SYNERGISING SURFACE MODIFICATION AND SOIL SUSPENSION FOR FABRIC CLEANING EFFICACY

by

ALESSANDRA VALENTINI

A thesis submitted to

The University of Birmingham

for the degree of

DOCTOR OF PHILOSOPHY

School of Chemical Engineering

College of Engineering and Physical Sciences

The University of Birmingham

February 2020

UNIVERSITY OF BIRMINGHAM

Abstract

There is a widespread interest in finding efficient ways to deliver cleaning on synthetic fabrics (eg. polyester), particularly in challenging laundry conditions that use low washing temperature and short rinse cycle.

This study advances understanding of using soil release polymers (SRPs) to modify polyester and cotton surfaces and deliver better cleaning in these challenging washing conditions. The effect of chemical structure of SRPs and deposition parameters such as pH and water hardness on surface modification was assessed. Streaming potential, scanning electron microscopy and thermal gravimetric analysis were used to characterize the fabric surface before and after polymer deposition, and results were correlated to bulk data coming from UV/vis spectroscopy, as well as to soil release and protein release/deposition data. Results showed that all SRPs analysed are effective in modifying polyester and improving grease release from fabrics compared to untreated polyester.

The interactions between SRPs and surfactants with different structure were studied by surface tension measurements to give insights on SRP-surfactant compatibility. The interactions between the same surfactants and typical components of food stains (amylose, protein, oil) were investigated via multiple methods and a structure-function correlation model was developed which correlated surfactant structures with strength of interaction with soil components. Insights into optimal surfactant structure required to achieve efficient cleaning with each of the analysed soil components were derived, as a result. The present findings provide new, essential insight into the behaviour of SRP-modified fabrics, facilitating the introduction of these new classes of SRPs in laundry detergent formulations, and enable the identification of cleaning mechanisms for complex food soils containing starch, oil and proteins.

Acknowledgments

First and foremost, I would like to acknowledge my supervisor Melanie Britton for her patience, her advice and her support during the last year. This PhD thesis would have not been the same without her guidance. Even if I joined Britton's group for a very short period, Melanie has always been able to convey her passion and her dedication to science. She has been an example to follow from a personal and professional point of view. I would like to thank Professor Gerardo Palazzo for his insights on the zeta potential world, for the hours spent discussing science and movies and for hosting me in his laboratory, making me feel part of the team. I wish to thank Serafim Bakalis and Konstantinos Gkatzionis for their guidance during the first two years of my PhD.

I owe my deepest gratitude to Anju Brooker and Eric Robles for their priceless support and help in my PhD and P&G journey. They have always believed in me and in my abilities as a scientist and as a person, encouraging me to show my ideas and to fight for what I believed was right for me, without any fear. I would like to thank Anju for the values she has conveyed to me, for her guidance throughout the project and in the P&G-jungle. My deepest gratitude goes to Eric for the never-ending conversations about science, I have learnt so much from him and I hope to always have the same enthusiasm that he has in doing his job. I would also like to thank Karl Braeckman for his constructive comments and warm encouragement, I have deeply enjoyed collaborating with you.

I would like to show my greatest appreciation to all the Bioclean students for sharing this path together, balancing stress and worries about the PhD with stimulating chats, and drinks, in the most beautiful places around Europe. A special mention goes to Helena, Hugo, Luca and Silvia…not by

chance the people I have shared more drinks with! Helena, for being the best lab-partner, for always catching the beauty in the world around us, for the infinite chats about life and for her true friendship. Hugo, for being the best music advisor I could have asked for, for the philosophical conversations in the middle of the night, for his assistance in spraining my wrist and for recognising myself as a "very conservative woman from the South of Italy". Thanks to Luca for the never-ending phone calls including guitar performances, podcast readings, books and life advice. Thanks to Silvia for being my roommate at conferences and meetings, for emptying an uncountable number of wine bottles together, for the chats that made me lose precious hours of sleep but that taught me how important is to never hide my feelings and my "Italian passion".

Thanks to Chiara, Clelia and Luisa for being my closest friends over the last 14 years. Even if my "emigration" decreases the chances to gain together, I have always felt them by my side. Every summer I have loved coming back to listen to the irrational adventures of Luisa, the ironic jokes from Clelia and the unexpected news from Chiara. Thanks to Gigi Milo for his morning pictures, for his creativity in reviewing lyrics and for being my techno music dance partner. Thanks to Claudia, Michele, Samuela, Francesco, Vincenzo and Gaia for welcoming me home every time.

I owe my deepest gratitude to the people I have met in Newcastle Innovation Centre. Thanks to the High five crew. Thanks to Despoina, for her straightforward advice, the deep chats over numerous cappuccinos and for listening to my complaints and very complicated stories. Thanks to Carlos, for the "Carlo's day phone calls" full of "who are you?", "nooooooooo" and "brava Ale!", for his true friendship and for the several pints we shared together. I'm glad I have shared so many lunches and afternoon coffees with Varun, I have learned how to look at life from a different point of view and to face whatever life offers you with a calm and positive attitude. Thanks to Laura for her craziness, for the cat pictures displayed in the toilet, for this friendship developed "a step by a step". Thanks to Lia for the office chats trying to convince ourselves that it was normal to stay in P&G until 7pm and that

tears that I made her cry any time that I was leaving, for all the times she had to ask for a kiss or a hug. She has shown me how to be a woman, from her I have learnt how to meet people everywhere I go and how important is making sacrifices for the people you love. Thanks to my brother Angelo, who remains an anchor in my life. He has always understood my choices, despite our different approaches in life. His rationality has always been able to calm my tumultuousness and he has often behaved as he was the older sibling. Family isn't something you choose…But I certainly would have chosen mine.

Abbreviations

3D	*Three dimensional*
AES	*Alkyl ethoxy sulfate*
AM	*Amylose*
AMP	*Amylopectin*
AO	*Amine oxide*
ARXPS	*Angle-resolved X-ray photoelectron spectroscopy*
AS	*Alkyl sulfate*
BCA	*Bicinchoninic acid*
BET	*Brunauer-Emmett-Teller*
BJH	*Barrett, Joyner and Halenda*
BS	*Back scattering*
BSA	*Bovine serum albumin*
cac	*Critical aggregation concentration*
Cap	*Coco amydo propyl*
CCA	*Convex constraint analysis*
CD	*Circular dichroism*
CIE	*Commission Internationale de l'Eclairage*
cmc	*Critical micellar concentration*
CTAB	*Cetyl trimethyl ammonium bromide*
DDAC	*Dodecyl dimethyl ammonium chloride*
DFT	*Density functional theory*
DI	*De-ionized*
DLVO	*Derjaguin, Landau, Verwey, Overbeek*
DNA	*Deoxyribonucleic acid*
DTAB	*Dodecyl trimethyl ammonium bromide*
EDL	*Electrochemical double layer*
EI	*Electron ionization*
EMR	*Electromagnetic resonance*
EO	*Ethoxylate*
EPS	*Extracellular polymeric substances*
ESI	*Electrospray Ionization*
FFR	*Fast field reversal*

FFT	*Fast Fourier transform*
FID	*Free induction decay*
IR	*Infra-red*
LAS	*Lauryl alkylbenzene sulfonate*
LDV	*Laser Droplet Velocimetry*
LOD	*Limit of detection*
LS	*Light scattering*
MALDI	*Matrix Assisted Laser Desorption Ionization*
MEMA	*Methoxyethyl methacrylate*
METAC	*methacryloyloxy*
MS	*Mass spectrometry*
NMR	*Nuclear magnetic resonance*
PA	*Polyacrylate*
PALS	*Phase Analysis Light scattering*
PBS	*Phosphate buffer saline*
PEG	*Poly(ethylene glycol)*
PET	*Polyethylene terephthalate*
PFG	*Pulsed field gradient*
PGSTE	*Pulsed gradient stimulated echo*
PMMA	*Poly(methyl methacrylate)*
POET	*Poly(oxyethylene terephthalate)*
psp	*Polymer saturation point*
Q	*Quadrupole*
QUATs	*Quaternary ammonium compounds*
RF	*Radiofrequency*
RH	*Relative humidity*
RNA	*Ribonucleic acid*
SA	*Surface area*
SAMs	*Self-assembled monolayers*
SANS	*Small angle neutron scattering*
SDS	*Sodium dodecyl sulfate*
SE	*Secondary electrons*
SEM	*Scanning electron microscopy*

SLS	*Sodium lauryl sulfate*
SRI	*Stain removal index*
SRP	*Soil release polymers*
TGA	*Thermal gravimetric analysis*
TIC	*Total ion chromatogram*
TM	*Mixing time*
Tof-SIMS	*Time of flight – secondary ion mass spectrometry*
Trp	*Tryptophan*
UV	*Ultraviolet*
UV/vis	*Ultraviolet-visible*
XIC	*Extracted Ion Chromatogram*
XPS	*X-ray photoelectron spectroscopy*
ZP	*Zeta potential*

Table of contents

List of Figures

List of Tables

Chapter 1. Introduction

Changes in consumer laundering habits have been observed in the last few decades as a consequence of higher consumer awareness of environmental problems. Recent surveys[1–5] have highlighted that, globally, typical washing temperatures are reducing ($\leq$ 40 °C) to minimize energy consumption. Moreover, washing cycles of 30 minutes are preferred to longer ones to save water, energy and time. However, in these washing conditions, grease removal from synthetic fabrics, such as polyester, is challenging. Therefore, there is research on finding efficient detergents that deliver cleaning on synthetic fabrics in this new challenging laundry environment. In this thesis, an investigation of polymer and surfactant classes that can be added in laundry detergents to enhance cleaning efficiency on synthetic fabrics has been carried out. The polymers under investigation are able to modify the surface of the fabric and improve the cleaning efficiency, as shown in this thesis. Additionally, the interactions between different types of surfactant and main components of the soil have been studied as a way to identify structural features that are needed in surfactants to enhance the interaction with the soil and deliver better cleaning.

1.1 Soil attachment on fabrics

1.1.1 Fabrics composition and structure

Textiles are widely used in many applications, including clothing, home interior and personal and healthcare. As a consequence, there is a growing interest in identifying chemical and physical processes which reduce textile cost, impove their durability and deliver specific benefits to the final product (e.g. superhydrophobicity; anti-wrinkling; stretchability). In most cases, these processes modify the surface of the material without affecting the bulk properties of the material, and the processes are strictly related to fabric structure and composition. Therefore, a deep understanding of surface modification of textiles goes hand in hand with an understanding of fabrics type and structure.

Fabrics are composed of fibres, which can be described as a single elongated piece of a given material with a cylindrical structure. Fibres that can be aligned and/or twisted together to create yarn which can then woven together to form a fabric.There are many different types of fibres (cotton, polyester, wool, nylon etc) which can be used, either on their own or in combination with each other to create blends of fabric (eg. polycotton is made from a combination of cotton and polyester fibres woven together). The fabric characteristics are related to the chemical properties of the fibres. Moreover, the arrangement of the fibres has an effect on fabrics durability, elasticity, wettability and wicking[6]. For instance, it is known that the contact angle measured on fabrics is influenced by their porosity and yarn diameters[7–9]. According to the arrangement of yarns and fibres, fabrics are classified as woven, knitted or non-woven fabrics[10]. The term woven-fabric is used to refer to fabrics where yarns are interlaced at a right angle (90°), therefore a repetitive geometric structure is obtained (Figure 1a). Instead, knitted fabrics are made of yarns that are interlacing, forming loops that can be easily stretched. This structure results in great elasticity and stretchability of the fabric (Figure 1b). If the fibres are directly entangled via chemical, mechanical or thermal treatment, without forming any yarns, the fabric is identified as non-wowen or flat (Figure 1c).
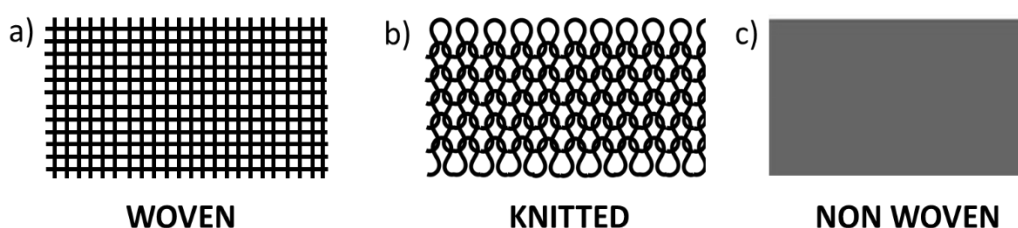
Figure 1 - Yarns arrangement for woven (a) and knitted (b) fabrics. Absence of yarns in the case of flat fabrics (c).

The most commonly used fabrics, nowadays, are cotton and polyester, which are characterized by different chemical and physical properties[10]. Cotton[11] is a fabric made of natural fibres mainly composed of α-cellulose and some uncellulosic polymers (carbohydrates, proteins), as minor components. Its fibres are characterized by high strength and fineness and they have diameters around 16-21 μm[12]. Cotton tends to be rigid and stiff and is very hydrophilic[13] due to the presence of hydroxyl groups, which interact with water molecules and result in high moisture retention.[10] Historically, cotton has been the

most used textile, but it has progressively been replaced by synthetic fibres. Among these, polyester has become one of the most common textile for clothing and home interior[14,15] and it is expected to become the most used fabric in the next decade. Polyester is composed of fibres which diameter is between 12-25 μm and which mainly contain polyethylene terephtalate (PET). It has high toughness and durability, and, therefore, it is used for clothing, household and medical applications[15].

One of the main differences between cotton and polyester is related to their surface energy and moisture management. Fast transportation of human sweat and water vapour through the fabric occurs in cotton because of its hydrophilicity and low thermal resistance[16], therefore cotton is a suitable textile for hot weather. Conversely, polyester is more hydrophobic, confirmed by its higher water contact angle, and has high thermal resistance, becoming an ideal textile for thermal insulating clothes. Because of their large use in textile industry, and their very different properties, cotton and polyester are the most studied textiles and leading to increased interest in their cleanability.

1.1.2 Soiling of fabrics

A detailed understanding of fabric cleaning processes requires improved understanding of the mechanisms of soil adhesion on fabrics. Soiling occurs when dirt (grease, oil, dust) deposits on the fabric surface, affecting fabric appearance as a consequence[12]. The resulting deposit is called *soil,* if the deposit is homogeneously distributed on the surface, or *stain,* if the deposit occurs in a discrete region. The origin and composition of the deposit can be different but, in general, soil is composed of a mixture of fluid and solid particles, where the fluid is adsorbed on the solid particle[17]. The fluid, which can be an oil, grease or resin, is responsible for binding and retaining the soil particles. This mechanism of soil particle entrapment is generally called *oil bonding* and it involves particles that can be organic or inorganic, macroscopic or microscopic. In some cases, it is also possible to have stains that are composed of a single component, as in the case of fluid stains, usually composed of only oil, or dry solid particulate stains (eg. clay)[18].

Soiling degree depends on the nature of the dirt as well as the properties of the surface where the soil deposits. An important parameter affecting soil deposition is the contact area between the soil and the textile. Therefore, soiling is highly dependent on the structure of the fabric and it has been observed that the soil accumulates in the space between yarns, in the pores between the fibres of a yarn or on the external surface of the fabric. As a consequence woven fabrics experience higher degree of soiling because of their higher surface area, whereas lower soil deposition occurs on non-woven fabrics[17].

The soiling process involves different kinds of interactions that can be distinguished in mechanical forces, electrostatic forces or adhesion forces. Among the mechanical forces, capillary pressure plays a primary role in the soiling process as it leads to penetration of the fluid soil in the textile structure with entrapment of the soil in the inter-yarn (micro-occlusion), pores (macro-occlusion) or between fibres[18]. Capillary pressure (ρ) is given by the following equation[18]:

$$\rho = \frac{2\gamma \, cos\theta_A}{r} \tag{1}$$

where γ is the surface tension of the liquid, θ_A is the advancing contact angle of the liquid on the surface fabric and r is the radius of the inter-yarn pore between fibres. Therefore, it is evident that fluid soil penetration depends on fabric structure (represented by the radius of the inter-yarn pore, r), on fabric wettability (θ_A) and on the fluid taken into consideration (γ). Considering a certain fabric substrate and a fluid (γ, r fixed), the penetration of the oil in the fabric pores and yarns occurs if $\rho > 0$. This means that the fluid has a lower surface tension than the fabric surface and, therefore, it will wet the fabric. A different driving force is involved in the deposition of dry particulate soils on fabrics, because the absence of a fluid component results in an absence of capillary pressure. Instead, the interaction between fibres and dry particulate soils is based on adsorption and geometric bonding, where the soil can get entrapped in the crevices in the fibres (micro-occlusion) or in the space between fibres or between yarns (macro-occlusion)[18].

The forces involved in the soiling process depend as well on the condition in which soil deposition occurs. In most cases, soiling occurs in dry conditions (while wearing or using the fabric), where mechanical forces and hydrophobic interactions are the main drivers for the deposition of the dirt. However, soiling also occurs in wet conditions[19], as in the case of laundry processes. In a washing machine the soil is suspended in the washing liqueur and, as they are in the presence of water, ionizable groups presents both on soil particles and on fabrics are in their dissociated form. Therefore, electrostatic attractions between these groups can occur, causing soil-redeposition on fabric surfaces.

1.1.3 Soil removal

Like soiling, soil removal is a complex process that involves a range of driving forces depending on the type of stain and fabrics. In the case of fluid soil, like oil for instance, fabric wettability plays an important role in determining the soil removal efficacy[19]. Removal of oil from textile occurs in three phases: *rolling up*[20]*, emulsification and solubilization.* The *rolling up* involves the displacement of the fibre-fluid interfaces and creation of two new interfaces: fibre-water and fibre-oil. As all processes, for being thermodynamic favourable it should have a negative value of free energy variation, defined as:

$$\Delta E = \gamma_{o/w} + \gamma_{f/w} - \gamma_{o/f} \tag{2}$$

where $\gamma_{o/w}$ is the surface free energy if oil/water interface, $\gamma_{o/f}$ is the surface free energy if oil/fabric interface and $\gamma_{f/w}$ is the surface free energy if fabric/water interface. For soil removal to be spontaneous, the following relationship needs to be true:

$$\gamma_{o/f} > \gamma_{o/w} + \gamma_{f/w} \tag{3}.$$

However, the kinetics of soil release needs to be taken into consideration. One of the simplest cases is the removal of oily fluid stains, which requires three steps[21]. The first step is called the induction period and is characterized by slow penetration of water in the fabric structure and slow release of the soil present on fabrics surface. After this, the soil-release period takes place, where rolling up, the dislodging of soil and water diffusion inside the fabric structure occur. Eventually, the last step occurs, called the final period, during which the amount of soil retained is constant. The rate determining step of the process is the induction period, which is controlled by the wettability of the fabric, which determines

the penetration of water within the fabric structure. Therefore, improving the wettability of a fabric increases the speed of the induction period, resulting in an enhancement of the kinetics of the soil removal process, thus delivering better cleaning.

Both the kinetic and thermodynamic of soil attachment and removal are related to the surface energy of the substrate and surface energy of the fluid soil that deposits on the fabric. For instance, polyester is easily wetted by oil, because of polyester hydrophobicity and low surface energy. The oil, which has a low surface energy spreads onto polyester surface with a low contact angle[22], resulting in a higher oil adhesion on polyester and, therefore, removal of oily stains from this type of fabrics is challenging.

There are several ways to ease the removal of fluid soil from a fabric surface; one possible way is to modify fabrics wettability before soiling occurs via plasma treatment for instance[23–25], increasing $\gamma_{o/f}$, shortening the induction period and enhancing oil removal from the substrate. However, this is an expensive technique and, therefore, it is not used to modify textile that are destined for clothing industry. An easier and more accessible way to enhance soil removal is addressed by using detergents during the washing process.

1.2 Soil removal via washing process

1.2.1 Laundry detergent composition

Soil removal from fabrics can be improved by addition of a detergent in the wash. In the literature, there are several definitions of a detergent. However, one of the most general is the description provided by Bourne and Jeggins who defined a detergent as *"any substance that, either alone or in a mixture reduces the work requirement for a cleaning process"*[26]. According to this definition, surfactants can be used as detergent. Surfactants are amphiphilic molecules that increase the water wetting ability of fabrics, lowering the surface tension of the solution (more details about their structure and characteristics will be given in section 1.2.3). In the case of laundry detergents, their role is to remove soil from the fabric surface and avoiding its re-deposition via soil emulsification, suspension or solubilization. Most

common detergents usually contain surfactants in combination with other substances that are able to improve the cleaning as well as delivering additional benefits[27].

It is known that many surfactants are hardness sensitive, which means they form complexes with hard water ions (eg. calcium and magnesium); this process is called saponification. These complexes, also called soaps, are insoluble and, therefore, precipitate and reduce the cleaning efficiency. As a consequence, it is very common in laundry detergent to have builders such as citrate and phosphate. The builders form complexes with water hardness ions, preventing their interaction with surfactant and enhancing cleaning efficiency of the detergent formulation.

Other additives widely used in laundry detergent formulations are dyes and bleaching agents. Dyes are molecules that deposit on a fabric's surface during the wash, increasing the whiteness appearance of the garments. In the case of white garments, the whiteness is usually achieved by addition of bleaching agents. The bleaching agents cause oxidization of compounds that initiate a series of chemical reactions to remove any colouring substance from the fabric. More recently, the use of polymers in laundry formulation has become very diffuse. Depending on the chemical structure of the polymer, several benefits are delivered during the wash, such as anti-re-deposition, soil-release, anti-static and dye-transfer inhibition. Fragrances are also added in the majority of detergent mixtures. These hydrophobic molecules deposit on fabric surface and produce a pleasant scent after the wash.

Some laundry detergents also include enzymes and suds-controlling agents. The enzymes are added to improve cleaning, by hydrolysing proteins, lipids or carbohydrates. The suds-controlling agents, on the other hand, are added to increase surfactant activity at the liquid-soil interface vs the liquid-air interface, in addition to the more practical purpose of avoiding foam leakage from the machine. For instance, in hand washing long-last suds are expected. Therefore, suds-stabilising agents are usually included in hand washing detergent products. On the other hand, suds-suppressors are commonly added in products

for dishwashers and washing machines, as excessive foam is perceived as a negative by the consumer and can lead to the foam leaking from the machine or remaining on the garments at the end of the wash.

1.2.2 Washing temperature and mechanical agitation effect on cleaning efficiency

Mechanical forces and washing temperature play an important role in promoting efficiency of soil removal. When mechanical forces are present in a wash, a higher mass transfer of detergents and stains takes places and this results in higher washing efficiency[28]. Washing temperature also has an effect on oil removal, where high washing temperatures lead to increased oil removal from fabric[29]. Both washing temperature and mechanical forces have a positive effect on the rolling up of the oil, which consists of the displacement of oil from the fibres and formation of oily large globules that can be easily removed by surfactants[30]. Therefore, use of high temperature and a high-spin cycle is advisable to enhance cleaning. However, this is in conflict with increasing global demands to reduce the amount of water and energy used, which leads to use of low-temperature and short washing cycles in laundry.

The importance of parameters, such as surface energy, surface topography, soil type and the presence of detergents, for determining the efficiency of soil removal has been mentioned (section 1.1.3). However, it is also important to understand what happens to the soil when it has been removed from fabric surface, as the soil might redeposit on the fabric if it is not efficiently emulsified or suspended in bulk. When the soil is suspended in the washing liquor, it interacts with the surfactants and other actives present in the laundry detergent. The type of soil-surfactant interactions occurring during the wash depend on the soil composition. In this study, an overview on the interaction between surfactants and main components of the soil is given and a structure-function relationship between surfactant structure and strength of interaction with the soil components is presented.

1.2.3 Surfactants

Surfactant are amphiphilic molecules possessing a hydrophobic alkyl tail, of typical chain length in the range of 12-18 carbon atoms, and a hydrophilic head group. Surfactants are classified according to the

charge and type of surfactant head group, of which there are four classes. The first class of surfactant comprises anionic surfactants, which have a negatively charged head group. Sulfate, sulfonate, carboxylate and phosphate are the most common surfactants belonging to this class and they provide good cleaning and anti-re-deposition benefits because of the electrostatic repulsion between heads. The second class of surfactant are the cationic surfactants, which have a positive head group, with the quaternary ammonium salts being the most common. Their effect on cleaning is similar to anionic surfactants, but they also have additional benefits. In particular, their positively charged head results in an increased tendency to deposit on the surfaces, which are generally negatively charged (e.g. hair, fabrics). For this reason, this class of surfactants is heavily used in hair conditioners and fabric softeners. The third class of surfactant comprises non-ionic surfactants, which head groups usually contain oxygen, and which are not involved by any de-protonation or protonation when in water (e.g. alcohol ethoxylates). As they are not charged, non-ionic surfactants are tolerant to water hardness and they are very often used as co-surfactant. The last class are the amphoteric surfactants, which contain both a positive and negative charge in their head group. The net charge of these surfactants depends on the pH, as each functional group can be protonated or deprotonated.

The surfactant head group has a high affinity for water and other hydrophilic media, while the alkyl chain prefers hydrophobic media. For this reason, surfactants will tend to go to the air-water interface, exposing their hydrophobic tail to the air (hydrophobic) while their hydrophilic head is in water (hydrophilic), lowering surfactant free energy and the liquid surface tension. An increase in surfactant concentration results in a decrease in the surface tension of the solution, as surfactant molecules segregate at the air-water interface and increase in concentration until reaching saturation. After a certain concentration, the formation of surfactant self-assembly structures, called micelles, occurs and surface tension remains constant. The concentration at which micelles start to form is called critical micellar concentration (*cmc*). It has been found that *cmc* is a function of the surfactant type and of pH and ionic strength of the solution. For instance, non-ionic surfactants have a lower *cmc* than ionic surfactants because of the lower solubility and higher packing of non-ionic monomers, which is due to

the absence of electrostatic repulsions between surfactant heads. At the same time, non-ionic surfactants are less affected by ionic strength, which strongly influence the *cmc* of ionic surfactants. Additionally, pH influences the *cmc* of amphoteric surfactant, which controls their solubility.

When micelles are formed in water, all the tails of the surfactants are kept together in the core, minimizing the contact with water, while the outside surface is occupied by surfactant heads. The driving force for this self-assembly are entropic and enthalpic as the surfactants tend to increase the number of tail-tail interactions and to minimize the interactions between surfactant tail and water. Other parameters that affect the surfactant self-assembly are electrostatic interactions (in the case of ionic and amphoteric surfactants) and steric interactions. Both the interactions determine the minimum distance at which surfactant monomers are placed inside the micelles. An important parameter which determines the surfactant aggregation number as well as the type of aggregate that is formed (spherical micelles, rod like micelles, etcetera) is the form factor, which is a function of the surfactant head volume and of the length of the surfactant alkyl tail. The interaction between surfactant and soil can involve both micelles and monomers, resulting in different effects and mechanisms. Moreover, the efficiency and occurrence of surfactant-soil interaction are strictly related to surfactant head type and charge.

1.2.4 Inefficient soil removal and biofilm growth

Soil removal is sometimes inefficient, particularly in the case of low temperature and short-cycle washing conditions. One of the main consequences of inefficient removal of soil from textiles is the development of biofilms (*biofouling*)[31,32]. A biofilm is an organized association of microbial organisms that are immersed in a matrix of extracellular polymeric substances (EPS), which is composed mainly of water (up to 97%[33]), and biopolymers, including polysaccharides, proteins, DNA and RNA. These biopolymers present in the EPS are the product of the lysis of bacteria cell or they are taken from the environment (eg. left-over soil). Polysaccharides are the main constituents of the EPS[34] and they define the structural and functional properties of the biofilm[35]. Moreover, they are also used as nutrients from the bacteria cell.

The development of a biofilm occurs when a substrate is in contact with an aqueous solution and involves three steps[36]. The first step is the deposition of a conditioning film, where proteins deposit on the surface of the substrate. This stage is necessary for bacteria adhesion because bacteria are unable to adhere to the substrate directly. Following this, planktonic bacteria cells present in the solution start adhering on the conditioned substrate. Initially, the adhesion is based on weak forces (Van der Waals). At this stage, the removal of bacteria from the surface is possible via shear forces or chemical action. After the initial attachment, bacteria start producing the EPS and communicating with each other (*quorum sensing*)[37]. New covalent bonds are formed between bacteria and the substrate or the surrounding EPS and this leads to an organized 3D structure. At this stage, the biofilm is resistant to mechanical and chemical action and hard to remove from the substrate, as a consequence. Biofilms can form from one or several bacteria strains. It has been observed that the bacteria present in the biofilm exhibit characteristics that are different from the one experienced by the same bacteria in the planktonic form, as they will have higher growth rate and resistance.

There are several aspects affecting biofilm growth that depend on the environment and/or the substrate. For instance, several studies show that biofilm attachment is enhanced on hydrophobic substrates (e.g. plastic) compared to hydrophilic substrates (glass). The reason for this is related to the hydrophobic nature of the wall of bacteria cells which results in hydrophobic forces being the main drivers of bacteria adhesion. The more hydrophobic the substrate, the higher the risk for the surface to experience biofouling. This is demonstrated in the Baier curve, which shows that minimum fouling is experienced if the surface tension of the substrate is around 22-24 mN/m [31,38]. Surface roughness has also an impact on biofilm attachment, as higher roughness implies easier bacteria attachment. However, as observed in nature, specific surface topographies can inhibit biofilm growth. In addition to the substrate features, environmental conditions determine an effect on biofilm development. As mentioned before, protein deposition on a substrate is the initial stage of the biofilm developing process. Therefore, if proteins are present in the aqueous medium and deposit on the substrate, an enhancement in bacteria attachment

occurs. Additionally, as for any deposition process, temperature, pH and ionic strength are important parameters to take in account for predicting bacteria adhesion to the surface. The presence of cations (Ca^{2+}, Mg^{2+}) results in a less negative surface charge on the substrate (e.g. glass), lowering electrostatic repulsion between the substrate and bacteria surface (usually negatively charged) and increasing the rate of attachment as a consequence.

Polyester fabrics are an ideal substrate for biofilm development as they have higher hydrophobicity and no negatively charged groups. The biofilm development on polyester fabric is even enhanced in presence of soil residues, as the proteins and the polysaccharides contained in the soil can become part of the EPS or being used as nutrients, increasing bacteria growth and attachment.

1.2.5 Antifouling and fouling-release

The term anti-fouling refers to the prevention of organisms attaching to a specific surface. Fouling-release is used, instead, to identify the removal of an already-attached biofilm from a substrate[31]. The development of biofilms represents the first stage of many infection diseases. Therefore, there has been a growing interest in anti-fouling and fouling-release strategies in the last few years. In all cases, the importance of these processes is undoubted, as the presence of biofilm lowers the performance of the affected device. One example is found in the filtration membrane industry, where fouling causes filtration flux decline[39]. For this reason, higher energy is required to achieve the same filtration efficiency of the membrane not conditioned by the biofilm and an earlier replacement of the membrane might be necessary.

Primarily, inhibition of biofilm growth on a substrate is achieved via protein repellence, which inhibits the formation of the proteinaceous conditioning film. There are several ways to promote anti-fouling on surfaces and they can be classified in physicochemical methods and physical methods. Physicochemical methods are based on a chemical modification of the substrate via deposition of anti-foulant agents or coatings. In the past, the main anti-fouling agents were metal (e.g. Ag). However,

metals are now known to be toxic for the environment. Therefore, there has been interest in identifying new green antifouling strategies in the last years. Among these strategies, deposition of self-assembled monolayers (SAMs) has shown relevant benefits in lowering protein attachment and biofilm growth, where the deposited SAMs are usually hydrophilic and neutrally charged. Other methods to deliver anti-fouling benefits involve the deposition of hydrogel or poly(ethylene glycol) films to achieve steric hindrance versus proteins[40].

In the case of fabrics, anti-fouling benefits are usually achieved via deposition of anti-microbial actives. This strategy involves the use of actives as silver (Ag), quaternary ammonium compounds (QUATs) and Triclosan. These actives can be deposited during the manufacturing process of the fabrics or when the fabric is washed. The presence of anti-fouling finishes on textile prevents growth of biofilms and, as a consequence, the development of infectious diseases in humans that wear or use the treated textile. A positive impact on the environment is also addressed by depositing anti-fouling finishes on garments. People tend to wash their clothes less often if anti-fouling finishes have been deposited and this leads to lower energy and water consumption[41]. However, anti-microbial agents are usually expensive, so are the detergent formulations in which they are included. For this reason, there is significant interest in finding alternative and cheaper ways to deliver anti-fouling benefits for fabrics. Among these, textile surface modification strategies show promising results.

1.3 Surface modification of fabrics

1.3.1 Surface modification of fabrics for anti-fouling benefits

Surface modification enables textiles to experience new features without changing their bulk properties. The methods used to perform fabric surface modification can be divided in physical methods and chemical methods[24]. Physical methods modify the surface of the fabrics via plasma and thermal treatments. On the other hand, chemical methods take advantage of grafting or crosslinking of polymer precursors or polymer adsorption to address new surface properties.

There is a rich literature on the efficacy of polymer coating in delivering anti-fouling benefits[32,40]. According to the type of polymer coating, the anti-fouling behaviour is achieved by different mechanisms[32]. In the case of hydrophilic polymeric coating, such as poly(ethylene glycol), poly(ethylene oxazoline), polyammides and zwitterionic polymers[42], the formation of a hydration layer occurs on the surface of the modified substrate. This layer causes a decrease in the conformational entropy of the protein when the protein approaches the surface, preventing its adhesion. For instance, hydrophilic coatings are used in filtration membranes, where amphiphilic co-polymers are added in the membrane casting solution and form a hydrophilic surface which repels foulants[39]. Alternatively, physical adsorption, plasma or UV treatments can be used to deposit poly(ethylene glycole) (PEG) on fabrics, releasing protein-fouling benefits[36]. There is also the opportunity to use hydrophobic polymer coatings as an anti-fouling treatment. In this case, the release of proteins deposited on the substrate is caused by the lower adhesion forces of the protein on the surface. An example of hydrophobic coating is the use of grafting methods to generate polymer brushes on polyester fabrics. The polymer-brush layer leads to super-hydrophobic surfaces which prevent proteins adhesion[43,44].

The deposition of polymer coating on fabric surfaces is usually based on strong covalent bounding between the polymer and the substrate. This surface modification approach can be achieved very easily in the textile industry, but it increases the price of fabrics. Alternatively, it is possible to modify fabric surfaces with polymers that bind to the substrate via hydrophobic forces or π- π interactions. In these cases, the polymer is added in a laundry detergent formulation and the surface modification is performed during wash.

1.3.2 Polymer deposition on fabrics

Polymers can deliver many types of benefits during the washing process. The polymers are primarily used as builders (binding calcium and magnesium ions present in water), anti-redeposition agents, soil-release agents, anti-static actives or dye transfer inhibitors[45,46].

As builders, the polymers bind calcium and magnesium ions, usually present in hard water, and avoid their deposition on fabrics. These polymers are often anionic polymers that use their negatively charged groups to bind to cations present in hard water. Acrylic co-polymers, which are derived by copolymerization of acrylic and maleic acids, are usually added as builders. The acrylic groups bind free calcium and magnesium, improving the tolerance of the detergent formulation to water hardness.

Anti-redeposition polymers are widely used in laundry detergents, and are usually anionic polymers such as carboxy methyl cellulose, poly-carboxylate, polyvinyl alcohols. When removed from a substrate by surfactants, the soil is transferred in solution. However, the soil might not be stable in solution and can precipitate on the fabric surface again. This results in soil re-depositing on areas of clothes that were initially clean, causing consumer dissatisfaction. Use of anti-redeposition agents enhances soil suspension and solubility, avoiding soil transfer and re-deposition. A similar re-deposition issue occurs with dye molecules, where the dye previously removed from an area of the garment can re-deposit on a different area of the fabric (or on a different garment), causing dye transfer. In this case, dye transfer inhibitors are used. As before, the polymer forms complexes with the dye, avoiding its re-deposition.

Dissatisfaction amongst consumers can also be due to excessive electrostatic charge accumulation on the fabric surface while wearing, resulting in consumer discomfort. This matter can be solved by adding conductive polymers (called antistatic polymers) to laundry formulations, improving fabric surface electric conductance.

Another class of polymer that is usually added in fully formulated laundry detergents are soil release polymers (SRPs). These are polymers that deposit on fabric surfaces and enhance the soil release via electrostatic repulsion, hydrophilization and/or steric repulsion, and improve the cleaning performance of the formulation. As secondary benefit, they can reduce biofilm growth by reducing the availability of nutrients for bacteria. SRPs are a topic of on-going research in laundry formulation and are the focus

of this thesis. Their presence has become increasingly important because of the low temperature commonly used in laundry processes and the global proliferation of hydrophobic synthetic fabrics.

1.4 Polymer-soil interactions

1.4.1 Soil release polymers

A Soil Release Polymer is a block copolymer that includes hydrophobic and hydrophilic blocks. The hydrophobic blocks are responsible of the deposition on the hydrophobic surface of the synthetic fabric, while the hydrophilic blocks face the fabric-liquid/fabric-air interface. Therefore, the surface of the fabrics become hydrophilic and the soil adhesion on it is weaker. As a result, the fabric exhibits soil-releasing benefits, with easier removal of oily soils from the textile surface by surfactant emulsification and/or via delamination of the polymeric film (Figure 2).
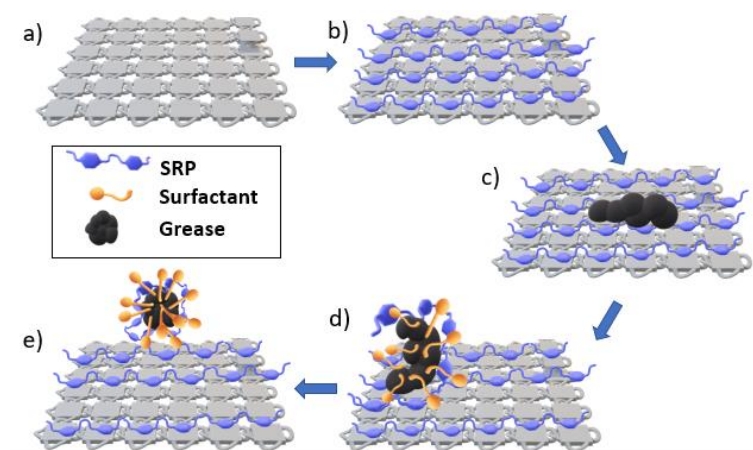
Figure 2- Schematic diagram showing the mechanism of action of a SRP. a) Untreated polyester fabric; b) fabric modified via SRP deposition; c) soil adhesion on fabric modified via SRP; d) soil removal from fabric surface via surfactant; e) emulsified soil in solution

SRPs can include a variety of different functional groups. In his review[47], O'Lenick mentions the use of polyacrylate (PA)/poly(methyl metacrylate) (PMMA) blocks polymerized with di-epoxide as SRPs used in textile curing process. This class of SRP leads to a net negative surface charge on fabric, due to the presence of the negatively charged acrylate groups, improving the water penetration in the fabric. Moreover, PA/PMMA co-polymers experience swelling in alkaline conditions and this behaviour seems

to play a role in soil release[17]. SRPs that contain fluorine in their structure are also used, as they lower the surface energy of the textile and deliver oil repellence even in dry conditions[17]. More recently, some SRPs that combine a silicone and polyethylene glycol (PEG) backbone with amino groups have been introduced.

The majority of the SRPs are based on poly(ethylene terephthalate)/poly(ethylene glycol) (PET-PEG) copolymers[48]. The chemical structure of these SRPs is very similar to the one of polyester fabrics, therefore these SRPs deposit on polyester. Among the two blocks, PET is the hydrophobic and is responsible for the deposition of the SRP on fabric. The driving force for deposition is the π-π interaction that occur between the terephthalate units of the polymer and the terephthalate groups on the fabric. Once deposition has occurred, the PEG water soluble chains orientate themselves above the fabric surface, forming a hydrophilic film. The PET-PEG soil release polymers are often functionalized with other chemical groups to deliver extra benefits in addition to soil release. For instance, the presence of anionic groups in the PET units leads to a net negative charged film on top of the polyester fabric. During the wash, the previously removed soil is suspended by anionic surfactant in solution and can re-deposit on the fabric. The presence of anionic groups in the SRP structure are able to prevent this, as there is an electrostatic repulsion between the negative charged groups on the fabric surface and the negative head groups of the surfactant (*soil repellence or anti-redeposition mechanism*).

The soil-release efficiency of the SRP depends on several factors, first among everything fabric type. In fact, these technologies are usually used for synthetic hydrophobic fabrics or for mixture of them with cotton (e.g. polycotton), while very little is known about SRP that are optimal for cotton[49,50]. In the same way, the number of times you wash with a detergent containing an SRP is relevant, as this determines the thickness and uniformity of the SRP film. The optimal SRP is one that modifies a large variety of fabrics types, requires a single cycle to generate a uniform layer on the surface of the textile and delivers soil release benefits at low dosage (less than 1% in laundry detergent formulation).

Moreover, as it needs to be included in a multi-component formulation containing surfactants, enzymes and solvents, the SRP must be compatible with other actives present. For instance, it has been observed that the use of anionic SRPs in fabric enhancer formulation is not advisable, as they form complexes, or coacervates, with the cationic surfactants[48] which prevent SRP deposition on fabrics Therefore, it is very important to assess the interactions of the SRPs with surfactants in bulk.

1.5 Polymer-surfactant interactions

Polymer-surfactant interactions have several applications in cosmetics, oil recovery and paint and there is widespread research on their characterization. One way to investigate these interactions exploits the changes in physicochemical properties that occur when polymers and surfactants are mixed. These changes refer to macroscopic phenomena (such as viscosity, surface tension, conductivity) or the environment in which the surfactant and polymers are immersed, assessed by diffusion Nuclear Magnetic Resonance (NMR), circular dichroism (CD) and Small Angle Neutron Scattering (SANS). Surfactants- polymers interactions are a consequence of electrostatic forces (acid-base interactions), dispersion forces, hydrophobic interactions and Van der Waals interactions. Mainly, the type of interaction depends on the charges of the surfactant and polymer. Moreover, the complexity of surfactant-polymer interactions is also increased by the possibility of the polymer to interact with individual surfactant molecules or with surfactant aggregates (*hemimicelles*). Sometimes, the formation of mixed surfactant-polymer micelles is also possible. The universally accepted model for polymer-surfactant interactions is called "pearls on a string model" or "necklace model"[51,52]. According to these models, surfactants start forming hemimicelles (surfactant aggregates) along the polymeric chain above a certain surfactant concentration, defined as critical aggregation concentration (*cac*). The surfactant monomers use their hydrophobic tails to interact with the hydrophobic domains of the polymer chain, forming hemimicelles along the polymer backbone, and the structure that is formed is similar to a pearl necklace. The *cac* of the surfactant-polymer system is lower than the *cmc*, as the interaction with the polymers stabilizes the surfactant aggregates. A more complex case is represented by the interaction between an ionic surfactant and an oppositely charged polyelectrolyte (Figure 3). In this case, polymer

and surfactants start interacting at concentrations below the *cac*, where the ionic surfactant heads interact with the charged sites of the polymer (*hairy-worm model*) in a non-cooperative way. The *cac* is reached when all the charged sites present on the polymer are saturated by surfactants.
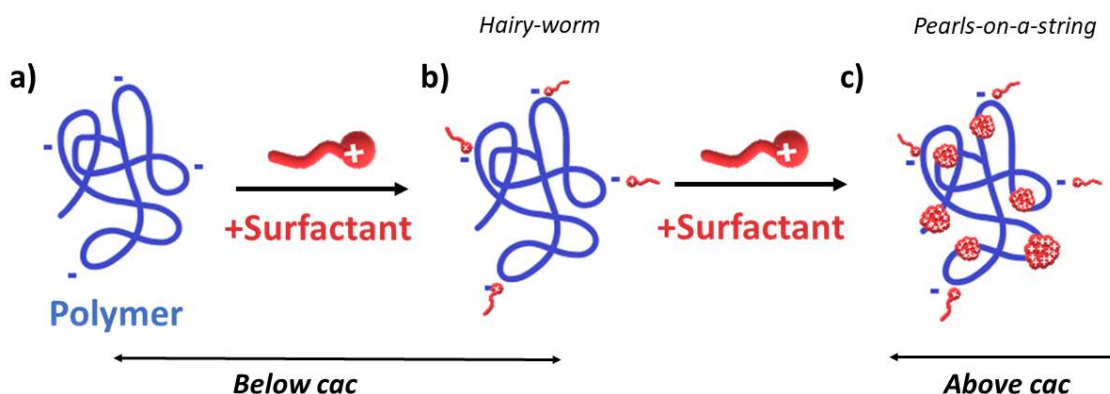
Figure 3- Schematic diagram of the interaction between a polyelectrolyte and an ionic surfactant: a) polymer by itself in bulk; b) Electrostatic interactions between surfactant heads and charged sites of the polymer; c) hemimicelles interaction with hydrophobic domain of the polymer.

The easiest way to assess the polymer-surfactant interactions is by measuring surface tension. In Figure 4, a schematic representation of the relationship for surface tension as a function of surfactant concentration is presented, in the presence and absence of polymer. In the case of surfactant, in the absence of polymer, there is an inflection point at the *cmc*. In the case of polymer-surfactant systems, three different areas can be identified in the graph[53]. For a concentration below the *cac*, the initial surface tension of the surfactant-polymer system is lower than surfactant system at the same concentration. This is a consequence of the so called *synergistic effect*, but is the case only for polyelectrolyte-ionic surfactant systems[54]. The first change in slope occurs at the *cac*, where the surfactants form hemimicelles along the polymer chain. The surface tension decreases for surfactant concentrations above the *cac* until reaching a concentration called the *polymer saturation point* (PSP), which is the *cmc* of the surfactant-polymer system. At the PSP, all the binding sites of the polymer are saturated by surfactants and, therefore, any extra surfactant monomer added is forming surfactant-only

micelles. After the PSP, the surface tension becomes constant and equal to the one for the surfactant-only system.
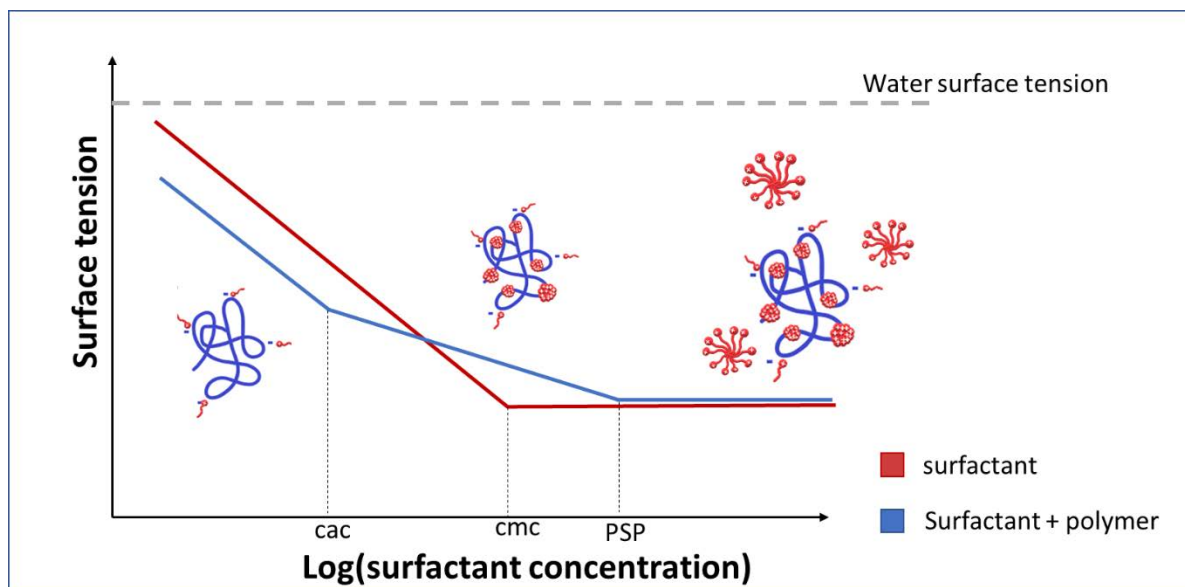
Figure 4 – Schematic representation of surface tension vs log(surfactant) for a system that contains only surfactant and a system that contains surfactant and polymer.

The *cac* value strongly depends on the strength of the forces involved in the interaction and on the type of surfactant and polymer. There are four different scenarios[55] that can occur. The first is an interaction between an ionic surfactant and an oppositely charged polyelectrolyte. In this case, the interactions between surfactant and the polymer are very strong, as they are electrostatic in nature, and this leads to a *cac* that is several orders of magnitude smaller than the *cmc* (*cmc* ~ 10000 *cac*). In the second scenario, weaker interactions occur between non-ionic surfactants and polyelectrolytes, mainly driven by hydrophobic forces. In this case, the *cac* is very similar to the *cmc* (*cmc* ~ 10 cac). The case of ionic surfactants and uncharged polymers results in closer values of *cac* and *cmc*, because the forces of interaction are extremely weak. The last scenario is when non-ionic surfactants interact with uncharged polymers. No interaction occurs in this case, therefore the two surface tension graphs overlap.

Other factors which influence the cac are surfactant chain length and polymer flexibility and conformation. Longer surfactant chain lengths, and less flexible polymers, result in higher *cac* values. Additionally, the *cac* depends on the polymer concentration.

1.6 Surfactant-soil interactions

In a washing cycle, surfactants are involved in interactions with not only the soil but also with polymers present in the detergent formulation. Surfactant-soil interactions are fundamental to the cleaning process, as they are responsible of removal of the soil from the fabric surface and emulsification/ complexation of the soil in bulk. However, some surfactant-soil interactions also have a negative effect on cleaning, as they lower the amount of free surfactant monomers available in bulk. The type of interaction, and its effect, depends on the type of surfactant, as well as the nature of the soil. Typically, soil is a complex mixture of grease (oil, solid fat), soluble and insoluble proteins and carbohydrates (such as starch). Each of these soil components experience different interactions with surfactants. In this thesis, the interactions between surfactant with soluble starch, soluble proteins and liquid oil are investigated

1.6.1 Surfactant interaction with oil: emulsion and emulsion stability

Oil is one of the main components of soil. When the SRP film is deposited on top of the fabric, oil removal is enhanced but requires the use of surfactants that lift the oil and emulsifies it. If the oil is not efficiently emulsified by the surfactant in solution, it will redeposit on the fabric, leaving them dirty. Therefore, good cleaning requires a surfactant system that efficiently emulsifies the oil, but the optimisation of such a surfactant system requires an understanding of the emulsification process and emulsion stability.

Oil and water are two immiscible liquids which spontaneously separate to minimize their interfacial area, creating an oil layer above the water phase. In the presence of agitation forces, as in a washing machine, homogenisation takes place, which leads to formation of oil droplets in water. These oil

droplets, called emulsions, are spherical, as this minimizes their interfacial area. Emulsion formation is the result of the action of Laplace pressure[56–58], expressed as:

$$\Delta P = \frac{2\gamma}{r} \tag{4}$$

where ΔP is the pressure between the inside and outside of the droplets, γ is the surface tension of the oil/water system and r is the radius of the droplets. Equation (4) highlights that the radius of the oil droplet depends on the surface tension of the system, which means that it is a function of the type of oil. The emulsification process generates new oil/water interfaces and, therefore, its free energy is positive. As a result, the emulsions are thermodynamically unstable, so they tend to coalesce and separate again because of gravity (oil being lighter than water). This process is called creaming and involves migration of droplets from the bottom to the top of the emulsion system, forming a floating layer. The time taken for the separation process is inversely proportional to the emulsion stability. The creaming velocity v is expressed by the Navier-Stoke's equation[59]:

$$v = \frac{2gr^2(\rho_w - \rho_{oil})}{9\eta} \tag{5},$$

where g is the gravitational acceleration, ρ_w is the density of the water, ρ_{oil} is the density of the oil and η is the viscosity of the system. From equation (5), it is evident that the density of the oil and the viscosity of the solution affect emulsion stability. Moreover, the equation suggests that smaller droplets lead to a more stable emulsion. For this reason, coalescence of oil droplets needs to be avoided in emulsions. The term coalescence refers to the process where two or more oil droplets collide and generate a bigger oil droplet, which is more unstable. As a result, a good emulsion system requires very low creaming velocity and stabilization against coalescence.

From a thermodynamic point of view, emulsions are unstable. However, they exist as metastable systems, where they are kinetically stable, and creaming and coalesce only occur after a long time. There are several ways to generate this metastability, but most of them based on a decrease in the creaming velocity or adding an emulsifier.

As mentioned before, increasing the viscosity of the solution can help decrease the creaming velocity and stabilize an emulsion. If we approximate oil droplets as hard spheres, the viscosity of the water/oil system is given by the Einstein equation[59]:

$$\eta = \eta_0(1 + 2.5\varphi) \tag{6},$$

where η_0 is the viscosity of the bulk phase and φ is the oil volume fraction. Therefore, increasing the oil volume fraction or the bulk viscosity enhances emulsion stability.

Metastability is also reached by addition of an emulsifier, which is a substance that generates a shell around the oil droplet. This shell prevents coalescence of oil droplets, via steric and electrostatic repulsion, and it helps stabilize the emulsion. Surfactants are known to be very good emulsifiers, orientating their hydrophobic tail in contact with the oil and their hydrophilic head in contact with the water. The use of surfactants as an emulsifier has found application in several industries[60] (food, cosmetic, painting) through their ability to lower the water/oil surface tension and stabilize the oil droplets. The stabilization of oil droplets is achieved when the surface area of the oil droplet is fully covered by surfactant monomers. The coverage efficiency strongly depends on surfactant structure and charge. As a general rule, ionic surfactants are better emulsifiers than non-ionic ones, as this results in higher zeta potential of the oil droplets and higher electrostatic repulsions. In line with the Derjaguin, Landau, Verwey, Overbeek (DLVO) theory [61,62], electrostatic repulsion prevents coalescence between oil droplets. However, the electrostatic repulsion between the charged head groups of the surfactant are also present within the surfactant film surrounding the oil droplets, which can lead to lower coverage. The increase of the ionic strength reduces repulsion within the film, therefore, emulsion stability is usually higher for ionic surfactants if water hardness is present. Among the non-ionic surfactants, ethoxylated surfactants, with high number of ethoxylated (EO) units, show higher emulsion stability due to steric repulsion between surfactant heads. However, higher EO content results in big surfactant head that requires longer surfactant alkyl chain to stabilize the emulsion. Alternatively, use of branched alkyl chain surfactants improves the packing around the oil droplets and this enhances emulsion

stability. At the same time, both the high ethoxylated and high branched surfactants have very low diffusion rate. Therefore, surfactant monomers can reach the oil droplet surfaces after that the oil droplets have already coalesced.

1.6.2 Surfactant-starch interactions: amylose helix complex formation

Another relevant interaction that can happen in the washing liquor is the one between surfactant and starch, which is a common component of food-derived stains. Starch is one of the major components of human diet and it is usually used as food thickener. Starch is made of granules with different shapes and it contains two types of polysaccharides, both based on glucose as building block: amylose (AM) and amylopectin (AMP)[63]. The amylose, that usually represents the 20-30 % (w/w) of starch [64], is a linear polysaccharide with molecular weight around 10^5-10^6 Da. On the other hand, amylopectin is a highly-branched polysaccharide, with molecular weight around 10^7-10^9 Da. Starch granules contain minor components such as lipids and proteins, which are present on the external shell of the starch granules or on the inside. External lipids are usually free fatty acids, triglycerides, glycolipids and phospholipids and they are usually present in cereal starch granules (e.g. wheat). Instead, proteins are usually the main component of the outer shell in potato starch granules.

When starch granules are heated in the presence of water, a disruption in the crystalline structure of the granules occurs. This process, known as gelatinisation, causes changes in the viscosity of the starch solution and a leaching out of the amylose present in the granules. Starch gelatinisation is less efficient for temperatures between 60 and 75°C, while it becomes more efficient in the range 75-90 °C.

It is known that surfactant can have an influence on starch gelatinisation. In fact, surfactant monomers can be involved in the formation of surfactant-amylose helix complex, as well as they can enhance or reduce starch swelling. There are many studies reporting the formation of amylose-helix complexes in presence of ligands as surfactants, iodine and lipids[65]. During gelatinisation, amylose leaches out from starch granules and it forms a single helix structure of diameter around 0.5 nm. This helical structure is hydrophilic on the outside, with a hydrophobic inner cavity that can host non-polar ligands. In the case

of surfactants, the alkyl tail is placed in the inner cavity, while the polar head is kept outside due to electrostatic and steric repulsion (Figure 5). However, there is poor understanding of the effect of surfactant structure on the gelatinisation. Recent studies[65] have suggested that helix-complex formation depends on the surfactant chain length, where longer alkyl tail results in higher hydrophobicity/lower solubility of the surfactant. As a consequence, C14-C18 surfactants are more able to be hosted in the amylose-helix cavity, forming inclusion complexes. Moreover, surfactant chain length influences starch pasting temperature for certain classes of surfactant (e.g. alkyl sulphate), where an increase in alkyl chain length (C_n) reduces pasting temperature for $n < 12$ (swelling enhancing). Instead, pasting temperature is increased if $n > 12$ [66].
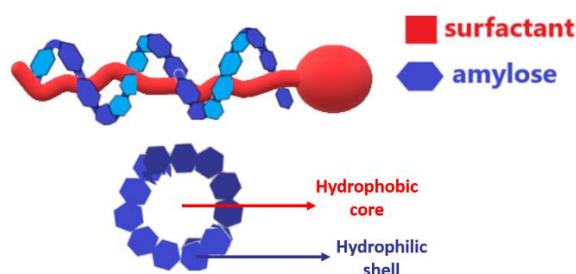
Figure 5 - Top: schematic representation of amylose-helix inclusion complex with surfactant, where the alkyl tail is entrapped in the inner core of the amylose helix. Bottom: a view from the top of the amylose helix and differentiation between the hydrophobic core and the hydrophilic shell.

1.6.3 Surfactant-protein interactions

Proteins are an important fraction of fabric soil and they can have animal or vegetable origins. Proteins are long peptides which are composed of amino acid monomers that are linked together via peptide bonds[67]. The sequence of amino-acids in the peptide chain is known as the primary structure of the protein. However, proteins also have secondary and tertiary structures. Secondary structure refers to the folding of proteins, as consequence of hydrogen bonds, into repetitive structures called α-helices, β-sheets and β-turns. The tertiary structure is related to the three-dimensional (3D) conformation of the protein in the space, which is usually determined by interactions between the R-side chain groups of the peptide chain and/or disulphide bridge formation. Quaternary structure is also used to describe proteins that are composed by two or more poly-peptide chains. In this case, interactions occur between

the different poly-peptide chains and the resultant structure defines the quaternary structure of the protein.

One of the most studied proteins, and the subject of this study, is bovine serum albumin (BSA). As the name indicates, BSA is a protein present in bovines and is a globular protein composed by a single polypeptide chain of 583 amino acids. It contains 17 disulphide bridges that are responsible for protein folding. Moreover, BSA contains a free SH group which leads to dimer formation at high protein concentration[68]. BSA is responsible for metabolite transportation in the blood but also has found applications in food and cosmetic industries, as well as drug delivery. The use of BSA in food, drugs and cosmetic products requires a deep understanding of its interaction with surfactants to understand which transformations can occur during the production process. These interactions are also important to understand the effect of proteins on cleaning.

Many studies have focused on analysing interactions between BSA and common anionic (eg. sodium dodecyl sulphate, SDS), cationic (eg. dodecyl trimethyl ammonium bromide, DTAB) and non-ionic (eg. polyethylene 8 lauryl ether, $C_{12}EO8$) surfactants. These studies have been carried out using techniques such as light scattering (LS)[68], nuclear magnetic resonance (NMR)[69], fluorescence spectroscopy[70], small angle neutron scattering (SANS)[71] and circular dichroism[72]. Fluorescence spectroscopy, for instance, takes advantage of the intrinsic fluorescence of BSA due to the presence of two Tryptophan residues (Trp). If BSA is irradiated with light of wavelength 280nm (λ_{ecc}), a fluorescence signal can be collected that is related to the tryptophan residues. In the native state of the protein, the tryptophan residues are placed in a hydrophobic "pocket" in the BSA structure and the resulting BSA emission spectrum has a maximum at 345nm (λ_{max}), where the intensity is I_0. However, surfactants can interact with proteins to induce their denaturation, which changes the secondary and tertiary structure of the protein. The denaturation results in moving the tryptophan residues into a more hydrophilic environment, where they interact with water molecules. As a result, there is a quenching of

the BSA fluorescence that is detected by a lowering of the intensity (I) of the fluorescent spectrum and a shift of λ_{max} to a lower wavelength. The higher the surfactant concentration, the more pronounced the fluorescent quenching. By plotting the ratio $\frac{I_0}{I}$ versus surfactant concentration ([surf]), it is possible to fit the data using the Stern-Volmer equation, resulting in the determination of the Stern-Volmer constant for the process (K_{SV})[73]:

$$\frac{I_0}{I} = 1 + K_{SV}[\text{surf}] \tag{7}$$

The resulting fluorescence emission spectrum of the protein-surfactant mixture can be deconvoluted by convex constraint analysis (CAA)[70], unhiding the presence of different emitting species. In the case of SDS, the peaks associated to the BSA-SDS complex (λ_{max}=325nm) and of partially denatured BSA (λ_{max}=323nm) are highlighted by the deconvolution.

The interaction between surfactant (S) and protein (P) can be described with the following equilibrium:

$$\text{P} + n\text{S} \leftrightarrow \text{PS}_n \tag{8}$$

where n is the number of surfactant molecules that can bind to the protein. The equilibrium constant of the process is described by equation 9:

$$K = \frac{[\text{PS}]}{[\text{P}][\text{S}]^{\text{n}}}. \tag{9}$$

It is possible to produce surfactant-protein binding isotherms by mean of fluorescence spectroscopy.[72] If we consider a certain surfactant concentration $C_{\text{surfactant}}$, it is possible to calculate α, the fraction of protein that is bound to the surfactant at a specific concentration:

$$\alpha = \frac{I_c - I_{\text{free}}}{I_{\text{min}} - I_{\text{free}}} \tag{10}$$

where I_c is the fluorescence intensity of BSA at a surfactant concentration $C_{\text{surfactant}}$, I_{free} is the BSA fluorescence intensity in absence of surfactant and I_{min} is the fluorescence intensity of BSA at saturation.

If C_{BSA} is the initial concentration of protein, it is possible to calculate v, the average number of surfactant molecules bound to the protein[70]:

$$v = \alpha \times \frac{C_{surfactant}}{C_{BSA}} \qquad (11).$$

The adsorption isotherm is obtained by plotting α vs $C_{surfactant}$ and four different areas can be distinguished (Figure 6)[68,72,74]. The first part of the plot (A) refers to the stage of the interaction called specific binding. This occurs at low surfactant concentration and it causes a slow rise of the binding isotherm. In this phase, the electrostatic binding between the surfactant charged headgroups and the ionic amino acids of the protein takes place. Therefore, this area is not present in the binding isotherms for non-ionic surfactant. After the specific binding, the binding isotherm starts to increase. This behaviour is due to the hydrophobic interactions between the hydrophobic domains of the protein and the surfactant alkyl tail, which lead to a partial unfolding of the protein. This region, indicated as B in the graph, refers to the non-cooperative binding between protein and surfactant monomers and its extension depends on the protein and surfactant type as well as polymer concentration. At the end of the non-cooperative binding regime, the protein has been partially unfolded by the hydrophobic interactions with surfactants. As a result, new hydrophobic domains are exposed to the surfactants that are then binding the protein in these new sites. This stage, indicated as C in the graph, is defined as cooperative binding. Finally, saturation (D) occurs when all the available sites of the protein have been bound by the surfactant monomers. Therefore, the binding isotherm does not change anymore as a function of surfactant concentration.
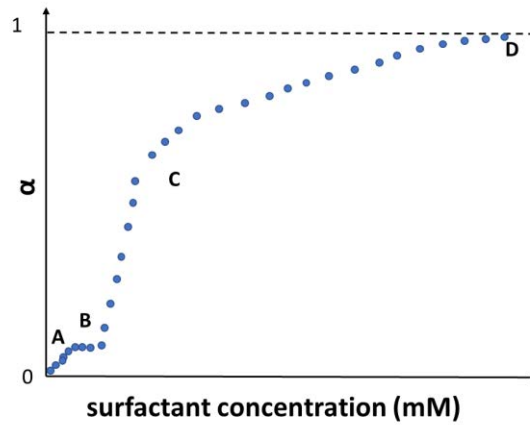
Figure 6 - Schematic representation of an adsorption isotherm between an ionic surfactant and a protein (e.g. BSA-SDS). Four different areas can be distinguished that are related to four different stages in the binding process: A) specific binding; B) non-cooperative binding; C) cooperative binding; D) saturation.

It is possible to assess if the surfactant-protein interaction involves a specific bonding region or not by the Scatchard plot. Considering a protein that has n binding sites and that link to a surfactant, present at a concentration C, with a binding constant equal to k, the mole of ligands r bound per mole of macromolecule is given by the following equation:

$$\frac{r}{C} = kn - kr \tag{12}.$$

The Scatchard plot ($\frac{r}{c}$ vs C) presents only a straight line if the binding is noncooperative, while a double trend in the plot, corresponding to the two type of binding sites, is observed in the case of cooperative binding.

The binding isotherms have been drawn for some of the most common surfactants (SDS, CTAB, C12EO etc) and the comparison between surfactant belonging to the same class has led to the conclusion that the binding isotherms trend depend on the surfactant charge. Surfactants with similar charge have similar binding isotherms and they bind the protein in similar way. For the same reason, binding of ionic surfactants is strongly influenced by pH, as demonstrated by Gelamo[70,73]. Changes in the pH results in varying the number of charged sites of the protein and, therefore, the number of available sites for specific binding.

1.7 Thesis outline

The work carried out and presented in this thesis is an overview of the efficiency of deposition of different classes of SRPs on cotton and polyester. The deposition data have bene correlated to stain removal and protein release/repellence data measured on SRPs-modified fabric. The interactions between surfactants and main soil components have been investigated as an additional way to enhance cleaning of fabrics in the washing process. In Chapter 1, an overview of the literature behind SRPs-deposition on textile and on the mechanism behind deposition and removal of soil from fabric surface has been presented. In Chapter 2, a list of the techniques used in this thesis is presented, focusing on the reasons why each technique has been identified as the most suitable to analyse our system. In Chapter 3 and 4 of this thesis, the deposition and efficacy of two different classes of soil release polymers have been investigated. Polyester and cotton have been tested in this contest, as the two most used textile in garments, because of the different properties they have. The first class of SRPs, presented in Chapter 3, investigated is composed of polyethylene glycol/polyoxyethylene terephthalate (PEG-POET) block copolymers and, among this class, two SRPs with similar molecular weight, but different charge, have been tested. The effect of charge of the SRP on the overall charge of the fabric has been assessed by means of streaming potential analysis. The use of UV/vis spectroscopy on SRP solution has enabled the indirect quantification of SRP deposition on polyester and cotton fabrics. In addition, a study of the kinetic of deposition as a function of pH, ionic strength and agitation has also been carried out. From the adsorption isotherms, information on the affinity of each SRP with the fabric has been deduced. Scanning electron microscopy (SEM) has been used to take image of modified fabrics, highlighting changes in fabrics roughness. Additionally, BET has been used to assess porosity of the fabrics in presence and in absence of the SRP film. Moreover, data have been collected via diffusion NMR to assess diffusion of water in the fabric structure when conditioned with SRPs as well as when no modification has been performed.

The second class of SRP, presented in Chapter 4, is composed of polyethylene glycol – 4 - methoxyethyl methacrylate/ methacryloyloxy ethyl trimethyl ammonium chloride (PEG-4-

MEMA/METAC) block copolymers and, for this class of polymers, the effect of the different ratio between the two blocks and different molecular weight has been evaluated.

For assessing the compatibility between the both classes of SRPs and the surfactants usually present in formulation, surface tension studies of surfactant-SRPs mixed system have been measured and results are shown at the end of Chapter 3 and 4. Insights on the formation of surfactant-polymer complexes and their adsorption at the air-water interface were collected.

In Chapter 5, an investigation of the effect of soil release polymer deposition on soil and protein release has been described. The removal of complex soil (sebum, lard, particulate soil) in the presence and absence of SRPs has been quantified via image analysis. Bovine serum albumin deposition and release has also been assessed via spectrophotometric assay and these data give insights on the use of the analysed SRPs as technologies for delivering anti-fouling benefits on fabrics via surface modification.

In Chapter 6 the mechanism behind the interaction of main surfactants used in formulation and main classes of soil have been investigated. First, the interaction between surfactant and the amylose helix have been analysed, as a possible rationale for surfactant depletion and cleaning inefficiency. Oil emulsion stability as a function of surfactant structure has been unravelled, as a necessary condition to fully remove the oil after that it has been released by the fabric surface. Finally, a screening of surfactant-protein interactions via fluorescence spectroscopy, mass spectrometry and surface tension has shown the importance of surfactant structure on the denaturing of bovine serum albumin, which has been used as model the protein in these studies.

Chapter 2. Experimental techniques

This thesis aims to achieve an understanding on the deposition of soil release polymers on cotton and polyester and on how surface modification via SRP deposition enhances soil removal from fabric surface. The choice of the analytical tool to investigate surface modification of fabrics via SRP deposition depends on the chemical and physical properties of the polymer as well as on the physical or chemical property of the surface under investigation. In this thesis, streaming potential was used to measure changes in zeta potential of the fabric when pre-treated with SRPs. The deposition of the polymer on fabric surface was confirmed via comparing the zeta potential of the SRP-treated fabrics to the zeta potential of the polymer in solution, measured via dynamic light scattering (DLS). However, changes in surface zeta potential had to be related to efficiency of deposition of SRPs on fabric. Therefore, the amount of SRP deposited onto fabrics was quantified via UV/vis spectroscopy or thermal gravimetric analysis (TGA), when polymers were not UV/vis active.

It was hypothesised that SRP deposition on fabrics had an impact on macroscopic properties of the surface, such as wettability, surface roughness and surface area. For this reason, contact angle measurements were used to assess changes in wettability of the fabric as a result of polymer deposition, whereas diffusion nuclear magnetic resonance (NMR) measurements were run to investigate changes in the restricted diffusion coefficient of water inside fabrics structure when SRPs were deposited onto the fabric surface. Instead, homogeneity of the deposition and changes in surface roughness and surface area were investigated via Scanning Electron Microscopy (SEM) and Brunauer–Emmett–Teller (BET) methods. SRPs, when present on the surface of fabrics during the wash, mainly interact with surfactants present in the laundry detergent and with components of soil that are present on fabric surface. Therefore, the interactions between SRPs and main classes of surfactants and common stains and soil components were studied. Surface tension measurements were used as a tool to investigate which surfactant classes interact the most with SRPs. Instead, image analysis and UV/vis spectroscopy were used to evaluate removal of an oily stain from fabric as well as removal and deposition of protein onto

fabric surface when SRPs were efficiently deposited. Eventually, interactions between surfactants and the main components of soil (starch, carbohydrates and proteins) were investigated, as these interactions have an effect on soil removal from fabrics. The choice of the analytical tools to investigate these interactions depends on the types of surfactants analysed, as well as on the parameters related to the interactions that have an impact on cleaning. Mass spectrometry (MS) analysis and surface tension measurements were carried out to study interactions between surfactant and starch or BSA and determine how much of the surfactant is involved in the interaction with these soil components, as this has an impact on cleaning efficiency. The effect of surfactant structure and concentration on denaturing of BSA was studied via fluorescence spectroscopy and compared to the results obtained via MS. Instead, the Turbiscan was used to assess emulsion stability as a function of surfactant structure, as higher emulsion stability leads to better cleaning.

2.1 Streaming potential

Streaming Potential is a technique that measures the zeta potential of flat and porous substrates. The zeta potential of a substrate is affected by any active deposited on the surface. Therefore, streaming potential can be used to confirm and monitor deposition of compounds (e.g. polymer) on a surface as function of time, pH and other parameters of deposition.

When a solid substrate is placed in contact with an electrolyte solution, a solid-liquid interface is generated. The solid substrate develops a surface charge due to the dissociation of acid or basic groups present on the surface (eg. sulfonate groups $-SO_3^-$; ammonium groups $-NH_3^+$) or because of the adsorption of hydroxide ions (OH^-) or hydronium ions (H^+). As a consequence, an electrochemical double layer (EDL, Figure 7) is generated in agreement with the Stern model[75].
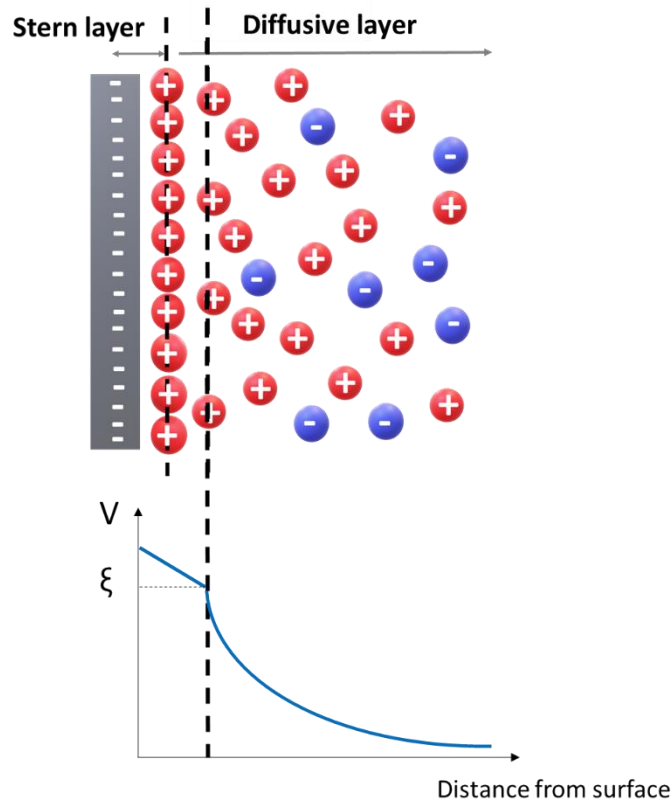
Figure 7- Stern electrochemical double layer at a solid-liquid interface (on the top) and resulting distribution of the potential in solution (on the bottom).

According to this model, the charge developed on the surface of the substrate induces a counterion distribution in bulk. It is possible to distinguish an inner plane or Stern layer, where counterions are so densely distributed that they are not free to move, and a diffuse layer, where counterions are free to move and they progressively reach the ion distribution typical of the bulk. The electric surface potential at the solid-liquid face is a quantity that cannot be experimentally measured. However, it is possible to evaluate a parameter that is strictly related to the surface charge of the sample and which is usually used as an approximation of the surface potential. This parameter, called zeta or electro kinetic potential (ξ), is the electric potential at the slipping plane, which is the plane close to the solid surface and within which the liquid is stationary. In the case of solid substrate, the zeta potential is usually measured via streaming potential analysis[76–79] and the scheme of a sample cell is shown in picture 8 (the case of a flat surface is shown for simplicity).
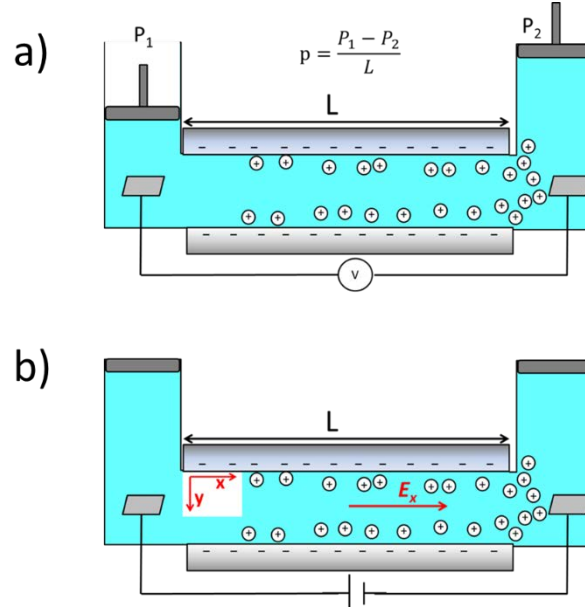
Figure 8 - Schematic representation of the electrokinetic phenomena occurring in the streaming potential channel. In Figure a, the hydraulic pressure is applied at the edge of the channel, causing a flow of the electrolyte solution. The counter ions are asymmetrically distributed in the channel as a result. When the hydraulic pressure stops (b), a streaming current starts flowing and the difference in electric potential is measured at the two electrodes at the edges of the channel.

The channel contains an electrolyte (usually KCl 1mM) which is in contact with the surface to analyse. Initially, a hydraulic pressure ΔP is applied at the edges of the channel and this causes a movement of the electrolyte ions in the same directions of the flow generated by the mechanical force. As a result, an asymmetric distribution of the counter ions in the channel is achieved which generates a potential difference inside the channel (Figure 8a). After the hydraulic pressure application, the ions tend to go back to an equilibrium distribution in the channel, generating a back current (Figure 8b). This back current is called streaming current (I_{str}) and it is influenced by the charge accumulated on the sample in contact with the electrolyte. The streaming potential current is related to the zeta potential of the sample via the Helmholtz-Smoluchowski equation:

$$\xi = \frac{dI_{str}}{d\Delta P} \times \frac{\eta}{\varepsilon \varepsilon_0} \times \frac{L}{A} \qquad (13)$$

where η is the viscosity of the solution, ε_0 is the vacuum permittivity, ε is the relative dielectric constant of the solution, and *L* and *A* are the area and the length of the streaming channel. Applying the Ohm law, according to which $I_{str} = U_{str}/R$, equation 13 could be rearranged as follows:

$$\xi = \frac{dU_{str}}{d\Delta P} \times \frac{\eta}{\varepsilon\varepsilon_0} \times \frac{L}{AR} \qquad (14).$$

In the case of fabrics, there is no information about the geometry of the samples, therefore the variables A and L are unknown. In this case, a new variable called electrical conductivity is introduced, which is defined as:

$$k = \frac{L}{R\,A} \qquad (15)$$

and the Helmholtz-Smoluchowski could be rewritten as:

$$\xi = \frac{dU_{str}}{d\Delta P} \times \frac{\eta}{\varepsilon\varepsilon_0} \times \frac{1}{k} \qquad (16).$$

2.2 Dynamic Light scattering

Dynamic light scattering (DLS) is one of the most used technique to determine particle size distribution and zeta potential in solution and it relies on Brownian motion. Comparing the zeta potential of a polymer in solution to the zeta potential of a surface immersed in a solution of the same polymer can give information on whether the polymer has deposited on the surface. DLS uses how light is scattered by particles and how light scattering changes as molecules diffuse. Particles in a solution experience collisions with solvent molecules. These collisions lead to a random motion of the particles where small particles move faster than bigger ones. The relationship between the speed of the particle, expressed as diffusion coefficient of the particle (D), and its size, expressed as hydrodynamic radius, is given by the Stokes-Einstein equation:

$$D = \frac{k_B T}{6\pi\eta R_h} \qquad (17)$$

where k_B is the Boltzmann's constant, T is the temperature and η is the viscosity of the solution[80].

If a light beam illuminates the sample, the photon interacts with the moving particles and, as a consequence of the elastic light scattering, they will be scattered in any directions. The detector is hit by the light scattered by each of the particles present in the sample, where the resulting scattered intensity is the sum of the intensities hitting the detector at a certain time t. As a result, the scattered

intensity pattern, at a time *t*, consists of dark and bright areas, because the interaction between intensities could be constructive (if intensities hit the detector with the same phase) or destructive (if the intensities have opposite phases when they hit the detector). However, as the particles move in the sample, the dark and bright areas in the scattered intensity pattern are also constantly moving and there is an intensity fluctuation across time[81]. The fluctuation depends on particle size, as a slow fluctuation of the scattered intensity I_s occurs when big slow particles are measured, whereas small particles cause fast changes in the intensity (Figure 9a). If we consider a certain point of the detector and we compare the intensity hitting the detector at a time *t=0* and at a time *t=δt,* the two intensities have a good correlation for very small *δt*, whereas this correlation decreases and tends to become 0 for long *δt*. If *θ* is the angle between the direction of incident light and the direction of the scattered light, the variable called scattering vector q is introduced, which is a function of the wavelength of the light (*λ*) and of the refractive index of the solvent (η_s), as shown in equation 18:

$$q = \frac{4\pi\eta_s}{\lambda} sin\left(\frac{\theta}{2}\right) \tag{18}$$

The normalised autocorrelation function $g^2(q, δt)$ is given by the Siegert equation[82,83] 19:

$$g^2(q, \delta t) = \frac{<I_s(q,0)\ I_s(q,\delta t)>}{<I_s(q,0)^2>} = |g^1(q, \delta t)| + 1 \tag{19}$$

where $g^1(q, δt)$ is the correlation function of the scattered light. The $g^2(q, δt)$ trend across time is shown in picture 9b.
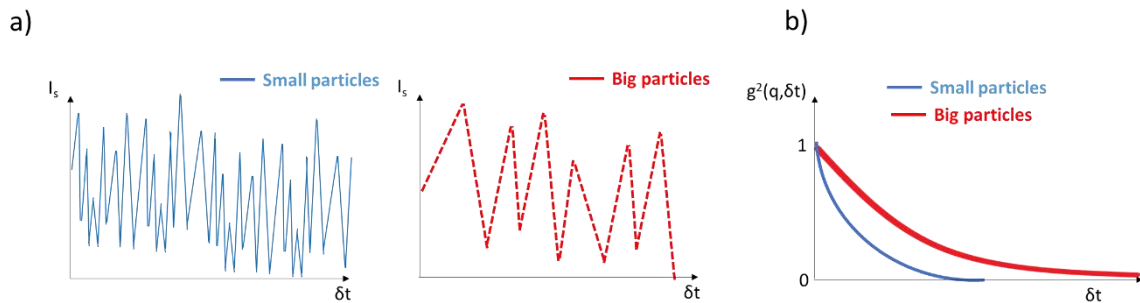
Figure 9 – a) Scheme of scattered intensities fluctuation across time for samples containing small or big particles; b) autocorrelation function in the case of small particles or big particles.

Each sample may be composed of particles with different sizes, where each particle experiences a different decay rate depending on its size. For each particle, a decay constant Γ is calculated, which is related to the diffusion coefficient by the following relationship:

$$\Gamma = Dq^2 \tag{20}$$

Therefore, the correlation function of the scattered light could be rewritten as:

$$g^1(q,\delta t)=\sum_{i=1}^{n}(c_i e^{-\Gamma\delta t}) \tag{21}$$

being c_i the normalised scattered intensity for the i particle. The decay factors are then obtained by applying the Laplace inverse transformation to equation 21 and the diffusion coefficients and the hydrodynamic radius of the particles are then calculated. As a result, the size distribution of the analysed sample is plotted. The most used distribution type is the size distribution by number, in which the area associated to each R_h is proportional to the number of particles with that specific R_h.

An important parameter to assess, in addition to particle size distribution, is the zeta potential of particles in solution. A charged particle in solution induces the EDL formation, as previously described for hard surfaces in streaming potential (section 2.1) and, therefore, the particle is characterized by a zeta potential. The zeta potential is an important parameter to the determine for particle stability, as the particles are stable only if their zeta potential is more positive than +30 mV or more negative than –30 mV. The zeta potential measurement of these type of systems is based on the analysis of electro-kinetic phenomena. If an electric field is applied at the edges of the solution, electrophoresis occurs and particles in the solution start moving in the direction of the electrode with opposite charge. However, viscous forces tend to oppose to the movement of particles in solution. When an equilibrium between the electrophoresis and the viscous forces is achieved, particle moves with a constant velocity, called electrophoretic mobility (μ_E), which is a function of the viscosity (η) and the dielectric constant (ε) of the solution, of the applied electric field and of the zeta potential of the particles. This electrophoretic mobility is related to the zeta potential of the particles (z) by the Henry equation:

$$\mu_E = \frac{2\, \varepsilon\, z\, f(k\alpha)}{3\eta} \tag{22}$$

where $f(k\alpha)$ is the Henry's constant that is equal to 1.5 in the case of moderate electrolyte concentration (Smoluchowsky approximation)[84] or 1 in the case of low electrolyte concentration (Huckel approximations)[84]. Zeta potential of particles in solution can be calculated from the electrophoretic mobility, measured via light scattering.

Light scattering can be used to detect the zeta potential of particles in solution by Laser Droplet Velocimetry (LDV) and M3-Phase Analysis Light scattering (PALS) analysis[85]. LDV combines the light scattered at 17° by colloidal particles in solution with the intensity of the incident beam. The resulting electromagnetic field hits the detector with a certain frequency and the rate of fluctuation of the hitting intensity is related to the particle velocity[85]. However, in the case of light scattering, the sample is usually loaded in a folded capillary tube, therefore the electroosmotic flow has to be considered. The electroosmosis is related to the motion of a liquid relative to a stationary surface, which is charged, when applying an electric field parallel to the surface. The electric field, applied to generate the electrophoretic flow of the colloidal particles in the capillary, results in an electroosmotic flow of the particles close to the wall that is compensated by a reverse flow in the centre of the capillary. The flow is stationary at the centre of the capillary, where the electroosmotic flow and the reverse flow have the same value and, therefore, their sum is equal to 0. Particles at the stationary layer are only subjected to the electrophoretic flow. Therefore, LDV measurements are performed in this area, which means that a good alignment of the cell is required to measure the electrophoretic mobility in absence of the electroosmotic contribution. A more recent approach uses the M3-PALS to measure the particle velocity at any point of the capillary and extrapolate only the electrophoretic mobility. According to this approach, two different reverse field are applied to the colloidal solution we are analysing. Initially, a slow field reversal mode (SFR) is applied to reduce the polarisation of the electrodes, reversing the field every 1 second. After this, a fast field reversal mode is applied (FFR), where the field direction is inverted after less than one second. In the FFR condition, the change in the electric field direction is so

fast that there is not enough time for the electroosmotic flow to develop. In this regime, a PALS measurement is performed, where the phase of the incident light and of the light scattered by the moving particles is compared. Both the light beams have the same phase but they experience a shift that is related to the velocity of the particle. The measured phase change is proportional to the change in the position of the particles. Therefore, the particle velocity (v_P) could be calculated via analysis of the phase (φ) plot against time, using equation 23:

$$\frac{d\varphi}{dt} = qv_P = qE\mu_P \qquad (23),$$

where E is the applied electric field, q is the scattering vector and μ_P is the particle mobility[86]. The particle zeta potential can be calculated by particle mobility, using equation 22.

2. 3 Ultraviolet-visible spectroscopy (UV/vis)

Ultraviolet visible spectroscopy (UV/vis) was used to indirectly assess the amount of soil release polymers deposited on fabrics at different concentration and in different conditions.[87] Moreover, the decrease of the absorbance of SRPs solution across time was used to track the kinetic of deposition of the polymers across time at different pH, agitation time and water hardness. An advantage of this approach is related to having no need of fluorescent tagging, which could have consequences on the efficiency and on the mechanism of deposition of the actives on fabrics. However, many other actives used in laundry detergents absorb in the UV region, e.g. brighteners. Therefore, this technique is generally used to assess deposition of SRPs in absence of detergents and other actives or in combination with actives that are not UV/vis active.

When incident radiation in the UV/vis range of the electromagnetic resonance (EMR) spectrum interacts with a molecule, the energy of the photons is absorbed and electrons present in the molecule are exited from the ground, or low electronic energy level, to empty, higher energy levels. The group of atoms that causes the adsorption of UV/vis radiation is called a chromophore and a compound is UV/vis active if it contains pi-electrons or non-bonding electrons[88]. Indeed, the transition between two

electronic states concerns non-bounding electrons or electrons involved in the π bond formation which are excited from a bonding orbital to an anti-bonding orbital. The transition only occurs if the energy of the photon absorbed is equal to the energy difference between the two electronic states (ΔE). The relationship between the ΔE between the electronic states and wavelength (λ) or frequency (v) of the electromagnetic radiation is expressed by equation 24:

$$\Delta E = h * v = \frac{hc}{\lambda} \tag{24}$$

where c is the speed of light in vacuum conditions and h is the Planck's constant.

Therefore, the specific wavelength absorbed by a molecule gives us information about the energy levels present in the molecule and about molecular structure. The intensity of light adsorbed is proportional to the concentration of an analysed substance, according to the Lambert-Beer law:

$$A = \varepsilon \, l \, C \tag{25}$$

where A is the absorbance at the wavelength of interest, ε is the molar extinction coefficient of the sample, l is the optical path of the incident light inside the solution and C is the molar concentration of the analyte.

The SRPs based on PEG-POET block copolymers, studied in this thesis, are UV/vis active due to the presence of conjugated double bounds in the terephthalate units and their maximum of adsorption is close to 240 nm. For this reason, UV/vis spectroscopy was used to measure decrease in absorbance, and therefore in concentration, of the SRPs and to indirectly assess the amount of SRPs deposited onto fabrics.

2.4 Thermal gravimetric analysis

Thermal gravimetric analysis (TGA) was used to assess amount of SRPs deposited onto polyester in the case of SRPs that were not UV/vis active. TGA is a useful technique to assess the effect of temperature on the mass of solid or liquid samples and gain information about their chemical composition and their resistance to heat. This is achieved using a high precision balance, which

measures the change in mass of a sample when the temperature is increased. Heating of the sample occurs in a controlled atmosphere, that usually contains a non-reactive gas (eg. nitrogen[89]). However, it is quite common to perform thermal gravimetric analysis also in presence of air or oxygen[90,91], so that the pyrolysis of the sample occurs and the carbon content in the sample is quantified. For instance, TGA is usually used to assess fabric's resistance to fire when a flame retardant coating is applied[90,92].

In our work, we used TGA to indirectly quantify the mass of non-UV/vis active SRPs deposited on our polyester, where the mass lost at the melting temperature of the polymeric film was an indicator of the mass of SRPs previously deposited. For this purpose, the analyses were performed on untreated and SRP-modified polyester and the thermograms of the samples were compared.
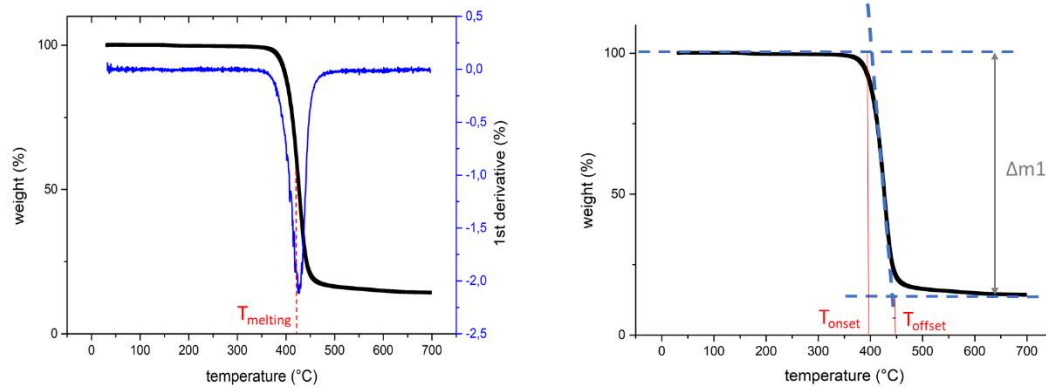
Figure 10 – Thermogram and its 1st derivative plotted for a sample of untreated polyester analysed in TGA. The thermal degradation has been done using a temperature ramp between 30 and 700 °C and a heating speed of 10 °C/min. The furnace has been filled with air

In TGA, the sample is typically placed in a platinum pan, after being cut into small pieces to maximize its surface area. The initial mass of the sample is recorded, and a thermal ramp is applied. The thermogram, obtained by plotting the percentage of mass decrease as a function of temperature, (Figure 10, black curve), has a S shape which is typical of single melting-point material. When the onset temperature is reached (T_{onset}), the material starts melting and its mass start decreasing. When the temperature reaches the offset value (T_{offset}), the process comes to an end and the amount of material that experienced thermal degradation is evaluated by the difference in mass % between the T_{offset} and the T_{onset}. The melting point ($T_{melting}$) is defined as the point with the greatest mass change in the

thermogram and it is usually given by the minimum in the first derivative of the thermogram (Figure 10, blue).

2.5 Scanning Electron Microscopy

Scanning Electron Microscopy (SEM) was used for imaging polyester before and after SRPs deposition and to estimate changes in surface roughness as a result of surface modification . In this technique, a primary electron beam is emitted by a tungsten filament, then it is accelerated by a series of condenser lenses and focused on the area of interest. The interaction between the electrons of the primary electron beam and the outer atoms of the surface leads to different phenomena, such as emission of X-rays and secondary electrons (SE). In the case of SEM, the secondary electron beam produced by inelastic scattering is focused by lenses and sent to the detector. The secondary electrons contain information about surface topography and they are used to reconstruct the image of the surface[93]. This is achieved by scanning the area of interest with the primary electron beam and encoding the information related to the secondary electron beam for each position of the sample. The spatial resolution of SEM could go down to 1 nm. If the sample is not conductive, a layer of metal ions is deposited on the surface of the sample to render the sample conductive and avoid artefacts in the images due to charging phenomena[94]. The sample metalization is achieved by depositing a thin layer of a metal (palladium, gold, chromium) or a conductive compund (osmium tetraoxide) . The initial layer avoids accumulation of an excess of charge on the substrate that can affect secondary electron emission.

A series of mathematical algorithms can be used to evaluate a roughness index associated to the SEM image, usually expressed as root mean square roughness (R_q), which is calculated as follow[95]:

$$R_q = \sqrt{\frac{1}{PQ}\sum_{i=1}^{P}\sum_{j=1}^{Q} z_{ij}^2} \qquad (26)$$

where P and Q are the number of pixels along the x and y directions and z_{ij} is the surface height for a specific point that is defined by the coordinate i and j in the picture. Moreover, the fast Fourier transform (FFT) can be applied to the images to provide information about spatial periodicity in the polymer deposition.

2.6 Contact angle measurements

The wettability of a surface is usually determined via contact angle measurements. When a drop of a liquid is dispensed on a substrate at a certain pressure and temperature, the liquid sits on the substrate with a specific contact angle that depends on surface roughness and wettability. The observed contact angle is the result of a balance between the surface tension at the liquid-solid interface (γ_{ls}), at the solid-gas interface (γ_{gs}) and at the liquid-gas interface (γ_{lg}), as shown in Figure 11 and in the Young equation:

$$\gamma_{gs} = \gamma_{ls} + \gamma_{lg} \cos \theta \qquad (27)$$
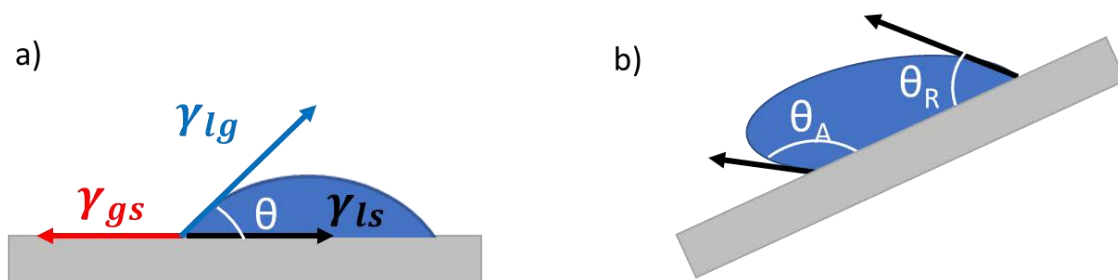
Figure 11 – Diagram of a liquid drop on a surface: γ_{ls} is the liquid-solid surface tension, γ_{gs} is the gas-solid surface tension, γ_{lg} is the liquid-gas surface tension and θ is the contact angle.

Contact angle of water on polyester before and after deposition of SRPs was measured to assess changes in surface wettability when SRPs are present. A substrate is defined as being hydrophilic if the contact angle of water is lower than 90°, while hydrophobic substrates have contact angles that are greater than 90°. For instance, a substrate is fully wetted by a liquid if the contact angle of the liquid on the substrate is equal to 0°. Moreover, the contact angle between a liquid and a solid is a dynamic quantity, where several contact angles may form as a consequence of motion impressed to the air-liquid-solid bounday or changes in the interficial forces[96]. If the sample is tilted, or if the liquid volume of the droplet deposited on the substrate is changed, dynamic contact angle is measured. The contact angle hysteresis is defined as the difference between the greatest (advancing contact angle) and the lowest contact angle (receding contact angle) that the liquid forms on a substrate. In any case, an equilibrium contact angle

could be calculated by measuring advancing (θ_A) and receding contact angle (θ_R) via volume changing method or sample tilting.

2.7 Diffusion Nuclear magnetic resonance

Nuclear magnetic resonance (NMR) is a technique which requires the presence of atoms that have a spin quantum number I which is not zero. The spin quantum number depends on the number of unpaired nucleons present in the atom, where each unpaired nucleons contributes a value of +1/2 to I.

NMR active nuclei have 2I+1 spin states[97], when in a static magnetic field, and in the case of ^{1}H, where $I = 1/2$, there are two possible spin states: $m_s = +1/2$ (α) and $m_s = -1/2$ (β). The nucleus is characterized by a magnetic momentum μ which is related to the spin quantum number by the equation 21:

$$\mu = \gamma I \tag{28}$$

where γ is the gyromagnetic ratio[97]. If a magnetic field $\boldsymbol{B_0}$ is applied, the magnetic momentum μ aligns to the direction of the magnetic field $\boldsymbol{B_0}$ and it processes around it. The frequency at which the spin precesses is called Larmor frequency ω_0 [88,98] and is defined as:

$$\omega_0 = -\gamma B_0 \tag{29}.$$

In the absence of a magnetic field, these spin states are degenerate. When $\boldsymbol{B_0}$ is applied, the two spin states are no longer degenerate:

$$E_m = -\frac{h}{2\pi}\gamma m B_0 \tag{30},$$

where h is the Plank's constant. The energy difference between the two spin states is given by:

$$\Delta E = \frac{h\gamma B_0}{2\pi} \tag{31}.$$

The population of spin states is described by the Boltzmann distribution:

$$\frac{N_\alpha}{N_\beta} = e^{-\frac{\Delta E}{k_B T}} \tag{32}$$

where k_B is Boltmann's constant and T is temperature [88,98]. There is an excess of nuclei in the lower spin state α and the difference in spin population produces a net magnetisation vector, defined as $M_0 = \sum \mu_i$ (Figure 12). This vector is aligned with the direction of the applied magnetic field, normally the z direction, and there is no detectable NMR signal[97].
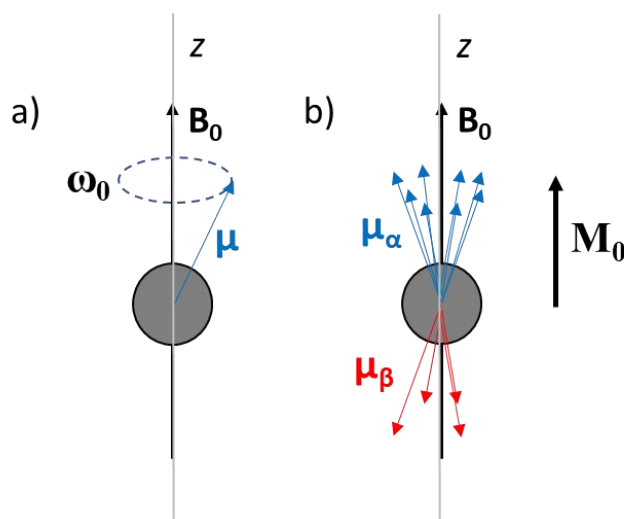
Figure 12– a) Scheme of the spin precession of a nucleus with magnetic momentum μ; b) distribution of different nucleus in the two spin state (α and β) and bulk magnetization M_0.

When radiofrequency energy is applied to the system, the magnetisation is moved into the *x-y* plane, resulting in the population in α and β being the same, and the NMR signal is maximum. All the nuclei in the *xy* plane are precessing, and the rotating magnetic moment, produces an electric field. This changing electric field is detected by an RF coil as the NMR signal. After the RF pulse is applied, the magnetisation begins to return to an equilibrium state, by processes known as relaxation. During relaxation, spins in the transverse plane return to thermal equilibrium and a decay of the NMR signal detected in the transverse plane across time occurs, which is called free-induction decay (FID). The spin relaxes can be described by two relaxation time: spin-lattice relaxation time (T_1) and spin-spin relaxation time (T_2). T_1 relaxation time is the time that spins require to go back to the Boltzmann distribution in the α and β levels. T_2 relaxation time is the time that spins take to de-phase when they are in the transverse plane.

The application of a Fourier transform to the FID produces an NMR spectrum of the analysed sample.

In this thesis, NMR was used because it enables to measure the self-diffusion coefficient of molecules at thermal equilibrium. This is achieved by applying a pair of pulsed magnetic field gradients (PFG) during the RF sequence. Each applied gradient varies the magnetic field across the sample, resulting in nuclei having different processional frequencies ω(r) in different parts of the sample. If G is the magnetic field gradient strength, the processional frequency is given by:

$$\omega(r) = \gamma B_0 + \gamma G r \tag{33}.$$

This information can be used to spatially encode where the nuclei are within the sample. If Δ is the observation time, the root square of the displacement of the molecules is related to the diffusion coefficient D by the following equation[99]:

$$d = \sqrt{2D\Delta} \tag{34}.$$

The diffusion coefficients for molecules can be calculated by measuring how the attenuation of the NMR signal changes as a function of observation times via diffusion NMR experiment.
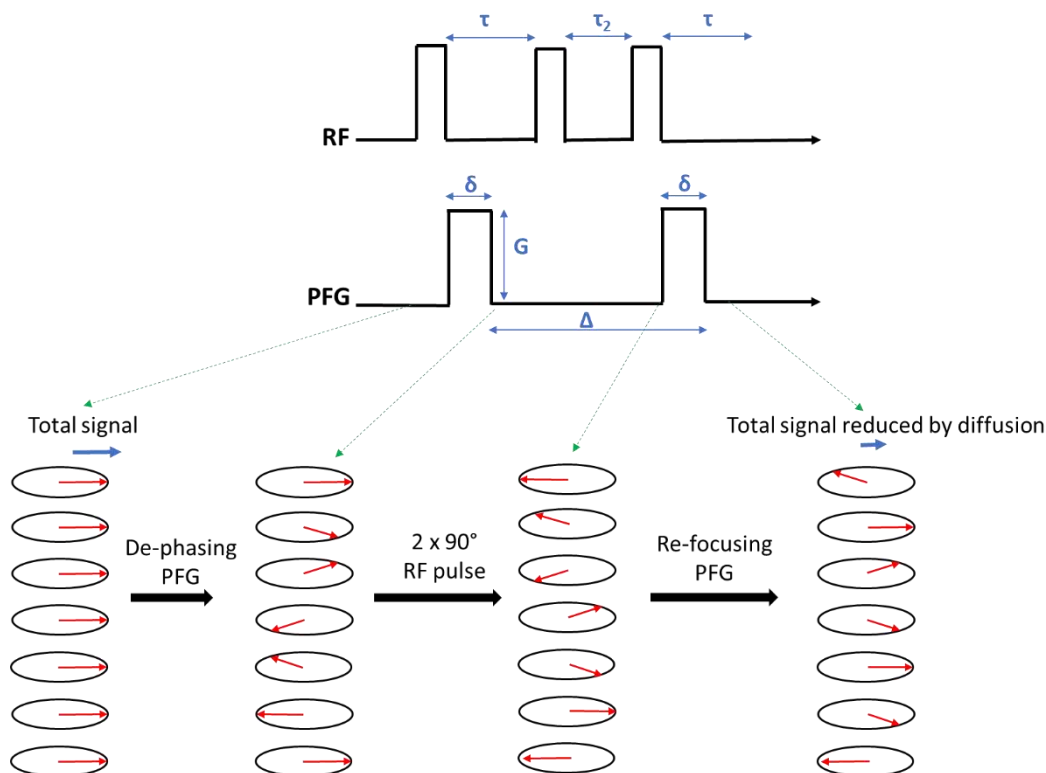
Figure 13 – On the top, sequence of RF pulse and pulsed field gradient applied to the sample in a Pulsed Gradient Stimulated Echo experiment. On the bottom, the spatial encoding of spins as a consequence of pulsed field gradient application and diffusion.

Diffusion NMR experiments are run by applying either a Pulsed Gradient Spin Echo (PGSE) or a Pulsed Gradient Stimulated Echo (PGSTE) sequence. A schematic of RF and PFG application in the case of PGSTE sequence is shown in Figure 13. This pulse sequence uses three 90° RF pulses. When the first RF pulse, M_0 is moved from the z axis into the *x-y* plane. Following the RF pulse, a magnetic field gradient is applied, called dephasing gradient. A second 90° RF pulse is applied after a time τ following the first RF pulse. The second RF pulse returns M_0 to the z axis, where it processes for a time τ_2, called the mixing time (TM). During this time, the magnetisation does not experience any T_2 relaxation. After this time, a third RF pulse is applied, followed by the second PFG, and M_0 is in the *x-y* plane. If no diffusion has occurred, between the application of the two gradient pulses, a full refocussing of the spins occurs. However, if molecular diffusion has occurred only a partial refocusing occurs and therefore there is a decrease in the NMR signal.

In a diffusion NMR experiment, several experiments are run by incrementing the pulsed magnetic field gradient strength G. The signal attenuation is plotted against the magnetic gradient field strength and a signal attenuation curve is obtained, which can be fitted by the Stejskal-Tanner equation[100] to obtain the diffusion coefficient:

$$\frac{S(G)}{S(0)} = e^{-\gamma^2 \delta^2 G^2 D \left(\Delta - \frac{\delta}{3}\right)} \tag{35}$$

It is possible that molecules are present within multiple environments. In this condition, the molecule exhibits different diffusion coefficients which all contribute to the signal attenuation. Therefore, signal attenuation curve cannot be fitted by a mono-exponential Stejskal-Tanner curve and a modification in equation 35 is needed. In the case of two different diffusion coefficients (D_1, D_2) exhibited within the sample, the Stejskal-Tanner relationship can be rewritten as follow[100]:

$$\frac{S(G)}{S(0)} = x e^{-\gamma^2 \delta^2 G^2 D_1 \left(\Delta - \frac{\delta}{3}\right)} + (1 - x) e^{-\gamma^2 \delta^2 G^2 D_2 \left(\Delta - \frac{\delta}{3}\right)} \tag{36}$$

2.8 Surface area, pore size and pore size distribution analysis

The diffusion of water inside porous substrates is related to the porosity of the substrate investigated. In this thesis, the diffusion coefficients of water inside polyester fabrics before and after SRPs deposition were correlated to surface area data collected for the same fabrics via Brunauer–Emmett–Teller (BET) methods. BET is a technique that enable the determination of surface area of porous materials, as well as pore size distribution, pore radius and volume. It is based on physical absorption of an inert gas on the surface of the sample analysed, where the mass of gas absorbed as a function of the pressure in the sample tube is measured.

The physical absorption of a gas onto a solid surface follows four different stages, dictated by the increase in gas pressure[101]. During stage I, at low gas pressures, only a few gas molecules are present, which are absorbed on the sample surface. At stage II, a gas monolayer is formed on the sample surface, as a consequence of the increased gas pressure. Further increase in the gas pressure leads to a thicker

gas layer adsorbed on the surface of the sample and the gas starts filling the pores, where the small pores are filled first (stage III). Knowing the gas pressure at which the pores filling occurs, enables an estimation of the pores size distribution and pores volume. During stage IV, saturation of the surface occurs, where mesopores and macropores are fully filled by gas. A desorption cycle is then performed on the samples, by decreasing the gas pressure across time. At this stage, an adsorption isotherm is obtained, where the volume of adsorbed gas against gas partial pressure (ratio between gas pressure and saturation pressure) is plotted. The isotherm is fitted to different models to determine pore volume, pore size and size distribution, verifying if the material is microporous (0.2-2 nm), mesoporous (2-50 nm) or macroporous (> 50 nm).

There are six different type of adsorption isotherms[102], as shown in Figure 14. Type I isotherm is known as the Langmuir isotherm and it is usually obtained for microporous materials, where the gas forms a monolayer and the absorbed volume reaches a plateau due to the inaccessibility of the smaller micropores. If the material is non-porous or nano-porous, multilayer formation is possible, and the equivalent absorption isotherm follows the Langmuir-Freundlich equation (type II). However, if the multilayer formation does not involve the formation of a preliminary monolayer, and a random clusterization of the gas molecules occurs due to weak adsorbent-adsorbate interaction, the isotherm is called Brunauer-Emmett-Teller (BET, type III). If molecular clusterization is followed by pore filling, type V adsorption isotherms are obtained. The gas adsorption on mesoporous materials follows type IV isotherms, where the multilayer formation is followed by gas condensation. Instead, type VI refers to non-porous material that experience multilayer formation. Therefore, fitting the experimental BET data to one of the following isotherms, an understanding of the sample porosity is achieved.
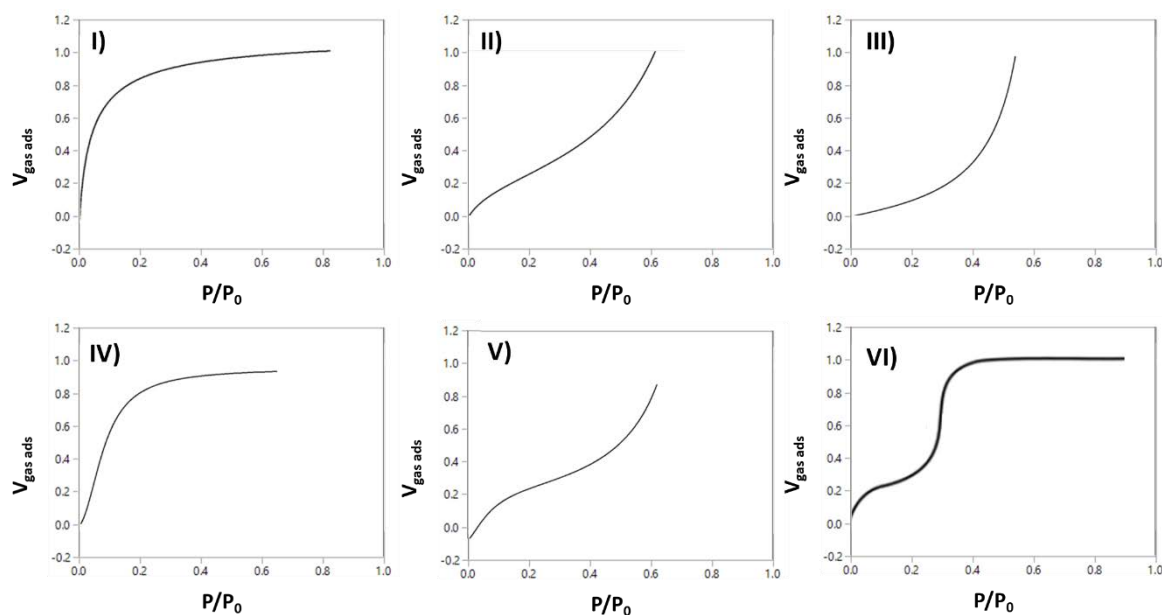
Figure 14 – Plots of adsorption isotherms type according to IUPAC classification[102]

2.9 Surface tension measurements

Surface tension measurements give information about which molecules are placed at the air/ water interface and they can be used to understand interactions between molecules present in solution, as in the case of surfactant-polymer interactions investigated in this thesis. When considering the molecules that are present in bulk in a certain phase, each molecule is surrounded by molecules of the same type. The molecules attract each other with an attraction force (called cohesion force, blue arrow in Figure 15) that has the same strength for each pair of molecules considered. As these cohesion forces are acting on the bulk molecule in all directions, the resulting force acting on the single molecule is zero. However, when considering a molecule placed at the interface with a second phase (eg. air-liquid), this molecule is subjected to cohesion forces with molecule of the same type only on one of its side. At the same time, a second type of forces, called adhesion forces (green arrow in Figure 15), is experienced with molecules belonging to the second phase. The adhesion forces are always weaker than cohesion forces, therefore, the molecule at the interface experience a resulting force that tend to drag the molecules in bulk. As a result, work has to be done against this force to bring the molecules at the interface with the second phase. The molecules in the system tend to arrange themselves in order to minimize the surface

51

area between the two phases and the work required to generate the interface. The surface tension is defined as the work W that is necessary to generate an increase ΔA of the interfacial area.

$$\gamma = \frac{W}{\Delta A} \tag{37}.$$
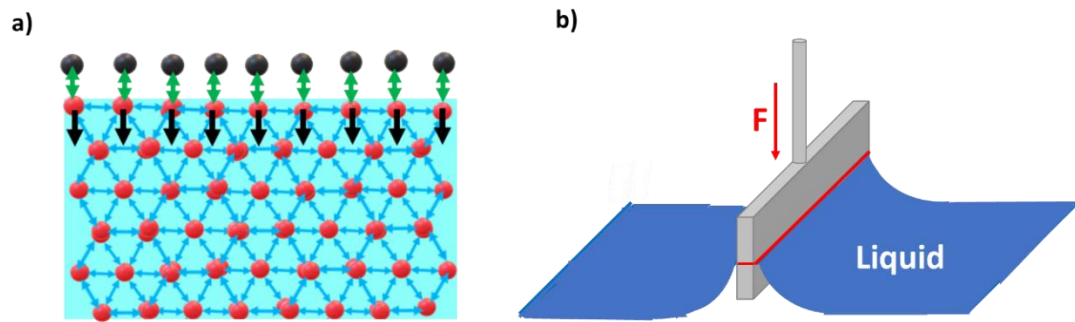
Figure 15 - a) Diagram of the adhesion forces (blue) and cohesion forces (green) acting on the molecules present in bulk and at the interface. b) Scheme of the Wilelmy method, where a platinum plate is immersed in a liquid and then extracted to measure the surface tension.

One of the main consequences of surface tension is the formation of water droplets. Water molecules experience very high cohesion forces due to hydrogen bonding, resulting in a very large value of surface tension (72 N/m at 25 °C). For this reason, water tends to achieve the minimum possible surface area when in contact with a different phase (eg. air) which correspond to the formation of a sphere.

The most used approach to measure surface tension for a liquid-air interface is the Wilhelmy method, which uses a plate of platinum-iridium that is dipped in the solution and then slowly extracted. This process brings to the formation of a liquid lamellae due to the wetting of the plate by the liquid. The plate is connected to a microbalance that measures the force, F, applied to the plate until the lamellae rapture. The measured force is related to the surface tension of the liquid via the following equation:

$$\gamma = \frac{F}{L \cos (\theta)} \tag{38}$$

where L is the wetted perimeter (equal to the perimeter of the plate) and θ is the contact angle. The choice of using a platinum-iridium plate is done to achieve full wetting of the plate by the liquid, so that $\cos(\theta)$ is equal to 1 and the equation is simplified.

Measuring the surface tension of a solution gives information about which molecules are placed at the air-water interface. In general, any solvent is characterized by a value of surface tension which is tabulated. In the case of solution, the surface tension value is different from the one measured for the solvent only if the solution contains surface active agents. For instance, this is the case of surfactant solutions. As explained in section 1.2.3, surfactants have high affinity to the air-water interface because of their amphiphilic structure. When placed at the air-water interface, they experience high cohesion forces with other surfactant molecules as well as high adhesion forces with the air molecules because of their hydrophobic tails. As a result, the resulting force acting on the surfactant molecule is weaker than the one experienced by water molecules and the energy requirement to keep the surfactant monomers at the air-water interface is lower. This reflects in a lower value of the surface tension in presence of surfactants. Moreover, surface tension could be used to understand interaction between surfactants and polymers. When the surface tension of pure surfactant solution is compared to the surface tension of the same surfactant in presence of a polymer (eg. SRPs, proteins or amylose) different scenarios can occur. If no interaction occurs between the polymer and the surfactant, the surface tension of the mixture is equal to the one of pure surfactant solution. If the polymer is surface active, both polymer and surfactant molecules are placed at the air/liquid interface and the surface tension is lower than the one measured for the surfactant solution. If an interaction is occurring between the surfactant and the polymer, there is a depletion of surfactant monomers at the air/liquid interface which reflects in an increase of the surface tension of the system.

2.10 Colour measurements for stain removal analysis

The efficiency of soil removal from textile are usually evaluated via colour change analysis and reflectance spectroscopy[18,19,28,103,104]. In most cases, a DigiEye digital image analyser (DigiEye plc,

Verivide, UK) is used instead of a simple spectrophotometer. This is because the DigiEye enables analysis of a wider area compared to a spectrophotometer and this minimize the error associated to the measurement, as different parts of the textile pattern are simultaneously analysed. The DigiEye is a lighted cabinet equipped with a Nikon digital camera that takes high quality and reproducible pictures of the stains. The system is set to use the D_{65} light which represents normal standardized day light conditions with a correlated colour temperature of 6500 K [105]. These conditions have been recognised as standard conditions by the Commission on Illumination (Commission Internationale de l'Eclairage, CIE)[106]. Pictures of the stains of interests are taken and the system uses these images to evaluate reflectance and colour of the stains and the output consist of colour coordinates that are in line with the *L*a*b** colour space, recognized as standard by the CIE. According to this, each image has a specific value of *L**, which is related to its lightness, of *a**, which gives information about the redness/greenness of the sample, and of *b**, which refers to the blue/yellow appearance of the stain. In our tests, the coordinates (L_i^*, a_i^*, b_i^*) were measured for the stains before (*i*=1) and after (*i*=2) laundering and analysed via DigiEye software 6.2. Differences in lightness (ΔLi^*), redness (Δai^*), and blueness (Δbi^*) for each stain in contrast to the background have been evaluated and the total difference was then calculated as:

$$\Delta E_{ab,i}^* = \sqrt{\Delta L_i^{*2} + \Delta a_i^{*2} + \Delta b_i^{*2}} \qquad (39).$$

The stain removal index is given by the following equation:

$$SRI(\%) = \left(\frac{\Delta E_1 - \Delta E_2}{\Delta E_1}\right) \times 100 \qquad (40).$$

2.11 Mass spectrometry

Mass spectrometry (MS) is a gas phase technique that lead to sample characterization via ionization and separation of the resulting ions according to their different mass-to-charge ratio (*m/z*). In general, mass spectrometers typically comprise the same key components which are an ion source, a mass analyser and a detector, where these could be different accordingly to the samples that needs to be analysed or to the resolution that needs to be achieved. One of the most common technique for

ionization used in MS is the ElectroSpray Ionization (ESI), where the liquid sample is vaporized and ionized before being transferred to a mass analyser. In an ESI interface, the liquid sample is forced through a capillary that has a very high potential applied and that is at atmospheric pressure. When a liquid is exposed to a high potential, the Taylor cone is formed[107] as a consequence of electrostatic repulsion between ions with the same charge (Figure 16). When the electrostatic repulsion becomes stronger than the liquid surface tension, an electrospray is formed and droplets containing analyte ions and solvent molecules are formed. These droplets are formed in the space between the capillary edge and the entrance of the spectrometer, where high vacuum is present. In this area, an inert gas as nitrogen (N_2) is flowing. As a result, solvent evaporation occurs and the droplets become smaller, with higher charge density. When the radius of the droplet reaches the Rayleigh limits[108], the repulsion between charged analytes in the droplets becomes too high and it leads to Coulombic fissions[109]. Smaller and smaller droplets form and they experience desolvation as before, until the Rayleigh breakup occurs again. The desolvation-Rayleigh breakup cycle repeats until a gas phase ion containing only one molecule of the analyte is formed. One of the main advantages of using ESI versus other ionization techniques (eg. Matrix Assisted Laser Desorption Ionization MALDI or Electron ionization EI) is that ESI belongs to the range of soft ionization techniques. Therefore, ESI is able to generate analyte ions without causing fragmentation of the analyte molecules. For this reason, it has found several applications in analysis of biological samples that usually experience fragmentation, as lipids and proteins. It is possible to distinguish ESI-(+) and ESI-(−) operation mode, where, accordingly to the potential applied to the capillary, positive or negative ions are generated respectively.
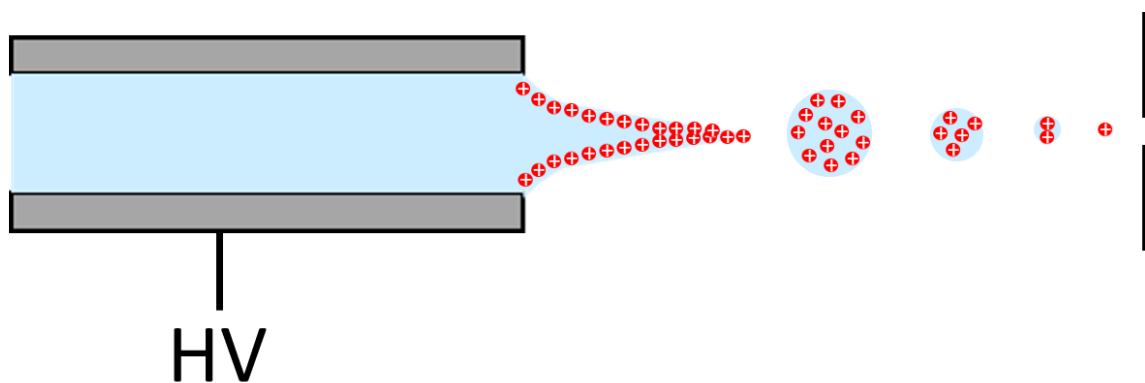
Figure 16 - Application of high voltage (HV) to the ESI capillary that contains the analyte solution. The steps of ESI ionization can be seen. Initially, Taylor cone is formed because of the high potential difference. When electric repulsion between charge exceed the solvent surface tension, analyte-solvent droplets are released and they undergo a series of Coulombic fissions until a single analyte molecule ion is formed.

The ions formed in the ESI source are characterized by a certain *m/z* and they are accelerated to the entrance of the spectrometer where the mass analyser is placed. There are different types of analyser, one of the simplest is the Quadrupole analyser (Q), which has been used in this work. In this type of analyser, an electric radio-frequency (RF) quadrupolar field is applied and used to separate ions according to their *m/z.* By scanning the RF, ions with different *m/z* pass through the quadrupole and reach the detector. The resulting signal recorded by the detector is directly proportional to the number of ions with a specific *m/z* hitting the detector when a certain RF is applied. The output of the technique is a mass spectrum, where the intensity is plot against *m/z*. Intensity is usually represented as a percentage, where the ion with the highest intensity has an intensity of 100% and the other ions intensities are normalised against this maximum. The area under the peak associated to each *m/z* is proportional to the abundance of the ion with that *m/z* in the sample, therefore it could be used for quantitative analysis.

2.12 Fluorescence spectroscopy

Fluorescence spectroscopy is one of the most used tools to assess interactions between proteins and surfactants, as decrease in fluorescence intensity associated to the tryptophan is strictly related to denaturation of the protein (as explained in section 1.6.3). Absorption of a photon by a molecule cause an electronic transition (as already explained in section 2.2), where the electron is excited from the

electronic ground state (S_0) to a higher energy electronic state (S_1). When the excitation occurs, the electron is transferred to any of the vibrational states of the excited electronic state S_1 (Figure 17). After the absorption, the molecule naturally undergoes a series of process as vibrational relaxation and/or internal conversion, where the energy is released as heat. These relaxation phenomena cause the decay of the electron from any of the vibrational excited states to the ground vibrational level in the S_1 electronic level. When the electron is in this ground vibrational state, it can decay to any of the vibrational states of the ground electronic level (S_0), releasing energy. The energy the electron releases is lower than the one previously absorbed, and the resulting emissive phenomenon is called fluorescence.
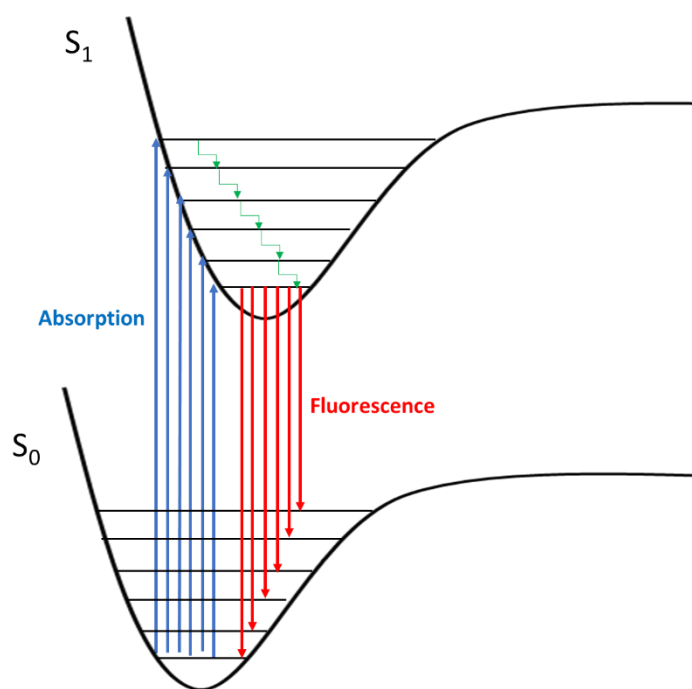
Figure 17- Jablonsky diagram for Absorption and Fluorescence. Electrons in the ground state (S_0) are excited by adsorption of light and they get promoted to any of the vibrational states of the excited electronic state (S_1). As a consequence of internal conversion or vibrational relaxation, the electrons decay to the fundamental vibrational state of S_1 where they are able to emit energy as light (fluorescence) and decay to any of the vibrational state of the ground electronic state. The resulting emitted light has a lower energy, and, therefore, a higher wavelength, than the light initially adsorbed.

The fluorescence emission spectrum has a maximum at higher wavelength compared to the absorption spectrum, as the photon emitted has a lower energy than the absorbed one. Moreover, the position of

this maximum in the emission spectrum is affected by several parameters, eg. the environment surrounding the fluorescent unit.

2.13 Turbiscan analysis

Turbiscan can be used to evaluate emulsion stability as a function of surfactant chemical structure. This tool investigates phenomena of instability related to emulsion formation by measuring the transmission (T_r) and the back scattering (BS) of an Infra-red (IR) light source. The wavelength of the Turbiscan light source is 850 nm (near IR) and the instrument is equipped with a double synchronized detector: a transmission detector, that lies in the same direction of the incident light ($\theta = 0$ °) and a back scattering detector, that is placed at 135 ° in respect to the original incident beam (Figure 18).
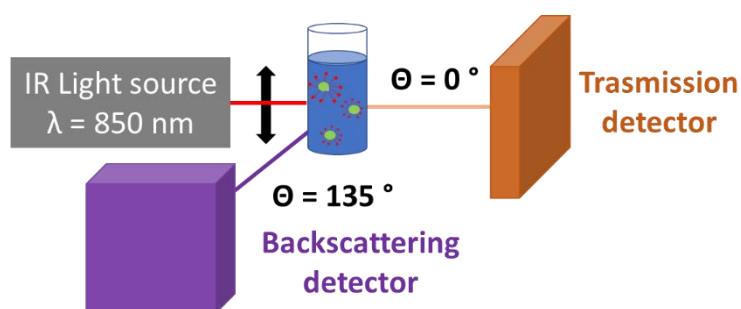
Figure 18– Diagrammatic scheme of the turbiscan instrument setup, where the IR source is moved along the length of the vial. The transmission and backscattering signals are collected by two different detectors, respectively placed at 0° and at 135°.

Emulsion formation occurs when two immiscible liquid (e.g. water and oil) are mixed together in the presence of agitation forces, leading to formation of spherical droplets. The emulsions are metastable system, which stability is increased by addition of an emulsifier, as surfactant for instance. However, because of their instability, emulsion tend to coalesce and separate as a consequence of gravity. The oil, which has a lower density, migrate to the air/water interface, causing phase separation. The changes in the oil distribution across the sample has an effect on the interaction between the analysed sample and the IR light.

The photon mean free path (λ) is defined as the average distance that the photon has covered between two successive collisions and this depends on different factors such as the density of the particles (n), particle mean diameter (d), the scattering extinction coefficient (Q_e) and the particle volume fraction (ϕ) [110]:

$$\lambda = \frac{1}{n\left(\frac{\pi d^2}{4}\right)Q_e} = \frac{2d}{3\phi Q_e} \tag{41}$$

In the case of anisotropic scattering, the photon is deflected after collision with a particle and moves in a direction that is different from the direction it pursued before the collision. Being θ the scattering angle, the asymmetry factor g related to the anisotropic scattering is given by the average cosine of the scattering angles that are considered in the phase function and its value is equal to 0 for isotropic Rayleigh or $0<g<1$ for anisotropic scatter. The photon transport mean free path is then expressed by:

$$\lambda^* = \frac{\lambda}{(1-g)} = \frac{2d}{3\phi(1-g)Q_s} \tag{42}$$

As a result of the collision, there is a lower number of photons travelling along the original direction of the incident light, which results in lower transmission. However, there is an increase in the backscattering signal, related to the size of the particle. Both the transmission and the back scattering are related to the photon mean free path by the following equations:

$$\text{BS} = \frac{1}{\sqrt{\lambda^*}} \sim \sqrt{\frac{\phi}{d}} \tag{43}$$

$$\text{T}_\text{r} = T_0 e^{-\frac{2r_i}{\lambda}} \tag{44}$$

where T_0 is the initial transmission and r_i is the internal radius of the measurement cell.

Therefore, analysing the backscattering and transmission profile of a sample across time gives information about the photon transport free path, which is related to emulsion formation and emulsion stability.

In Figure 19, the different phases of emulsions analysis via Turbiscan are shown. Initially (Figure 19a), the transmission and the backscattering profile of the surfactant solution in absence of any soil are analysed, as these values are then used for normalizing the transmission and backscattering profiles. After few minutes, oil is added in the vial and emulsions are generated via mixing. When mixing stops, the emulsions formed are uniformly distributed in the solution and the transmission is lower than before the addition of oil (Figure 19b). Emulsions are unstable and, therefore, they tend to migrate and phase separate. This process, called creaming, results in the migration of oil droplets to the air/water interface as consequence of gravity (oil being lighter than water). As a result, the transmission at the bottom of the vial increases due to the lower amount of oil droplets in this region. At the same time, the formation of the oil layer on top of the solution cause a decrease of the transmission signal at the top of the vial (Figure 19c). In combination to the creaming, flocculation occurs, where the oil droplets coalesce and generate bigger oil droplets that are more unstable. This has an effect on the back scattering, as bigger particle scatter more, causing an increase in the backscattered signal.

An advantage of the use of turbiscan for emulsion analysis is related to the possibility of using data fitting to achieve particle size distribution. Particle size is related to creaming velocity, which could be calculated by fitting the transmission or back scattering data across time at each height. The case of transmission is shown in Figure 20: Figure 20a shows the shape of a transmission profile recorded across time for a certain height of the vial (h_i). The increase of transmission at the end of the agitation is related to the creaming process, where a plateau in T_r is achieved after a certain time that is strictly related to the emulsion stability as well as to the emulsion droplet size. The increase of T_r vs time follows an exponential trend and it could be fit to the equation 45 in order to determine the variable τ_i, time required to achieve the equilibrium transmission:

$$T_r = e^{\tau_i} \tag{45}.$$

The values of τ_i at each h_i could be used to evaluate the creaming velocity:

$$v_i = \frac{h_i}{\tau_i} \tag{46},$$

that could be substituted in the Navier-Stokes' equation (equation nr 5) to obtain the radius of the droplet size r at each height[111] .
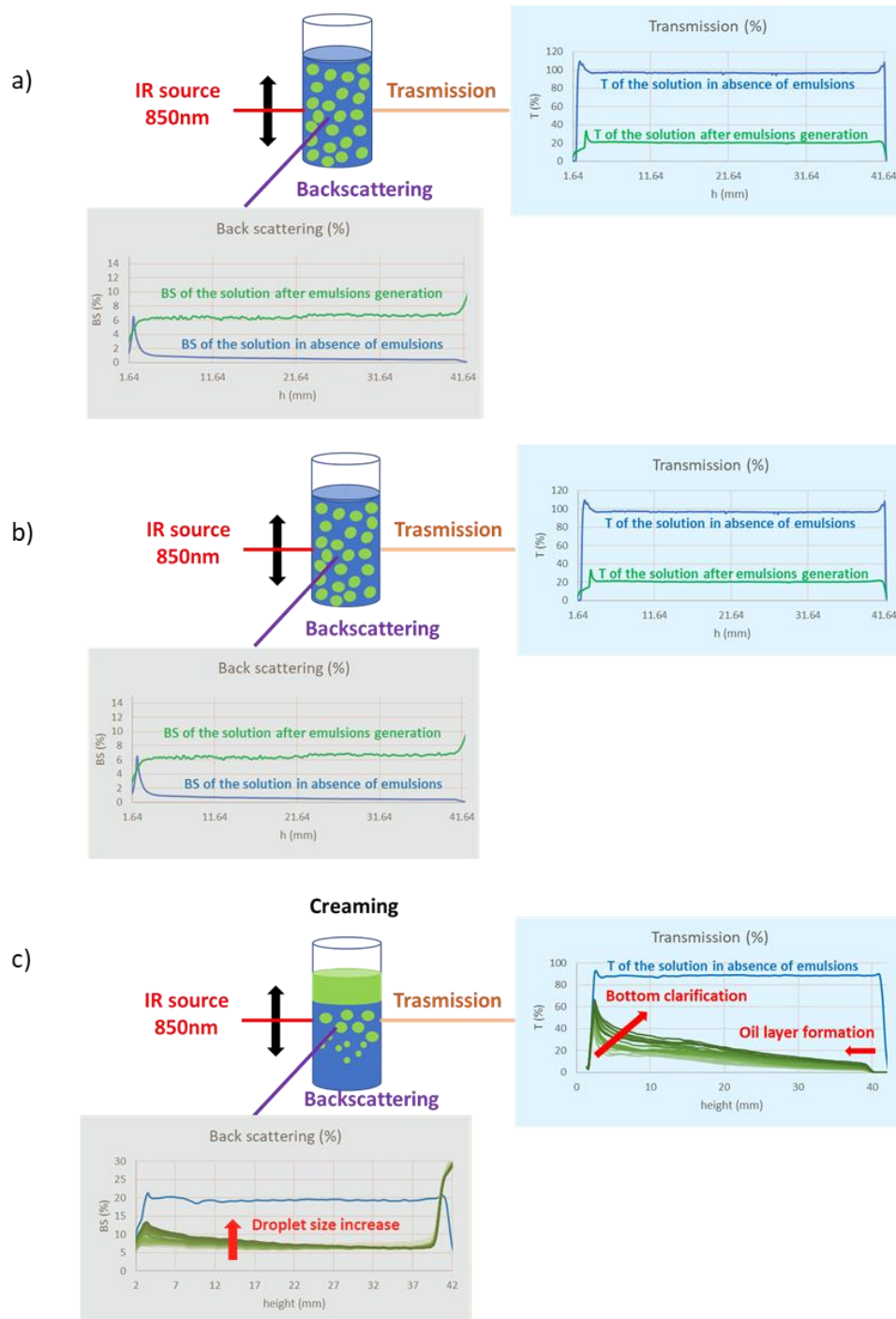
Figure 19– Transmission (blue boxes) and back scattering profile (grey boxes) across vial height of a surfactant solution in absence of oil (2a), just after emulsion generation (2b), and after that creaming has occurred (2c).
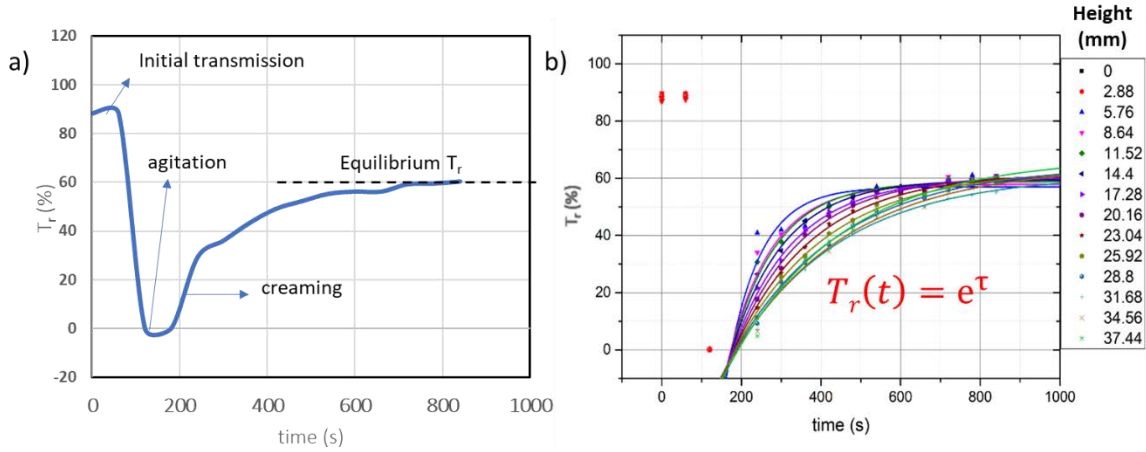
Figure 20 – a) Transmission profile across time for a generic height h_i where the phases of agitation and creaming are highlighted. b) Comparison between different Transmission profile at different vial heights.

2.7 Models for data fitting

2.7.1 Langmuir and Langmuir-Freundlich adsorption isotherms

Adsorption isotherms represent an easy tool to have information about the affinity between the adsorbate and the substrate, which can be used to assess which polymers have a higher affinity towards polyester via measuring the affinity constant. There are several models used to fit the adsorption isotherms and the best fitting is dictated by the type of adsorption sites and of absorbate. In the simplest case, as already described in section 2.5, the adsorption isotherm follows the Langmuir model. The adsorption isotherm relates the amount of adsorbate (per gram of adsorbent) q_E occupied sites to the concentration of adsorbate at equilibrium, $[P]_e$:

$$q_E = Q_{sat} \frac{K\,[P]_e}{1+K[P]_e} \tag{47}$$

where Q_{sat} denotes the saturation level of the solid and K (Langmuir's constant) is the equilibrium constant for the adsorption process reflecting the adsorption energy. A real solid surface is generally heterogeneous, characterized by adsorption sites with different adsorption energies and therefore different Langmuir's constant. For heterogeneous systems the overall adsorption isotherm is obtained

62

integrating the Langmuir's isotherms over all the K_L-values[112] obtaining the following isotherm often called Langmuir−Freundlich or Sips isotherm.

$$q_E = Q_{sat} \frac{K([P]_e)^m}{1+L([P]_e)^m} \tag{48}$$

The variable K is related to the median binding affinity (K0) via $K_0 = K^{1/m}$. In this model m is the heterogeneity index, which varies from 0 to 1. For a homogeneous material, $m = 1$, and we retrieve the Langmuir isotherm. A heterogeneity in the affinity of the surface for noninteracting adsorption sites corresponds to $m < 1$. However, when multiple adsorption sites occur, another phenomenon connected with inhomogeneity can emerge. The polymer affinity for an adsorption site can depend on the occupancy of the neighbouring sites. In such a case, the adsorption is said to be cooperative. In the case of positive cooperativity, the presence of occupied binding sites makes the further ligand binding favourable and $m > 1$. In the case of negative cooperativity, the binding to a site reduces the affinity of the ligands for the other sites and $m < 1$.

Chapter 3. PEG-POET SRPs

3.1 Introduction

The primary goal of this work was to identify suitable soil release polymers to enable surface modification of fabrics and enhance soil removal from synthetic hydrophobic textiles, such as polyester. According to literature, the optimal candidate is a block copolymer that is composed of hydrophilic and hydrophobic units, where the hydrophobic moieties are necessary for deposition onto polyester. In this chapter, polyethylene glycol – polyoxyethylene terephthalate (PEG-POET) block copolymers were investigated as soil release polymers for cotton and polyester. A combination of streaming potential and UV/vis spectroscopy was employed to investigate the effect of deposition parameters, such as pH, water hardness and agitation speed, for SRP adhesion on fabrics. This study helped to identify the experimental conditions needed to achieve efficient deposition of PEG-POET SRPs on polyester. In addition to the deposition parameters, the presence of surfactants in the environment can have an effect on SRPs deposition due to coacervation of SRPs with surfactant molecules or changes in polymer conformation. Therefore, interactions between the soil release polymers and different types of surfactants were investigated to assess which surfactants are able to interact with the SRPs during the wash.

As explained in section 1.4.1, the enhancement of soil removal from SRP-modified textiles is a consequence of the hydrophilization, and pore occlusion, experienced by the textile as result of polymer deposition. This chapter provides an overview of the effect of PEG-POET SRPs on polyester with respect to surface wettability. Changes in surface area and surface porosity due to SRPs deposition are investigated, as these parameters can be related to soil removal performances, which will be discussed further in Chapter 5.

3.2 Experimental

3.2.1 Polyethylene glycol – polyoxyethylene terephthalate (PEG-POET) soil release polymers

The first class of SRPs analysed in this work is based on a polyethylene glycol – polyoxyethylene terephthalate (PEG-POET) block copolymers, which general structure is shown in Figure 21a. The PEG block is hydrophilic, whereas the hydrophobic POET block is responsible of the deposition on the hydrophobic fabrics. Among this class, two different SRPs were studied, both commercialized by Clariant Gmbh (Muttenz, Switzerland). The first SRP is the SRA300F, an anionic SRPs where the terephthalate group has been functionalized with sulfonate groups that are not present in the non-ionic SRN240, also used for this work. The two polymers have very similar structure, as the length of the hydrophobic and hydrophilic block are the same for both the SRPs. Therefore, the main difference between the two actives is associated with the presence of the sulfonate groups along the SRA300F chain, which could lower the strength of the hydrophobic interactions with the textiles for the anionic SRP.
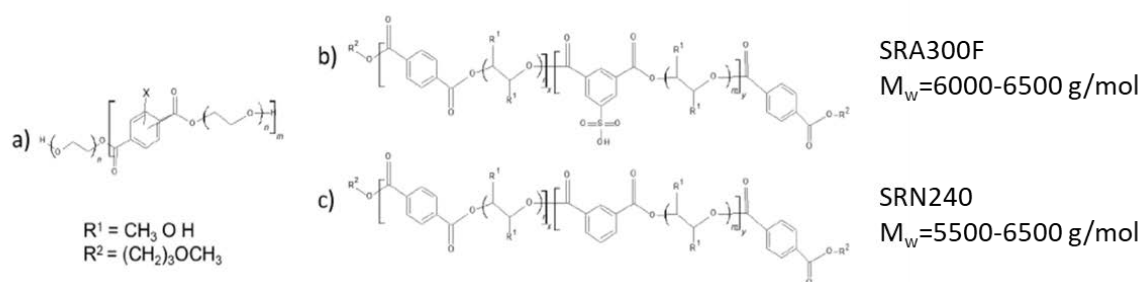
Figure 21 - a) General structure of the PEG-POET block copolymers used in this research; b) structure of SRA300F, the anionic SRP used in this work; c) structure of SRN240, the non-ionic SRPs used in this work.

In this work, the effect of the different chemical structure on deposition on fabrics surfaces as well as on soil removal performances was investigated. As mentioned, the main difference among the two polymers is the charge, where the presence of the anionic group on the SRA300F is expected to lower the hydrophobic interaction with hydrophobic materials.

3.2.2 Surfactants

A wide variety of different surfactant molecules, containing different head group type and size, different chain lengths and different degree and type of branching was investigated. The surfactants used are listed in Appendix I, which were selected in order to achieve a good representation of different chain lengths (from octyl to myristic alkyl chains), head group sizes (from small as alkyl sulfate to big as cocoamido propyl) and charge (cationic, non-ionic, amphoteric, anionic) and branching degrees (from 0% to 95% branching). The final aim was to unravel the mechanism behind surfactant-soil interaction as a function of surfactant and polymer chemical structures.

3.2.3 Fabrics pre-conditioning with PEG-POET SRPs and streaming potential analysis

Two types of fabrics with different wettability were selected for our tests: polyester and cotton. Polyester is more hydrophobic than cotton[10], so it is the substrate of preference of SRPs. Both fabrics were purchased from WFK Testgewebe GmbH, cut into 5×5 cm^2 pieces and they were washed in deionizied (DI) water at 60°C for 30 minutes to remove any finish from the fabric production process. Stock solution of SRA300F and SRN240 were dissolved in Milli-Q water at 5000 ppm concentration (around 1 mM for both the polymers) and then diluted to the required concentration, according to needs. The pH of the solution was adjusted by addition of NaOH and HCl (Sigma Aldrich).

For streaming potential analysis, the fabrics were conditioned with SRP solution in a tergotometer (Copley Scientific, Nottingham, UK) at 35 ± 1 °C, keeping the ratio of SRP solution to fabric constant at a value of 24, which is in line with the normal load for Europe and North America[113]. Most of the tests were carried at an SRP concentration equal to 50 ppm, which represents 1% polymer content in a normal washing product. However, for the adsorption isotherms, concentrations of the polymers

between 25 and 200 ppm of SRP were used. De-ionized water, agitation speed of 200 rpm and a washing pH equal to 8 were used in most of the experiments. Changes in the washing condition were applied to assess the effect of parameters, such as pH (pH 4 vs pH 8), agitation speed (100 rpm vs 200 rpm) and water hardness (15 dH vs DI). Treated fabrics were dried overnight at (20 ± 2) °C and at a relative humidity (RH) of 50%. Samples were analysed by measuring zeta potential at the same pH used during pre-treatment of fabrics. A 1 mM solution of potassium chloride (KCl) was used as electrolyte solution and a pressure drop between 200 and 600 mbar was applied at the edge of the streaming potential cell. Three zeta potential values were measured for each sample (three internal replicates) and then mean averaged. Zeta potential data shown are the average of zeta potential values measured on three different samples (three external replicates).

3.2.4 Kinetic analysis of SRP deposition via UV/vis

The UV/vis measurements were run with a Cary 8454 (Agilent technologies, USA), using a dip probe with an optical path of 1 cm. The probe of the spectrophotometer was immersed in the polymer solution, in contact with the fabric, and the UV/vis spectrum of the solution between 200 and 600 nm was measured. The absorbance of SRP in solution was measured every 5 minutes for a total pre-treatment time of 30 minutes, which is the time required to reach the equilibrium of deposition. The amount of SRP adsorbed on polyester was measured indirectly from the concentration left in the bulk solution, after incubation of the polyester fabric in SRP solution at different washing conditions. As in the case of streaming potential analysis, most of the analyses were carried at an SRP concentration equal to 50 ppm at pH 8 and at 35 ± 1 °C, using an agitation speed of 200 rpm. Changes in washing condition were tested by varying pH (pH 4 vs pH 8), agitation speed (100 rpm vs 200 rpm) and water hardness (15 dH vs DI). For the adsorption isotherms, concentrations of the polymers between 25 and 200 ppm of SRP were used.

3.2.5 Contact angle measurements of SRP-modified fabrics

The contact angle measurements were carried with a OCA-200 (Dataphysics, Germany). The instrument is equipped with a high speed camera which has a maximum frequency of acquisition of 250 Hz. This feature is fundamental in the case of fabrics where the water adsorption occurs very rapidly.

Contact angle values were measured every 4 ms for a total analysis time of 10 minutes. Stripes of untreated or SRP-modified polyester were taped on glass microscope slides without excessive stretching of the textile. In the case of SRP-modified polyester, a polymer concentration of 50 ppm was used to wash the fabrics in tergotometer before measuring contact angle. A temprature of 35 °C, an agitation speed of 200 rpm and DI water were used as experimental conditions. Contact angle values were measured for water (surface tension γ_w = 72.80° @20 °C, drop volume 12.5 µL), using a dispensing speed of 2 µL/s. At least 10 measurements were collected for each samples and averaged.

3.2.6 Analysis of fabrics via scanning electron microscopy

Scanning electron microscopy (SEM) was used to analyse fabrics with and without pre-conditioning of SRPs. Fabrics were pre-treated using an SRP concentration of 50 ppm at 35 °C in DI water, using an agitation speed of 200 rpm in tergotometer. Fabrics were dried overnight, cut in small pieces (about 0.5×0.5 cm^2) and they were metallized via deposition of palladium, as the SRP pre-trated samples showed high charging behaviour when metalization was not used. The metalization was performed via electron beam deposition of palladium on the substrate. The images were taken with the help of Dr. Cinzia Di Franco, based in the Istituto di Fotonica e Nanotecnologie, CNR (Bari).

The SEM instrument used is a Field Emission Zeiss ΣIGMA (Jena, Germany, tension 3 kV; emission 120 µA). The SEM images were used to estimate the surface roughness of the polyester before and after the SRPs deposition. This was done by using the software Gwydion 2.5.3 which uses a series of mathematical algorithms to evaluate a roughness index associated to the image that has been processed, as explained in section 2.5.

3.2.7 Diffusion nuclear magnetic resonance experiments

Diffusion NMR experiments were run in collaboration with Gabriele Cimmarusti, Ph.D. student based in the University of Birmingham. Polyester fabrics (5×3 cm^2) untreated and pre-treated with SRPs at a concentration of 50 ppm were dipped in water at 15 dH. Excess of water was removed and the fabrics were folded and inserted in 10 mm NMR tubes. The diffusion NMR experiments were performed using a Bruker Avance Neo spectrometer with a 11.74 T vertical bore magnet. Sample temperature was fixed

at 25 °C and controlled by a chiller BCU-II unit and a probe heater. Typical parameters used in these experiments were: δ = 1 ms and γ = 2.67 10^8 $s^{-1}T^{-1}$. ^{1}H NMR diffusion measurements were performed by applying a pulsed gradient stimulated echo sequence (PGSTE). An observation time, Δ, between 10 and 2000 ms was used, using a repetition time of 2s, and the signal attenuation as a function of magnetic gradient field strength was obtained. Echo attenuation data were fit to the minimum number of diffusion coefficients by using the Stejskal-Tanner equation[114] (equation 29) and two diffusion coefficients were found. M_1 and D_1 are the weight and restricted diffusion coefficient of free water, whereas M_1 and D_1 are the weight and restricted diffusion coefficient of water experiencing restricted diffusion.

3.2.8 Surface area analysis via Brunauer-Emmett-Teller method

Physisorption isotherms were collected for untreated and SRP-treated polyester in BET using nitrogen and carbon dioxide as gas for the analysis. The samples have been analysed with the help of William Caufield (Scientist) and Simon Greener (Senior scientist), both based in P&G Newcastle Innovation Centre. The samples were cut in small pieces (about 3 x 3 mm^2) and loaded in physisorption tubes. Each tube was mounted in a degasser unit, where the tube is evacuated, reaching a pressure of 10 mmHg. The samples were degassed at 40°C overnight, as polymer melting (SRN240) or glass transition (SRA300F) were observed in the DSC thermograms for the two polymers for a temperature above 50 °C (Appendix II). For BET analysis, untreated and SRPs treated fabrics were cut in small pieces. The sample was then loaded for the analysis and was cooled down with liquid nitrogen. The absolute pressure was increased until 100 kPa and the mass of gas adsorbed across time was measured. The resulting isotherm was analysed using the software MicroActive for the analysis, the exact mass of the dried sample was added as input and the adsorption isotherms were fitted by using the Brunauer–Emmett–Teller (BET) and Barrett, Joyner and Halenda (BJH) models. The BET is the most common model used for analysis of micro- meso- and macro-porous materials[115,116], whereas BJH model is one of the most used for mesoporous materials, if the mesoporous are bigger than 10 nm. [117]

3.2.9 Surface tension measurements of polymer-surfactant solutions

Surface tension values of surfactant solution were measured with a tensiometer K100 (Kruss, Germany) both for pure surfactant solutions and for surfactant solutions in combination with SRPs. A stock solution of each surfactant at 3000 ppm was prepared by dissolving the surfactant in DI water. The stock solution was then diluted with DI water to the desired surfactant concentration, varied between 5 and 3000 ppm, and surface tension was measured for pure surfactant solution at each of the concentrations prepared. Stock solutions of SRPs were prepared by dissolving SRA300F and SRN240 in DI water. The SRP stock solution was diluted by adding surfactant solutions and DI water to address a final SRP concentration of 50 ppm, where the surfactant concentrations analysed in combination with SRPs were the same analysed for pure surfactant solutions. All the measurements were collected in replicates at 25 °C and the resulting values were averaged.

3.3 Thermodynamic and kinetic of deposition of PEG-POET SRPs

3.3.1 PEG-POET SRPs deposition at pH 8

The results of streaming potential analysis for untreated and SRP-treated polyester are shown in Figure 22. A typical value of zeta potential for untreated polyester was found to be between −60 and −65 mV, which is in agreement with literature.[118] The negative charge has been previously associated with adsorption of OH^- ions on the surface of the polyester fiber.[119] Increasing pH is found to cause a progressive decrease in zeta potential because of the increasing amount of available OH^- ions present in the bulk electrolyte solution, which consequently increases their absorption on polyester. As expected, there is a change in zeta potential when the polyester has been pre-treated with a SRP.
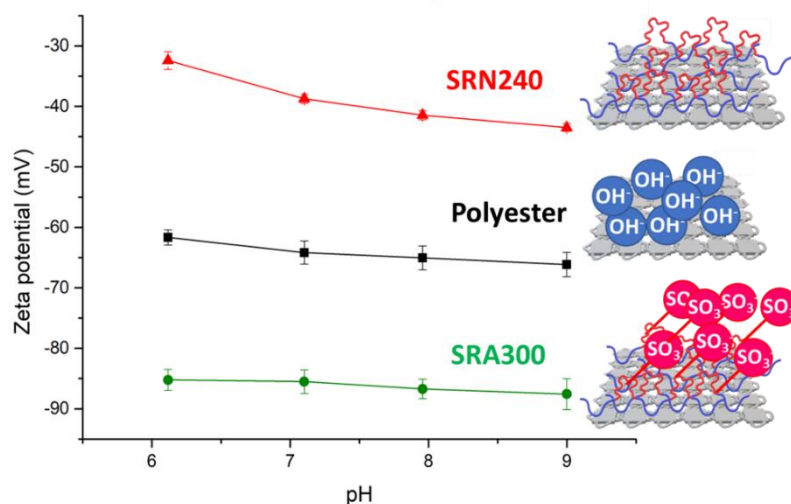
Figure 22– Electro-kinetic curves of polyester fabrics in the presence and absence of SRPs. The curve for untreated polyester (■) is compared with same material after deposition of SRN240 (▲) and SRA300F (●). Zeta potential values at each pH are the result of the average between three replicates for three different samples.

Polyester pre-treated with SRA300F results in a lower value of zeta potential, i.e., shifting the surface zeta-potential to a more negative value (around −90 mV).[75] This shift is expected, as SRA300F is an anionic polymer and, therefore, its deposition on top of the fabric renders the charge on the polyester surface to be negative due to the sulfonate groups present in SRA300F. Further evidence of this behaviour is indicated in the small variation of zeta potential between pH 6 and 9, given the pKa of the polymer expected to be below pH 6. Conversely, SRN240 causes a shift of the zeta potential for polyester to less negative values, because of the non-ionic character of this polymer. Hence, the SRN240 polymer chains are expected to displace the OH⁻ ions adsorbed onto the polyester surface or at least decrease their density on the surface with uncharged moieties. Moreover, a progressive decrease of zeta potential, with increasing pH, confirms that, for this sample, OH⁻ adsorption on the surface of polyester is still the main driver for surface charging. As shown in Figure 22, the two SRPs have an opposite effect on the streaming potential, as a result of their different charge nature. There is a shift in the zeta potential for the fabrics, after SRP deposition compared to the untreated polyester, and the difference in zeta potential is almost the same for both polymers. This might suggest that the two SRPs have the same efficiency of deposition. To test this hypothesis, the amount of adsorbed polymer was measured, indirectly, by UV/vis. The decrease in absorbance after SRP deposition was used to quantify the amount

71

of SRPs deposited by comparison with calibration curves previously obtained. Results showed that about (26.0 ± 0.2) ppm (51.2% w/w) of SRN240 deposited on polyester while only (7.82 ± 0.10) ppm (15.6% w/w) for SRA300F, disproving the initial hypothesis. Based on this, it can be concluded that the zeta potential shift cannot be used to assess efficiency of deposition, as it strongly depends on the charge density of the SRP. In fact, lower amount of SRA300F is deposited, but the difference in zeta potential vs untreated polyester is about the same (but with opposite sign) observed for higher amount of SRN240. Hence, the negatively charged SRA300F, even at a lower degree of deposition, is sufficient to significantly reduce the zeta potential. Conversely, the neutrally charged SRN240 is only able to change the zeta potential by a similar amount because of the significantly higher degree of deposition. The lower efficiency of deposition of SRA300F can be justified by the less hydrophobic character of the SRPs, due to the presence of the sulfonate groups present along its backbone, as well as possible electrostatic repulsion between the anionic polymer and the negative surface charge of the polyester fabric.

Streaming potential analysis were performed as well on cotton fabrics before and after pre-treatment with SRN240 and SRA300F, and are shown in Figure 23. From these data, no significant difference can be observed in the zeta potential between SRP-treated samples, and no differences in SRP concentration in bulk at the end of the pre-treatment were confirmed via UV/vis (where SRP concentration was measured as explained in section 2.3). This might be explained by the lower affinity of cotton for POET block adsorption which confirms that this SRP structure is not compatible to deposition on natural fibers.
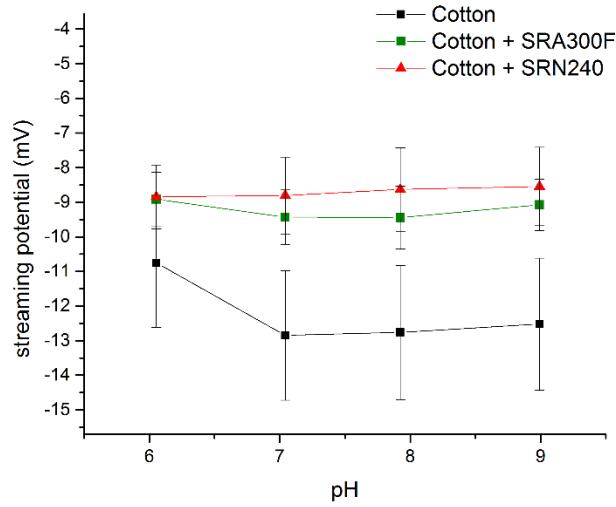
Figure 23- Electrokinetic curves of cotton fabrics with and without conditioning stage with soil release polymers (1 h, 35 °C). The curve for untreated cotton (■) is compared with same material after deposition of SRN240 (▲) and SRA300F (●). Zeta potential values are the result of the average between three replicates for three different samples

3.3.2 Kinetic of deposition of PEG-POET SRPs on polyester

The kinetics of deposition on polyester was monitored both for SRA300F and SRN240 at pH 8. The polyester fabrics were washed with SRP solution at 50 ppm and the absorbance of SRP in solution was measured every 5 minutes for a total pre-treatment time of 30 minutes, which is the time required to reach the equilibrium of deposition. The deposition of a polymer P on a substrate S can be described as a first order kinetic process:

$$P + S \rightarrow PS \tag{49}$$

Initially, the polymer is at a concentration P_0 equal to 50 ppm, then the polymer concentration in solution decreases across time t and reaches a plateau concentration ($P_{saturation}$). The rate of deposition (k) is equal to the rate of decrease of SRPs absorbance in bulk. Therefore, k is calculated by fitting the absorption data to the following equation:

$$[P] = [P_0] + (P_{saturation} - [P_0]) \times (1 - e^{-kt}) \tag{50}.$$

An example of fitting for SRA300F is shown in Figure 24.

Parameter	Estimate	Standard Error
P_0 (ppm)	49.4	1.4
K (s^{-1})	3.5×10^{-3}	7×10^{-4}
$P_{saturation}$	29.5	0.8
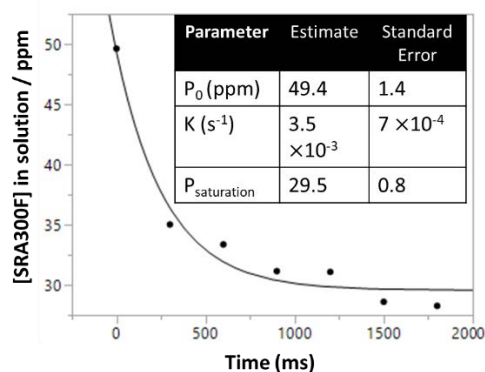
Figure 24– Fitting of SRA300F concentration in bulk across time via equation 50. The deposition of SRA300F has been run on polyester fabrics at pH 8, 35 °C and 200 rpm agitation speed.

Results of the fitting shows that, at pH 8, the rate of deposition of SRN240 is $(5.6 \pm 0.5) \times 10^{-3}$ s^{-1}, while only $(3.8 \pm 0.7) \times 10^{-3}$ s^{-1} for SRA300F. The higher rate of deposition SRN240 vs SRA300F is due to the higher hydrophobicity of SRN240 and the lack of electrostatic repulsion between SRN240 and the surface of the polyester, which is negatively charged. As a result, deposition on polyester is faster for the non-ionic SRP SRN240.

3.3.3 Absorption isotherms of PEG-POET SRPs on polyester

The adsorption isotherms of the two SRPs to polyester were plotted from UV absorbance data at different SRP concentration[120–124] and then fit to the Langmuir (equation 47) and Langmuir-Freundlich equation (equation 48), as shown in Figure 25.
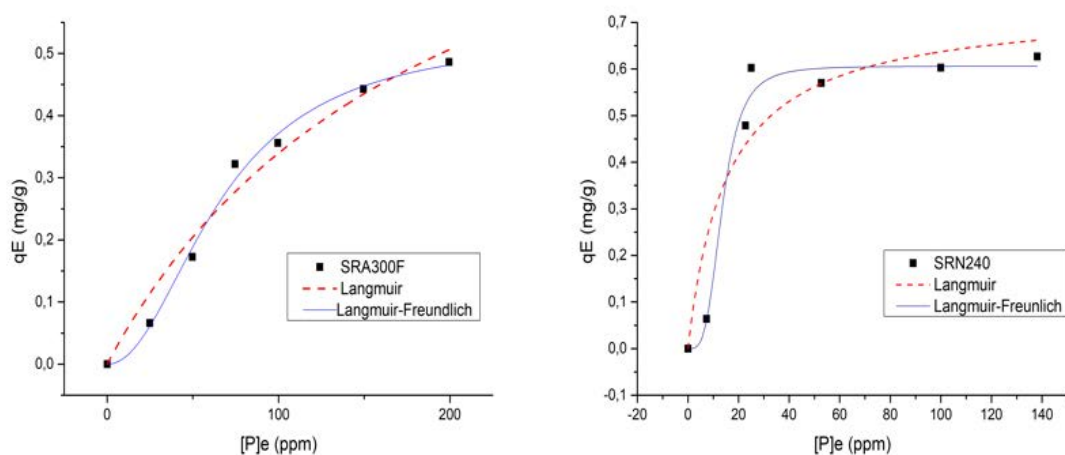
Figure 25 - Adsorption isotherms fittings for SRA300F (left) and SRN240 (right) at pH 8. Estimated fitting parameters associated with Langmuir (dashed line) and Langmuir−Freundlich (solid line) models are listed in Table 1.

Table 1 – Fitting parameters obtained by fitting adsorption isotherms for SRA300F and SRN240 on polyester at pH 8 with Langmuir and Langmuir-Freundlich models.

	SRA 300F	SRN240
Langmuir		
Q_{sat} (mg/g)	1.0 ± 0.3	$(7.3 \pm 1.1) \times 10^{-1}$
K (ppm)	$(5.0 \pm 0.2) \times 10^{-3}$	$(6 \pm 4) \times 10^{-2}$
Langmuir-Freundlich		
Q_{sat} (mg/g)	$(5.3 \pm 0.4) \times 10^{-1}$	$(6.0 \pm 0.2) \times 10^{-1}$
K (ppm)$^{-m}$	$(1.6 \pm 0.2) \times 10^{-4}$	$(9.0 \pm 0.2) \times 10^{-5}$
m	2.1 ± 0.4	3.6 ± 0.9

From the fitting, it is clear that the Langmuir-Freundlich model fits the data best and the fitting parameters are shown in Table 1. The use of Langmuir-Freundlich models is due to the cooperative effect that deposition of polymer chain has on the neighbouring adsorption sites, as shown by the *m* values for both the polymers. Most likely, the cooperative binding is due to polymer-polymer interaction, which promotes the deposition of more SRP when the polymer is already deposited on fabric. By comparing the binding affinities for SRN240 $(7.5 \pm 0.2) \times 10^{-2}$ s^{-1} and SRA300F (1.6 ± 0.5)

$\times 10^{-2}$ s^{-1}, it is evident that SRN240 has a higher affinity towards polyester probably because of its non-ionic charge. A low concentration of SRN240 is required to saturate the surface of polyester and the concentration of saturation is low, which suggests that SRP forms a homogeneous layer on the fabric outer surface, thereby locking the pores of the fabric and preventing soil penetration via capillary action.

3.3.4 Effect of water hardness on PEG-POET deposition on polyester
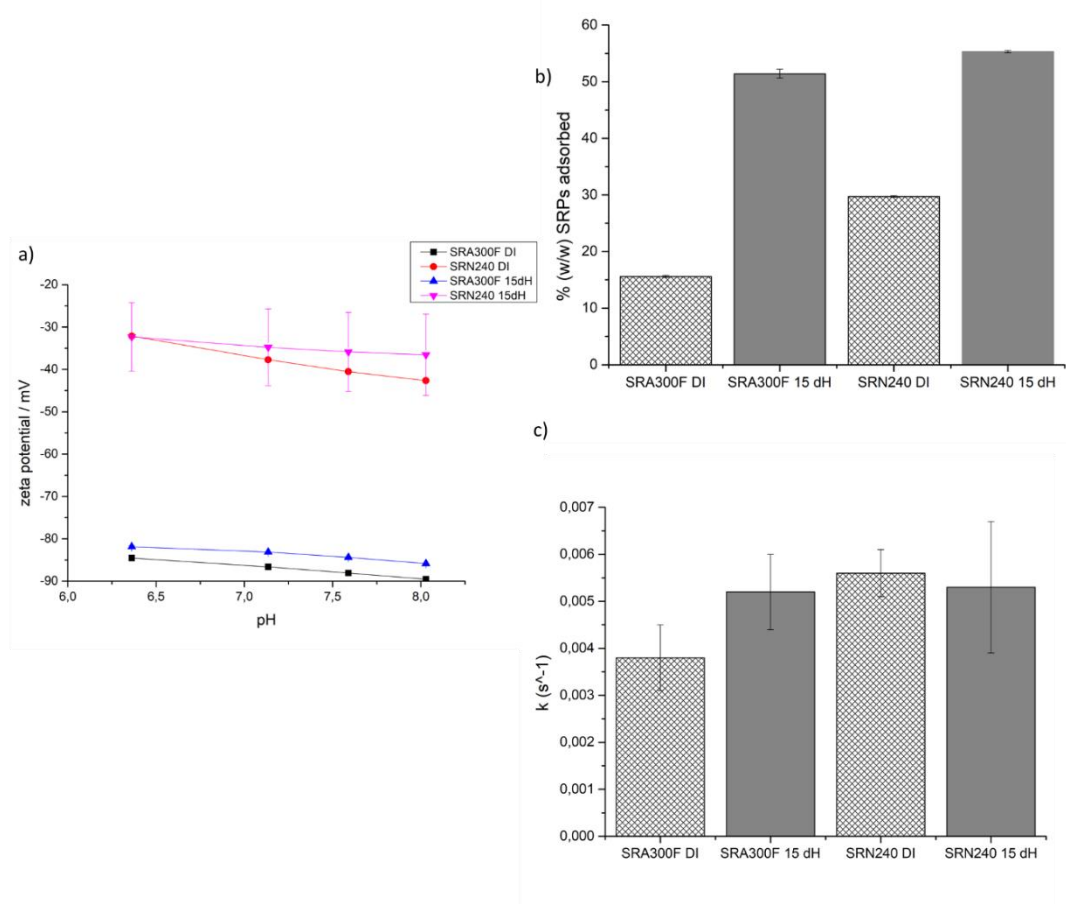
Figure 26 – a) Electro-kinetic curve of polyester fabrics pre-treated with SRN240 (•,∇) and SRA300F (▲,■) in DI water (•,■) or in water at 15 °dH (∇,▲). Pre-treatment was run for 1 hour at pH 8 and 35 °C, using an agitation speed equal to 200 rpm; b) percentage of SRA300F and SRN240 adsorbed on polyester fabrics in DI (patterned) and in 15 °dH water (solid); c) rate constant of deposition for SRA300F and SRN240 on polyester in DI (patterned) and in 15 °dH water (solid).

The effect of water hardness on SRPs deposition was investigated by comparing previous results (section 3.3.1) to streaming potential and UV/vis data generated for polyester that had been pre-treated with SRP in presence of CaCl$_2$·2H$_2$O, MgCl$_2$·6H$_2$O and NaHCO$_3$ (total hardness of water was 15 °dH).

In Figure 26a, the electro-kinetic curves of fabrics, with and without pre-conditioning with SRPs, are shown. There is a large standard deviation associated to the ζ of polyester that had been pre-treated with SRN240 in 15 °dH. This is a consequence of the fast and reversible displacement of OH^- ions by the cations present in the water (Ca^{2+}, Mg^{2+}, Na^+), which leads to changes in the ζ measured. Therefore, no meaningful differences are observed between the electro-kinetic curve of polyester modified with SRN240 in DI or 15 °dH. On the other hand, ζ measured on polyester modified with SRA300F in water at 15 °dH is less negative than the ζ measured in DI water, which suggests pairing between the SO_3^- groups of the polymers and the cations present in the water. The UV/vis data (Figure 26b) show an increase of the concentration of SRA300F deposited on polyester when water hardness is used, whereas no differences were observed for SRN240. The enhanced deposition of SRA300F is justified by the shielding effect of cations on the electrostatic repulsion between polyester and SRA300F, both negatively charged, which boosts the deposition of the anionic SRP. Instead, no effect of water hardness was observed on the percentage of deposition of SRN240, being non-ionic. For the same reasons, rate of deposition increases when conditioning polyester with SRA300F in hard water, whereas the rate is not meaningfully changed in the case of SRN240 (Figure 26c).

3.3.5 Effect of agitation on PEG-POET deposition on polyester

The effect of agitation speed on SRPs deposition on polyester was explored by comparing results at an agitation speed of 100 rpm, with those at 200 rpm [75]. The zeta potential curves of fabrics pre-treated at 100 and 200 rpm are similar (Figure 27a) and this suggest that there is no meaningful effect of the agitation speed on deposition. Further confirmation is found in the UV/vis data (Figure 27b), being the amount deposited at 100 and 200 rpm the same for both polymers. However, agitation does have a role on the kinetics of deposition, where a lower deposition rate was found when fitting the data at 100 rpm to equation 50. The use of lower agitation speeds decreases the SRPs flow through fabrics, leading to lower efficiency of deposition.
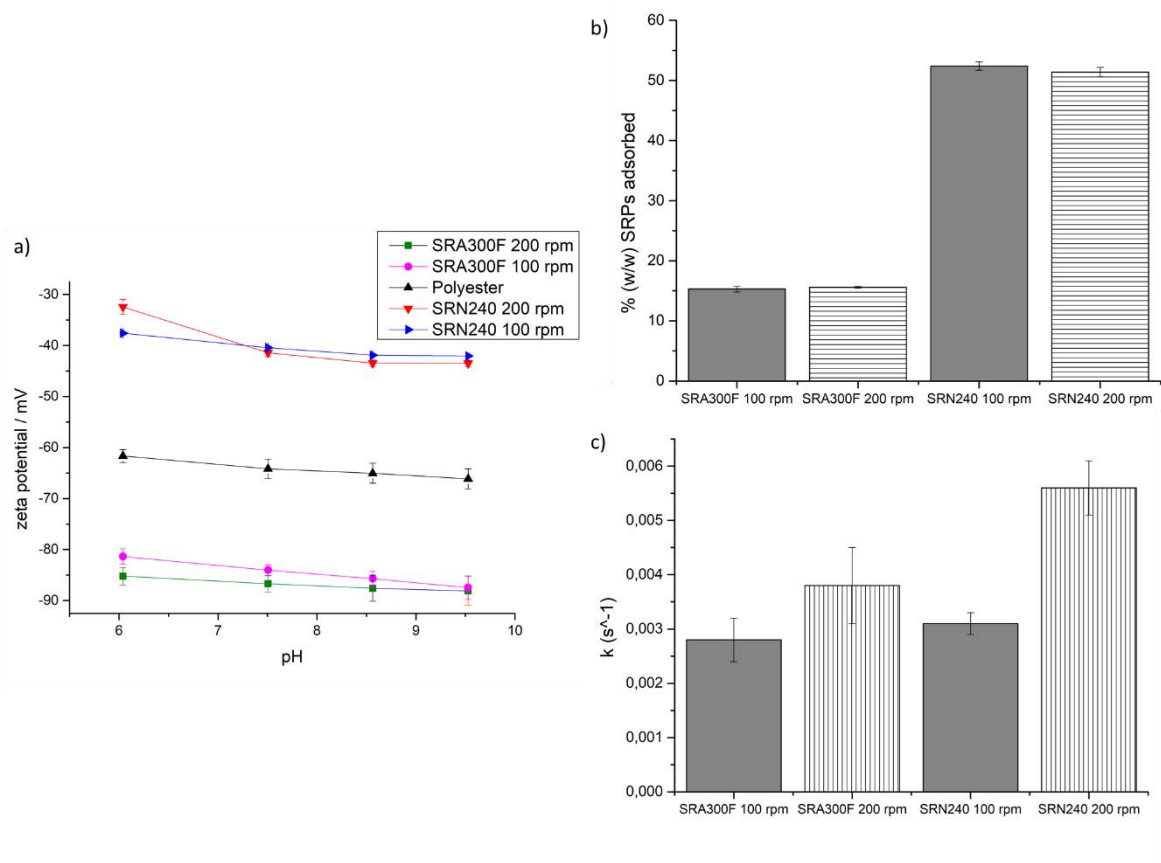
Figure 27 - a) Zeta potential of polyester fabric pre-treated per 1 h at 35 °C with SRA300F (■, ●) and SRN240 (▼, ▶) using an agitation speed of 200 rpm (■, ▼) and at 100 rpm (●, ▶) vs untreated polyester (▲). b) percentage of SRA300F and SRN240 adsorbed on polyester fabrics using an agitation speed of 200 rpm (patterned) and 100 rpm (solid); c) rate constant of deposition for SRA300F and SRN240 on polyester using an agitation speed of 200 rpm (patterned) and 100 rpm (solid).

3.3.6 Effect of pre-treatment pH on PEG-POET deposition on polyester

The deposition of SRPs on polyester was run at pH 4 to assess the effect of low pH on efficiency of deposition. At acidic pH (eg. pH 4), polyester has a lower negative charge due to the lower amount of OH⁻ available. The polyester is more similar to cotton at pH 4, as its zeta potential is about −27 mV (in line with literature values[125]), and, as such, it appears to be more hydrophilic. As in the case of pH 8, the two polymers cause a shift in opposite direction of the zeta potential due to their different charge and the difference in zeta potential compared to untreated polyester is almost the same both for SRA300F and SRN240 (Figure 28a). The amount of SRPs deposited was quantified via the use of UV/vis (as explained in section 3.2.4) and results showed that about (22.2 ± 0.5) ppm (44 % w/w) of SRN240 deposited on polyester while (17.2± 0.2) ppm (34.39 % w/w) for SRA300F (Figure 28b). It

can be concluded that at pH 4 the amount of SRA300F deposited increases but the amount of SRN240 deposited reduces at pH 8. Changes in the percentage of deposition can be explained by considering the higher hydrophilicity of polyester at this pH, which results in a higher affinity of SRA300F to the surface because of the sulfonate hydrophilic groups. On the other hand, the higher hydrophobicity of SRN240 leads to a reduced deposition compared to the same polymer at pH 8. From a kinetic point of view (Figure 28c), the rate of the deposition is improved at pH 4 for both the polymers, with higher boosting effect on the anionic SRA300F. The increase in rate of deposition for SRA300F at pH 4 is linked to the lower electrostatic repulsion towards the surface of polyester at this pH, due to the lower negative charge of polyester. Instead, the increased rate for SRN240 is less obvious and is probably related to the lower number of OH⁻ ions which are present on the polyester surface and which have to be displaced ahead of deposition of SRN240.
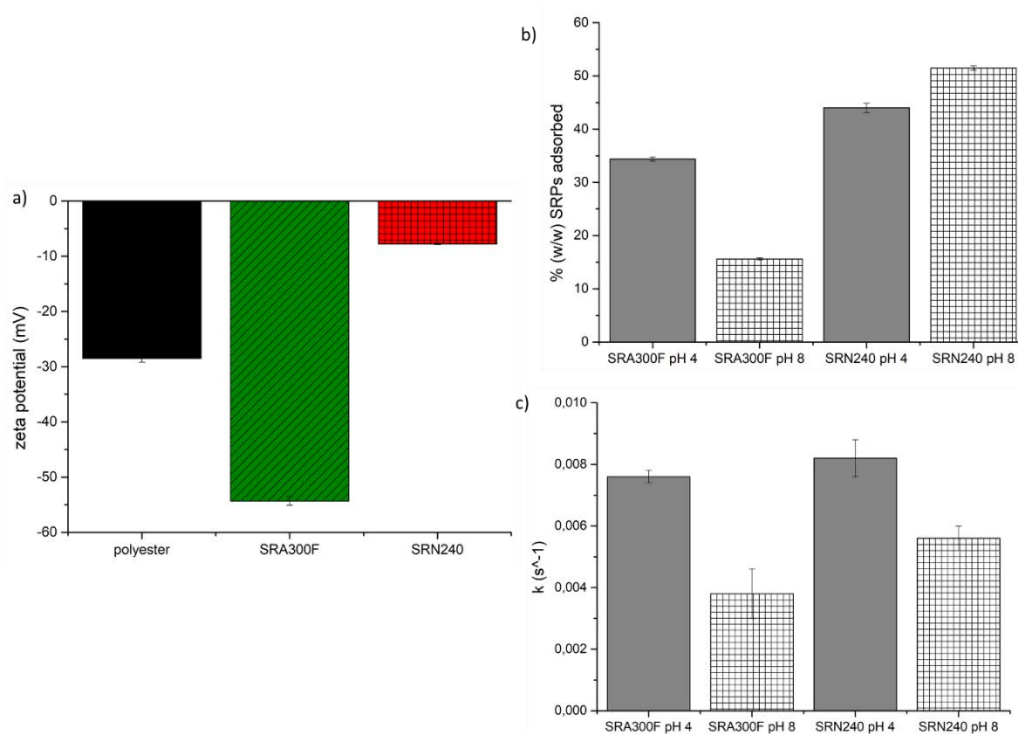
Figure 28 - a) Zeta potential at pH 4 of polyester fabrics in the presence and absence of SRPs. The value of zeta potential at pH 4 for untreated polyester (black) is compared with same material after deposition of SRN240 at pH 4 (red) and SRA300F at pH 4 (green). Zeta potential values are the result of the average between three replicates for three different samples; b) b) percentage of SRA300F and SRN240 adsorbed on polyester when the pre-treatment is run at pH 8 (patterned) and pH 4 (solid); c) rate constant of deposition for SRA300F and SRN240 on polyester when the pre-treatment is run at pH 8 (patterned) and pH 4 (solid).
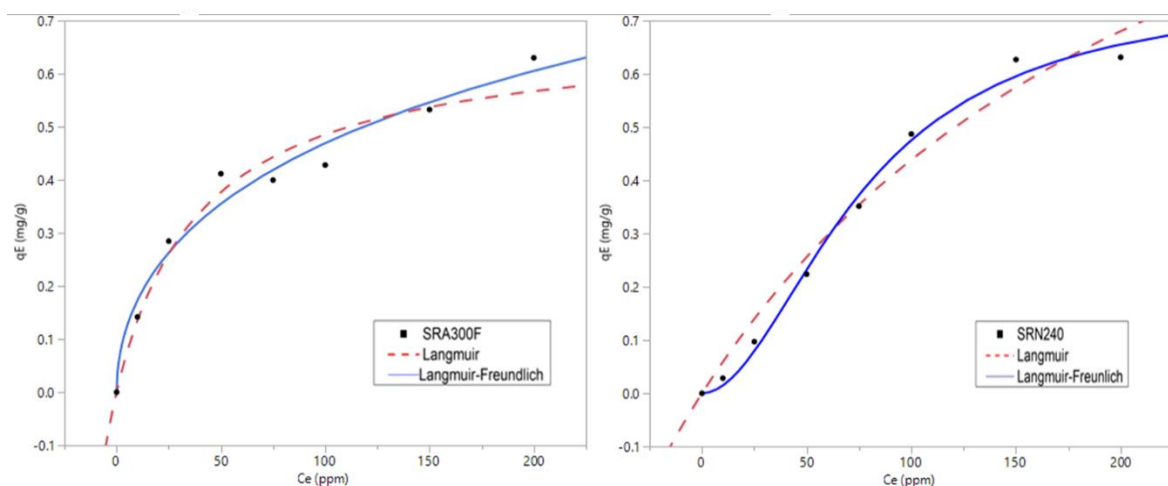
Figure 29 - Adsorption isotherms fittings for SRA300F (left) and SRN240 (right) at pH 4. Estimated fitting parameters associated with Langmuir (dashed line) and Langmuir−Freundlich (solid line) models are listed in Table 2.

Differences in the deposition of SRPs on polyester, at pH 8 and pH 4, were confirmed by comparing the adsorption isotherms for the two polymers. Both at pH 8 (Figure 25) and 4 (Figure 29), the Langmuir-Freundlich model fits the experimental data best, confirming the heterogeneity of the deposition sites on the surface of the fabric. Moreover, by comparing the fitting parameters obtained for the two models (Table 2), at the two values of pH, it is evident that lower pH values lead to a lower affinity for the polyester with the non-ionic SRN240, whereas it enhances the deposition of the anionic SRA300F.The affinity constants for the two polymers can be calculated as mth root of the fitting parameter $K,$ found by fitting the data to equation 48. The affinity constant of SRN240 towards polyester decreases from $(9.0 \pm 0.2) \times 10^{-5}$ at pH 8 to $(2.5 \pm 0.2) \times 10^{-5}$ at pH 4, reflecting lower affinity of SRN240 to the polyester, which is more hydrophilic at this pH. Instead, the binding constant of SRA300F significantly increases from $(1.6 \pm 0.2) \times 10^{-4}$ to $(3.8 \pm 2) \times 10^{-2}$ at pH 4, which confirms lower electrostatic repulsion between the polymer and the fabric surface at low pH. Furthermore, the heterogeneity index m for SRA300F moves from 1 (pH 8) to 0.5 (pH 4). The decrease in m as the pH decreases suggests that there is negative cooperativity in the deposition of SRA300F chains on the polyester, which means that binding of SRA300F to polyester surface is more difficult when SRP is already bound to the polyester, probably as a consequence of the stronger electrostatic repulsion between the polymer units.

Table 2 - Fitting parameters obtained by fitting adsorption isotherms for SRA300F and SRN240 on polyester at pH 8 and 4 with Langmuir and Langmuir-Freundlich models.

	SRA 300F		SRN240	
	Langmuir			
	pH 8	pH 4	pH 8	pH 4
Q_{sat} (mg/g)	1.0 ± 0.3	0.68 ± 0.05	$(7.3 \pm 1.1) \times 10^{-1}$	1.5 ± 0.4
K (ppm)	$(5.0 \pm 0.2) \times 10^{-3}$	$(25 \pm 6) \times 10^{-3}$	$(6 \pm 4) \times 10^{-2}$	$(4.1 \pm 1.4) \times 10^{-3}$
	Langmuir-Freundlich			
	pH 8	pH 4	pH 8	pH 4
Q_{sat} (mg/g)	$(5.3 \pm 0.4) \times 10^{-1}$	1.41 ± 0.17	$(6.0 \pm 0.2) \times 10^{-1}$	0.75 ± 0.06
K (ppm)$^{-m}$	$(1.6 \pm 0.2) \times 10^{-4}$	$(3.8 \pm 2) \times 10^{-2}$	$(9.0 \pm 0.2) \times 10^{-5}$	$(2.5 \pm 0.2) \times 10^{-5}$
m	2.1 ± 0.4	0.5 ± 0.3	3.6 ± 0.9	1.9 ± 0.2

3.4 Hydrophilization of polyester via PEG-POET SRPs

The contact angle of water, on untreated and SRP-treated polyester, was measured across time. In Figure 30a, a comparison between the initial contact angle of polyester and SRP-treated polyester is shown. The initial water contact angle (WCA) of untreated polyester was found to be 117 ° (Figure 30b), which is in line with literature values[126] and confirms the hydrophobicity of PET. The initial contact angle of water on polyester changes dramatically when SRPs are deposited, confirming hydrophilization of polyester due to the surface modification. Between the two SRPs, SRN240 leads to a lower initial WCA than SRA300F. Moreover, a faster decrease of contact angle value across time and lower wicking time were observed on polyester modified with SRN240, which suggests that SRN240 hydrophilizes polyester more than SRA300F. Indeed, the non-ionic SRP increases the wicking speed of polyester three times more than the anionic SRA300F, despite the lower hydrophilicity due to the absence of

sulfonate groups, and this can be justified by the higher efficiency of deposition of SRN240 on polyester.
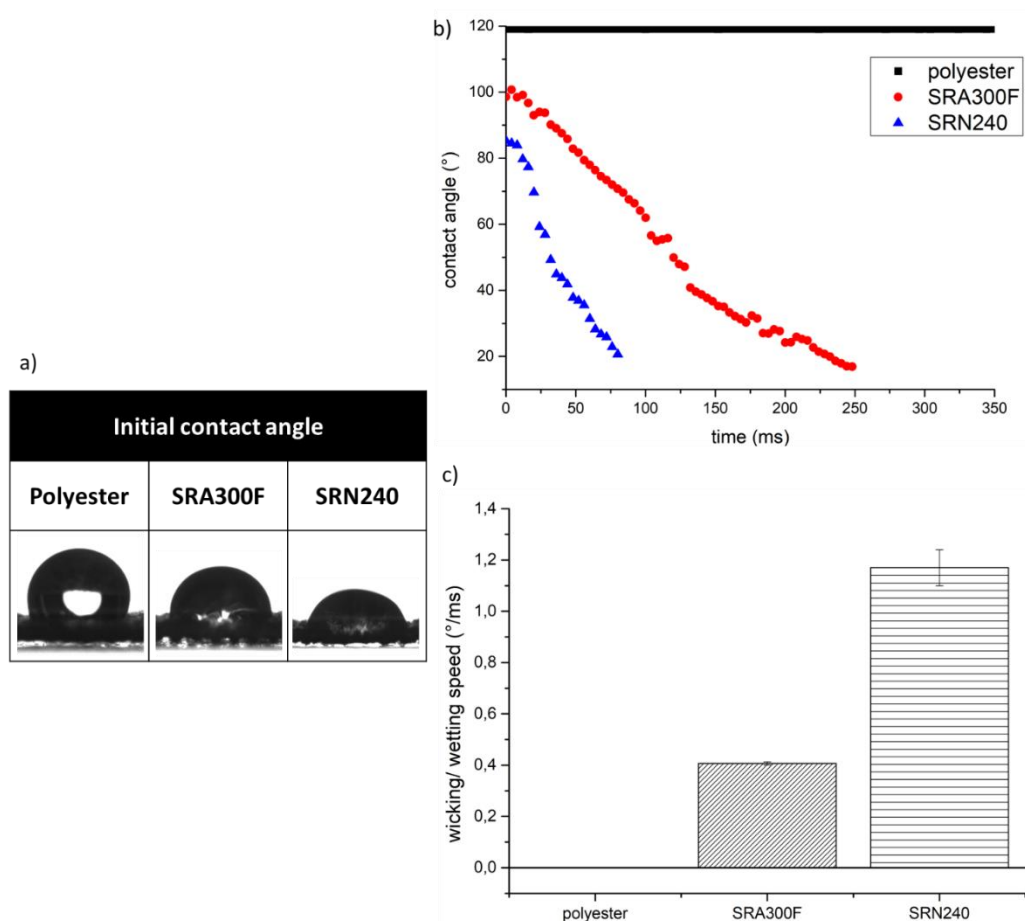
Figure 30 – a) initial water contact angle for untreated polyester and polyester treated with SRA300F and SRN240. The contact angle measurements were run using DI water, dispensed with a dosing rate of 2 μL/s and with a drop volume of 12.5 μL. The measurements were run at 25 °C under humidity control. b) diagrammatic representation of water contact angle measured across time for untreated and SRPs treated polyester. The values are an average of 10 replicates and a fast speed camera was used, using 250 Hz as frequency of acquisition. c) wicking and wetting speed of water by untreated and SRPs treated polyester, obtained as absolute value of the slope in the linear fitting of the contact angle vs time plot.

3.5 Effect of PEG-POET SRPs on surface roughness

SEM pictures of untreated and SRP-modified polyester were acquired after metallization with palladium. Differences in fabric morphology were observed, even at low magnification (Figure 31), with a change of roughness of the fibre surface versus unmodified polyester. However, in the same picture some nonhomogeneous areas were detected, probably due to unmodified areas of the fabric. The deposition seemed more homogeneous on the fibers for SRA300 (Figure 31e), which suggests that

SRA300F is forming a film on top of the polyester, whereas SRN240 might penetrate inside the pores of the fabric. This hypothesis might justify why SRN240 induces a higher wicking speed than SRN240, as shown in section 3.4.
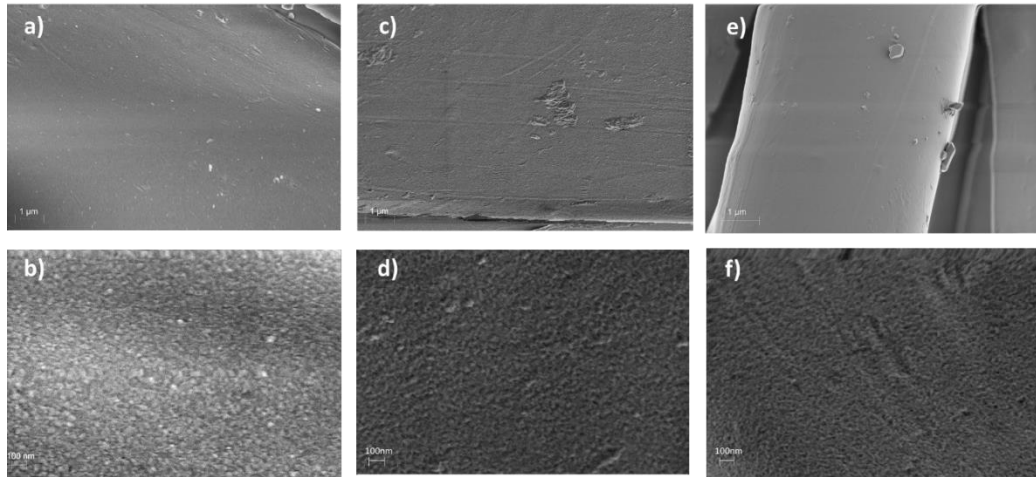
Figure 31 - SEM images of untreated and SRP-modified polyester at 10000× (a, c, e) and 50 000× (b, d, f) magnification. Figures represent untreated polyester (a, b) and polyester pre-treated with SRA300 F (c,d) and SRN240 (e, f). In all cases fabrics have been metalized by electron-beam deposition with palladium.
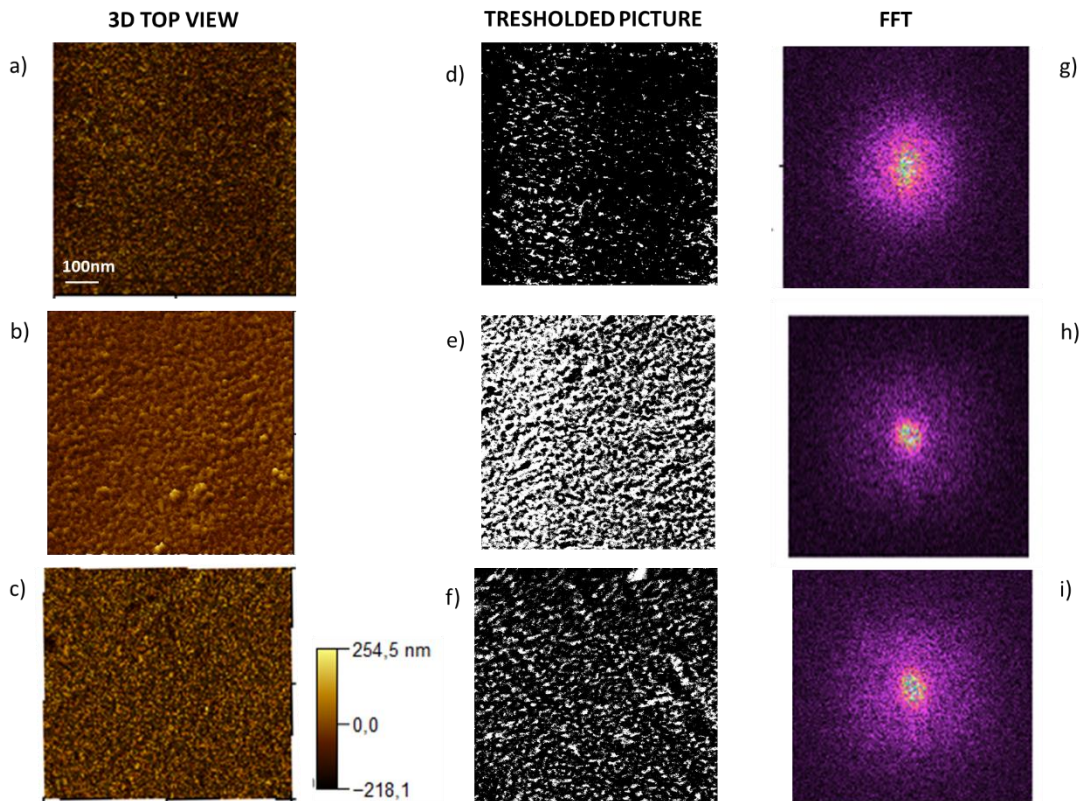
Figure 32 – 3D top view (a,b,c), tresholded image (d,e,f) and Fourier transform (FFT, g,h,i) of the SEM picture for untreated polyester (a,d,g) and polyester modified with SRA300F (b,e,h) and SRN240 (c,f,i)

An estimation of the surface roughness was performed by processing the images at 50000× magnification with the software Gwydion. Changes in the value of root mean square deviation (R_q) confirmed that the SRP deposition had occurred. The R_q value for polyester (calculated by equation 26) is 8.2 ± 0.7, which is lower than the R_q values found for polyester modified by polymer deposition (R_q =14 ± 3 for SRA300F and 10.2 ± 1.4 for SRN240). Therefore, an increase in the surface roughness is observed when the polymer is deposited on the polyester. Moreover, the higher R_q values for SRA300F vs SRN240 seems to confirm that SRA300F sits on the surface of the polyester, whereas SRN240 penetrates inside the pores. In Figure 32e and 32f it is possible to identify darkest and lightest regions on the fabric surface, which represent hard and soft domains of the polymers. The PEG blocks are the soft domains, visible as lighter regions in the picture, whereas the POET blocks are the hard domains, which have the tendency to separate in structures that are more compact (darker areas). A phase separation can be observed on the surface, as the hard and soft block follows a pattern in which characteristic length scales can be observed on the polyester. This can be better assessed analysing the Fourier transforms of the surfaces from the SEM images. The FFT of SRPs treated fabrics show some concentric rings that suggest that the pattern of the polymer is isotropic and that a short-range order and a long-range order can be observed.

3.6 Effect of PEG-POET SRPs on water diffusion

Untreated and SRP-treated polyester fabrics were analysed using diffusion NMR experiments. The signal attenuation, as a function of gradient strength (as explained in section 3.2.7), were fitted to the Stejskal-Tanner equation[114] (equation 29). Two diffusion coefficients were found and their trend versus observation time is presented in Figure 33.
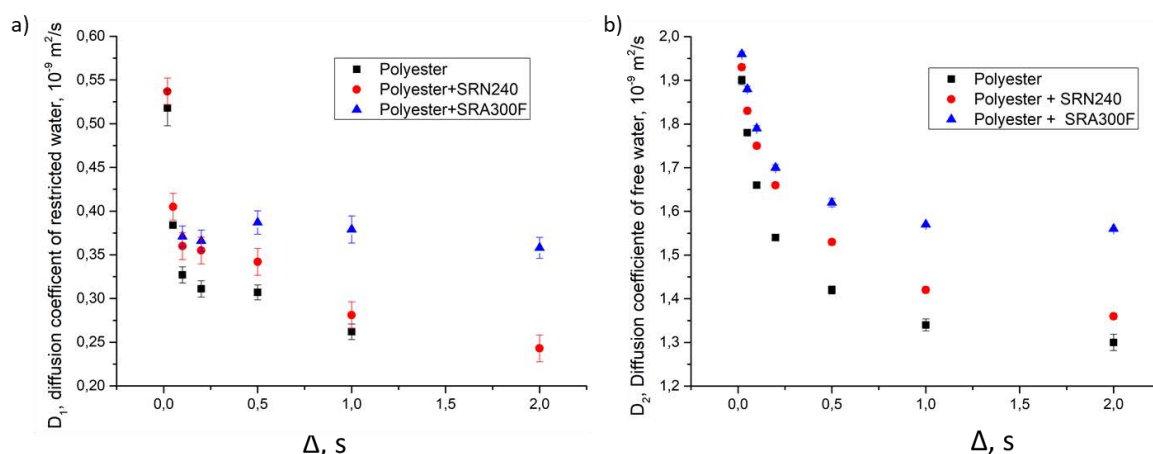
Figure 33 – Self-diffusion coefficients of bulk water (b) and restricted-diffusion water (a), measured by diffusion NMR. The measurements were run at 25 °C on fabrics previously wet with 15 °dH water. The percentages of contribution for each self-diffusion coefficient are expressed in table 3.

Table 3 – Relative contributions for each diffusion coefficient of a fraction of a molecule, diffusing as restricted water (M1) or as free water (M2) for polyester, with and without polymer conditioning.

Δ (s)	Polyester				SRN240				SRA300F			
	D_1 (10^{-9} m²/s)	D_2 (10^{-9} m²/s)	M_1	M_2	D_1 (10^{-9} m²/s)	D_2 (10^{-9} m²/s)	M_1	M_2	D_1 (10^{-9} m²/s)	D_2 (10^{-9} m²/s)	M_1	M_2
0.02	1.90	0.52	0.92	0.08	1.93	0.54	0.92	0.08	1.96	0.56	0.93	0.07
0.05	1.78	0.38	0.92	0.08	1.83	0.40	0.91	0.09	1.88	0.44	0.93	0.07
0.1	1.66	0.33	0.92	0.08	1.75	0.37	0.90	0.10	1.79	0.37	0.93	0.07
0.2	1.54	0.31	0.90	0.10	1.66	0.36	0.88	0.12	1.70	0.36	0.93	0.07
0.5	1.42	0.31	0.86	0.14	1.53	0.34	0.84	0.16	1.62	0.39	0.89	0.11
1	1.34	0.26	0.83	0.17	1.42	0.28	0.82	0.18	1.57	0.38	0.86	0.14
2	1.31	0.24	0.78	0.22	1.36	0.24	0.78	0.22	1.56	0.36	0.82	0.18

Diffusion coefficient D_2 is expected to be associated with water that is diffusing in the space between the yarns of polyester, as it has a comparable value for D as bulk water[127,128]. The second diffusion coefficient, D_1, is due to water that is restricted by the structure of the fabric[129]. Focusing on a single observation time (e.g. Δ = 0.05 s), it can be seen that the restricted diffusion coefficient (D_1 = 0.38 × 10^{-9} m² s⁻¹) is lower than the diffusion coefficient of bulk water (D_2 = 1.78 × 10^{-9} m² s⁻¹). This means that the water is not able to move further than the confined region and it appears to have a slower diffusion coefficient. The area accessible to the diffusion of the water is smaller and the displacement of molecules is smaller, as a consequence. In Figure 33, values for D_1 and D_2 are plotted as a function of the observation time for samples with and without pre-conditioning with SRPs. A decrease in diffusion coefficient with observation time was found, which is typical of porous substrates, where restricted diffusion occurs.[130] In the case of self-diffusion coefficient of bulk water (D_2), it can be

observed that the reduction in diffusion coefficient is more rapid or untreated polyester than polyester modified with SRA300F and SRN240. This confirms that an hydrophilization of the sample occurs when polymers are applied, as it is known that hydrophilic substrates lead to slower short-time dynamics of water molecules[131]. In Figure 33a, D_1 approaches an asymptote for SRA300F more rapidly, with increasing observation time, than SRN240. Also, the value of D at the plateau is higher for polyester, which might be a consequence of a slower rate of exchange between free water and restricted-diffusion water. These observations for SRA300F suggests that water is unable to penetrate inside the fabric mesoporous structure. The more restricted the diffusion coefficient observed for SRA300F is consistent with the formation of a polymer film that covers the polyester surface, as confirmed by the SEM images (section 3.5). In the case of SRN240, the restricted diffusion coefficient is similar to the one measured for SRA300F at short $\varDelta$, reflecting the presence of restricted diffusion due to pore occlusion by the polymer. However, at higher observation times the restricted diffusion coefficient is equal to the one measured for polyester. Considering that there is an exchange between water diffusing as free water and water experiencing restricted diffusion, this suggest that SRN240 fills the pores in the fabric, but does not saturate all the pores because of the low concentration of polymer used in the pre-treatment. As a result, at large observation times the diffusion of water in the unclogged pores is measured and, therefore, D_1 is the same observed for untreated polyester. This is in line with what observed in SEM, where uncovered areas of the fabric were identified in the case of SRN240.

Further confirmation of the different mechanisms for deposition between SRA300F and SRN240 is given by the relative contributions for each diffusion coefficient in the samples analysed. The results are listed in table 3, where M_2 refers to the diffusion of bulk water and M_1 is the weight of the restricted diffusion coefficient. It can be seen that M_1 and M_2 are about the same at all observation times, suggesting that there is almost no exchange between the two diffusion domains. As expected, most of the water is freely diffusing and has a diffusion coefficient comparable with bulk water. By comparing M_2 values for polyester, SRA300F and SRN240, it can be seen that the amount of restricted water is comparable for polyester and SRN240, indicating the presence of unclogged pores in the case of

SRN240 and polyester. Conversely, lower values for M_2 are found for SRA300F, and the difference in values found for polyester and SRN240 increases with observation time. This observation suggests that water diffusion is more restricted in the case of SRA300F, where the polymeric film prevents water accessibility to the pore.

3.7 Effect of PEG-POET deposition on fabric surface area

The adsorption isotherms for polyester, with and without pre-conditioning by SRPs, are shown in Figure 34. Comparing the collected isotherms, with the different IUPAC classified[101] adsorption isotherm types, it can be seen that the isotherms are closest to type V (section 2.8), as they have a nearly horizontal trend across P/P$_0$, which is typical of mesoporous materials. Therefore, this indicates that polyester fabrics are mesoporous and their gas adsorption involves the formation of monolayer/multilayer inside the pores followed by gas-condensation[132]. A similar quantity of gas was adsorbed by untreated and SRA300F-modified polyesters. However, a lower amount of gas was adsorbed by polyester when SRN240 was present, which can be linked to a lower pore volume inside the fabric.
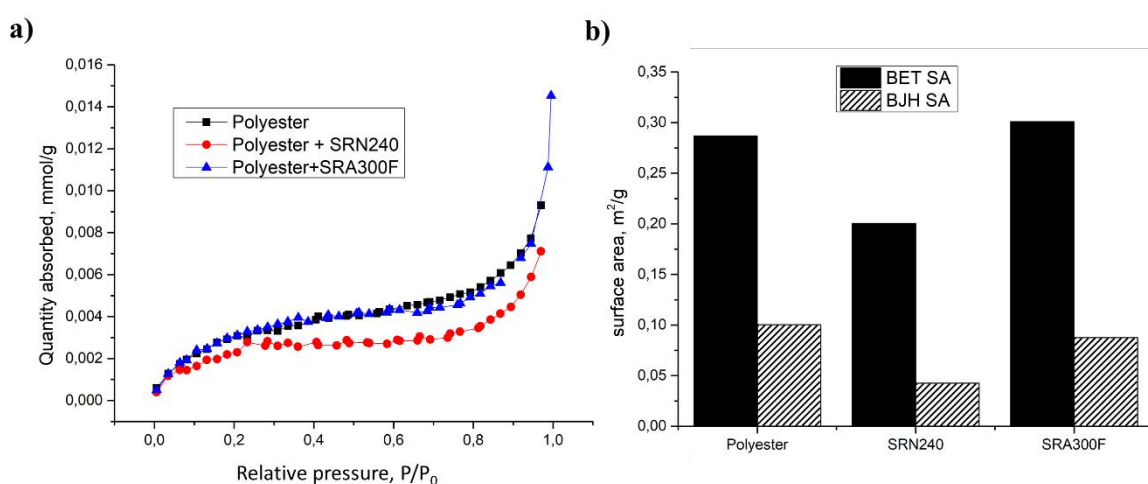
Figure 34 – a) Nitrogen absorption isotherms of untreated polyester (■) and polyester treated with SRN240 (•) and SRA300F (▲). The isotherms were collected using a Micromass 2020N after degassing samples at 40 °C overnight. B) surface area of the fabrics with and without SRPs pre-conditioning calculated by BET (black, solid) and BJH (black, patterned) models.

The surface area (SA) calculated with BET and BJH models are presented in Figure 34a and it can be observed that the area estimated by BET model is bigger than the one estimated by BJH model. This was expected, as BET model does not take in to account interactions occurring between absorbed molecules or heterogeneity of absorption sites[133]. According to Micromass (Waters Corporation, Milford,MA, USA), an accurate measurement of SA requires at least 40 square meters of total surface area in the sample, which would have required 100 g of fabrics for each test. However, the sample tube was able to host only 10 g of fabrics in our test. As a result, the absolute value of SA and pore size cannot be trusted, but a comparison between samples can still be performed.

The SA, calculated by BET and BJH models and shown in Figure 34a, is sensibly small (~0.1 - 0.3 m^2/g). These values were compared to the SA estimation based on fabrics geometry. A value of SA = 0.13m^2/g was calculated for polyester, assuming a fibre diameter equal to 20 μm, a cross sectional area of 314.16 $μm^2$ and a density of the fibre equal to 1.49 g/cm^3 (from the manufacturer). It can be seen that the calculated area is similar to the value obtained by using the BJH model or from literature[36], which suggests that this technique works sufficiently well, despite a loss in resolution. SA values were compared for untreated polyester and modified-polyesters. Results shown that the lowest SA value was obtained for SRN240-modified polyester (0.04 m^2/g). This observation is in line with observations from the diffusion NMR data, indicating a clogging of the pores by SRN240, which leads to pores that are inaccessible to the gas, and hence a lower surface area is detected. The SA for SRA300F (0.08 m^2/g) was lower than the one of untreated polyester (0.10 m^2/g) but higher than the one calculated for SRN240. This is surprising, as it would have been expected that the lowest SA is achieved when SRA300F is deposited on polyester. This observation can be rationalized by considering that SRA300F forms a film onto polyester surface but it has as a low efficiency of deposition. However, further investigation is needed to confirm this hypothesis.

3.8 SRPs interaction with surfactants in bulk

Surface tension was measured on surfactant solutions with and without SRPs. The surfactants analysed were SDS, AE$_3$S, AO, CapAO, LAS and Isalchem. As shown in Appendix I, AE$_3$S and AO have same chain length combination (C$_{12}$-C$_{14}$) but different head group charge at pH 8 (AE$_3$S is anionic, whereas AO is not charged at this pH). Conversely, AO and CapAO, as well as SDS and AE$_3$S, have same head group charge but they differ for the head group size, being the CapAO head group bigger. Moreover, the effect of branching was studied by comparing LAS (50% branched alkyl benzene sulfonate) and Isalchem (95% branched alkyl sulfate) to SDS. First, the *cmc* values for each the surfactant were found (Figure 35) and they are shown in table 4. The *cmc* is lower for surfactants with large head group size because of the lower number of surfactant monomers needed to saturate the air/water interface, as highlighted by the comparison between AO and CapAO. The *cmc* decreases as well when using branched surfactant (Isalchem vs SDS[134]), where the steric hindrance due to the lateral branching leads to a lower packing at the air/water interface.

Table 4 – Critical micellar concentration calculated for surfactants analysed in this work. Measurements were run in replicate at 25 °C, in DI water and at pH 8.

Surfactant	*cmc* (ppm)	Standard deviation (ppm)
AE$_3$S	69.71	0.18
LAS	170.687	0.016
AO	97.02	0.02
CapAO	93.08	0.03
Isalchem	513.799	0.003
SDS	2348.07	0.05
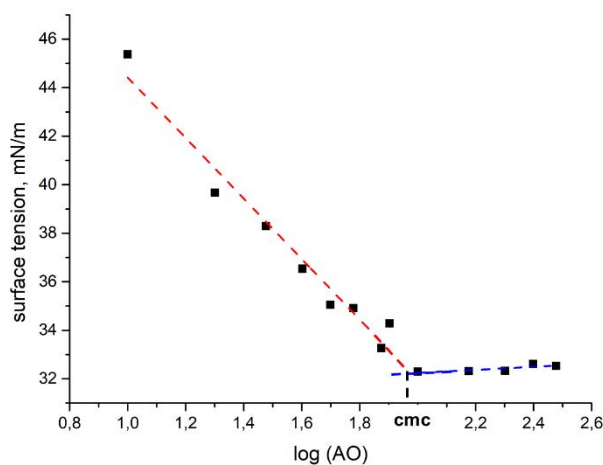
Figure 35 – Surface tension plot versus logarithmic concentration of surfactant for C12-C14 Amine Oxide (pH 8, DI water). Measurement were run in replicates at 25 °C via Wilhelmy method.

The comparison between the curves of surface tension for the surfactant alone and in combination with SRPs at 50 ppm leads to identify which surfactants interacts with the polymers at this concentration. As expected, no interaction was observed between the anionic SRA300F and the negatively charged LAS (Figure 36b) and Isalchem (Figure 36c), which is a consequence of the electrostatic repulsion between surfactant and polymer[55]. Surprisingly, the surface tension values for AE3S in the presence of SRA300F and SRN240 are higher than the one measured for the surfactant alone (Figure 36a). The surface tension values for solution of SRA300F and SRN240 at 50ppm are (60.15 ± 0.12) mN/m and (58.34 ± 0.09) mN/m respectively, which are close to the surface tension measured in the case of the AE_3S/SRP system at the lowest surfactant concentration. Therefore, it can be deduced that initially only SRPs are at the air/water interface and then, progressively, also surfactant monomers go at the interface, lowering the surface tension. Moreover, the surface tension at the plateau is still higher for the AE_3S/SRP system versus pure AE3S, which suggest that polymers lie at the air/water interface even after that surfactant reaches the *cmc*. Most likely, no interaction between the polymers and the surfactant can be hypothesised as a consequence. As for AE_3S, the surface tension measured at low SDS concentration is close to the one of pure SRP solution, suggesting the presence of the polymer at the air/water interface

(Figure 36f). As the surfactant concentration increases, the surface tension curve becomes closer to the one of pure SDS. In the case of SRA300F, the curves of pure surfactant and surfactant in combination with SRPs almost overlap, suggesting no meaningful interactions, whereas a very weak interaction is found for SRN240, as expected.
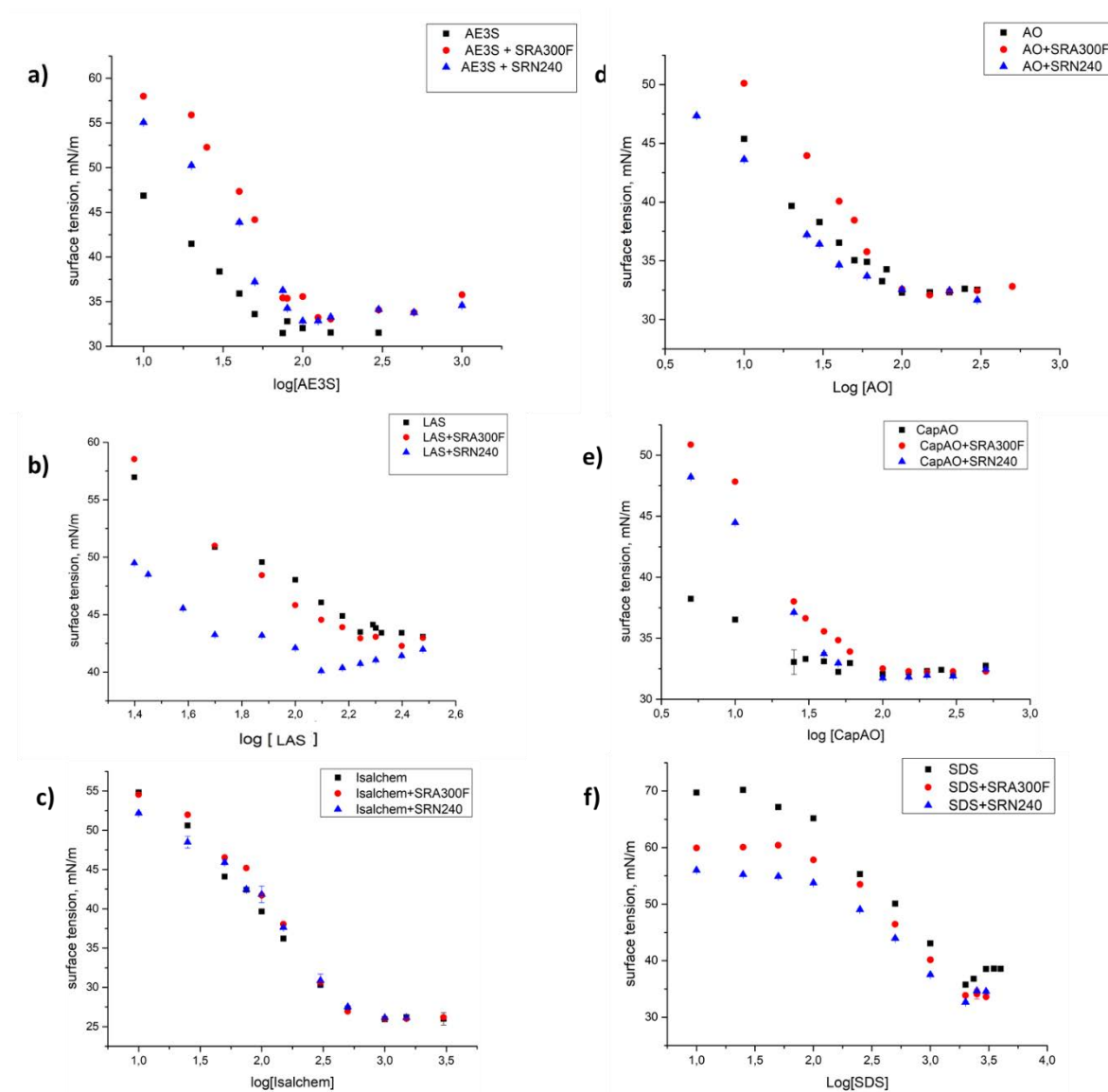
Figure 36 – Surface tension plot versus logarithmic concentration of surfactant for AE₃S (a), LAS (b), Isalchem (c), AO (d), CapAO (e) and SDS (f) at pH 8 in DI water. The measurements were run in replicates for surfactant on its own (□) and in the presence of SRA300F (•) and SRN240 (Δ) at 25 °C via Wilhelmy method.

In the case of CapAO (Figure 36e), surface tension of polymer-surfactant mixture is higher than the one of pure surfactant solution. In this case, differences were observed between SRA300F and SRN240. For SRN240, the curve in combination with the SRP overlaps with the one of CapAO after the *cmc* of

the surfactant, which indicates that the higher surface tension is due to the presence of the SRP at the air/water interface but there is no interaction between the surfactant and the polymer, as expected in the case of non-ionic polymer and not-charged surfactant[135]. Instead, an inflection point was found in the case of SRA300F for a CapAO concentration of 40 ppm (*cac* of our system), suggesting the absorption of surfactant hemimicelles along the polymer chain. The *psp*, which is the surfactant concentration at which all the available domains of the polymer are saturated by the surfactants, is close to the *cmc* of pure surfactant. This is a consequence of the weak interaction between an anionic polymer and a non-charged surfactant. A similar scenario was observed when combining LAS and SRN240. In this case, the surface tension in presence of the SRP is lower than the value of surface tension measured for the surfactant alone, which reflects an interaction between the surfactant and the polymer[54,136]. The *cac* for a mixture of LAS-SRN240 was found to be 50 ppm, while the *psp* is reached for a LAS concentration equal to 125 ppm. After the *psp*, an increase of the surface tension values as surfactant concentration increase was found and the curve overlaps to the one of pure LAS for a high surfactant concentration. This is driven by saturation of air/water interface with LAS monomers and LAS micelles formation. No interaction was observed between the SRN240 and AO, as they are both not electronically charged, whereas AO interacts with SRA300F. The interaction starts around 50 ppm, as in the case of CapAO, due to the similar structure of AO and CapAO. The last case is represented by Isalchem, which does not interact either with SRA300F and SRN240. This result was expected for SRA300F, as both surfactant and polymer are negatively charged. However, a weak interaction would have been expected for the non-ionic SRN240. An explanation of this behaviour can be given by the high branching level of Isalchem which inhibits the formation of the surfactant hemimicelles along the polymer chain.

3.9 Conclusions

In this chapter, an understanding of the efficiency of deposition on cotton and polyester for PEG/POET SRPs as a function of pH, water hardness, agitation and SRPs concentration was found. Use of streaming potential and UV/vis measurements highlighted that SRA300F and SRN240 are effective in modifying polyester but not cotton. SRN240 was found to have a higher deposition efficiency on

polyester than SRA300F at pH 8, which is probably related to the electrostatic repulsion between polyester and SRA300F, both negatively charged. This hypothesis seems confirmed by the increase in amount of SRA300F deposited when water hardness is present, whereas no enhancement in deposition was observed for SRN240 in the same conditions. Use of pH 4 during the pre-conditioning of fabrics leads to higher amount of SRP deposited on polyester than at pH 8, while no effect of agitation on percentage of the two SRPs deposited was found, as expected.

The kinetics of deposition was assessed by use of UV/vis and results showed that use of pH 4 and higher agitation speed during the conditioning of fabrics increases rate of deposition for both SRA300F and SRN240. Instead, the presence of hardness in the water only improves the rate of deposition in the case of SRA300F, as a consequence of lower electrostatic repulsions between SRP and polyester.

Adsorption isotherms were found to fit a Langmuir-Freundlich model and the binding constants are higher at pH 4 than 8, confirming the enhanced deposition at low pH for the two SRPs on polyester.

The contact angle of water on fabrics, with and without pre-conditioning with PEG/POET SRP, was measured, highlighting the hydrophilization of polyester as a consequence of SRPs deposition. On the same fabrics, SEM showed changes in roughness of the fabric as a consequence of polymer deposition. SRA300F was found to form a more homogenous layer when deposited, suggesting formation of a film on top of the fabrics, whereas SRN240 exhibits uncovered areas of the fabric, in spite of its higher efficiency of deposition. A mechanism based on pore clogging was hypothesised for SRN240, as a consequence. The self-diffusion coefficient of water, measured via diffusion NMR, confirmed the hypothesis, as a more restricted diffusion was observed on polyester modified via SRA300F, whereas a diffusion coefficient closer to untreated polyester was found for SRN240, as some of the pores are unclogged and accessible to water.

The interactions of PEG/POET SRPs with surfactants in bulk was assessed via surface tension measurements. Similar interactions were observed between the two SRPs and AE$_3$S and SDS, being

SRPs initially at the air/water interface and little by little substituted by surfactant monomers as surfactant concentration increases. No interaction between SRPs and surfactants was hypothesised in this case. In the same way, no interaction was found to occur between Isalchem and SRA300F and SRN240. Instead, LAS showed interactions with SRN240 but not with SRA300F, as expected in the case of an anionic surfactant-anionic polymer system. Conversely, the amphoteric AO and CapAO, which are not-charged at the pH of analysis, showed interaction with SRA300F, whereas no meaningful interaction was found with SRN240.

Chapter 4. PEG-4-MEMA/METAC SRPs

4.1 Introduction

In Chapter 3, the mechanism behind the deposition of PEG-POET SRPs was investigated, highlighting the effect of water hardness, agitation speed and pH on efficiency of deposition of SRPs on polyester. It was found that this class of SRPs is not suitable to modify cotton fabrics, probably as a consequence of the high hydrophobicity of the polymers or electrostatic repulsion between cotton surface and the polymer, in the case of anionic SRP. Therefore, an alternative class of SRPs, which can deposit on cotton, was investigated. Polyethylene glycole-4-Methoxyethyl methacrylate/ 2-(Methacryloyloxy) ethyl trimethylammonium chloride (PEG-4-MEMA/METAC) SRPs are positively charged, which suggests that they may deposit on cotton as a consequence of electrostatic attraction to the hydroxyl groups present in cotton.

In this chapter, streaming potential was used to assess the deposition of PEG-4-MEMA/METAC SRPs on cotton and polyester, as a function of pH. When deposition occurred, an estimation of the efficiency of deposition of each SRP on fabrics was made via thermal gravimetric analysis, as a means of judging the effect on deposition of different ratios of PEG-4-MEMA and METAC. As in the case of PEG-POET SRPs, the interactions between PEG-4-MEMA/METAC SRPs and some common surfactants were investigated in bulk via surface tension measurement. The final aim of these measurements was to assess which SRPs have higher chance to interact with surfactants during the wash.

4.2 Experimental

4.2.1 Polyethylene glycole-4-Methoxyethyl methacrylate/ 2-(Methacryloyloxy) ethyl trimethylammonium chloride soil release polymers

The second class of SRPs analysed in this works is obtained by copolymerization of poly (ethylene glycol) methyl ether methacrylate (PEG-4-MEMA) and [2-methacryloxy]ethyl] trimethyl ammonium chloride (METAC) block copolymer structure (Figure 37a) and they are commercialized as Sokalan polymers from BASF (Germany). The structure feature of the three polymers used in this work is

presented in Figure 37b, where it could be observed that 65/35 PEG-4-MEMA/ METAC (listed as A in the table) and 40/60 PEG-4-MEMA/ METAC with low molecular weight (listed as B in the table) have similar molecular weight, but they differ because of the different ratio between the two blocks, being A more hydrophobic than B. On the other hand, PEG-4-MEMA/ METAC with high molecular weight (listed as C in the table) has the same ratio between the two monomers but higher molecular weight than B.

name	% PEG-4-MEMA (Mol%)	METAC (Mol%)	M_w (kDa)
A	65	35	147.1
B	40	60	132.4
C	40	60	969.4

Figure 37 – a) chemical structure of poly (ethylene glycol) methyl ether methacrylate (PEG-4-MEMA) and [2-methacryloxy]ethyl] trimethyl ammonium chloride (METAC) used as monomers for the synthesis of the block copolymers analysed in this work. b) Molar ratio between the PEG-4-MEMA and METAC content and molecular weight of the three polymers analysed in this work.

4.2.2 Fabrics pre-conditioning with PEG-4-MEMA/METAC SRPs and streaming potential analysis

Swatches of polyester and cotton, purchased from WFK Testgewebe GmbH, were pre-treated in a tergotometer with SRPs solution at 35 °C, keeping the ratio of polymer solution to fabric equal to 24. The SRPs solutions were prepared by dilution of a stock solutions of SRP A, B and C at a concentration of 5000 ppm in Milli-Q water. A final SRP concentration of 50 ppm was used for conditioning the fabrics and the pH was adjusted by adding HCl or NaOH. The SRPs-treated fabrics were dried overnight at (20 ± 2) °C and at a relative humidity (RH) of 50%. Polymer concentrations between 10 and 200 ppm were used to assess the effect of SRP concentration on the surface zeta potential of polyester, as done for PEG-POET SRPs (section 3.3.3).

Polyester and cotton fabrics, cut in 5 × 5 cm^2 pieces and washed in DI water at 60 °C for 30 minutes, were washed with SRPs solution in tergotometer. The conditions of the pre-treatment were the same used for PEG-POET SRPs (section 3.2.3), where an agitation speed of 200 rpm and 35 °C were used for all the tests. The effect of pH on deposition was assessed by using pH 4 and pH 8 during polyester

pre-conditioning. For the adsorption isotherms, concentrations of the polymers between 25 and 200 ppm of SRP were used. For streaming potential analysis, the conditions used were the same used for fabrics pre-treated with PEG-POET SRPs (section 3.2.3).

4.2.3 Thermal gravimetric analysis of fabrics

A Perkin Elmer Pyris 1 TGA was used for running thermal gravimetric analysis of SRP samples and of polyester fabrics. In the case of TGA analysis of pure polymer, 5 mg of SRP were weighted in the platinum pan. Instead, for TGA analysis of fabrics, swatches of polyester, previously washed with SRPs solution at 50 ppm at pH 8 (as explained in section 4.2.2), were cut in small pieces (about 0.5×0.5 cm^2) and placed in a desiccator overnight. The samples were transferred to a platinum pan, which was then inserted in the furnace of the TGA instrument and a nitrogen flow of 20 mL/min was used to fill the furnace. The initial weight of the sample was measured, where the mass used for the analysis was usually around 5 mg, and a thermal ramp was applied. For our tests, a ramp from 30 °C to 700 °C was applied, using a heating rate of 10 °C/min. The software used for analysing the TGA data was Pyris.

4.3 Deposition of PEG-4-MEMA/METAC SRPs

4.3.1 Streaming potential measurements of fabrics modified via PEG-4-MEMA/METAC block copolymers at pH 8

Streaming potential measurements of untreated and SRPs-treated polyester fabrics are shown in Figure 38 and a shift of the zeta potential (ZP) of the polyester to positive values was found when the SRPs are present (Figure 38). This shift indicates that deposition of PEG-4-MEMA/METAC block copolymers occurs on polyester. Sign reversal for zeta potential values was measured on SRP-treated polyester which is in line with literature[137], where positive surface charge is expected even for low concentration of cationic actives on hydrophobic surfaces because of their high deposition. The zeta potential of SRPs in solution was measured via light scattering and it was found to be (18.0 ± 0.4) mV for A, (18.8 ± 0.5) mV for B and (15.0 ± 0.2) mV for C. Since all the analysed PEG-4-MEMA/METAC polymers are positively charged, the efficiency of deposition can be determined by comparing the surface zeta-potential of the fabrics with the zeta-potential for the SRP in solution. The closer the two

values of zeta potential, the higher the efficiency of deposition. By comparing zeta potential in solution and on fabrics, it was found that polymer B (ZP = 16 mV) has the best efficiency of deposition among the analysed SRPs, followed by polymer C (ZP = 7 mV) and polymer A (ZP = 9 mV). This suggest that a better efficiency of deposition is achieved for higher content of METAC, probably because a 40:60 ratio for PEG-4-MEMA:METAC leads to the optimum hydrophobicity for depositing onto a polyester surface.
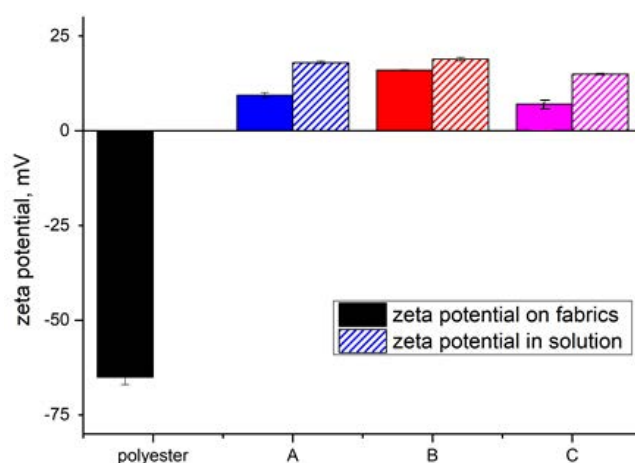
Figure 38 - Zeta potential values of polyester fabrics untreated or pre-treated with SRPs at pH 8 in tergotometer (solid fill). The values are the average between three replicates for three different samples. The surface zeta potential of the fabrics is compared to the zeta potential of the SRPs in solution in the same condition (patterned bars).

Deposition of PEG-4-MEMA/METAC block copolymers on cotton was investigated via streaming potential analysis of untreated and SRP treated cotton in order to compare the results with deposition data on polyester. Cotton has hydroxyl groups which are expected to induce electrostatic attraction between the fabric surface and the cationic SRPs, leading to deposition. However, very small differences were observed between the zeta potential values of untreated cotton and SRPs-treated cotton both at pH 4 and pH 8 (Figure 39). This suggests that there is poor deposition of these class of SRPs on cotton, probably because of the hydrophobicity of the polymer due to the PEG-4-MEMA content.
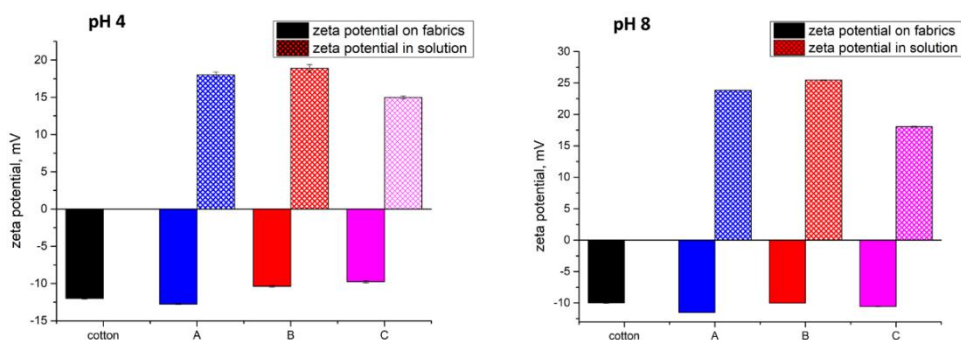
Figure 39 – Zeta potential values of untreated and SRPs-modified cotton (solid fill) at pH 4 (on the left) and pH 8 (on the right). The values are the average between three replicates for three different samples. The surface zeta potential of the fabrics is compared to the zeta potential of the SRPs in solution in the same condition (patterned bars).

As already shown for PEG-POET SRPs in section 3.3.1, an estimation of the amount of the polymer deposited onto polyester has to be done to confirm the hypothesis about the effect of METAC content on deposition. However, PEG-4-MEMA/METAC polymers are not UV/vis active, therefore the absorbance in solution cannot be used to indirectly quantify the amount deposited. For charged SRPs, the depletion in solution conductivity can be used to quantify the amount of polymer deposited on fabrics. Notwithstanding, conductivity measurements are challenging in this case as fabrics release fibres and fabric-finishes during the pre-treatment, even after fabric boiling step. Background conductivity measured on pure polyester was found not constant, as it depends on the specific piece of fabric used in the pre-treatment, therefore it cannot be subtracted from the overall measurement. As a result, an alternative way to estimate the amount of polymer deposited on the fabric was found which is based on the use of TGA.

4.3.2 Thermal gravimetric analysis of polyester modified with PEG-4-MEMA/METAC block copolymers

The thermal gravimetric analysis (TGA) were initially performed on untreated polyester, and the resulting thermogram is shown in Figure 40a. A step in the thermogram corresponds to a mass loss as result of temperature increase. In the case of untreated polyester, a single mass loss was observed in the thermogram, which corresponds to the decomposition of polyester fabric and release of volatile gas, as already reported in literature[138,139]. The temperature of decomposition was found to be 421 °C and the

residual weight percentage after decomposition was 15%, both values in line with literature values[138].

The TGA was run on pure SRPs to assess thermal degradation experienced by the polymers in the same temperature range (Figure 40b). The thermogram of PEG-4-MEMA/METAC 65:35 (called A, for simplicity) shows three mass losses. The first mass loss corresponds loss of water, which was expected as the PEG-4-MEMA/METAC SRPs are sold as 40% solution in water. The second mass loss, which melting temperature is 285.06 °C, is related to the melting of the METAC blocks [140,141], while the melting of the PEG-4-MEMA unit occurs at higher temperature[142] (usually methyl methacrylate melts around 400 °C).
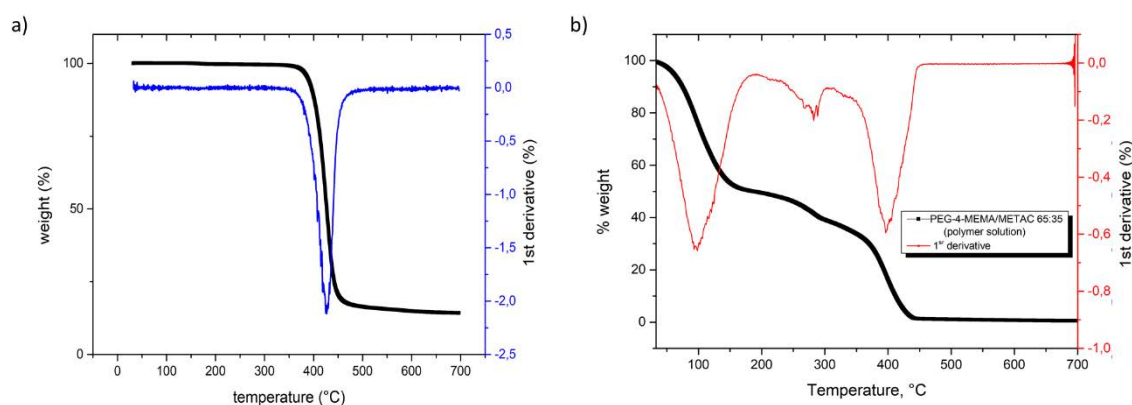
Figure 40 – a) Thermogram (black) and its 1st derivative (blue) for sample of untreated polyester. The TGA was run in presence of nitrogen between 30 and 700 °C using a heating rate of 10 °C/min; b) thermogram (black) and its 1st derivative (red) for a sample of PEG-4-MEMA/METAC 65:35. The conditions for the TGA were the same used for polyester.

Table 5 – List of TGA parameters calculated for untreated polyester and for polyester modified with the PEG-4-MEMA/METAC block copolymers. Melting temperature and mass losses were calculated from the thermograms, while full width at half maximum (FWHM) and area were obtained by the 1st derivative of the thermograms. The standard deviation, not shown in the table, was always lower than 10%.

	$T_{m\,1}$ °C	$T_{m\,2}$ °C	Δm_1 %	Δm_2 (%)	A_1	$FWHM_1$	A_2	$FWHM_2$	Ratio A_2/A_1
Polyester	421	/	84	/	83.98	33.9	/	/	/
PEG-4-MEMA/ METAC 65:35	415	587	87	12	83.98	34.18	11.96	52.50	0.138
PEG-4-MEMA/ METAC 40:60 low Mw	422	599	86.6	12.6	86.40	35.14	12.66	55.88	0.147
PEG-4-MEMA/ METAC 40:60 high Mw	422	601	86	12.82	85.95	86.45	35.28	12.04	0.140
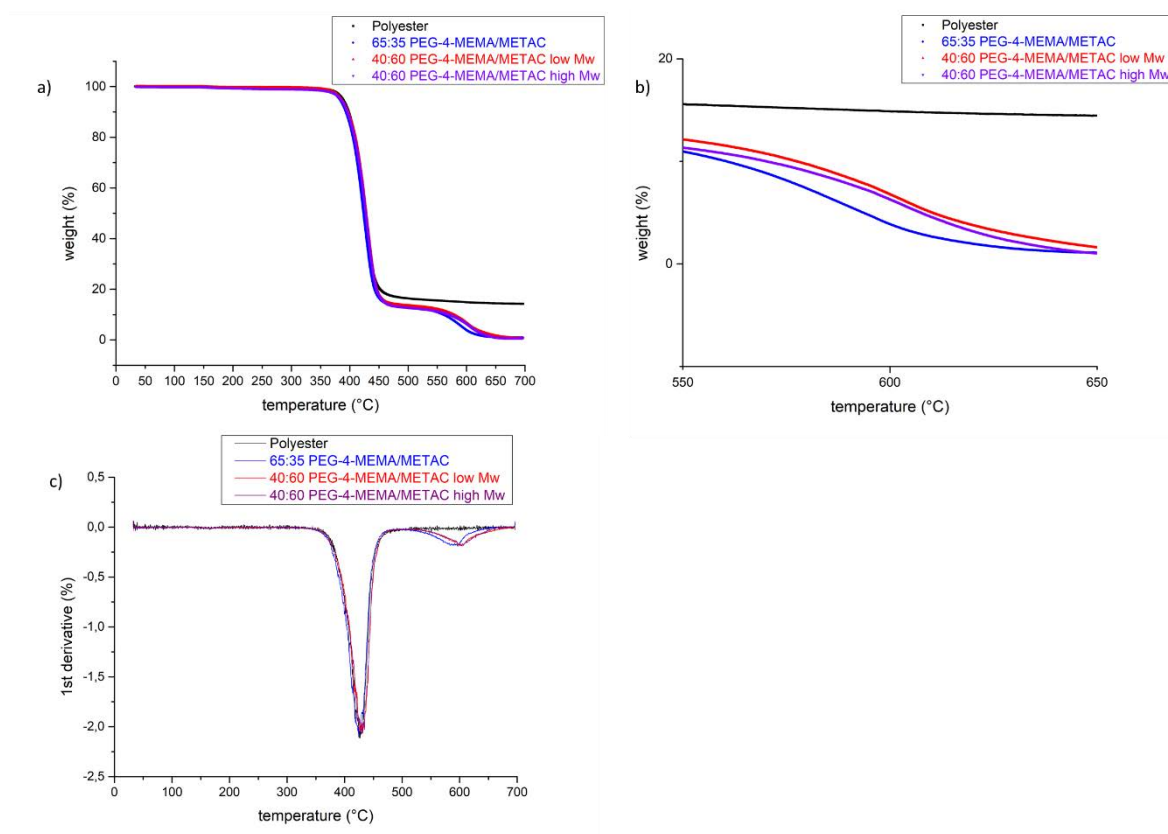
Figure 41 – a) Thermogram of untreated (black) and SRPs treated polyester exposed to a heating ramp between 30 and 700 °C in presence of nitrogen. b) Magnification of the thermograms at the METAC melting point; c) Magnification of the thermograms between 550 and 650 °C, temperature range for the curing of the polyester with SRPs.

The comparison between the thermograms of polyester and SRPs-treated polyester is shown in Figure 41a. The mass loss occurring at about 420 °C is higher for the fabric pre-conditioned with SRPs compared to untreated polyester. This may be explained by suggesting that, perhaps, at this temperature both polyester and polymer undergo decomposition, therefore the higher mass loss is related to the degradation of both. Moreover, a small shift of the T_m to lower temperature was observed when the polymer is present, which means that the polymer decreases the thermal stability of polyester. However, a second mass loss appears in the sample pre-treated with the PEG-4-MEMA/METAC copolymers. As this decomposition is not typical of the polymer or of the fabric, we hypothesis that it has to be related to the interactions between the polymer and the fabric, where the adsorption of the polymer on the fabric leads to easier thermal degradation of the polyester and release of volatile components. This mass loss seems to be strictly related to the structure of the SRPs, as both polymer B and C have the same decomposition temperature (Figure 41b) which is higher than the one experienced by polyester pre-

treated by polymer A. A higher $T_{m\,2}$ was found for SRPs with higher METAC content (B and C) and might be related to the lower number of PEG-4-MEMA units involved in the interaction with the polyester, resulting in higher thermal stability of the sample. The first derivative of the thermograms was calculated to quantify the area associated to each thermal degradation, where the ratio between the area associated to the two peaks can be used as a semi-quantitative indication of the amount of polymer deposited. The ratio is shown in table 5 and the higher ratio A_2/A_1 was observed for polyester pre-treated with PEG-4-MEMA/METAC 40:60 with low molecular weight (B). This output confirms that, in line with streaming potential results, polymer B has the highest efficiency of deposition on polyester at pH 8 and that C has higher efficiency than A.

4.3.4 Effect of pH on polyester conditioning via PEG-4-MEMA/METAC block copolymers

Deposition of PEG-4-MEMA/METAC block copolymers onto polyester was carried at pH 4 to assess the effect of pH on deposition. The modified fabrics were analysed in streaming potential and zeta potential of the fabrics measured at pH 4 was compared to the zeta potential of SRPs in solution at the same pH, as shown in Figure 42. The zeta potential measured for polyester pre-treated with SRPs is more positive than zeta potential measured in solution for the same polymer. The excess of surface charge detected might be related to the change in the SRP conformation when deposition occurs. Indeed, SRPs are usually presented as polymer coil in solution, where only few of the positive amine groups are exposed, contributing to the zeta potential of the polymer in solution. The deposition of the polymer induces an unfolding of the polymer coil, therefore more amine groups are exposed and contribute to the zeta potential charge of the treated polyester. As a result, the surface charge is more positive than the zeta potential of the polymer in solution.
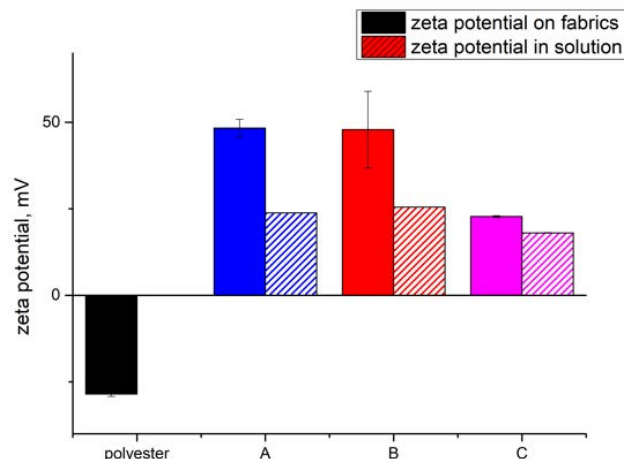
Figure 42 - Zeta potential values of untreated or SRPs-treated polyester fabric at pH 4 (solid fill). The values are the average between three replicates for three different samples. The surface zeta potential values of fabrics are compared to the zeta potential of the SRPs in solution in the same condition (patterned bars).

Measurements of zeta potential and size of the polymer in solution at different pH were performed to proof this hypothesis and they are shown in Figure 43. It can be seen that the PEG-4-MEMA/METAC SRPs experience a change in size in addition to a change in zeta potential as a function of pH, confirming that these polymers can uncoil in different conditions.

Deposition was observed for all the SRPs, where A and B have higher efficiency of deposition than D. As mentioned before, at this pH the polyester is less hydrophobic, therefore deposition of PEG-4-MEMA/METAC polymers is most likely driven by the electrostatic attractions between OH$^-$ ions on polyester and the polymer. As the ZP of SRPs in solution is 23.82 mV for A, 25.47 mV for B and 18.05 mV for C, the higher efficiency of deposition for A and B can be justified considering a stronger electrostatic attraction with polyester surface.
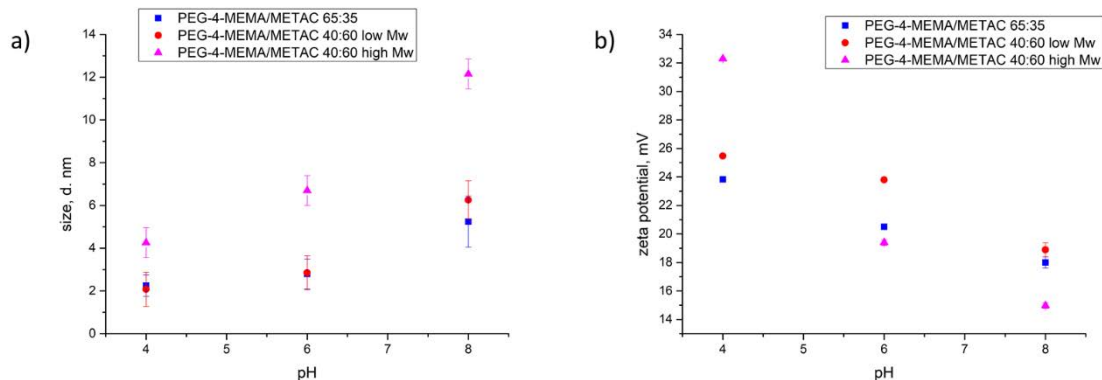
Figure 43 – Size (a) and zeta potential (b) of the PEG-4-MEMA/METAC polymers in solution at different pH, measured via light scattering. The measurements were run at 25 °C after trimming the solution to the desired pH with NaOH and HCl 0.05N.

4.4 SRPs interaction with surfactants in bulk

Surface tension measurements were used to assess interactions between PEG-4-MEMA/METAC block copolymers and surfactants at pH 8, as shown for PEG/POET SRPs in section 3.4. The surface tension of the PEG-4-MEMA/METAC polymers was found to be (58.01 ± 0.11) mN/m for A, (63.78 ± 0.09) mN/m for B and (60.51 ± 0.08) mN/m for C, and therefore lower than the one of pure water (72.80 ± 0.05) mN/m [143]. The amphoteric surfactants are expected to interact the least with the cationic polymers, as only hydrophobic interactions between surfactant tails and hydrophobic domains of the polymer occur in this case. This was confirmed by measuring surface tension of AO and CapAO in combination with SRPs. In the surface tension plot of AO (Figure 44d), three main areas can be identified. Initially, the surface tension of SRP-surfactant mixture is higher than the one of the pure surfactant, reflecting the formation of monolayer of the polymer and surfactant monomers at the air/water interface [144]. As surfactant concentration increases, a decrease in surface tension is observed due to higher number of surfactant monomers at the air/water interface. The *cac* is reached for a surfactant concentration around 40 ppm for the three SRPs, where the surface tension variation is null or poor due to the interactions between the polymer and the new surfactant monomers added. After *cac*, surface tension decreases and reaches the same plateau of pure surfactant system. The *psp* of the polymer (150 ppm) is slightly higher than the *cmc* of pure surfactant (about 90 ppm), as a higher concentration of surfactant monomer is required to form pure surfactant micelles after that mixed polymer-surfactant micelles are formed.
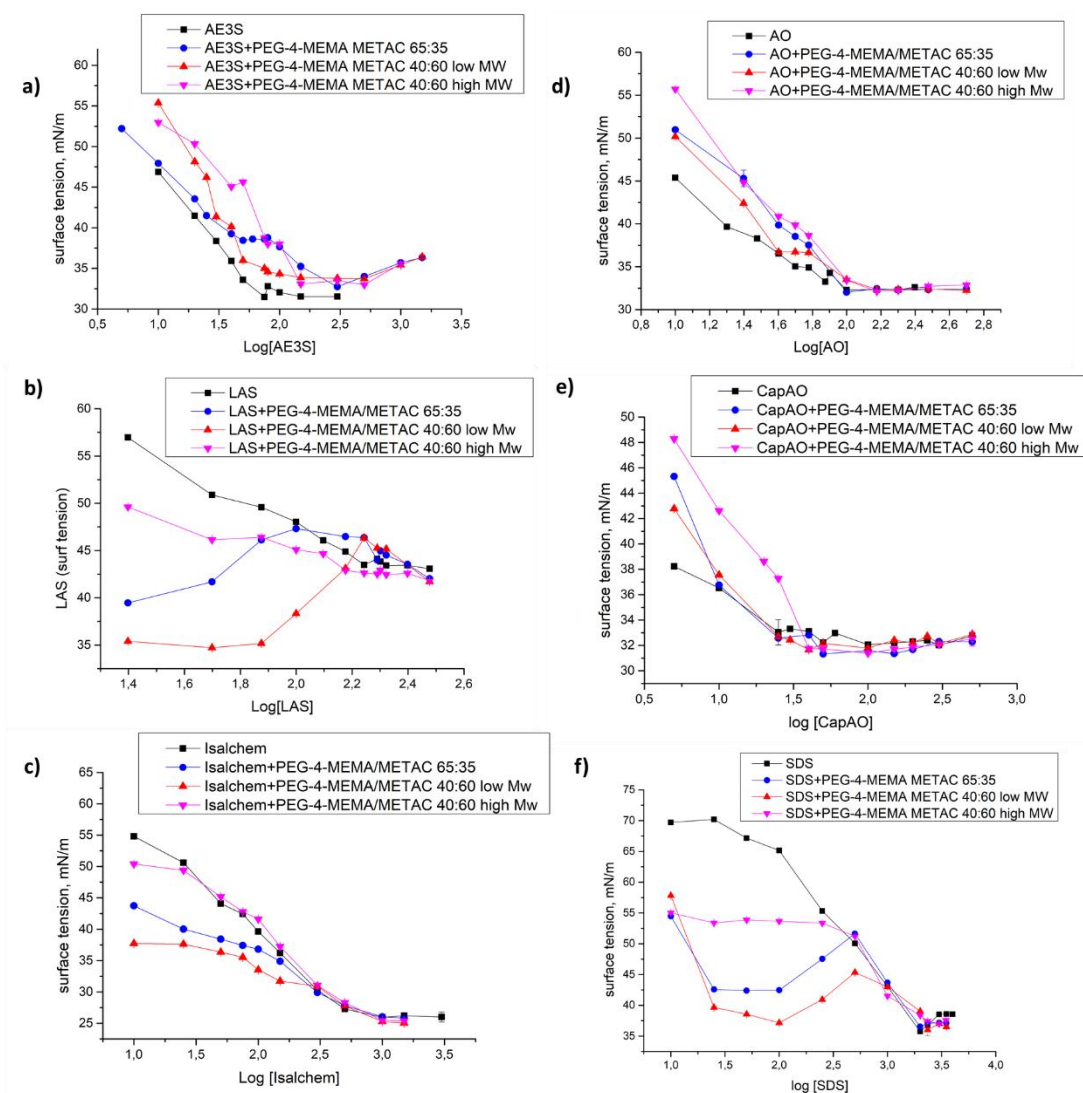
Figure 44 – Surface tension plot versus logarithmic concentration of surfactant for AE3S (a), LAS (b), Isalchem (c) AO (d), CapAO (e) and SDS (f) at pH 8 in DI water. The measurements were run for surfactant on its own (□) and in the presence of PEG-4-MEMA/METAC 65:35 (•) and PEG-4-MEMA/METAC 40:60 low molecular weight (▲) and high molecular weight (∇).

If combining the SRPs with AE_3S (Figure 44a), the surface tension at low surfactant concentration is the same of the pure polymer, confirming the presence of a SRP monolayer at the air/water interface. The PEG-4-MEMA/METAC 65:35 (A) has the closest surface tension to the surfactant, probably because of the lower number of cationic groups presents along the chain, therefore its *cac* is the latest (about 40 ppm). Instead, the interactions with the SRPs with a 60% content of METAC (B and C) occurs already at a very low surfactant concentration (15 ppm), as in these cases the number of positively charged groups interacting with the surfactant monomers is much higher. The *psp* is higher for polymer

105

C (150 ppm) than B (75 ppm), probably because C has a higher molecular weight but same ratio between the blocks than B, therefore there are more sites where surfactant can absorb along polymer chain. Polymer A has the latest *psp*, as it has a higher content of hydrophobic domains (PEG-4-MEMA) available for the interaction with surfactant monomers.

In the case of LAS (Figure 44b), the initial surface tension of the surfactant-polymer mixture is lower than the one of pure surfactant. The interaction between surfactant and polymer occurs at low surfactant concentration (*cac* is lower than 5 ppm, as a plateau in the surface tension is already observed for this concentration). An increase in surfactant concentration causes an increase in surface tension, probably because of the cooperative nature of the interaction, as in most of the interactions between ionic surfactant and oppositely charged SRPs[145]. The hydrophobic interactions between surfactant tails are thermodynamically favoured, therefore more surfactant monomers adsorb when other surfactant molecules are already present along the polymer chain. Similarly, surface tension plots of SDS combined with PEG-4-MEMA/METAC SRPs (Figure 44e) show initial surface tension values that are close to the values expected for solution containing only SRPs, reflecting the presence of the polymers at the air/water interface. An increase in surfactant concentration leads to a decrease in surface tension, where the delta versus the surface tension of pure SDS solution is related to the strength of the interaction between SRP and SDS. In all cases, the surface tension values do not experience significant changes between 25 and 100 ppm, suggesting that any addition of surfactant monomers in this range reflects in the interaction of the surfactant with the polymer. The *cac* for the system is therefore lower than 25 ppm and its low value suggests strong electrostatic interactions between anionic head of the SDS monomers and the positive METAC groups along the polymer chain. For a SDS concentration > 100 ppm, the surface tension of the polymer-surfactant system increases, probably because all the polymer chains present at the air/water interface have interacted with the surfactants in solution. Any extra SDS monomers added in the system go at the air/water interface, giving surface tension values closer to the one of a pure SDS solution. The *psp* of SDS was found to be 500 ppm for polymer A and C, whereas a SRP concentration equal to 1000 ppm is required to form pure SDS micelles in the case of polymer B. The lower *psp* of A is due to the its zeta potential, which is less positive than in the case

of B and C and results in a lower amount of SDS monomers interacting with the SRP. By comparing surface tension values of B and C combined with SDS at 50 ppm, C can be deduced to have weaker interaction than B with SDS. Indeed, surface tension value of C+SDS is not meaningfully different from the one measured for C solutions and the *psp* is lower.

In the case of Isalchem, no interaction was observed when the surfactant is combined with polymer C. Instead, SDS interacts with A and B at a concentration of the surfactant that is lower than 5 ppm, and the polymer-surfactant curve overlap to the curve of pure surfactant for a SDS concentration equal to 50 ppm for A and 200 ppm for B. Again, the *psp* of B+SDS system is higher than the *psp* of A+SDS system because of the higher number of cationic groups present in B and that interact with the surfactant monomers.

4.5 Conclusions

In this chapter, streaming potential measurements were used to assess deposition of PEG-4-MEMA/METAC block copolymers in different conditions. It was found that this class of SRPs efficiently deposits on polyester both at pH 8 and 4, whereas no deposition was observed for cotton. This suggests that hydrophobic interactions play a meaningful role on deposition of SRPs on fabrics. Therefore, no deposition occurs on cotton that is hydrophilic, even if an electrostatic attraction would be expected between the anionic groups present on cotton surface and the quaternary ammonium present in the SRPs structure. The zeta potential measured at pH 4 on fabrics that had been conditioned with SRPs was more positive than the one measured for the same SRPs in solution. This was rationalized as a consequence of polymer uncoiling before deposition and exposure of a larger number of positive groups than in the coiled form.

TGA was used to analyse polyester pre-treated with SRPs at pH 8 and indirectly compare the efficiency of deposition of the PEG-4-MEMA/METAC SRPs. The data collected suggested that B has a higher

deposition efficiency than C, which is more efficient than A. As a result, higher METAC content was identified as an important parameter for deposition efficiency on polyester.

Surface tension measurements were run to understand how PEG-4-MEMA/METAC SRPs interact with different surfactant types. One of the main challenges is due to the absorption of SRPs at the air/water interface, which reflects in surface tension values that are closer to the one of a pure SRP solution for a low surfactant concentration. Weak interactions were observed between SRPs and amphoteric surfactants at pH 8, as expected. The strongest interaction for amphoteric surfactants occurs with C, probably as a consequence of the higher content of hydrophobic domains due to its higher molecular weight. The comparison between AO and CapAO highlighted that presence of big head most likely reduces the interaction with the SRPs, as the surface tension plot of CapAO with A and B overlap with the one of pure CapAO for lower surfactant concentration than in the case of AO.

In the case of anionic surfactants, a strong interaction was expected for cationic SRPs. The SRPs concentration we looked at were low, as only 50 ppm of polymers were added in the solution. Therefore, *cmc* of the surfactant and *cac* of the polymer-surfactant system are quite close in most of the cases. However, some understanding on the effect of surfactant and polymer structure on the interaction was developed. SDS, AE_3S and LAS were found to interact with all the SRPs analysed, whereas Isalchem did not show any interaction with C.

Chapter 5. Soil release and BSA release/repellence of fabrics pre-treated with soil release polymers

5.1 Introduction

An investigation on the deposition of PEG-POET and PE-4-MEMA/MEETAC SRPs on cotton and polyester was carried in Chapter 3 and 4, using streaming potential, UV/vis and thermal gravimetric analysis (TGA) as screening tools. The effect of parameters such as pH, agitation speed and water hardness on deposition were studied, and the optimal conditions for the deposition of each SRP were determined. In Chapters 3 and 4, PEG-POET and PEG-4-MEMA/METAC block copolymers were found to efficiently deposit onto polyester at pH 8 and 4, suggesting that they can be used as soil release polymers for this fabric. In the case of PEG-POET SRPs, it was found that polymer deposition onto polyester leads to an hydrophilization of fabrics, which can translate to a lower adhesion of greasy soil onto polyester and an enhancement of soil removal from the fabric surface. In order to assess if polymer deposition results in an improvement of grease release, from SRPs-modified fabrics, stain removal tests were run on unmodified and SRPs-modified fabrics and the results are presented in this chapter. Common hydrophobic stains, such as lard and sebum, were used to stain fabrics after that SRPs were deposited and the percentage of soil removed from polyester and cotton was measured via image analysis.

Enhanced soil removal from polyester can lead to higher cleaning efficiency[24] even in challenging washing conditions, such as low temperature and short-cycle washing conditions. However, it can be expected that part of the soil will be left on fabric, leading to biofilm growth, as explained in section 1.2.4. The chances of biofilm growth on fabric surface can be reduced by preventing protein adhesion on fabrics. Indeed, the formation of a conditioning film, made of protein, on the fabric surface enhances bacterial adhesion and proliferation[36]. If proteins are repelled or more easily released by fabric surface, biofilm growth can be avoided. Therefore, in this chapter, the BSA adhesion and release from

unmodified and SRPs modified polyester was tested via streaming potential analysis and bicinchoninic acid assay (BCA). The ultimate aim of the study was to assess if the deposition of SRPs on polyester can provide benefits on cleaning from enhancing protein release or repellence, or if the resulting hydrophilization of polyester has a negative impact on the formation of protein conditioning film and on biofilm growth, as a consequence.

5.2 Experimental

5.2.1 Soil removal test

Stain removal indexes (SRI) were evaluated for polyester and cotton fabrics and results are shown in this chapter. In all cases, SRI values were determined for untreated fabric and for fabrics pre-treated with the different types of SRPs, using an SRP concentration equal to 50 ppm at pH 8 (as explained in sections 3.2.3 and 4.2.2). Swatches of untreated and SRP-treated fabrics were sent to Lubrizol Advanced Materials Inc. (Netherlands) for circular stain application. Commercially available round stains of artificial sebum[146], *collar and cuff* soil and lard[147] (Lubrizol, Netherlands) were mixed with a purple/red dye and applied on 5×5 cm^2 squares of polyester and cotton. Collar and cuff soil is an artificial body greasy soil that has artificial sebum and particulates (clay, soot, etc.) as its main components. It is intended to be representative of soils created from human and external sources, known to be a relevant, and hard to remove soil normally accumulating in the collar and cuff. Stain removal tests were run in an automatic tergotometer with addition of a normal laundry detergent formulation at 25 °C for 20 min at 1800 rpm, followed by a 7 min rinse cycle at 7200 rpm.

5.2.2 BSA deposition on untreated and SRPs-treated polyester via streaming potential

Samples of polyester, previously washed at 60 °C to remove fabric finishes, were cut into 5×5 cm^2 pieces and inserted in the cylindrical cell for streaming potential measurements. The initial zeta potential of fabrics was measured in presence of pure 1.7 mM KCl (similar ionic strength to PBS), at either pH 4 or 7.2. PBS solution was prepared by dissolving one PBS tablet (Sigma Aldrich) in DI water. A stock

solution of BSA, at a concentration of 10 mg/mL, was prepared by dissolving BSA (heat shock fraction at pH 7 from Sigma Aldrich, purity grade ≥ 98%), without excessive stirring, in either PBS or in water at pH 4, according to pH needed for testing. The pH was measured and adjusted with NaOH and HCl (Sigma Aldrich, solutions at 0.1 M in water). The stock solution of BSA was diluted directly in the beaker within the streaming potential instrument and the KCl solution was replaced every time that BSA concentration was increased. Solutions, over a range of concentrations of BSA (0.2 – 1 mg/mL), were used to pre-condition polyester in the streaming potential, by rinsing the fabrics ten times with BSA solution to achieve BSA deposition and sample equilibration. The zeta potential, for each BSA concentration, was measured 10 times, the values were mean averaged, and standard deviation was calculated. The test was run both at pH 4 and 7.2, to assess the effect of pH on BSA deposition on polyester.

5.2.3 BCA assay for protein deposited on untreated and SRPs-treated polyester

Polyester fabrics were conditioned with SRPs at pH 4 and 8, using an SRP bulk concentration of 50 ppm (as explained in sections 3.2.3 and 4.2.2). Fabrics were dried overnight under temperature and humidity control (25 °C, 20% RH) and then incubated with BSA. For incubation, a BSA stock solution at 10 mg/mL was diluted to a concentration of 1 mg/mL in PBS or water at pH 4. The incubation was carried out in 10 mL glass petri dishes, where 0.4 g of each untreated or pre-treated fabric sample was incubated with 8 mL of BSA solution at 1mg/mL. The petri dishes were left under agitation at 150 rpm overnight. The quantity of BSA deposited on the fabric was measured using the bicinchoninic acid assay (BCA), which is an assay for total protein quantification when protein concentration is between 0.2 and 1 mg/mL. The principle of the method is formation of a complex between cysteine, cystine, tyrosine and tryptophan amino acids present in proteins and Cu^{2+}, which is added as $CuSO_4 \cdot 5H_2O$, provided as 1% (w/v) in the BCA kit from Sigma Aldrich. The Cu^{2+} present in the complex is reduced by adding a mixture, provided in the BCA kit, of sodium carbonate, sodium tartrate, sodium bicarbonate and bicinchoninic acid at basic pH and incubating at 60 °C. The complex between Cu^+ and the protein, formed during the incubation, has a violet colour and absorbs at 562 nm. In our test, calibration curves of BSA between 0.2 and 1 mg/mL were produced, using incubation times of 30, 45 and 60 mins and

trimming the pH to 4 and 7.2. The absorbance at 562 nm was measured after incubation for 30, 45 and 60 mins and the absorbance values were substituted in the calibration curves to obtain the mass of BSA in the sample. Values coming from different incubation times were mean averaged and the standard deviation calculated. Three replicates were run for each polymer.

5.2.4 BCA assay for protein released from untreated and SRPs-treated polyester

A stock solution of BSA at 10 mg/mL was prepared by dissolving pure BSA in PBS or in water at pH 4 and trimming the pH to the desired values via addition of NaOH and HCl. The stock solution was diluted to a final concentration of 2 mg/mL. As from previous test, it was found that, in this condition, the quantity of BSA released by the fabric was in the range of 0.5 mg/mL, therefore it was quantified via BCA assay. Samples of untreated and SRPs-treated fabrics were prepared and placed on aluminium foil, then 2 mL of the BSA solution at 2mg/mL were deposited on each sample via drop casting. The samples were left to dry overnight under controlled humidity and temperature conditions (20% RH, 35 °C) to ensure the BSA deposited onto the polyester surface. The samples conditioned with BSA were incubated with 4 mL of PBS or water at pH 4. in petri dishes for 24 hours under agitation (150 rpm) and then the concentration of BSA released by the fabric surface was quantified with BCA assay.

5.3 Effect of soil release polymers deposition on soil removal from fabrics

5.3.1 Soil release benefits due to deposition of PEG-POET SRPs on polyester

A stain removal test was performed on polyester samples with and without preconditioning with PEG-POET SRPs. Stain removal indexes (SRIs) were calculated as explained in section 2.10 via image analysis of stains before and after the washing process, and they are shown in Figure 45. The composition of the stains applied on the fabrics is listed in section 2.5.1 and the greasy soil removal was tested, as a function of surface modification. In the case of untreated polyester, a low SRI was determined for all the analysed stains. The poor cleanability of polyester is due to the strong

hydrophobic interactions occurring between the hydrophobic surface of the fabric and the hydrophobic soil analysed. Comparison of SRIs, between untreated and treated polyester, suggests that SRPs deliver soil-release benefits at the low concentrations (50 ppm) typically used in washing formulations. Indeed, the SRI measured for both the SRPs are much higher than the value observed for untreated polyester for all the analysed stains[75]. The SRI achieved for the stains is comparable for the two SRPs, except on the collar and cuff soil, where SRN240 was shown to deliver superior cleaning results. This may be due to the higher efficiency of deposition of SRN240 polymer, compared to SRA300F, resulting in lower adhesion efficacy of the soil on the surface and hence making it easier to remove complex soil mixture including particulates from polyester via this mechanism.

Figure 45 – a) Chart of stain removal index for polyester fabrics that have been washed with and without SRPS and then stained with artificial sebum (in red), lard (in blue), and collar and cuff (in black). b) Picture of collar and cuff stains before and after the wash for untreated and SRP-treated polyester.

5.3.2 Soil release benefits due to the deposition of PEG-POET SRPs on cotton

Cotton fabrics, with and without preconditioning with PEG-POET SRPs, were stained with the hydrophobic soils listed in section 2.5.1 and the stain removal indexes were determined. The results are shown in Figure 46 and, when compared with the SRI for virgin polyester (Figure 45), it can be deduced that grease removal and emulsification is easier in the case of cotton. Indeed, SRI values on cotton are higher than the one observed for unmodified polyester, which reflects the higher hydrophilicity of cotton and the lower adhesion of soil due to the week dipole – induced-dipole forces. No meaningful increase was observed on stain removal indexes when the fabrics were pre-treated with PEG-POET

SRPs, which is further confirmation of the poor deposition of these polymers on cotton, as previously discussed in section 3.3.1.
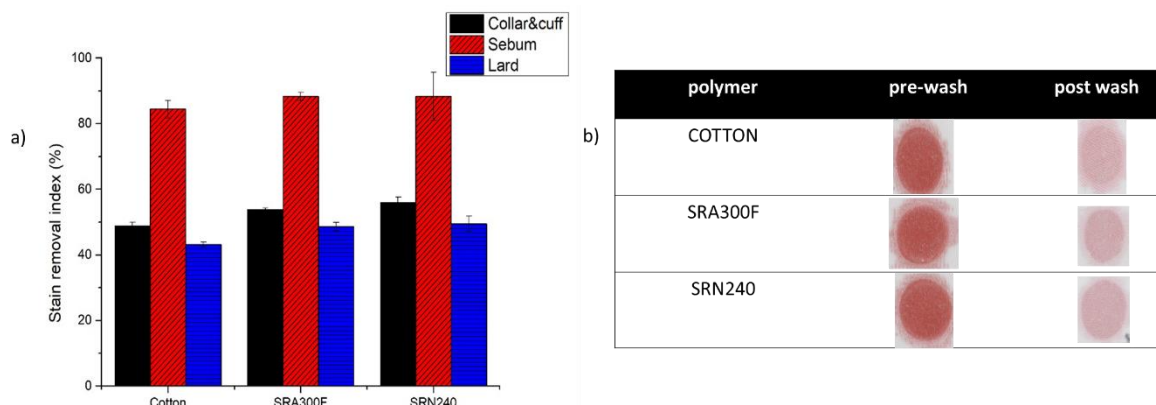
Figure 46 - Chart of stain removal index for cotton fabrics that have been washed with and without SRPS and then stained with artificial sebum (in red), lard (in blue), and collar and cuff (in black). b) picture of collar and cuff stains before and after the wash for untreated and SRP-treated polyester.

5.3.3 Soil release benefits due to the deposition of PEG-4-MEMA/METAC on polyester

Circular stains of lard mixed with blue dye were deposited on polyester fabrics with and without preconditioning with PEG-4-MEMA/METAC SRPs. The samples were washed with a normal laundry detergent and the stain removal indexes were measured via image analysis and they are shown in Figure 47. The SRIs were higher for SRPs-treated polyester, which demonstrate that the deposition of SRPs on top of polyester enhances the removal of lard, confirming the soil release benefits delivered by this class of SRPs. However, no meaningful differences were observed among the three polymers, which suggests that the percentage of SRP deposited for each polymer is about the same. This is in line with TGA data shown in section 4.3.2, where the percentage of polymer deposited onto polyester was about the same for the three SRPs.
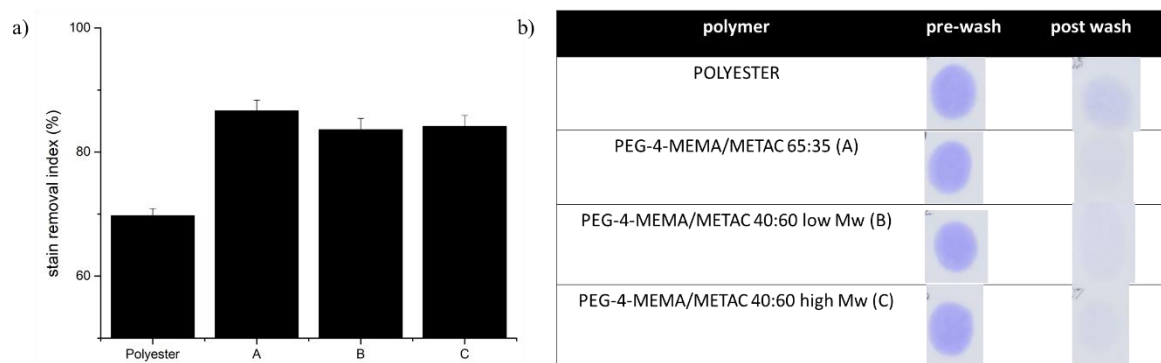
Figure 47 – a) Chart of stain removal index for polyester fabrics that have been washed with and without SRPS and then stained with lard. b) picture of lard stains before and after the wash for untreated and SRP-treated polyester.

5.3.4 Soil release benefits due to the deposition of PEG-4-MEMA/METAC on cotton

A stain removal test was run on cotton fabrics with and without pre-conditioning with PEG-4-MEMA/METAC SRPs. As in section 5.2.1, lard stains were applied, and the stain removal was calculated via image analysis, as explained in section 2.10. The stain removal indexes for untreated cotton and SRP-modified cotton are shown in Figure 48 and no meaningful enhance in soil removal was observed when cotton had been washed with PEG-4-MEMA/METAC SRPs. The outcome of the stain removal test is in line with streaming potential results, shown in section 4.3.1, which suggested that poor or no deposition occurred on cotton for this class of SRPs.
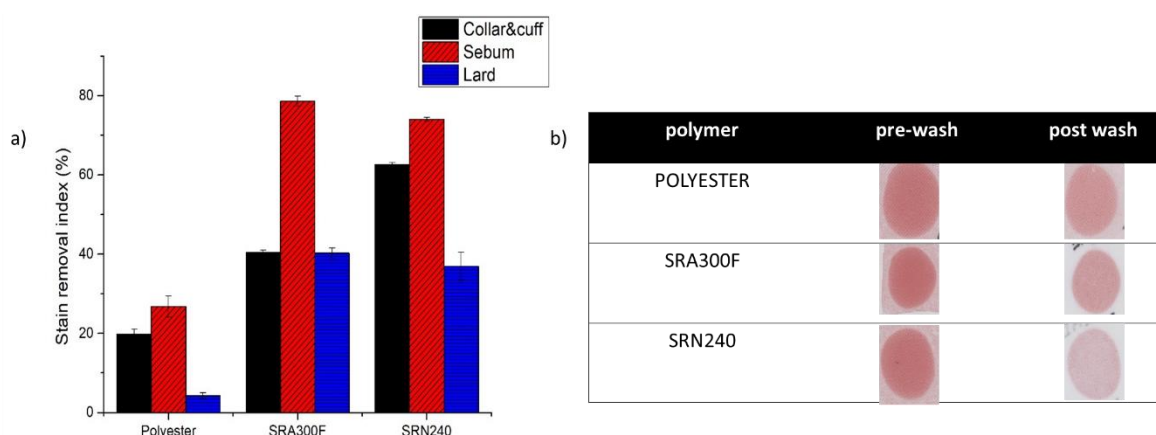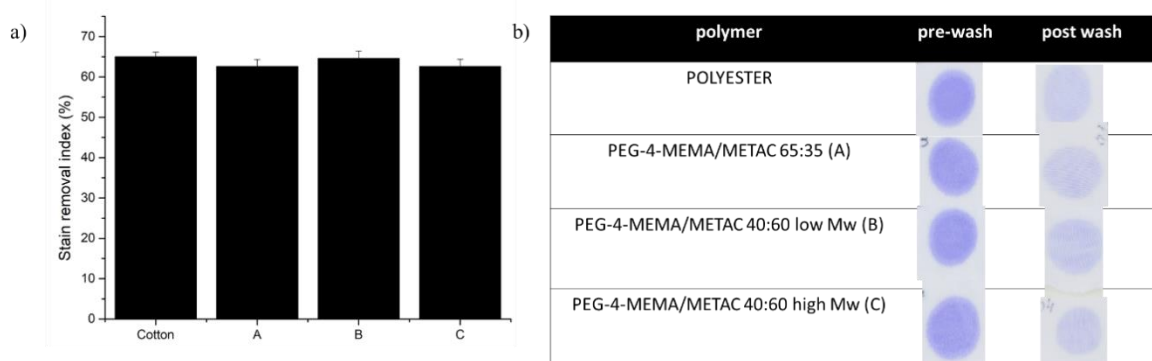

Figure 48 – a) Chart of stain removal index for cotton fabrics that have been washed with and without SRPS and then stained with lard. b) picture of lard stains before and after the wash for untreated and SRP-treated polyester.

5.4 Protein deposition on polyester

Polyester samples were analysed in streaming potential after equilibration with an increasing concentration of BSA. The zeta potential values, as a function of BSA concentration, are shown in Figure 49 and are compared to the zeta potential of BSA in solution. The zeta potential of a 1 mg/mL BSA solution was found to be –26.0 m V at pH 7.2 and 20 mV at pH 4 by light scattering measurements, in line with literature values[148]. The isoelectric point of BSA is reported[149–151] to be around 5 , which means that in PBS (pH 7.2) most of the functional groups present on the amino acids of the BSA are deprotonated and the average charge of the protein is negative. Instead, at pH 4, the protonation of ionizable groups of the BSA occurs, and the net charge of BSA is positive.

It is evident that the zeta potential of polyester pre-treated with BSA approaches the zeta potential of BSA in solution, as the protein concentration ([BSA]) increases. A plateau is observed in the zeta potential plot, which is close to the ZP of pure BSA in solution (the excess of positive charge in the case of pH 4 has been explained in section 4.3.4). The data follow a Langmuir isotherm model and, therefore, fitted using equation 51, which is the Langmuir isotherm model modified to take in account the initial zeta potential of the fabrics (ZP_{initial}):

$$ZP = ZP_{\text{initial}} + \frac{Q_{\text{saturation}}*K*[\text{BSA}]}{1+K*[\text{BSA}]} \qquad (51).$$

The Langmuir constants, K, for BSA deposition onto polyester, at different pH values, are shown in table 6. It can be seen that K is higher at pH 4 than in PBS. This can be explained by considering that polyester has a negative zeta potential at both pH values, whereas BSA is positively charged at pH 4 and negatively charged at pH 7.2. Therefore, at pH 4, BSA experiences an electrostatic attraction due to the negative charge of the polyester and deposits more, even for low concentration of BSA (Figure 49b). Instead, at pH 7.2, polyester and BSA are both negatively charged and repel each other. Therefore, a higher BSA concentration is required to achieve BSA deposition on polyester and to observe a shift

of the zeta potential measured on fabrics. Thus, to summarise, the formation of a protein conditioning film on polyester is easier at pH 4 than 7.2.
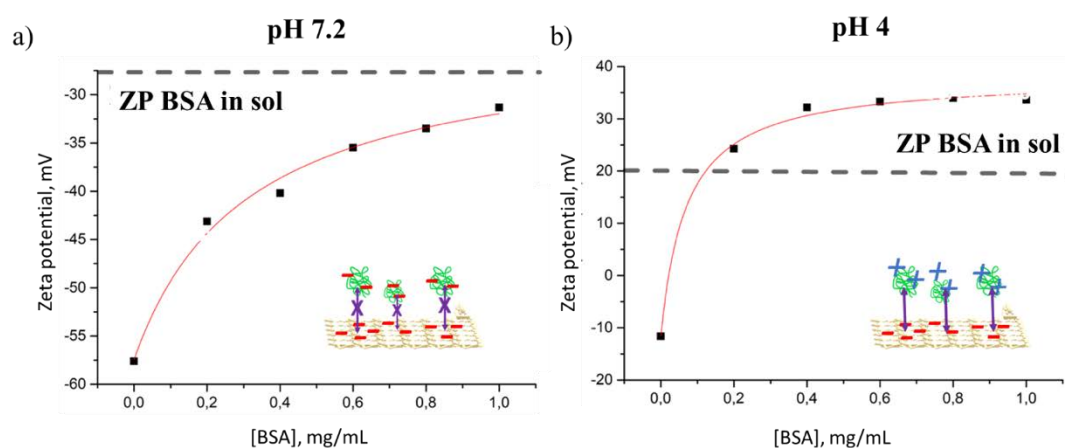
Figure 49 – Zeta potential of polyester equilibrated with different concentrations of BSA in PBS (a) and pH 4 (b) as a function of BSA concentration. The data have been fitted to equation 51 and the value of the Langmuir constants are listed in table 6

Table 6 – Langmuir adsorption constant of BSA on polyester at pH 4 and pH 7.2

substrate	pH	K (mL/mg)
polyester	7.2	(3.2±0.8)
polyester	4	(14±2)

5.5 Protein repellence from polyester pre-treated with SRPs

5.5.1 Protein deposition in presence of SRPs coating at pH 8

In Figure 50a, the percentage of BSA deposited in PBS on polyester untreated or pre-treated with 50 ppm SRPs solution at pH 8 is shown. The 16% of BSA solution at 1 mg/mL, was observed to deposit onto pure polyester, which resulted in 1.28 mg of BSA depositing on untreated polyester. In PBS, the BSA is negatively charged and its adsorption onto polyester is mainly driven by hydrophobic interactions, involving the hydrophobic domains of the protein. The low percentage deposited is related to the hydrophobicity of the textile that, therefore, has a lower affinity for polyester than natural

fibres[152]. If an anionic SRP, such as SRA300F, is applied, this leads to a net negative charge on polyester surface, therefore the percentage of BSA deposited on the modified textile is lower than in the case of untreated polyester due to the electrostatic repulsion between BSA negative groups and sulfonate groups present on SRP-modified polyester. Instead, if a positively charged polymer is deposited on polyester (as in the case of the PEG-4-MEMA/METAC polymers), an increase in the amount of BSA depositing on a fabric is observed, due to electrostatic attraction between the positive amine groups presents along the polymer chain and the negatively charged groups of the BSA. Surprisingly, a decrease in BSA deposition was also observed also when the non-ionic SRN240 is deposited on polyester, despite the higher hydrophilicity of the polyester when the SRP is applied (section 3.4). This observation can be justified by considering the presence of the PEG loops on the fabric surface, that contain 34 and 45 PEG units[153,154]. These loops, most likely, create steric hindrance that prevents the BSA from adsorbing onto the polyester surface.

Figure 50 – a) Percentage of BSA deposited on polyester, in presence and in absence of SRPs coating, in PBS. b) zeta potential of the fabrics before and after BSA deposition.

The zeta potential of untreated and SRP-treated polyester was measured before and after the incubation with BSA (Figure 50b) as further confirmation of BSA deposition on fabrics. It is evident that, in all cases, there is a shift of the zeta potential compared to the initial value, supporting the observation that deposition occurs. Moreover, the final zeta potential is very close to the zeta potential of BSA in PBS, suggesting that the main active present on the fabric surface after the incubation is the protein.

Therefore, it can be confirmed that, in PBS, the BSA deposition occurs both in presence and in absence of SRPs.

Figure 51 - Plots of zeta potential for SRP-treated polyester, equilibrated with different concentrations of BSA in PBS, as a function of BSA concentration. The polyester was pre-treated with SRA300F (a), SRN240 (b), PEG-4-MEMA/METAC 65:35 (c), PEG-4-MEMA/METAC 40:60 low M_w(d), PEG-4-MEMA/METAC 40:60 low M_w(e). The data have been fitted to equation 51 and the value of the Langmuir constants are listed in table 7.

The Langmuir constants for BSA deposition on fabrics were calculated in the case of SRP-treated polyester. As in the case of untreated polyester, the deposition was done in the streaming potential (as explained in section 5.2.2) on fabrics that had been previously pre-conditioned with the analysed SRPs. The Langmuir constants were obtained by fitting the experimental data (Figure 51) to equation 51 and

119

these are listed in table 7. In the case of SRA300F, there is a decrease of the Langmuir constant, and the affinity of the BSA to the fabric as a consequence, which is in line with the BCA assay. The decreased affinity confirms the negative impact of electrostatic repulsion between the anionic polymer and negative charged BSA. A slight decrease in the affinity constant, compared to the untreated polyester, was observed in the case of SRN240, though the difference is not significant. This might confirm the effect of the steric hindrance due to PEG loops on BSA deposition. In the case of the PEG-4-MEMA/METAC block copolymers, the Langmuir constant value remains higher, than in the case of untreated polyester, confirming higher affinity of BSA to the substrate due to the presence of the positive charged groups of the SRPs.

Table 7 – Langmuir adsorption constant of BSA in PBS on polyester pre-treated with SRA300F (a), SRN240 (b), PEG-4-MEMA/METAC 65:35 (c), PEG-4-MEMA/METAC 40:60 low Mw(d), PEG-4-MEMA/METAC 40:60 low M_w(e).

substrate	pH	K (mL/mg)
polyester	7.2	(3.2±0.4)
SRA300F	7.2	(0.9±0.2)
SRN240	7.2	(2.7±0.2)
PEG-4-MEMA/METAC 65:35	7.2	(8.8±0.8)
PEG-4-MEMA/METAC 40:60 low Mw	7.2	(4.1±0.6)
PEG-4-MEMA/METAC 40:60 low Mw	7.2	(9,0±0.6)

5.5.2 Protein deposition in presence of SRPs coating at pH 4

Polyester fabrics, previously pre-treated with SRPs solutions at 50 ppm and pH 4, were incubated with BSA, at a concentration of 1 mg/mL, overnight in acidic condition and under agitation, and the percentage of BSA deposited was quantified via BCA assay (Figure 52). It is observed that the presence of SRA300F on top of the polyester increases the percentage of BSA deposited, this was expected as the protein is positively charged at pH 4 and is attracted by the anionic soil release polymers, as a result. The deposition of non-ionic SRP SRN240 decreases the percentage of BSA depositing on polyester, which seems to confirm the steric effect of the PEG groups on protein adsorption hypothesised in the case of PBS. In the case of PEG-4-MEMA/METAC SRPs, which are positively charged polymers, no

meaningful deposition was observed on polyester, which suggests that the positive charge introduced on fabrics via SRP deposition leads to electrostatic repellence to BSA and prevents or reduces protein deposition. The zeta potential of fabrics, before and after incubation with BSA, was measured in streaming potential and results are shown in Figure 52b. The zeta potential of fabrics after incubation with BSA becomes very close to the zeta potential of the BSA in solution, which confirms the occurred deposition for BSA. The zeta potential slightly changes also, in the case of PEG-4-MEMA/METAC SRPs, which suggests that there is probably a certain quantity of BSA deposited when these SRPs are present on the fabric surface. However, the reduction in concentration, due to the BSA deposition on fabrics, may be lower than the sensitivity of the BCA assay and, therefore, below the level of detection for this test.
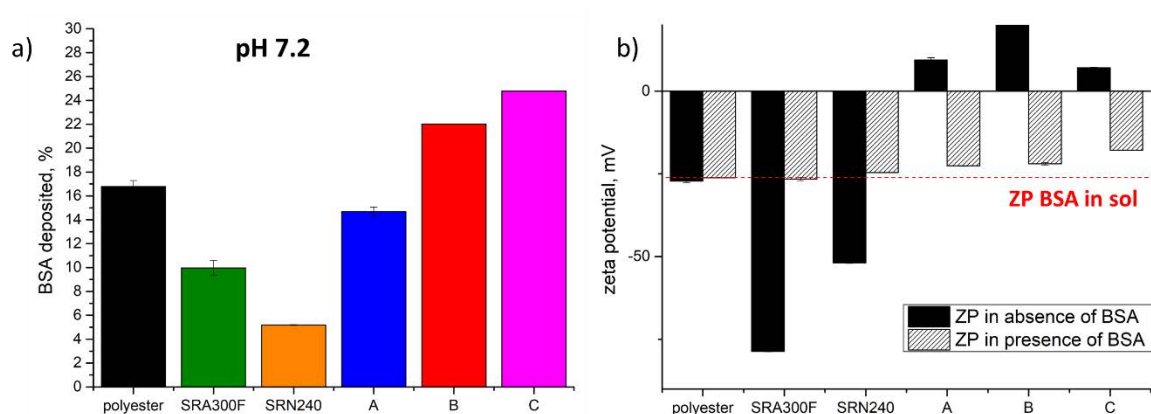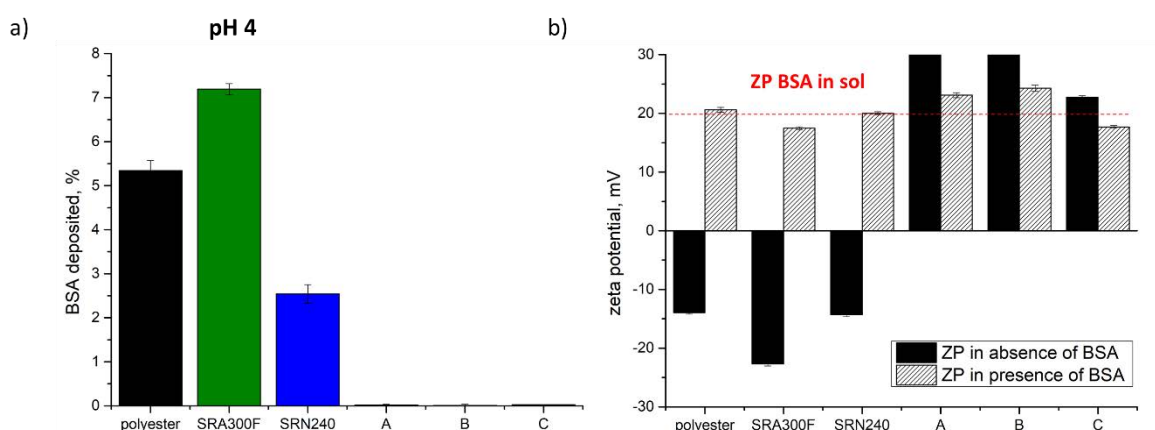

Figure 52 – a) Percentage of BSA deposited on polyester in presence and in absence of SRPs coating at pH 4. B) Zeta potential of the fabrics before and after the BSA deposition.

As explained in section 5.2.2, polyester fabrics with and without SRPs pre-conditioning were conditioned with increasing concentration of BSA in the streaming potential cell, using BSA dissolved in 1 mM KCl at pH 4 as streaming solution. The zeta potential for fabrics rinsed with BSA solution, until reaching deposition equilibrium, was measured and the data were plotted against BSA concentration. The results for the 5 polymers analysed are shown in Figure 53 and the data were fitted to equation 51 to obtain the Langmuir constant associated to BSA deposition on SRPs pre-treated polyester. The Langmuir constants determined are listed in table 7.
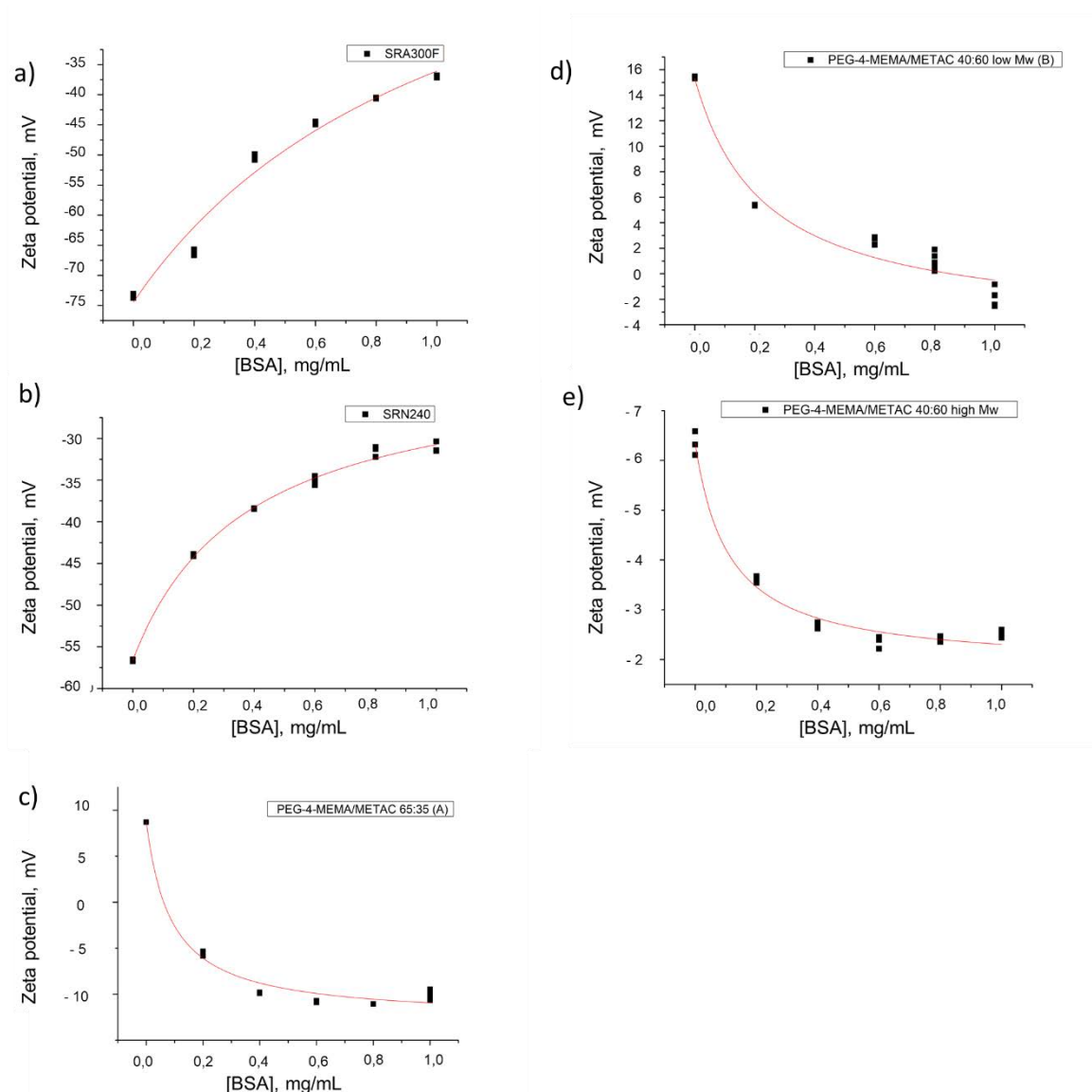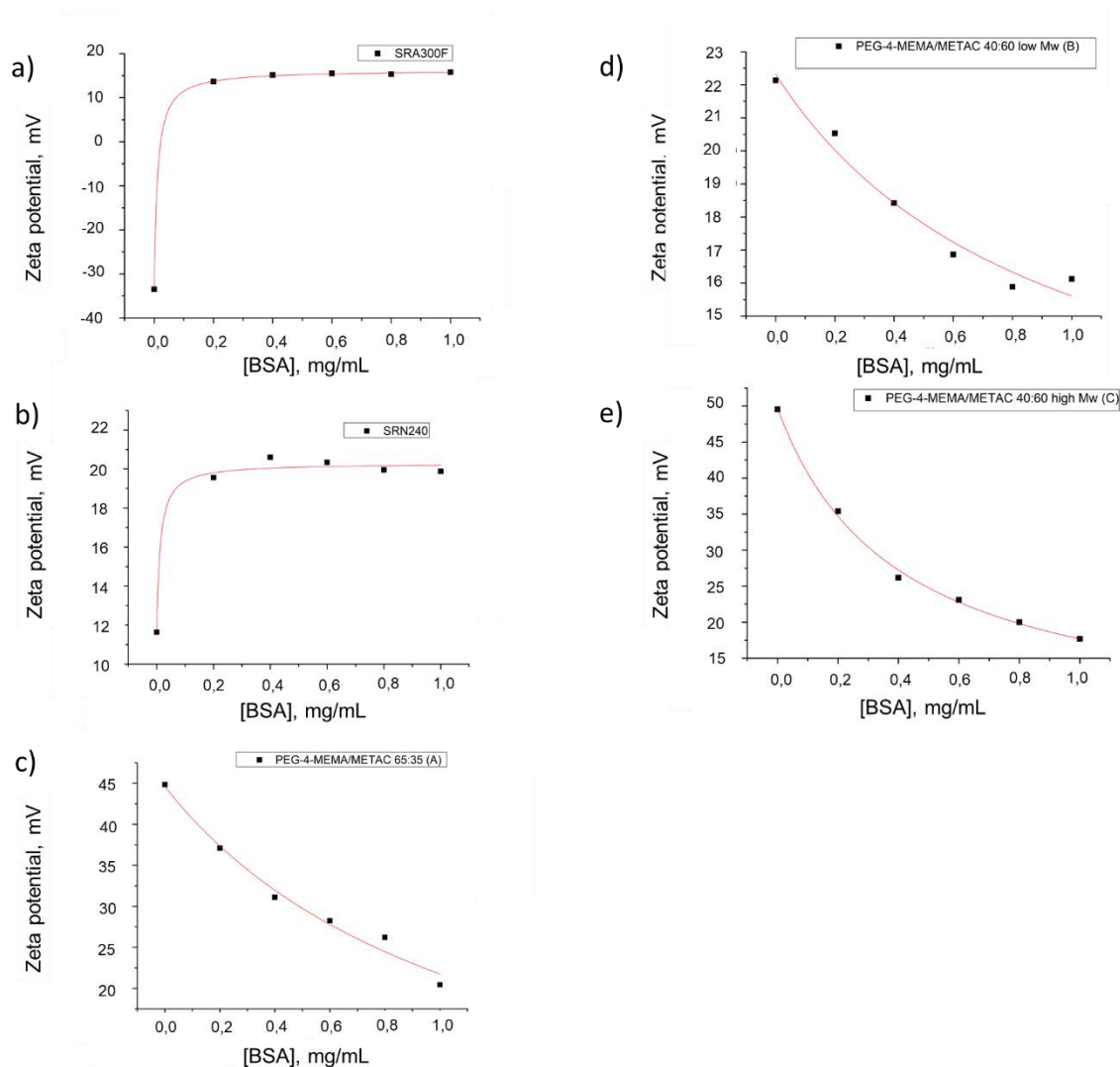
Figure 53 - Plots of zeta potential for SRP-treated polyester, equilibrated with different concentrations of BSA at pH 4, as a function of BSA concentration. The polyester was pre-treated with SRA300F (a), SRN240 (b), PEG-4-MEMA/METAC 65:35 (c), PEG-4-MEMA/METAC 40:60 low M_w(d), PEG-4-MEMA/METAC 40:60 low M_w(e). The data have been fitted to equation 51 and the value of the Langmuir constants are listed in table 8.

The trend observed in the Langmuir constant values is in line with the BCA assay results. A low binding constant was found for PEG-4-MEMA/METAC SRPs, which did not indicate deposition in the BCA assay. BSA deposits on this class of SRPs, as confirmed by the variation in zeta potential wen increasing protein concentration. However, the affinity for the modified fabric is very low. This can be justified by considering the electrostatic repulsions that occur between fabric surface, which is positively charged as a consequence of PEG-4-MEMA/METAC deposition, and BSA, which is positively charged at pH

4. Polyester modified with SRN240 has a lower affinity to BSA than untreated polyester at pH 4, as demonstrated by the smaller binding constant measured for SRN240. The low BSA deposition can be due to the lower negative charge found on polyester when modified with SRN240, where BSA experiences lower electrostatic attraction to the surface as a consequence. Conversely, deposition of SRA300F on polyester enhances the deposition of BSA. The positively charged BSA is strongly attracted by the anionic sulfonate groups present on the modified fabric. As a result, the Langmuir constant for SRA300F-modified fabrics is about 6 time higher than the one obtained for un-treated polyester, which is in line with the increased percentage of BSA deposited on polyester when SRA300F is deposited.

Table 8 – Langmuir adsorption constants of BSA at pH 4 on polyester pre-treated with SRA300F (a), SRN240 (b), PEG-4-MEMA/METAC 65:35 (c), PEG-4-MEMA/METAC 40:60 low Mw(d), PEG-4-MEMA/METAC 40:60 low M_w(e).

substrate	pH	K (mL/mg)
polyester	4	(14±2)
SRA300F	4	(49.7±0.2)
SRN240	4	(8.0±0.5)
PEG-4-MEMA/METAC 65:35	4	(0.9±0.4)
PEG-4-MEMA/METAC 40:60 low Mw	4	(1.1±0.6)
PEG-4-MEMA/METAC 40:60 low Mw	4	(2.5±0.3)

5.6 Protein release from polyester modified with SRPs

5.6.1 Protein release from SRP-treated fabrics in PBS

The percentage of BSA released, in the case of untreated or SRP-modified polyester, is shown in Figure 54. It can be seen that a high percentage of BSA deposited was released, as the BSA was in excess and probably the use of a drop casting approach avoided the formation of strong bond with the fabric surface. In general, all the polymers resulted in a lower percentage of BSA released from the polyester. An explanation for this could be that the BSA solution is wetting the fabric and, therefore, the presence of SRPs, which are increasing the fabric wettability, promotes the penetration of BSA inside the fabric's

porous structure. Indeed, SRN240, that was found to cause the highest hydrophilization of the polyester, has the lowest percentage of BSA released. The percentage of BSA released in the case of PEG-4-MEMA/METAC block copolymers is lower than in the case of untreated and SRA300F-treated polyester, probably as a consequence of the higher electrostatic attraction between negative charged BSA, due to the use of PBS, and positively charged polymers. No meaningful differences were observed in the case of polyester and SRA300F, probably because in both cases the polyester surface is negatively charged. It can be noted that the differences in the percentage of BSA released are relatively small, as for all the polymers the percentage release is between 80 and 90%, therefore it can be concluded that SRPs do not provide significant benefits for protein release at pH 7.2.
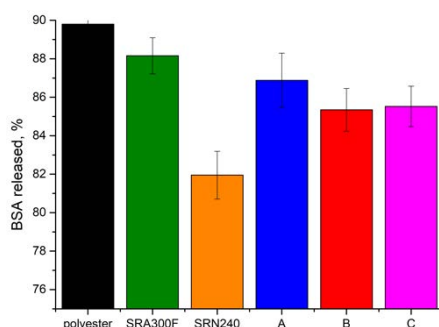
Figure 54 - Percentage of BSA released from untreated and SRPs treated polyester after incubation with PBS overnight. The mass of BSA initially deposited on the fabrics was 2mg.

5.6.2 Protein release from SRP-treated fabrics at pH 4

The percentage of BSA, released after depositing BSA via drop casting on untreated and SRP-treated polyester and incubating the fabrics in water at pH 4, was measured via BCA assay and the results are plotted in Figure 55. It can be seen that the percentage of BSA released by untreated polyester when incubated at pH 4 is slightly lower than that released in PBS. The highest retention in acidic conditions is due to higher electrostatic attraction between negatively charged polyester and the positively charged BSA. From the histogram, it is evident that there is a different effect on BSA-release, depending on the polymer structure. Deposition of both SRA300F and SRN240 results in lower percentage of BSA released from the fabric. Again, this might be due to the hydrophilization of the textile that causes BSA

penetration in the textile and higher adhesion, being the BSA being hydrophilic. Instead, relevant benefits were observed in the BSA release from fabrics pre-treated with PEG-4-MEMA/METAC soil release polymers. The higher released percentage of BSA in the latest case might be related to the lower adhesion of BSA on the fabric, which is a consequence of the electrostatic repulsion between the positively charged protein and the amine groups present on the polymer chain. Therefore, it can be deduced that the deposition of PEG-4-MEMA/METAC block copolymers improves BSA release in acidic conditions.
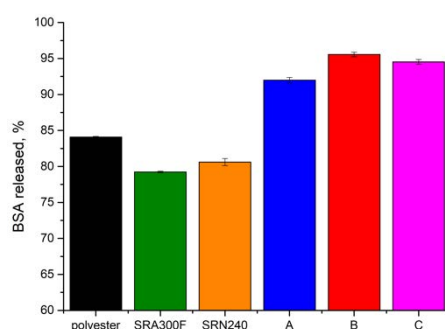
Figure 55 – Percentage of BSA released from untreated and SRPs treated polyester after incubation with water at pH 4 overnight. The mass of BSA initially deposited on the fabrics was 2mg.

5.7 Conclusions

In this chapter, the effect of SRP modification on greasy soil release, BSA release and repellence was investigated. It was found that PEG/POET block copolymers deliver soil release benefits on polyester, but not on cotton. The highest soil removal indexes were found for SRN240. This can be related to the higher hydrophilicity and to the occlusion of fabric pores due to SRPs deposition (as explained in section 3.5), which results in weaker capillary forces and lower soil adhesion when SRN240 is deposited. Lard removal was measured on fabrics modified with PEG-4-MEMA/METAC SRPs and results showed that this class of SRP deliver benefits on polyester, but not on cotton. The stain removal data were in line with the hypothesis on efficiency of deposition in Chapter 3 and 4, where the SRPs were found not to deposit on cotton.

Polyester affinity to BSA deposition was assessed by combining streaming potential and BCA assay data. It was found that polyester has a higher affinity to BSA at pH 4 than 7.2 (PBS). This result can be explained by considering that polyester is negatively charged at both pH, whereas BSA charges moves from positive, at pH 4, to negative, at pH 7.2. Therefore, higher electrostatic attraction between polyester and BSA was observed at pH 4. The same approach was used to assess the effect on BSA release from the surface of the fabric when SRPs are present. The BCA assay showed that PEG-4-MEMA/METAC co-polymers enhance the deposition of BSA onto polyester in PBS, as a result of electrostatic attractions. Yet, PEG/POET co-polymers reduce the quantity of BSA deposited onto polyester in PBS. The mechanism of BSA repellence was related to electrostatic repulsion in the case of SRA300F and to steric hindrance in the case of SRN240. A decrease in amount of BSA deposited compared to un-treated polyester was found for all the analysed SRPs at pH 4, except in the case of SRA300F. This can be justified when considering the electrostatic attraction between BSA and SRA300F-modified polyester at this pH, where PEG-4-MEMA/METAC block copolymers lead to electrostatic repulsion, and lower mass of BSA deposited, as a consequence.

Binding constants of BSA to polyester with and without SRPs pre-conditioning were obtained by fitting to equation 51 the streaming potential values of fabrics exposed to BSA as a function of BSA concentration. Results are in line with the BCA assay data.

BSA release from fabrics with and without pre-conditioning with SRPs was assessed with BCA and results showed that PEG-4-MEMA/METAC and SRN240 increased BSA retention on the fabric surface in PBS. Conversely, the BSA retained is higher for PEG/POET block copolymers and lower for PEG-4-MEMA/METAC block copolymers than polyester at pH 4.

Chapter 6. Surfactant – soil interactions in bulk

6.1 Introduction

In previous chapters, the efficiency of deposition of some SRPs classes on cotton and polyester was studied by mean of streaming potential measurements, UV/vis and TGA. This study led to the identification of the deposition parameters which impact on the deposition of SRPs onto polyester and explained why SRPs are inefficient in modifying cotton. Fabrics, with and without SRP pre-conditioning, were stained with some common greasy soils, such as lard, sebum and *collar and cuff,* and stain removal indexes were evaluated via image analysis. Surface modification of polyester via the deposition of SRPs was found to enhance soil removal from polyester, as a consequence of the lower adhesion of each soil onto the fabric surface. However, it is necessary to prevent re-deposition of soil on fabrics and this can be achieved by emulsifying oil and grease or removing proteins and carbohydrates from solution via interactions with surfactants. As a result, an efficient cleaning of polyester requires the presence of free surfactants in solution which interact with soil components.

In this chapter, an investigation of the interactions between different classes of surfactants and primary soil components was undertaken. Starch was chosen as model soil for carbohydrates, BSA was used as a representative of proteins and corn oil was used as model for liquid oil. For all the model soils, the interaction with surfactants at a concentration of 300 ppm was studied, where 300 ppm is the surfactant concentration normally experienced by consumer in a sink during dish washing. Surfactants with different structure properties were selected so that an understanding on the effect that surfactant structure has on the interaction with soil can be achieved. The mechanism behind surfactant inclusion, inside amylose helices, was unravelled in this chapter, as this interaction is responsible for the depletion of surfactant monomers present in solution. The effect of surfactant chemical structure on the formation of amylose-inclusion complexes was studied in this work and optimal degree of branching, alkyl chain length and head group size were identified to prevent inclusion of surfactant monomers in the amylose helix. The effect of the same parameters on protein denaturation and complexation was investigated in

this chapter, as well, as these mechanisms can lead to a more efficient removal of protein from washing solutions. This investigation used mass spectrometry, surface tension measurements and fluorescence spectroscopy to investigate the effect of surfactant charge, chain length, level of branching and size of surfactant head on interactions with proteins. Moreover, emulsion stability as a function of surfactant structure was studied by analysing transmission profiles collected with the Turbiscan, as oil was one of the main components of the stains analysed in Chapter 5. As a result, some surfactant properties were identified in this thesis to optimize the interaction between soil components and surfactants and improve cleaning of clothes in laundry.

6.2 Experimental details

6.2.1 Preparation of surfactant solution with and without addition of starch and BSA

Stock solution of surfactants (listed in Appendix I) at a concentration of 3000 ppm were prepared by solubilizing surfactant in mass spectrometry (MS) quality water (Sigma Aldrich). Stock solutions were kept in the fridge and diluted to the desired concentration via addition of MS quality water before each use. In the case of samples containing only surfactant without addition of starch and BSA, the stock solution was diluted to a final concentration of 300 ppm, trimming the pH to 8 via NaOH or HCl and adding 10 mM ammonium carbonate as buffer.

In the case of samples containing starch, 2 g of wheat starch (Sigma Aldrich) was dissolved in 10 mL MS water. The suspension was heated to 60°C, under agitation, for 1 hour, to enable *leach out* of the amylose from the wheat granules. After this step, 5 ml of surfactant solution and 35 mL of water were added and samples were left to equilibrate for 30 minutes. The final surfactant concentration was 300 ppm and the starch content was 2% (w/w).

For the analysis of interactions between surfactants and BSA, a 10 mg/mL stock solution of BSA was prepared by dissolving BSA in MS water and adjusting the pH to 8 via addition of NaOH and HCl 0.05N, using an ammonium carbonate buffer (1mM) to avoid pH changes. The stock solutions of BSA and of the surfactant were diluted with MS water to reach a final concentration of BSA equal to 1 mg/mL and a final surfactant level of 300 ppm. The solution was stirred gently to avoid excessive foaming.

In both cases, 1:10 dilution of the surfactant with and without BSA and starch was used for injection into the mass spectrometer (Micromass ZQ 2000 ,Waters Corporation, Milford,MA, USA) and filtered with nylon 45 μm syringe filter (VWR International Ltd, Luttterworth, UK), to avoid presence of contaminants that precipitate at the electro-spray ionization (ESI) interface and occlude the ESI capillary. No filtration or dilution were used for samples analysed via surface tension measurements, instead.

6.2.2 Experimental conditions and data minding for MS analysis of surfactant

In our work, a Micromass ZQ 2000 (Waters Corporation, Milford,MA, USA) was used to collect the mass spectra of surfactant solutions in the presence and absence of starch and BSA. For each sample, spectra were collected both in positive and negative modes, to enable the detection of both negative (eg. alkyl sulfates) and positive surfactant species (e.g. amine oxides). Data analysis was performed using Micromass Mass Lynx software (v 3.4, Waters, Milford, MA). Initially, the MS spectrum of each surfactant was analysed to identify the different isomers present in the sample (as most of the analysed surfactants contain different chain length). As soon as the characterization was completed, the eXtracted Ion Chromatogram (XIC) for each *m/z* of interest was extracted, using a window of ± 0.5 atomic mass unit (amu). The area under each peak, in the XIC trace, was measured and recorded for each surfactant isomer. These areas were then used to calculate the concentration of surfactants using calibration curves previously prepared. These calibration curves were prepared, for each *m/z* ratio of interest, using surfactant concentrations equal to 1, 5, 10, 30 and 50 ppm. An example of calibration curve, referring

to the C11 CapAO (m/z = 301.5), is shown in Figure 56 and the LOD was calculated by using the intercept (b) and the standard deviation associated to the slope and (δa), according to the following equation:

$$LOD = \frac{3\ \delta a}{b} \qquad (51)$$
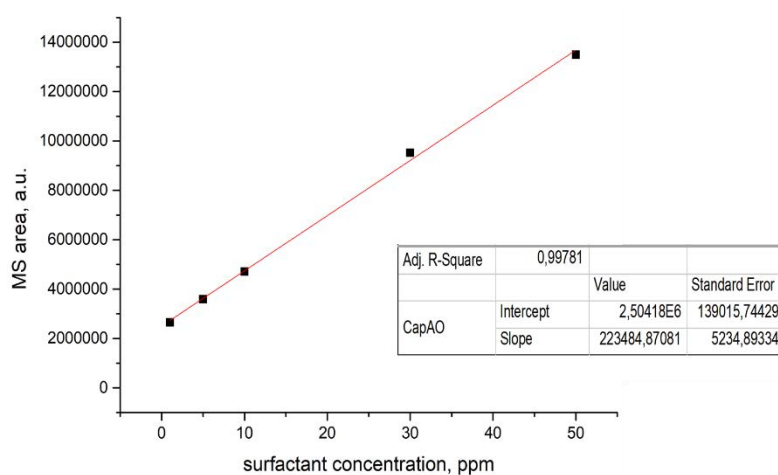
Figure 56 – *Calibration curve for C11 CapAO isomer determined by plotting the area under each XIC associated to the m/z=301.5 for samples at different concentration of the surfactant. In all cases, samples were filtered, and the pH was trimmed to 8.*

The comparison between the concentrations in the surfactant solution in the presence and in the absence of starch led to quantify the percentage of each isomer depleted as a consequence of the interaction with starch. For each surfactant studied, the XIC of one or more *m/z* ratios were extracted for the quantification, depending on the composition of the surfactant considered. The full list of the *m/z* ratio considered for this work is shown in Appendix III, including information about the ESI mode used for the analysis (+ or -) and the structure of the isomer they referred to. It was not possible to distinguish between linear and branched isomers because no chromatographic separation was performed ahead of MS analysis.
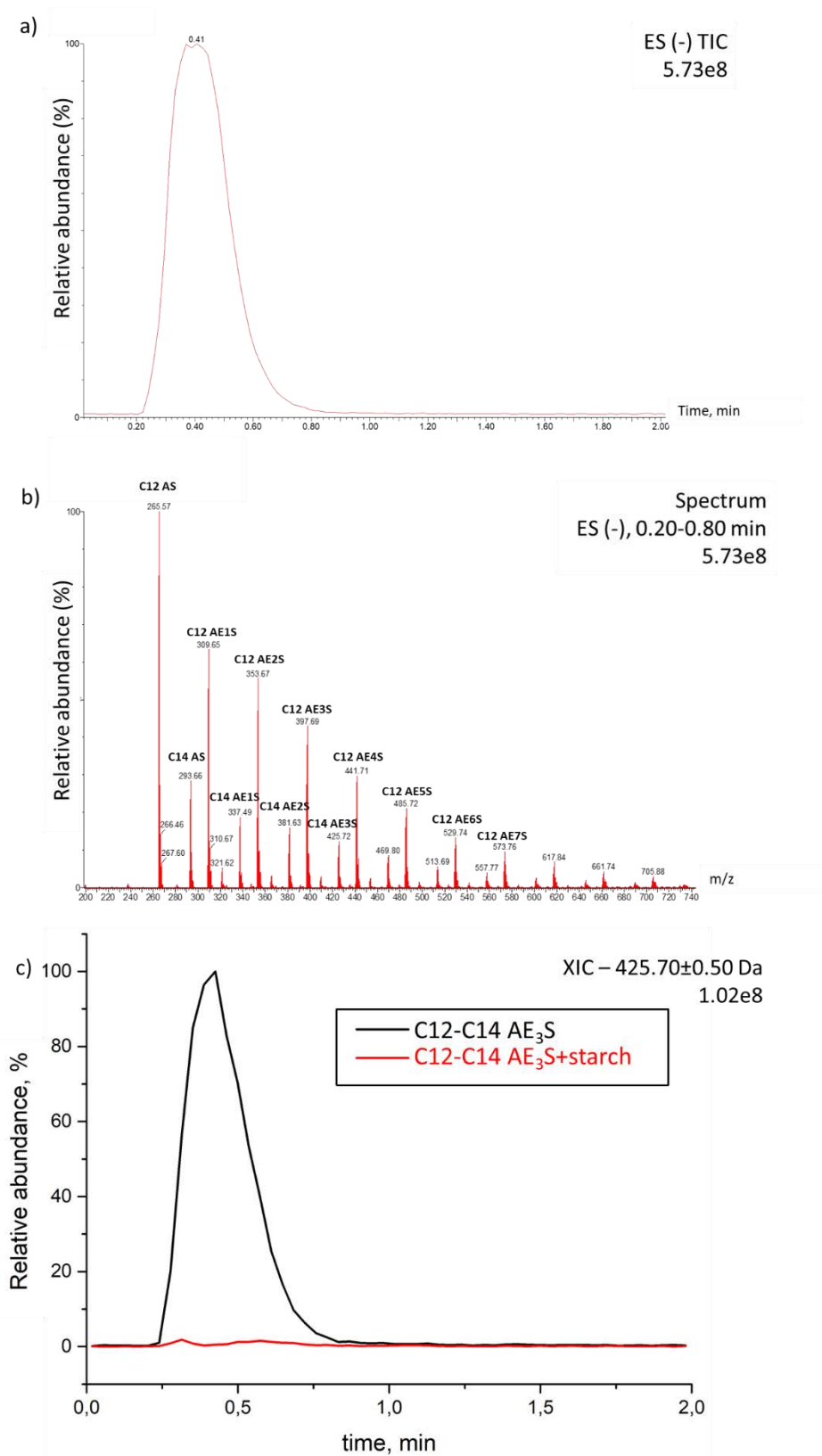
Figure 57 – a) Total ion current chromatogram (TIC) of a sample of C24 AE₃S injected in the mass spectrometer and analysed in negative ESI-(-) mode for 2 minutes; b) ESI-(-) spectrum averaged under the surfactant band present in the TIC between 0.2 and 0.8 minutes and related to the elution and ionization of the C24 AE₃S sample; c) eXtraxted Ion Current (XIC) chromatogram obtained for the m/z ratio

The sample was injected in the mass spectrometer and the MS signal was detected both in positive and negative mode for 2 minutes. A typical total ion chromatogram (TIC) for a surfactant solution injected in the MS analyser is shown in Figure 57. The mass spectrum was averaged under the band present in the TIC (Figure 57b) and the main m/z ratio in each surfactant sample were identified, so that the corresponding eXtracted Ion Current (XIC, Figure 57c) was extracted. The band in the XIC was integrated to obtain the area associated to the specific m/z ratio extracted and the area was substituted in the calibration curves to extrapolate the concentration of the specie with the m/z ratio in the sample. The percentage of surfactant concentration after interaction with starch or BSA was calculated as follow:

$$depletion\ in\ surfactant\ concentration, \% = \left(\frac{A_{m/z}^{no\ soil} - A_{m/z}^{soil}}{A_{m/z}^{soil}}\right) * 100 \quad (52),$$

where $A_{m/z}^{no\ soil}$ is the area associated to the XIC for a specific m/z in the pure surfactant solution and $A_{m/z}^{soil}$ is the area associated to the XIC in the case of surfactant-starch suspension.

6.2.3 Surface tension analysis of surfactant solutions with and without addition of starch and BSA

Surface tension measurements were performed for solutions of surfactants, in the presence and absence of protein or starch. The samples were prepared as described in section 6.2.1 and analysed using a K100 tensiometer (Kruss, Germany). Samples were analysed at 25 °C using a platinum-iridium plate, as previously described in section 3.2.5. The final surfactant concentration was 300 ppm, and the concentrations for starch and soil were 2% (w/w) and 1mg/mL, respectively. Measurements were averaged over 3 replicates for each sample.

6.2.4 Sample preparation for fluorescence spectroscopy

The fluorescence spectrophotometer used was a Varian Cary Eclipse (Agilent Technology, USA) which was equipped with a Peltrier thermostatted multicell holder. The excitation wavelength was 280 nm and the slit width was fixed at 5 nm. Fluorescence emission spectra were recorded between 200 nm and 600

nm, using a slit width of 5 nm. Solutions of BSA, with and without surfactants, were prepared via dilution from stock solutions. A 10 mg/mL BSA stock solution was prepared by dissolving pure BSA in PBS. Surfactant solutions at a concentration of 5000 ppm were prepared in PBS solution (preparation described in section 5.2). Aliquots of the stock solutions of BSA and surfactants were diluted in PBS to achieve the final desired concentration. A BSA concentration of 1mg/mL was used for all the samples, with the surfactant concentration varied between 25 and 2000 ppm. The emission spectra, collected over the range 297 - 500 nm, were recorded for pure BSA and for BSA in combination with some anionic (SDS, LAS, Lial, AE_3S), cationic (DDAC), amphoteric (C_{10} AO, CapAO, CapBetaine, C_{12-14} AO) and non-ionic (C_{10} EO) surfactants.

The fluorescence emission spectrum of thermally-denatured BSA was collected over the range 297 – 500 nm and compared to the emission spectra of BSA in presence of surfactants. Thermal denaturation was performed by increasing the temperature of a solution of BSA 1 mg/mL from 25 and 93 °C, at a heating speed of 1 °C/ min, and measuring the fluorescence emission spectrum of the protein in the end.

6.2.5 Emulsion preparation and analysis via turbiscan

Solutions of different surfactants, at a concentration of 300 ppm, were prepared in water at 15 German degrees (°dH) water hardness and stored at 35 °C. The Turbiscan vial were carefully filled, to avoid foaming, with 20 mL of surfactant solutions. The initial intensity of light transmitted through surfactant solution in absence of oil was measured. Emulsions were generated by mixing 1 mL of corn oil (Mazola) to the surfactant solution. A propeller laboratory shaker (Eurostar 60, IKA, Germany), set at 1600 rpm for 2 minutes, was used to mix the emulsions. Transmission and back scattering across vial height were recorded each minute for 30 minutes after mixing. Transmission and back scattering was measured using a TurbiscanTM LAB (Formulaction SA, France) and the data analysed using the software Turbisoft LAB (Formulaction SA, France).

6.3 Bulk interaction of surfactant with starch

6.3.1 Surfactant depletion in presence of starch via MS analysis

Figure 58 shows the depletion in surfactant concentration, expressed as a percentage versus the initial concentration, for *m/z* ratio present in the analysed surfactants. The higher the depletion percentage, the more the surfactant is included in the amylose helices. As explained in section 1.6.2, surfactants can form amylose inclusion complexes because of their amphiphilic nature.
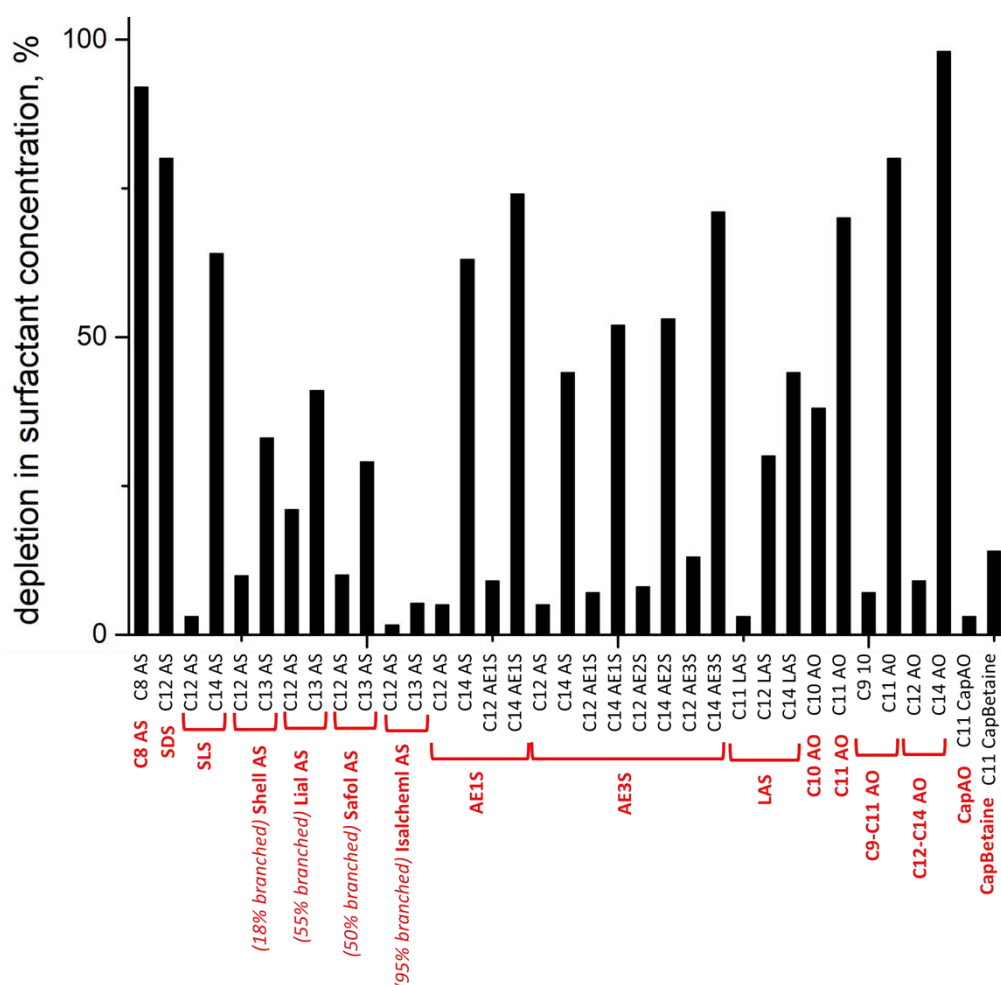
Figure 58 – Bar charts showing the depletion in surfactant concentration, expressed as percentage versus initial concentration, due to the interaction with starch for a range of isomers present in the surfactants analysed in this thesis. The depletion was calculated by comparison between the initial XIC area underneath the surfactant band in absence of starch and the band detected in MS after equilibration with starch. the XIC area associated to the main peaks (in black) was measured.
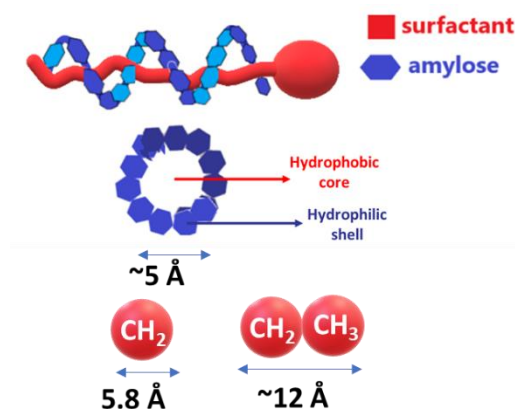
The hydrophobic tail of the surfactant is inserted into the inner core of the helical structure of amylose, which is hydrophobic, and the starch-surfactant interaction is stabilised because of hydrophobic and Van der Waals interactions. In this research, our aim was to assess the affinity of the surfactant, for inclusion in the amylose helical structure, based on the surfactant chemical structure. In the case of C8 alkyl sulfate (C8AS) and SDS, a total depletion of surfactant concentration in solution was measured via MS analysis when starch is added. This observation can be justified by considering that diameters of surfactant tail and of the amylose helix. Indeed, these surfactants are linear, with the diameter of the tail around 5.8 Å (calculated as cubic root from the values used in Tanford equation[156]), and therefore the tail can enter and be inserted into the helix, which inner diameter is around 5 Å[155] (Figure 59). The depletion in concentration observed for SDS and C8AS was compared with the percentage depletion for the other alkyl sulfates.It can be seen that, in the case of surfactant mixture (eg. SLS, which is a mixture of C12 and C14 AS), there is a preferential inclusion of the fraction with the longer chain length, whereas the shorter surfactant is mostly left free in solution. The preferential inclusion of surfactants with longer chain lengths can be explained by their increased hydrophobicity, which increases their affinity with the hydrophobic core of the helix as a consequence. Moreover, by comparing SLS (linear), Shell AS, Lial AS, Safol AS and Isalchem surfactants, the effect of branching on amylose inclusion complex formation can be deduced. It was found that the higher the percentage of branched isomers present in the mixture, the lower the depletion in presence of starch. This can be easily justified by considering that the diameter of a linear tail is around 5.8 Å, while the presence of a

methyl branch connected to the methylene unit increases the diameter to about 12 Å. As a consequence, the presence of methyl branching inhibits the inclusion in the helical structure of the amylose, which diameter is smaller (5 Å).

The effect of charge of surfactant head on surfactant inclusion in the helix was studied by comparing SLS with C12-C14 AO. SLS is an anionic surfactant, while C12-C14 amine-oxide is not charged at pH 8 (pH of analysis). Figure 58 shows that inclusion is preferred for uncharged surfactants, most likely as a consequence of the higher hydrophobicity due to the absence of a net charge. It can be hypothesised that, for mixture of ionic and non-ionic, or amphoteric, surfactants, ionic surfactants are preferentially included in the helical structure of the amylose and, therefore, depleted in bulk.

It was found that the nature of surfactant head group controls the amount of surfactant included in the helical structure of amylose. Comparing C11 AO to C11 CapAO, a decrease in inclusion in the helix for CapAO was found, where the main difference is the presence of a big head group in the case of CapAO. Indeed, the bigger head group of CapAO probably introduces additional steric hindrance for the interaction with amylose, therefore, CapAO is almost not included inside the amylose helix. The same behaviour is observed in the case of CapBetaine, which exhibits low depletion in concentration after addition of starch. This is true for anionic surfactants as well, where the inclusion of AE_3S lower than the inclusion of AE_1S in average.

6.3.2 Surface tension measurements of surfactant-starch mixture

The surface tension of pure surfactant solutions (300 ppm, 15 °dH water) were measured using the Wilhelmy method and results are shown in Figure 60 (black charts). From these data, the effect of surfactant structure on the surface tension of the solution can be observed. By comparing SDS (pure C12 AS) and SLS (C12-C14 AS), as well as by comparing C11 AO and C9-C11 AO, it is deduced that a combination of surfactants leads to a lower surface tension than single surfactant by improving surfactant packing at the air/water interface. Surfactant packing is also enhanced by the presence of

branches along the surfactant alkyl tail, as shown in the alkyl sulfate series. However, an excess of branched surfactant monomers (Isalchem) seems to lead to an increase in surface tension.

The values of surface tension for pure surfactant solutions were compared to the surface tension measured for the same surfactants with 2% starch and presented as red bars in the chart (Figure 60). The results show an increase in surface tension that can be hypothesised to depend on the depletion of surfactant at the air/water interface, due to the inclusion of surfactant in the helical structure of the amylose.
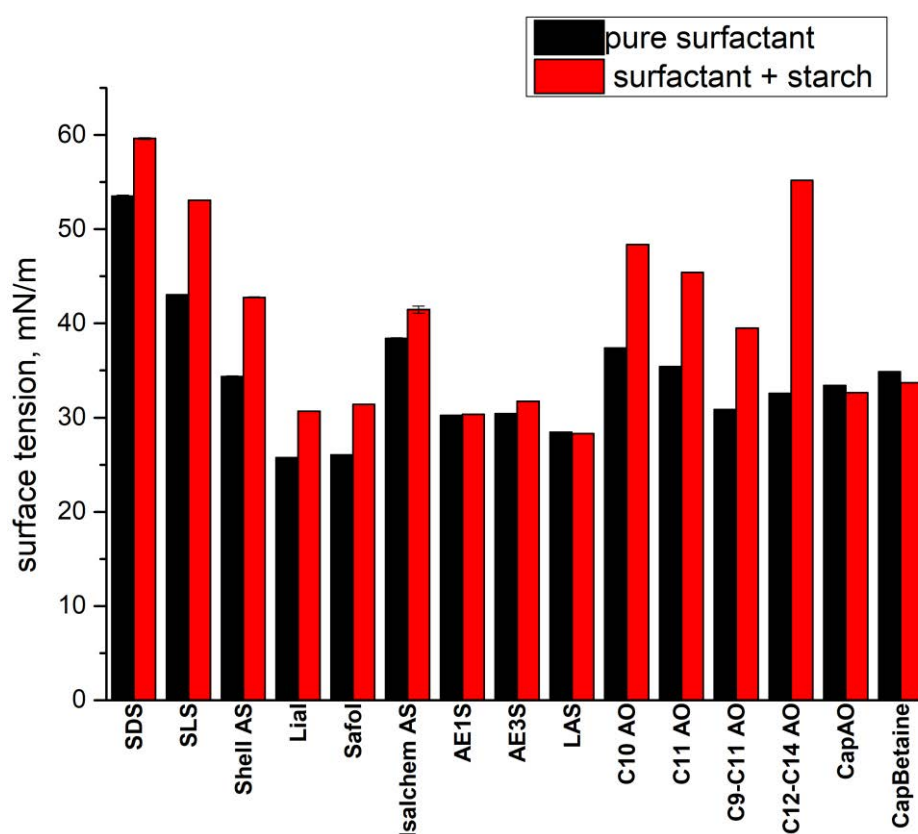
Figure 60 – Surface tension of surfactant solution at 300 ppm in absence (black) and in presence of 2% (w/v) wheat starch (red). The surface tension values were measured at 20 °C via Wilhelmy method using a platinum plate.

There is a good agreement between the increase in surface tension values and the percentages of depletion in MS data (Figure 58). Indeed, high depletion of surfactant concentration in the MS data results in an increase in surface tension for surfactant-starch mixture. In the case of alkyl sulfates, an

increase in surface tension is always observed, confirming the inclusion in helical structure of amylose for this class of surfactant. Moreover, larger differences in surface tension values were observed in the case of SLS, SDS and Shell AS, which had no or lower-degree of branching and, therefore, were the most affected by the interaction with amylose. Small differences were observed for AE_1S and AE_3S, probably because there is a high content of C12 alkyl sulfate available for stabilizing the air/water interface. An increase in surface tension is observed for amine oxides, where the highest variation was observed for C12-C14 AO, which also exhibited the highest depletion in MS signal after start addition. Further confirmation of the resistance of CapAO and CapBetaine to the inclusion in helical structure of amylose is found in the negligible variation of surface tension values for these surfactants. Indeed, the values for surface tension in the presence of starch are very close to the value measured for pure surfactant, which suggests that the surfactant content at the air/water interface is the same even in presence of amylose. As a consequence, the structure-function model developed via MS analysis was confirmed by surface tension data.

6.3.2 Structure-function model for starch- surfactant interactions

The results of MS analysis and surface tension measurements lead to develop a structure – function model for surfactant monomer inclusion inside amylose helix, and the results are shown in Figure 61. The hydrophobicity of surfactant monomers was found to be the main factor affecting the formation of amylose-inclusion complexes. The longer the surfactant alkyl tail, the more hydrophobic the surfactant, therefore the inclusion in amylose helix is enhanced for surfactants with longer chain length. Head group type also impacts interaction with amylose. Indeed, ionic surfactants are more soluble than non-ionic and amphoteric surfactants, hence they are less included in amylose helix than surfactant without a net charge. Moreover, the presence of a big head or of branching introduces additional steric hindrance for the interaction with amylose.
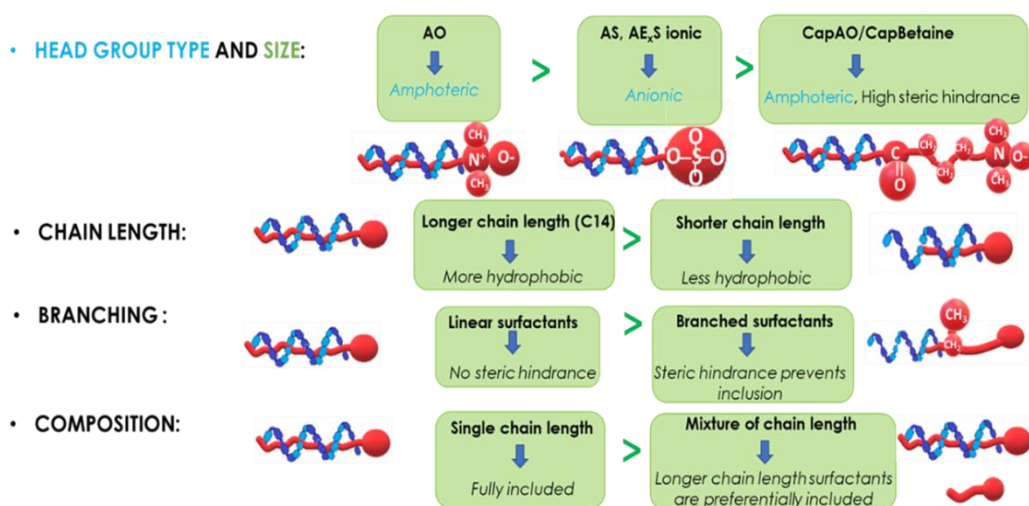
Figure 61 - Structure-function correlation models developed for interactions between surfactant and amylose helix. The model was based on surface tension measurements and mass spectrometry results, both run at a surfactant concentration of 300 ppm and at 35 °C.

6.4 Bulk interaction of surfactant with protein

6.4.1 Surfactant depletion in presence of BSA via MS analysis

The use of mass spectrometry enabled quantification of the amount of surfactant depleted by the interaction with BSA (Figure 62). Overall, it can be observed that all the surfactants are affected by the interaction with proteins, as a depletion in surfactant concentration was detected in most of the cases. It can be observed that the surfactants most affected by the interaction with BSA are Lial AS, Safol AS and LAS. This suggests that the presence of branching enhances the interaction with protein, posssibly because branching stabilizes the unfolded domains of the protein when BSA denatures. However, lower and higher degrees of branching (eg.Shell, Isalchem) appear to reduces the efficiency of the interaction. Alkyl ethoxy sulfate surfactants also exhibits high depletion of the XIC area associated to the surfactant in presence of BSA. Most likely the presence of ethoxylated head enhances protein denaturation, as it improves the packing around the hydrophobic domains. As widely reported in the literature, SDS is widely used for protein denaturation[157–159] because of the strong interaction that SDS has with BSA. This is confirmed by the large depletion experienced for the SDS *m/z* ration in presence of BSA.
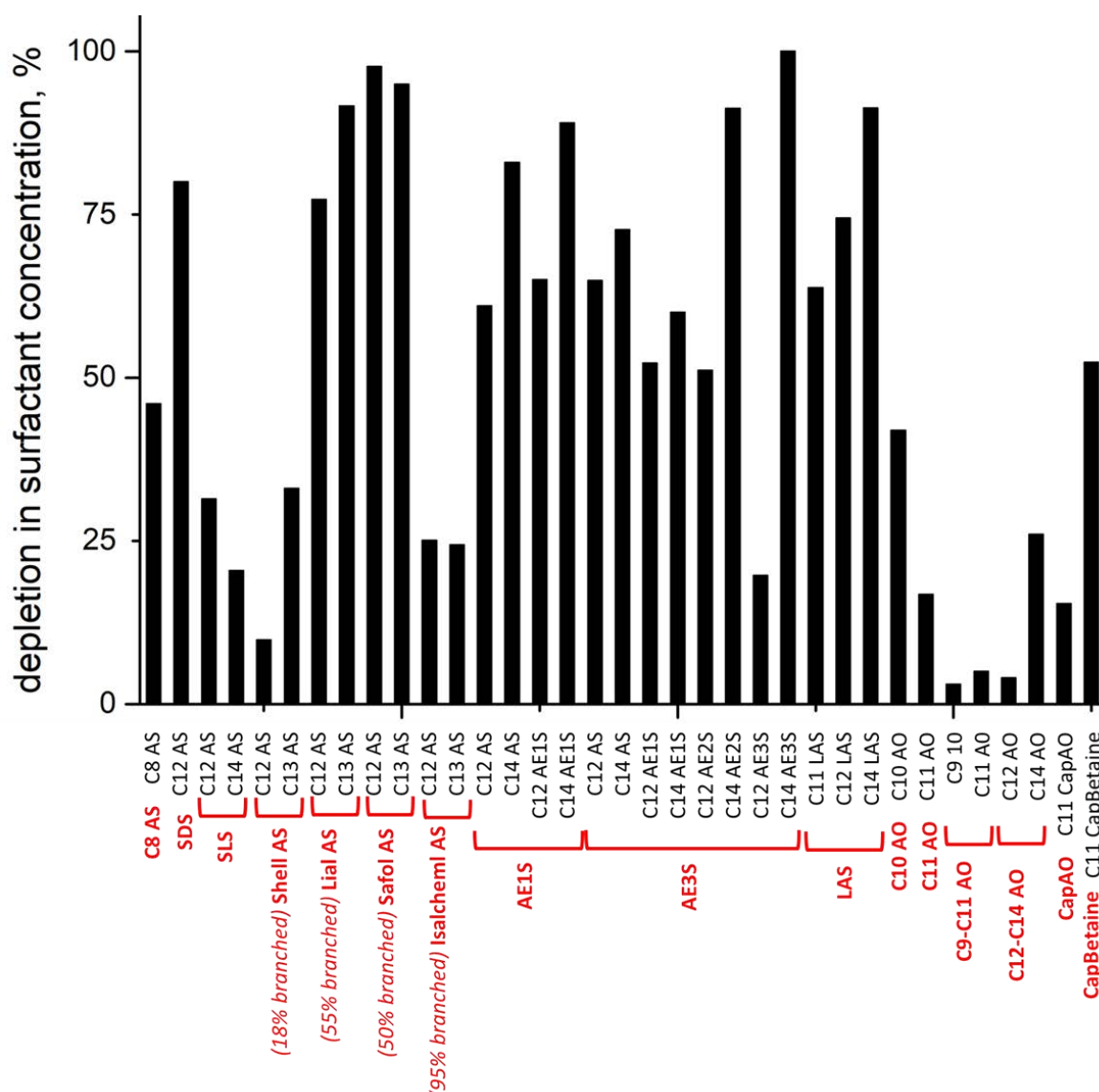
Figure 62 – Bar charts showing depletion in surfactant concentration, expressed as percentage versus initial concentration, due to the interaction with BSA for a range of isomers present in the surfactants analysed in this thesis. The depletion was calculated by comparison between the initial XIC area underneath the surfactant band in absence of starch and the band detected in MS after equilibration with starch. For each surfactant (in red) the XIC area associated to the main peaks (in black) was measured.

The amine oxide class results is the least affected by the interaction with BSA at this pH. In the case of anionic surfactants, as described in section 1.6.3, the interactions with the protein occurs much faster because of the electrostatic attraction between the surfactant charged head and the charged groups along the protein chain. This interaction, called specific binding, is not present in the case of amine oxide, and non-ionic/amphoteric surfactants in general, where the interaction with the protein is solely based on hydrophobic interaction between the surfactant tail and the hydrophobic domains of the protein. As a

result, amine oxide surfactants are less involved than anionic surfactant in the interaction with the BSA at this concentration.

6.4.2 Surface tension measurements of surfactant-BSA mixture

Surface tension measurements were run on samples of surfactants with and without BSA to further unravel the interactions between surfactants and proteins. It was observed that, in the case of Lial, Safol and LAS, a significant increase in surface tension was observed when BSA was added (Figure 63). This confirms the strong interaction between branched surfactants and BSA. However, the correlation between the surface tension data and the MS analysis is less straight forward than in the case of starch, most likely as a consequence of the surface activity of BSA. For instance, it is known that SDS and BSA interact and MS analysis showed that a high amount of SDS is involved in the interaction. Despite this, the surface tension of the BSA/SDS system is lower than the one measured for the pure SDS solution and is closer to the value measured for pure BSA solution. It might be hypothesised that the surface tension is still low, in spite of the depleted amount of free SDS monomers, as there are proteins absorbed at the air/water interface. For the same reason, we can justify the increase in surface tension for C10 AO and C11 AO, where no meaningful interaction was observed in MS. The increase in surface tension might be explained by preferential absorption of BSA at the air/water interface, where the protein has higher surface tension than the surfactant.
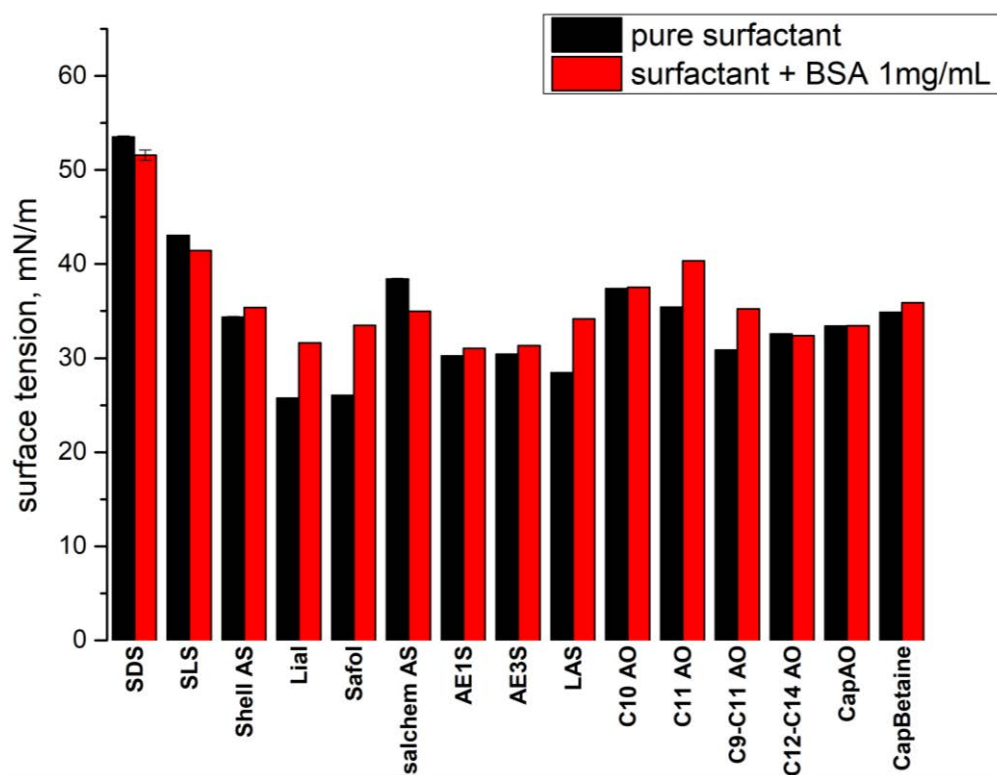
Figure 63 – Bar charts showing the surface tension values of surfactant solutions at 300 ppm in absence (black) and in presence of 1 mg/mL BSA (red). The surface tension values were measured at 20 °C via Wilhelmy method using a platinum plate.

6.4.3 Surfactant-BSA interaction via fluorescence spectroscopy

Fluorescence spectroscopy was used to assess the interactions between surfactants and proteins, as well as a mean of comparison with MS and surface tension data. The data in this section were collected at the Department of Chemistry in the University of Bari in collaboration with Helena Mateos Cuadrado (Ph.D. student). As already mentioned in section 1.6.3, bovine serum albumin exhibits intrinsic fluorescence related to the presence of Tryptophan units. When BSA is in its native form, the fluorescence spectrum has a maximum at 345 nm. This maximum shifts to lower wavelengths when denaturation occurs and the Tryptophan is exposed to a hydrophilic environment. Therefore, denaturation of this protein, by interactions with surfactants, can be followed by monitoring the shift in the maximum of the fluorescence emission spectrum as a function of the surfactant concentration. Fluorescence intensity provides information about the amount of protein that has been denatured by the surfactant, and consequently the strength of the interaction.
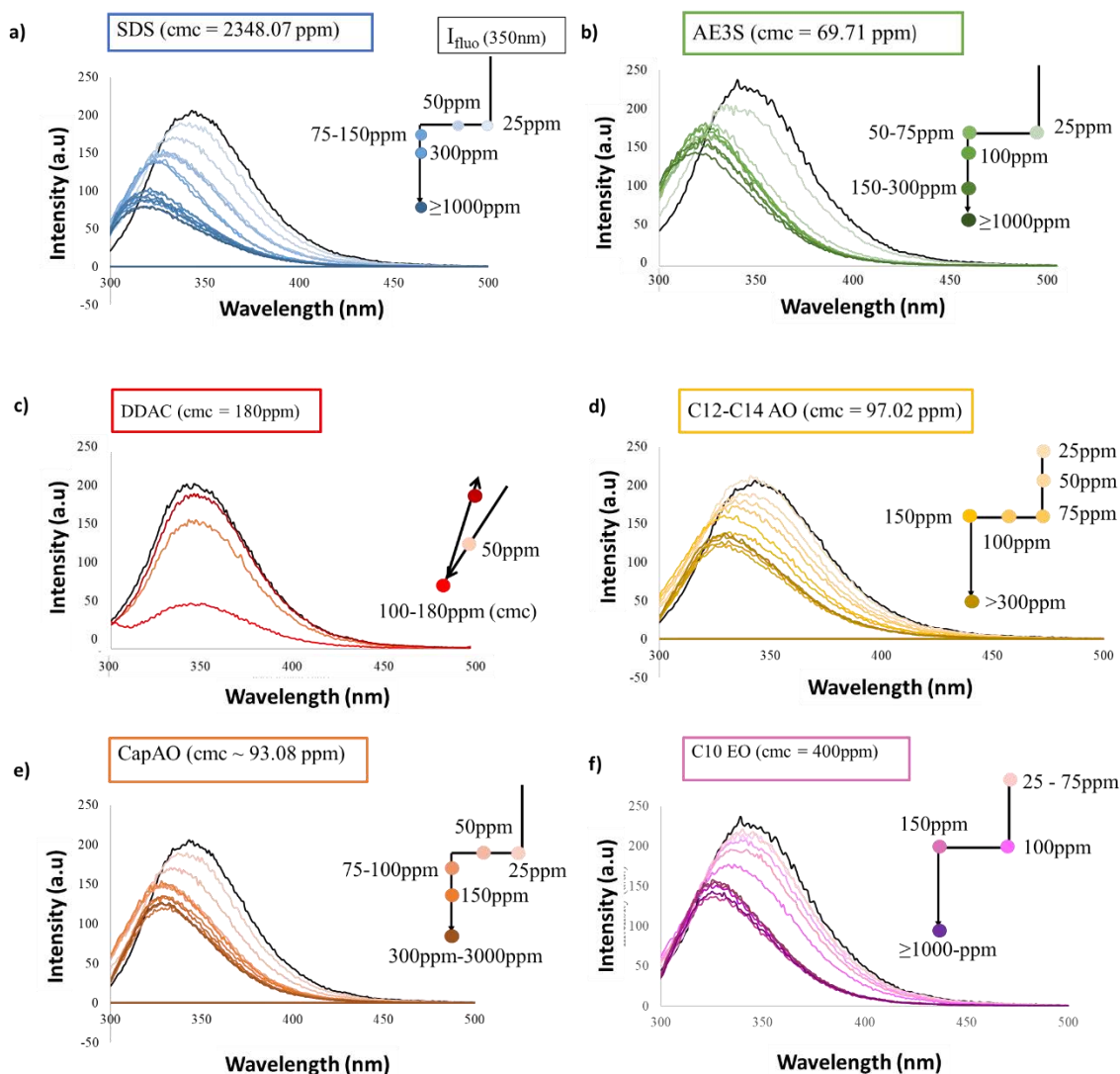
Figure 64 – Fluorescence spectra of BSA-surfactant mixtures at different surfactant concentrations. The surfactant analysed are SDS (a), AE3S (b), DDAC (c), C12-C14 AO (d), CapAO (e) and C10 EO8 (f). In all cases, BSA concentration was kept equal to 1 mg/mL and fluorescence was measured at 20 °C.

Initially, emission spectra of BSA 1 mg/mL were collected for pure protein, as well as in combination with surfactants over a range of concentrations. Emission spectra are shown in Figure 64, where different types of surfactant were selected to assess the effect of surfactant head charge and size on BSA denaturation. It can be observed that the emission spectrum of pure BSA (in black in the charts) exhibits a maximum at 345 ± 1 nm when excited at 280 nm. When the BSA is mixed with surfactant, a decrease in the fluorescence intensity (I_{fluo}) as well as a shift in the maximum position (λ_{max}) occurs in most cases.

However, differences can be observed on the quenching of BSA fluorescence according to the surfactant type.

Among the anionic surfactants, SDS and AE3S were analysed, which have the same head group charge, but different size, with AE3S having a bigger head group size than SDS. In the case of SDS, three species can be discerned, as already described in literature[70]. In addition to native BSA, a second specie is found for SDS concentration between 50 ppm and 300 ppm, which has its maximum of emission at 327 ± 2 nm which is related to the formation of a SDS-BSA complex. Instead, for higher SDS concentration, a peak corresponding to denaturated BSA, which λ_{max} is aroun 320 ± 1 nm, is found. It can be observed that, in the case of AE_3S (Figure 64b), I_{fluo} reaches its minimum and λ_{max} is fully shifted to lower wavelength for a lower surfactant concentration (around 75 ppm). Moreover, this concentration is very close to the cmc of AE_3S (69.71 ppm). This result suggests that there is a strong interaction between AE_3S and BSA, where the interaction between surfactant monomers and protein occurs at a surfactant concentration below 50 ppm (higher I_{fluo} and λ_{max}), whereas the interaction between surfactant micelles and hydrophobic domains of BSA becomes the main mechanism even at 75 ppm. When BSA interacts with surfactant micelles, according to the pearl necklace model[51,52], protein unfolding occurs and the surfactant monomers are tightly packed around the hydrophobic domains of the protein because of the big size of AE_3S head. Instead, the *cmc* of SDS is much higher than the one of AE_3S, therefore the interaction with surfactant monomers is the main mechanism for most of the surfactant concentrations analysed. In this case, the quenching starts at low concentration and changes in protein conformation occurs, but a higher surfactant concentration is required to cause a full decrease in I_{fluo} and λ_{max} (~300 ppm, Figure 64a).

An interesting case is represented by DDAC, which is a cationic surfactant with a quaternary ammonium head group. DDAC has a similar head charge density than SDS but it is oppositely charged.

144

When looking at the quenching of BSA fluorescence as a function of DDAC concentration (Figure 64c), it can be observed that the minimum in I_{fluo} and λ_{max} is reached for a surfactant concentration of 180 ppm, which is the *cmc* of the surfactant. However, at concentrations above the *cmc*, the fluorescence intensity increases again, and the emission spectrum is very similar to the one of native BSA. This is in line with what already observed for CTAC by Gelamo[70]. This behaviour can be rationalized by the assumption that the interaction between BSA and DDAC only occurs when the surfactant in present as a monomer, whereas the DDAC micelles are not involved in any interaction with the protein. This has been confirmed by carrying the same measurements on a BSA-DDAC mixture where the DDAC concentration is progressively increased. It was found that the same behaviour is observed if surfactant titration is carried in the presence of BSA, as shown in Figure 65. Addition of DDAC above its cmc results in a recovery of fluorescence and the resulting solution appears transparent.
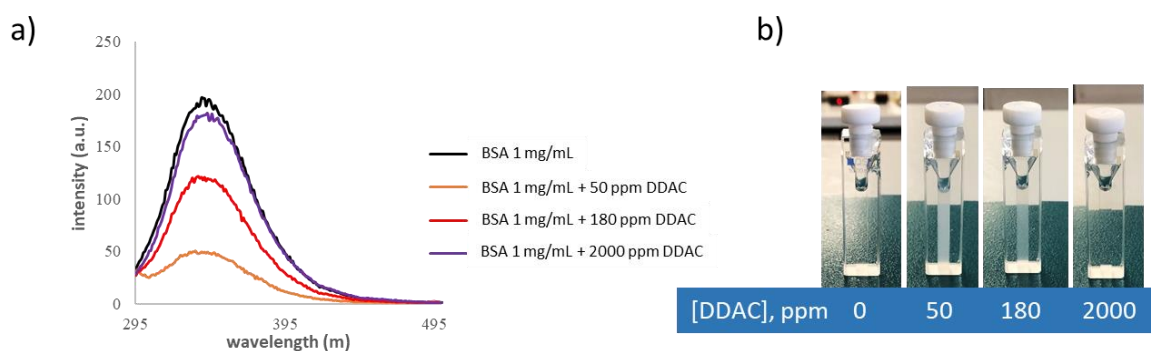
Figure 65 – a) Fluorescence spectra of BSA mixed with DDAC at different concentrations (0, 50, 180, 2000 ppm) in water and corresponding pictures of the samples (b). In all cases, BSA concentration was kept equal to 1 mg/mL and fluorescence was measured at 20 °C.

The interaction between amphoteric surfactants and BSA was studied by looking at C12-C14 AO and CapAO (Figure 64d and e). Fluorescence spectra were measured in PBS, where both the surfactants do not have a net charge. As observed when comparing SDS and AE_3S, the presence of a big head (CapAO vs C12-C14 AO) induces faster quenching of BSA fluorescence. A minimum in λ_{max} is observed for a CapAO concentration equal to 75 ppm, instead of 150 ppm needed for C12-C14 AO. Furthermore, the amphoteric surfactants were compared with a non-ionic surfactant ($C10\ EO_8$), which is not charged. In the later case, the interaction between surfactant and BSA required an even higher concentration than

in the case of C12-C14 AO and CapAO. Therefore, it can be deduced that the interaction with BSA is favoured in the case of ionic surfactants, followed by amphoteric surfactants, while non-ionic surfactants are the one interacting the least with the protein.
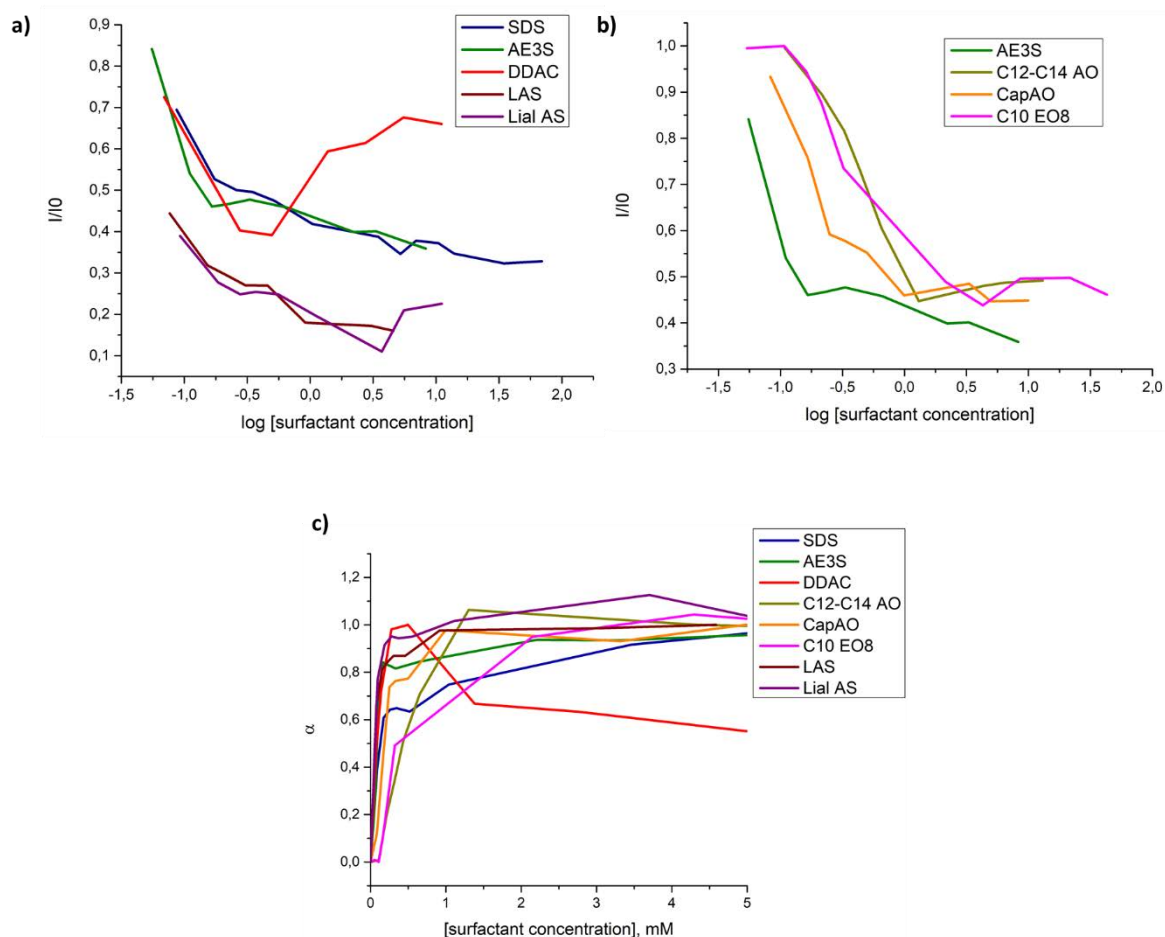
Figure 66 - Plots of fluorescence intensity of BSA-surfactant system (normalized versus fluorescence intensity of pure BSA at 1mg/mL) as a function of surfactant concentrations for ionic surfactants (a) and non-ionic/amphoteric surfactants (b). c) Diagram of fraction of surfactant bound to the BSA (α) as a function of surfactant concentration.

The effect of surfactant type on the interaction with BSA is highlighted by plotting the normalized fluorescence intensity as a function of surfactant concentration for all the surfactants analysed (Figure 66). The normalized intensity is calculated, as explained in section 1.6.3, by dividing the intensity at 350 nm measured for the surfactant-BSA system at a certain concentration (I) by the intensity of pure BSA at 350 nm (I_0). In Figure 65a, the plot for ionic surfactants is shown. It can be seen that the initial decrease of I/I_0 is steep for this type of surfactants, confirming a fast interaction between the surfactant

and the BSA. The trend is steepest for AE_3S, suggesting that the greatest effect on protein denaturation is due to the size of surfactant head. Moreover, the normalised intensity was plotted also for LAS and Lial AS, which are branched surfactants. From the chart, it can be deduced that the presence of branching induces higher denaturation of the protein, as the intensity detected is much lower than the one observed for linear ionic surfactants. An explanation for the enhanced interaction between the branched surfactants and proteins can be related to the improved packing achieved by branched surfactants around the hydrophobic domains of the protein. The unfolded protein is heavily stabilized even at lower surfactant concentration, as a consequence.

Table 9 - Binding constant to BSA of some of the surfactants analysed in this work. The binding constant was determined by fitting the plot of the fraction of surfactant bound to the protein vs surfactant concentration using the Langmuir equation (equation 47).

Surfactant type	Surfactant	Binding constant ($K_{L, mmol}^{-1)}$)
Anionic surfactants	SDS	(6.8 ± 0.9)
	AE_3S	(15.2 ± 0.5)
	Lial	(34.4 ± 0.8)
	LAS	(26 ± 3)
Amphoteric surfactants	C12-C14 AO	(1.9 ± 0.6)
	CapAO	(5.5 ± 1.4)
Non-ionic surfactants	C10 EO8	(1.7 ± 0.5)
Cationic surfactants	DDAC	(9 ± 2)

In Figure 66b, the amphoteric and non-ionic surfactants are compared to AE_3S. A delay in protein quenching due to amphoteric and non-ionic surfactants can be highlighted by the chart, as the decrease

of normalised intensities occurs at a higher surfactant concentration. In the case of CapAO, the rate of decrease in I/I_0 is close to the one observed for AE$_3$S, which proves the importance of surfactant head in the protein denaturation process. Instead, the decrease of I/I_0 in the case of C12-C14 AO is less steep, which confirms that the interaction between amphoteric surfactants and BSA requires higher surfactant concentration to cause changes in protein conformation. The non-ionic surfactant (C10 EO8) reaches the plateau in I/I_0 for the highest surfactant concentration, probably because in this case solely hydrophobic interactions are responsible for the interaction with BSA and more surfactant monomers are required to unfold the protein.

The adsorption isotherms for the surfactant-protein interaction were produced by plotting the surfactant fraction bound to the protein (α, calculated using equation 10) as a function of surfactant concentration. Results are shown in Figure 66 c and data were fitted to Langmuir equation (equation 47) so that the binding constant of the interaction was found. The Langmuir constants for each surfactant are shown in table 9. The binding constants are in line with the learnings coming from fluorescence emission spectra. The highest affinity for the BSA is observed for Lial and LAS, which are branched anionic surfactants, followed by AE$_3$S (big head anionic surfactant), SDS and DDAC (for a concentration lower than the cmc). Among the amphoteric, CapAO has a higher binding constant than C12-C14 AO to BSA, confirming the enhancement due to big head group. Instead, the lowest affinity is experienced by the non-ionic surfactant, C10 EO$_8$.

The MS and surface tension data, at a surfactant concentration of 300 ppm, were compared with fluorescence emission spectra for BSA 1mg/mL over a range of different surfactants, at the same concentration (Figure 67). As reference, the fluorescence emission spectrum for a 1 mg/mL solution of thermally denatured BSA was included, to enable the efficiency of surfactants, at 300 ppm, for denaturing BSA to be deduced. The comparison between the fluorescence emission spectra of BSA in combination with different surfactants at 300 ppm highlights that, at this low concentration, the only

surfactants that already succeed in denaturing BSA are the anionic surfactant, with a higher denaturation efficiency in the case of branched surfactants. Amphoteric and non-ionic surfactants, instead, interact with the protein to change partially the protein conformation, but are unable to achieve full exposure of the tryptophan to the hydrophilic environment. Moreover, a good correlation was found between the fluorescence data and the MS data (Figure 62) at 300 ppm, where LAS and Lial are mainly affected by the interactions with the protein, whereas the amine oxide are the least interacting with BSA at this level.
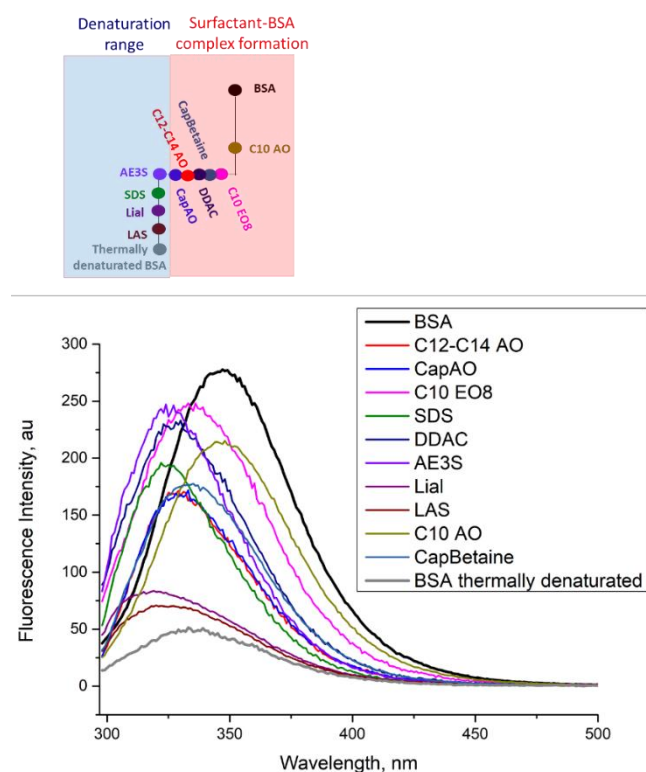
Figure 67 – Plot of fluorescence intensity of BSA at 1 mg/mL in absence (black) and in presence of surfactants at 300 ppm concentration or after thermal denaturation.

6.5 Oil emulsification by surfactants

An understanding of the interaction between surfactant and oil was investigated by looking at emulsion stability for a range of surfactants. As in the previous cases analysed in this chapter, the target surfactant concentration is 300 ppm, which represents the average surfactant concentration in a sink where dishes are hand washed via dipping and scrubbing processes. Therefore, analysis of emulsion stability on different surfactant types were run at this concentration in Turbiscan. The results are shown in Figure

66, where the higher transmission at the plateau is related to a more extensive creaming. As a result, a lower transmission at the plateau indicates better emulsification. In Figure 68a, the comparison between different surfactant classes is shown and the effect of different parameters as head group size and branching degree can also be highlighted. The resulting structure-function model for surfactant emulsion stability is presented in Figure 69 and it was found that the efficiency of surfactant packing around oil droplets impacts emulsion stability. In general, the lower transmission was observed for amine oxides surfactant (C9-C11 AO, C11 AO, C10 AO). This outcome was expected, as these surfactants are not charged at pH 8. When the surfactant monomers are packed around oil droplets, the absence of accumulated charge on surfactant head enables the surfactant to get closer (as no electrostatic repulsion is experienced) and an increase in the packing is obtained as a result. The increased packing induces a stabilization of oil droplets which avoids or causes a delay in the creaming. For the same reason, anionic surfactants have the higher transmission and worst emulsion capacity. The electrostatic repulsion between surfactant heads requires larger distances between surfactant when they are around oil droplets, therefore the packing is worst, and the emulsion is less stable.

The effect of surfactant head size can be seen by comparing C11 AO with C11 CapAO. Both surfactants have the same alkyl chain length, but the head group in the CapAO monomers is bigger than C11 AO. It can be deduced that the presence of a bigger head group leads to less stable emulsions, as demonstrated by the lower transmission measured in the case of CapAO. The lower emulsion stability for big head surfactants can be explained by considering that, when surfactant with big head groups pack around oil droplets, there is empty space between surfactant tails, and water can penetrate and destabilize the emulsions. This is also confirmed in the case of alkyl sulfate surfactants (Figure 67b), as the transmission is higher in the case of AE_3S and AE_1S surfactants compared to SDS. When analysing different types of alkyl sulfate surfactants, lower transmission was observed in the case of branched surfactant, as the branching improves the packing around oil droplets. Moreover, an optimum degree of branching needed for emulsion stability was found by analysing the transmission data. In fact, Lial AS (55% branching) is more stable that Isalchem AS (95% branching) and Shell AS (18% branching).

Therefore, a branching degree around 50% most likely induces a better packing around oil droplets than a lower (where there is still residual water between the alkyl tail) or higher branching degree (probably because of steric hindrance due to the high content of branched monomers). The type of branching affects the emulsion stability as well, as deduced by the comparison between Lial AS and Safol AS. The presence of C2-methyl branching leads to better emulsion stability than terminal cyclic branching, as in the case of Safol AS. This can be justified by considering that the branching in terminal position leads to lower packing around oil droplets and to less stable emulsions, as a consequence.
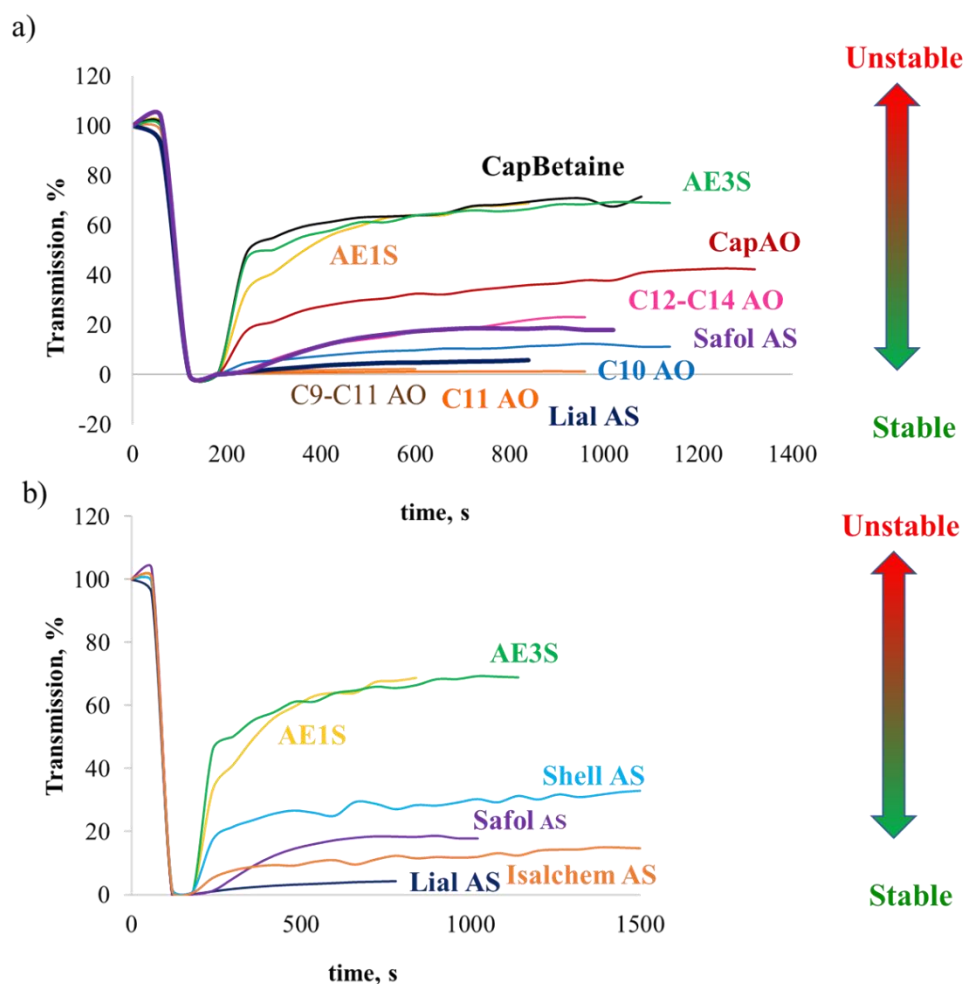
Figure 68 – Plot of average light transmission as a function of time for corn oil emulsions generated in Turbiscan. The emulsions were obtained via addition of 5% corn oil in 20 mL of surfactant solution at 300 ppm in water at 15 °dH. The emulsions were generated by mixing for 2 minutes at 1600 rpm and at 35 °C and the transmission was measured in the centre of the vial for about 20 minutes. On the left (a), a series of different surfactant classes are compared. On the right 9b), transmission profiles for alkyl sulfate with different surfactant head size and branching degree are shown.

Figure 69 – Structure-function model for emulsion stability. The model is based on turbiscan data collected for surfactant at 300 ppm and 35 °C.

6.6 Conclusions

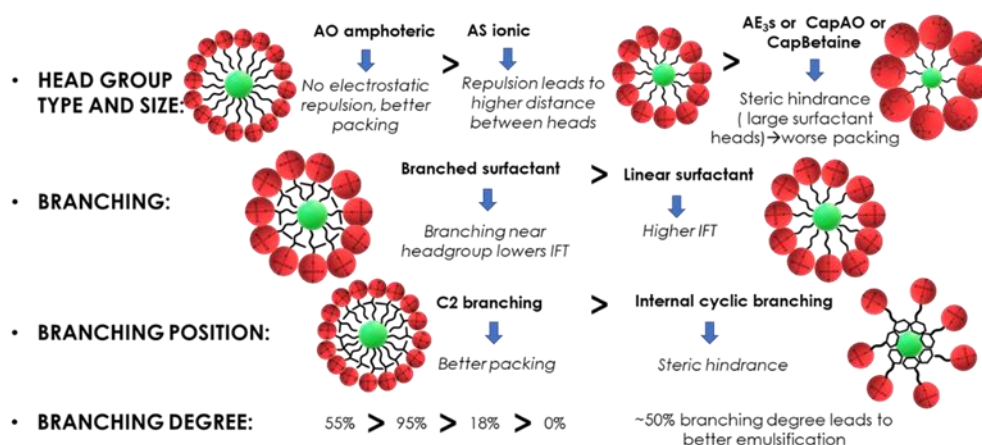In this chapter, the interactions between surfactants with common components found in food soil (eg. starch, BSA and corn oil) were investigated. Surfactants with different structure properties were studied to achieve an understanding on the effect that surfactant structure has on the interaction with soil components. Our aim was to identify which surfactant properties are needed to lower the interaction between surfactants and starch or proteins and enhance emulsion stability, so that cleaning is enhanced.

The interaction between surfactants and starch, through surfactant inclusion in the amylose helix, was assessed via surface tension and mass spectrometry. Comparison between mass spectra of the surfactant solutions, with and without 2% starch, led to the quantification of the percentage of surfactant inclusion in the amylose helical structure. A structure-function relationship was found for surfactant inclusion in amylose and the efficiency of inclusion was found to depend on the surfactant chain length, head group size and type, as well as the presence of branching in the alkyl chain. The model shows that surfactants with shorter chain length, because of their lower hydrophobicity, are less affected by the interaction with amylose than the ones with longer alkyl tails. Moreover, if the surfactant has a large head group, a decrease in surfactant inclusion, within the amylose helix, was observed, as a consequence of steric hindrance. For the same reason, the presence of branching prevents the inclusion in the helical structure,

as this results in a surfactant diameter that is bigger than the inner diameter of the amylose helix. It is also important to consider the head group charge of the surfactant, as amphoteric surfactants are more hydrophobic than ionic surfactants and they are more involved in the interaction with amylose, as a consequence. The MS data were confirmed via surface tension, where an increase in surface tension was observed when starch was added to a surfactant that is highly included in the amylose helix.

The same parameters related to surfactant structure were found to be significant when determining the strength of the interaction with BSA. As with starch, a relationship between the surfactant structure and the efficiency of denaturation of BSA was found. The main factors controlling protein denaturation were found to be surfactant head group charge and chain length. In general, anionic surfactants denaturate BSA more efficiently than amphoteric and non-ionic surfactants, as specific binding occurs. Moreover, longer alkyl tail surfactants are better denaturing agents, as the hydrophobic interactions between the surfactant alkyl tail and the hydrophobic domains of the BSA are stronger. For surfactants with similar head group charges, the interaction with BSA is enhanced by the presence of branches or by bigger head size, as these features help to stabilize the unfolded protein by increasing packing around hydrophobic domains.

Emulsions were generated by adding corn oil and the transmission of light through each emulsion suspension was measured to investigate the relationship between surfactant structure and emulsion stability. The charge of surfactant head group charge was found to be an important parameter for emulsion stability, as amine oxide class was found to lead to better emulsification at pH 8. This is a consequence of the closer packing achieved by uncharged surfactant around oil droplets because of the absence of electrostatic repulsions between surfactant head groups. The size of surfactant head group was found to also have an influence, with bigger head groups leading to worse packing and more unstable emulsions. Branching also impacts emulsion stability, where a 50% degree of branching was

found to be the optimum for emulsion stability. Moreover, C2-methyl branched surfactants are more efficient in stabilising emulsions than surfactant with branches placed at the end of the alkyl tail.

The work carried out in this chapter has, therefore, identified what structural properties a surfactant should have, in order to enhance the interaction with food soil components. These findings can be employed to identify which surfactants should be ideally included in a detergent formulation in order to maximize the interactions with the components of the soil, and hence enhance the cleaning.

Chapter 7. Concluding remarks and future works

7.1 Conclusions

In this thesis, surface modification of polyester and cotton fabric via soil release polymer deposition was studied. Different classes of SRP were selected, based on charge and/or chemical structure of the polymer, and deposition parameters such as pH, agitation speed and water hardness were investigated. It was found that all classes of SRP investigated were effective in modifying polyester, but not cotton, probably because of the higher hydrophilicity of the latter.

In Chapter 3, the use of streaming potential and UV/vis absorption measurements provided insights into the thermodynamics and kinetics of deposition of PEG-POET SRPs. Among this class of SRP, the non-ionic SRN240 showed better efficiency of deposition at pH 8 than the anionic SRA300F, which is probably related to the electrostatic repulsion between polyester and SRA300F, both negatively charged. It was found that faster kinetics and higher efficiency of deposition were achieved for both SRPs at pH 4, than pH 8. Yet, the use of water hardness was found to enhance the deposition of only SRA300F, as a consequence of lower electrostatic repulsions between SRP and polyester. Changes in surface roughness, hence surface area, were found on PEG-POET-modified polyester. Moreover, PEG-POET-modified polyester was found to be more hydrophilic than unmodified polyester. NMR measurements of the self-diffusion coefficient of water, inside these SRP-modified fabrics, suggested that two different mechanisms of deposition were possible, depending on the SRPs. It was hypothesised that SRA300F forms a film on top of the polyester, wherease a mechanism based on pore clogging was hypothesised for SRN240.

In Chapter 4, deposition of PEG-4-MEMA/METAC SRPs on cotton and polyester was investigated. The use of thermal gravimetric analysis (TGA) and streaming potential measurements indicated SRPs with higher MEMA content (60%) resulted in greater deposition on polyester at pH 8, probably as a

consequence of stronger hydrophobic interactions. No meaningful deposition of PEG-4-MEMA/METAC was observed on cotton,s even if electrostatic attraction was expected to occur between the cationic SRPs and cotton, which is negatively charged.

In Chapter 5, the effect of SRPs deposition on soil removal was evaluated for all SRPs, both on cotton and on polyester. The poor grease removal from cotton fabrics which had been pre-treated with SRPs appeared to confirm the hyphotesis that the SRPs classes investigated did not deposit on cotton. Within the PEG-POET class of SRP, SRN240 was found to lead to better soil removal than SRA300F, suggesting a correlation between efficiency of deposition of SRPs and soil removal. Similar benefits were found for lard removal on polyester pre-treated with PEG-4-MEMA/METAC SRPs, compared to untreated polyester, confirming the hypothesis that a similar amount of the three polymers was deposited. An understanding on BSA affinity to polyester, with and without pre-conditioning with SRPs, was reached. A combination of streaming potential and bicinchoninc acid (BCA) assays were used to assess the amount of BSA deposited. Results showed that BSA has a higher affinity to polyester at pH 4, than pH 8, probably because of electrostatic attraction between positively charged BSA and negatively charged polyester at this pH. Moreover, it was found that BSA deposition is enhanced by PEG-4-MEMA/METAC SRPs and decreased by PEG-POET SRPs at pH 7.2, whereas the opposite occurs at pH 4. These results suggest that deposition of BSA on polyester is mainly driven by electrostatic interactions. Release of BSA from the fabrics after deposition was also assessed, highlighting that SRPs don't deliver any benefits on BSA release at pH 7.2. An improvement in the quantity of BSA release was found for PEG-4-MEMA/METAC SRPs at pH 4, probably as a consequence of the lower adhesion of BSA to the fabric when the polymer is present.

In Chapters 3 and 4, the interactions between SRPs and surfactants, commonly used in laundry detergents, were assessed in bulk by surface tension measurements. A lack of interactions in solution between surfactants and SRPs is usually required, so that SRPs are free to deposit on polyester and

surfactants are in solution, interacting with the soil and leading to cleaning. Studies on the interaction between SRPs and anionic and amphoteric surfactants were carried out in Chapter 3 and 4 Results showed that Isalchem AS, which is a lauryl alkyl sulfate containing 95% of C2-methyl isomers, did not interact with any of the SRPs at this level. SDS, AE_3S and LAS interacted with PEG-4-MEMA/METAC SRPs, as expected, being SRPs cationic and analysed surfactants anionic. Instead, SRA300F did not interact with any of the anionic surfactants, in line with what described in literature[160]. Interactions between amphoteric surfactants (not charged at pH 8) and cationic/ anionic SRPs were observed. The non-ionic SRN240 showed weak interactions with SDS and AE_3S, which is in line with results from Yang and Rathman at this SRP concentration[160]. To sum up, Isalchem AS is a good surfactant to combine with SRPs as it does not interact with these polymers, while amphoteric surfactants are only suitable to be combined with non-ionic SRN240, as there is no meaningful interactions in this case. Anionic SRA300F can be used in combination with of AE_3S, LAS or SDS (and anionic surfactants, more in general) in order to prevent any coacervation or surfactant-polymer complex formation. This, demonstrates that the selection of the SRP most appropriate for a laundry formulation is influenced by the charge of the surfactants within the formulation.

In Chapter 6, the interactions of surfactants with model components commonly found in food stains were investigated. It was observed that soil removal is enhanced from polyester surfaces where SRPs were deposited. However, it is equally important to prevent the re-deposition of any removed soil, which can be achieved by including surfactants, which promote good emulsion stability and efficient protein denaturation, in laundry detergent formulations. To this end, certain interactions between surfactants and soil components should be avoided, as they result in lowering the amount of surfactant monomers available in solution, affecting the efficiency of cleaning. For instance, the inclusion of surfactant monomers in the helical structure that amylose forms in solution reduces the number of surfactant monomers left in solution. In this thesis, we investigated the interaction between food soil components, such as starch, BSA and oil, and several surfactants, which differ in respect to head group size and charge, length of the alkyl tail and branching degree. Starch was chosen as a representative of

polysaccharides, typically present in many stains of food origin. The efficiency of inclusion in the amylose helix structure as a function of surfactant structure was investigated by mass spectrometry and surface tension. It was observed that structural features of surfactant that enhanced inclusion in amylose helix are the ones that leads to high surfactant hydrophobicity, as presence of linear and long alkyl tail, as well as small and not charged head. The effect of surfactant structure on BSA quenching and denaturation was studied by fluorescence spectroscopy and mass spectroscopy. The interaction was found to be favoured in the case of ionic surfactants, because of specific binding occurring between surfactant heads and charged amino acids presents along the protein chain. Branched and/or big head surfactants were found to denature BSA more, as there is a better stabilization of the hydrophobic domains in the unfolded protein. The effect of surfactant chain length on the interaction with protein was highlighted, where the longer the tail, the stronger is BSA quenching, as already reported in literature[161]. Finally, emulsion stability as a function of surfactant structure was investigated, identifying a relationship between surfactant structure and speed of creaming. Turbiscan data suggested that the best surfactant to stablise the emulsion was an amphoteric/non-ionic surfactant with a small head group size and that had a 50% branching degree. Our observations on the interactions between surfactant and different soil components suggests that there is no single surfactant that is poorly included in the amylose helix and that efficiently denaturates protein at the same time. The use of branched surfactants seem to be the most promising option to achieve an optimum for these interactions. However, a balance between poor inclusion in amylose helix and efficiency in denaturatig protein has to be found when choosing charge and size of surfactant head and length of the alkyl tail, as opposite structural features are needed to optimize the interaction with starch, proteins and oil.

7.2 Future Work

The results presented in this thesis help to design a laundry formulation including a SRP that efficiently deposit on polyester, improving its cleanability. However, further studies are needed to determine the most appropriate surfactant-SRP combinations leading to improved cleaning. While understanding of the surfactant-SRPs interactions in bulk was achieved, the next step will be to assess how the presence

of surfactants affects the pre-conditioning of polyester with SRPs.. This will need to be achieved by assessing changes in surface charge, soil removal index, surface wettability, roughness and surface area, in the presence of surfactants. Indeed, different effects on these parameters can be expected if there is competition or enhancement in deposition between surfactant monomers and SRPs. The selection of surfactants SRP combinations should be based on the structure-function correlation model developed in this thesis on surfactant-soil interactions.

Lastly, this work has focused on the interactions between single food soil components and surfactants. In reality, most stains are composed of a combination of oil, proteins, polysaccharides and solid particles. Therefore, the next step in this research would be to assess the effect of a combination of different soil components on surfactant availability. A correlation between the structure-function models developed in this thesis andstain removal indexes for real food stains would be achieved. The use of scattering techniques as SAXS and SANS may help to characterise any resulting complexes between surfactants with SRPs, starch or amylose, while X-ray reflectometry (XRR) may give insights on the composition of polymer-surfactant mixture at the air/water interface.

References

(1)   A.I.S.E. Pan-European consumer survey on sustainability and washing habits https://www.aise.eu/documents/document/20151020151708-aise_consumershabitssurvey_summary2015-def.pdf.

(2)   A.I.S.E., Stamminger, I. Laundry Washing Habits - Diverse profiles across Europe https://www.aise.eu/documents/document/20151102183240-lowtemp_projectdescription_update_2nov2015_final.pdf.

(3)   A.I.S.E. Perceptions of cleanliness and hygiene-cleaning habits, sustainability and safety https://www.aise.eu/documents/document/20180528165059-aise_consumershabitssurvey2017_summary_final.pdf.

(4)   A.I.S.E. Pan-European consumer habits research https://www.aise.eu/our-activities/information-to-end-users/consumer-research.aspx.

(5)   Mylan, J. The Business of "Behaviour Change": Analysing the Consumer-Oriented Corporate Sustainability Journey of Low-Temperature Laundry. *Organ. Environ.* **2017**, *30*, 283–303.

(6)   Holme, I. Adhesion to Textile Fibres and Fabrics. *Int. J. Adhes. Adhes.* **1999**, *19*, 455–463.

(7)   Hasan, M. M. B.; Calvimontes, A.; Synytska, A.; Dutschk, V. Effects of Topographic Structure on Wettability of Differently Woven Fabrics. *Text. Res. J.* **2008**, *78*, 996–1003.

(8)   Hossai, M. M. Plasma Technology for Deposition and Surface Modification - Doctoral Dissertation, Universitat Bremen, 2009.

(9)   Yanılmaz, M.; Kalaoğlu, F. Investigation of Wicking, Wetting and Drying Properties of Acrylic Knitted Fabrics. *Text. Res. J.* **2012**, *82*, 820–831.

(10)   Hatch, K. L. *Textile Science*, 2nd ed.; Delmar, Ed.; West Pubblishing company: Eagan, 1993.

(11)   Gordon, S., Hsieh, Y. L. *Cotton: Science and Technology*; Woodhead Publishing Limited, 2007.

(12)   Getchell, N. F. Cotton Quality Study III : Resistance To Soiling. *Text. Res. J.* **1955**, *25*, 150–194.

(13)   El Messiry, M.; El Ouffy, A.; Issa, M. Microcellulose Particles for Surface Modification to Enhance Moisture Management Properties of Polyester, and Polyester/Cotton Blend Fabrics. *Alexandria Eng. J.* **2015**, *54*, 127–140.

(14) Butola, B. S. Advances in Functional Finishes for Polyester and Polyamide-Based Textiles. In *Polyesters and Polyamides*; Woodhead publishing limited: Cambridge, 2008; pp 325–353.

(15) Maida, J. BizVibe: Cotton, Polyester, and Smart Textile Markets on the Rise https://www.businesswire.com/news/home/20170324005625/en/BizVibe-Cotton-Polyester-Smart-Textile-Markets-Rise.

(16) Huang, J. Review of Heat and Water Vapor Transfer through Multilayer Fabrics. *Text. Res. J.* **2016**, *86*, 325–336.

(17) Chowdhury, A. K. R. Antistatic and Soil-Release Finishes. In *Principle of Textile finishing*; woodhead publishing limited: Cambridge, 2017; pp 285–318.

(18) Smith, S.; Sherman, P. Textile Characteristics Affecting the Release of Soil During Laundering. *Text. Res. J.* **1968**, *310*, 441–449.

(19) G.M. Venkatesh, N.E. Dweltz, G. L. M. A Study of Textiles and Development of Anti-Soiling and Soil Release Finishes: A Review. *Text. Res. J.* **1974**, *33*, 352–362.

(20) K. Ogino, W. A. A Study of Removal of Oily Soil by Rolling up in Detergency. *Bull. Chem. Soc. Japan* **1976**, *49*, 1703–1708.

(21) Kissa, E. Mechanisms of Soil Release. *Text. Res. J.* **1981**, *51*, 508–513.

(22) Coulson, S. Plasma Treatment of Textiles for Water and Oil Repellency. In *Plasma technology for textile*; Woodhead Publishing Limited: Cambridge, 2007; pp 183–201.

(23) De Geyter, N.; Morent, R.; Leys, C. Surface Modification of a Polyester Non-Woven with a Dielectric Barrier Discharge in Air at Medium Pressure. *Surf. Coatings Technol.* **2006**, *201*, 2460–2466.

(24) Gotoh, K.; Yoshitaka, S. Improvement of Soil Release from Polyester Fabric with Atmospheric Pressure Plasma Jet. *Text. Res. J.* **2013**, *83*, 1606–1614.

(25) Ferrero, F. Wettability Measurements on Plasma Treated Synthetic Fabrics by Capillary Rise Method. *Polym. Test.* **2003**, *22*, 571–578.

(26) Bourne, M. C.; Jennings, W. G. Definition of the Word "Detergent." *J. Am. Oil Chem. Soc.* **1963**, *40*, 212–212.

(27) Bajpai, D.; Tyagi, V. K. Laundry Detergents: An Overview. *J. Oleo Sci.* **2007**, *56*, 327–340.

(28) Mercadé -Prieto, R.; Bakalis, S. Methodological Study on the Removal of Solid Oil and Fat Stains from Cotton Fabrics Using Abrasion. *Text. Res. J.* **2014**, *84*, 52–65.

(29)   Breen, N. E.; Durnam, D. J.; Obendorf, S. K. Residual Oily Soil Distribution on Polyester/Cotton Fabric after Laundering with Selected Detergents at Various Wash Temperatures. *Text. Res. J.* **1984**, *54*, 198–204.

(30)   Adam, N. K. Detergent Action and Its Relation to Wetting and Emulsification. *J. Soc. Dye. Colour.* **2008**, *53*, 121–129.

(31)   Magin, C. M.; Cooper, S. P.; Brennan, A. B. Non-Toxic Antifouling Strategies. *Mater. Today* **2010**, *13*, 36–44.

(32)   Damodaran, V. B.; Murthy, N. S. Bio-Inspired Strategies for Designing Antifouling Biomaterials. *Biomater. Res.* **2016**, *20*, 18–20.

(33)   Sutherland, I. W. The Biofilm Matrix-an Immobilized but Dynamic Microbial Environment. *Trends Microbiol.* **2001**, *9*, 222–227.

(34)   Donlan, R. M. Biofilms: Microbial Life on Surfaces. Emerg Infect Diseases. *Emerg Infect Dis.* **2002**, *8*, 881–890.

(35)   Sutherland, I. W. The Biofilm Matrix--an Immobilized but Dynamic Microbial Environment. *Trends Microbiol.* **2001**, *9*, 222–227.

(36)   Schollmeyer, E.; Ulbricht, M.; Wego, A.; Bahners, T.; Klingelhöller, K. Photo-Chemical Surface Modification for the Control of Protein Adsorption on Textile Substrates. *J. Adhes. Sci. Technol.* **2011**, *25*, 2219–2238.

(37)   Solano, C.; Echeverz, M.; Lasa, I. Biofilm Dispersion and Quorum Sensing. *Curr. Opin. Microbiol.* **2014**, *18*, 96–104.

(38)   Pereni, C. I.; Zhao, Q.; Liu, Y.; Abel, E. Surface Free Energy Effect on Bacterial Retention. *Colloids Surfaces B Biointerfaces* **2006**, *48*, 143–147.

(39)   Asatekin, A.; Kang, S.; Elimelech, M.; Mayes, A. M. Anti-Fouling Ultrafiltration Membranes Containing Polyacrylonitrile-Graft-Poly(Ethylene Oxide) Comb Copolymer Additives. *J. Memb. Sci.* **2007**, *298*, 136–146.

(40)   Zhao, J.; Shi, Q.; Luan, S.; Song, L.; Yang, H.; Shi, H.; Jin, J.; Li, X.; Yin, J.; Stagnaro, P. Improved Biocompatibility and Antifouling Property of Polypropylene Non-Woven Fabric Membrane by Surface Grafting Zwitterionic Polymer. *J. Memb. Sci.* **2011**, *369*, 5–12.

(41)   Windler, L.; Height, M.; Nowack, B. Comparative Evaluation of Antimicrobials for Textile Applications. *Environ. Int.* **2013**, *53*, 62–73.

(42)   Mi, L.; Jiang, S. Integrated Antimicrobial and Nonfouling Zwitterionic Polymers. *Angew.*

Chemie - Int. Ed. **2014**, *53*, 1746–1754.

(43)   Luzinov, I. Nanofabrication of Thin Polymer Films. In *Nanofibers and Nanotechnology in Textiles*; woodhead publishing limited: Cambridge, 2007; pp 448–469.

(44)   Zdyrko, B.; Luzinov, I. Polymer Brushes by the "Grafting to" Method. *Macromol. Rapid Commun.* **2011**, *32*, 859–869.

(45)   Bertleff, W.; Neumann, P.; Baur, R.; Kiessling, D. Aspects of Polymer Use in Detergents. *J. Surfactants Deterg.* **1998**, *1*, 419–424.

(46)   ean Gauthier-Lafaye, Robert Gresser, Gilles Guerin, D. J. Polymers in Detergency. In *Proceedings of the 4th World Conference on Detergents: Strategies for the 21st century*; Arno Cahn, Ed.; Pearl river, New York, 1999; pp 190–200.

(47)   O'Lenick, A. J. Soil Release Polymers. *J. Surfactants Deterg.* **1999**, *2*, 553–557.

(48)   Showell, M. S. *Powdered Detergents*, 1st editio.; CRC press: Boca Raton, 1998.

(49)   Manohar, K. S.; Alan, W. R.; Paul, G. E. Cotton Soil Release Polymers. 6,087,316, 1997.

(50)   Gosselink, Eugene Paul; Price, K. N. Cotton Soil Release Polymers. 6,071,871, June 6, 2000.

(51)   Sen, S.; Sukul, D.; Dutta, P.; Bhattacharyya, K. Fluorescence Anisotropy Decay in Polymer−Surfactant Aggregates. *J. Phys. Chem. A* **2001**, *105*, 7495–7500.

(52)   Cabane, B. Structure of Some Polymer-Detergent Aggregates in Water. *J. Phys. Chem.* **1977**, *81*, 1639–1645.

(53)   Bit, G.; Ali, M.; Debnath, B.; Saha, S. K. Solution Properties of a Polymer-Nonionic Surfactant Mixed System. *J. Dispers. Sci. Technol.* **2010**, *31*, 1085–1090.

(54)   Jain, N.; Trabelsi, S.; Guillot, S.; McLoughlin, D.; Langevin, D.; Letellier, P.; Turmine, M. Critical Aggregation Concentration in Mixed Solutions of Anionic Polyelectrolytes and Cationic Surfactants. *Langmuir* **2004**, *20*, 8496–8503.

(55)   Diamant, H.; Andelman, D. Onset of Self-Assembly in Polymer-Surfactant Systems. *EDP Sci. EPL* **1999**, *48*, 1–7.

(56)   Walstra, P.; Smulders Pauline E. A. Formation of Emulsion. In *Modern aspect of emulsion science*; Becher, P., Ed.; The Royal Society of Chemistry: Cambdridge, 1983.

(57)   K.A. Lucassen-Reynders; E.H. Kuijpers. The Role of Interfacial Properties in Emulsification. *Colloids and Surfaces* **1992**, *65*, 175–184.

(58)   Godwin J.W. Emulsions and Microemulsions. In *Colloids and Interfaces with Surfactants and*

Polymers - An Introduction; Godwin J.W, Ed.; John Wiley and Sons, Ltd, 2004.

(59)   Abbott, P. S. *Surfactant Science : Principles and Practice*; DEStech Publications, Ed.; Lancaster, 2017.

(60)   Chen, G.; Tao, D. An Experimental Study of Stability of Oil-Water Emulsion. *Fuel Process. Technol.* **2005**, *86*, 499–508.

(61)   Salou, M.; Siffert, B.; Jada, A. Study of the Stability of Bitumen Emulsions by Application of DLVO Theory. *Colloids Surfaces A Physicochem. Eng. Asp.* **1998**, *142*, 9–16.

(62)   Binks, B. P.; Lumsdon, S. O. Stability of Oil-in-Water Emulsions Stabilised by Silica Particles. *Phys. Chem. Chem. Phys.* **1999**, *1*, 3007–3016.

(63)   Buléon, A.; Colonna, P.; Planchot, V.; Ball, S. Starch Granules: Structure and Biosynthesis. *Int. J. Biol. Macromol.* **1998**, *23*, 85–112.

(64)   Bertoft, E. *Analyzing Starch Molecular Structure*; Elsevier Ltd, 2017.

(65)   Putseys, J. A.; Lamberts, L.; Delcour, J. A. Amylose-Inclusion Complexes: Formation, Identity and Physico-Chemical Properties. *J. Cereal Sci.* **2010**, *51*, 238–247.

(66)   Mira, I.; Eliasson, A. C.; Persson, K. Effect of Surfactant Structure on the Pasting Properties of Wheat Flour and Starch Suspensions. *Cereal Chem.* **2005**, *82*, 44–52.

(67)   Bradshaw, R. A.; Purton, M. *Proteins : Form and Function*, 1st editio.; Academic Press: Cambridge, 1990.

(68)   Valstar, A.; Almgren, M.; Brown, W.; Vasilescu, M. The Interaction of Bovine Serum Albumin with Surfactants Studied by Light Scattering. *Langmuir* **2000**, *16*, 922–927.

(69)   Chen, A.; Wu, D.; Johnson, C. S. Determination of the Binding Isotherm and Size of the Bovine Serum Albumin-Sodium Dodecyl Sulfate Complex by Diffusion-Ordered 2D NMR. *J. Phys. Chem.* **1995**, *99*, 828–834.

(70)   Gelamo, E. L.; Tabak, M. Spectroscopic Studies on the Interaction of Bovine (BSA) and Human (HSA) Serum Albumins with Ionic Surfactants. *Spectrochim. Acta - Part A Mol. Biomol. Spectrosc.* **2000**, *56*, 2255–2271.

(71)   Chodankar, S.; Aswal, V. K.; Kohlbrecher, J.; Vavrin, R.; Wagh, A. G. Surfactant-Induced Protein Unfolding as Studied by Small-Angle Neutron Scattering and Dynamic Light. *J. Phys. Condens. Matter* **2007**, *19*, 1–12.

(72)   De, S.; Girigoswami, A.; Das, S. Fluorescence Probing of Albumin-Surfactant Interaction. *J. Colloid Interface Sci.* **2005**, *285*, 562–573.

(73)   Gelamo, E. L.; Silva, C. H. T. P.; Imasato, H.; Tabak, M. Interaction of Bovine (BSA) and Human (HSA) Serum Albumins with Ionic Surfactants: Spectroscopy and Modelling. *Biochim. Biophys. Acta - Protein Struct. Mol. Enzymol.* **2002**, *1594*, 84–99.

(74)   Paul, B. K.; Samanta, A.; Guchhait, N. Exploring Hydrophobic Subdomain of the Protein Bovine Serum Albumin in the Native, Intermediate, Unfolded, and Refolded States by a Small Fluorescence Molecular Reporter. *J. Phys. Chem. B* **2010**, *114*, 6183–6196.

(75)   Valentini, A.; Gkatzionis, K.; Palazzo, G.; Cioffi, N.; Franco, C. Di; Robles, E.; Brooker, A.; Britton, M. M. Combined Use of Streaming Potential and UV / Vis to Assess Surface Modification of Fabrics via Soil Release Polymers. *Ind. Eng. Chem. Res.* **2019**, *58*, 14839–14847.

(76)   Bukšek, H.; Luxbacher, T.; Petrinić, I. Zeta Potential Determination of Polymeric Materials Using Two Differently Designed Measuring Cells of an Electrokinetic Analyzer. *Acta Chim. Slov.* **2010**, *57*, 700–706.

(77)   Scales, P. J.; Grieser, F.; Healy, T. W.; White, L. R.; Chan, D. Y. C. Electrokinetics of the Silica-Solution Interface: A Flat Plate Streaming Potential Study. *Langmuir* **1992**, *8*, 965–974.

(78)   Erickson, D.; Li, D. Streaming Potential and Streaming Current Methods for Characterizing Heterogeneous Solid Surfaces. **2001**, *289*, 283–289.

(79)   Werner, C.; Körber, H.; Zimmermann, R.; Dukhin, S.; Jacobasch, H.-J. Extended Electrokinetic Characterization of Flat Solid Surfaces. *J. Colloid Interface Sci.* **1998**, *208*, 329–346.

(80)   Clark, N. A.; Lunacek, J. H.; Benedek, G. B. A Study of Brownian Motion Using Light Scattering. *Am. J. Phys.* **1970**, *38*, 575–585.

(81)   Pecora, R. *Dynamic Light Scattering: Applications of Photon Correlation Spectroscopy*, 1st editio.; Plenum Press: New York, 1985.

(82)   Ruf, H.; Haase, W.; Wang, W. Q.; Grell, E.; Gärtner, P.; Michel, H.; Dufour, J. P. Determination of Size Distributions of Submicron Particles by Dynamic Light Scattering Experiments Taking into Account Normalization Errors. In *Trends in Colloid and Interface Science VII*; Steinkopff, 2008; pp 159–166.

(83)   Farooqi, Z. H.; Siddiq, M. Temperature-Responsive Poly(N-Isopropylacrylamide-Acrylamide-Phenylboronic Acid) Microgels for Stabilization of Silver Nanoparticles. *J. Dispers. Sci. Technol.* **2015**, *36*, 423–429.

(84)   Hunter, R. J. *Introduction to Modern Colloid Science*; Oxford University Press: New York,

1995; Vol. 99.

(85)   Clogston, J. D.; Patri, A. K. Zeta Potential Measurement; 2011; pp 63–70.

(86)   Mateos, H.; Valentini, A.; Robles, E.; Brooker, A.; Cioffi, N.; Palazzo, G. Measurement of the Zeta-Potential of Solid Surfaces through Laser Doppler Electrophoresis of Colloid Tracer in a Dip-Cell: Survey of the Effect of Ionic Strength, PH, Tracer Chemical Nature and Size. *Colloids Surfaces A Physicochem. Eng. Asp.* **2019**, No.

(87)   Yang, C.; Rathman, J. F. Adsorption-Solution Structure Relationships of PET/POET Polymeric Surfactants in Aqueous Solutions. *Polymer (Guildf).* **1996**, *37*, 4621–4627.

(88)   Lampman, G. M.; Vyvyan, J. R.; Pavia, D. L.; Kriz, G. S. *Introduction to Spectroscopy*, 4th editio.; Brooks/Cole Cengage learning, 2001.

(89)   Grassie, N.; Speakman, J. G. Thermal Degradation of Poly(Alkyl Acrylates). I. Preliminary Investigations. *J. Polym. Sci. Part A-1 Polym. Chem.* **1971**, *9*, 919–929.

(90)   Mostashari, S. M.; Baghi, O.; Mostashari, S. Z. Thermogravimetric Analysis of a Cellulosic Fabric Treated with Nickel Sulfate Hexahydrate as a Flame-Retardant. *Cellul. Chem. Technol.* **2009**, *43*, 95–98.

(91)   Mostashari, S. M.; Zanjanchi, M. A.; Moafi, H. F.; Mostashari, S. Z.; Chaijan, M. R. B. Thermogravimetric Analysis of a Cellulosic Fabric Incorporated by Synthetic Ammonium Magnesium Phosphate as a Flame-Retardan. *Polym. - Plast. Technol. Eng.* **2008**, *47*, 307–312.

(92)   Devaux, E.; Rochery, M.; Bourbigot, S. Polyurethane/Clay and Polyurethane/POSS Nanocomposites as Flame Retarded Coating for Polyester and Cotton Fabrics. *Fire Mater.* **2002**, *26*, 149–154.

(93)   Garche, J. *Encyclopedia of Electrochemical Power Sources*; Elsevier, 2009.

(94)   Zhou, W.; Apkarian, R. P.; Lin Wang, Z.; Joy, D. Fundamentals of Scanning Electron Microscopy. In *Scanning Microscopy for Nanotechnology: Techniques and Applications*; Springer: New York, 2006; pp 1–40.

(95)   Alshibli, K. A.; Alsaleh, M. I. Characterizing Surface Roughness and Shape of Sands Using Digital Microscopy. *J. Comput. Civ. Eng.* **2004**, *18*, 36–45.

(96)   Johnson, R. E.; Dettre, R. H.; Brandreth, D. A. Dynamic Contact Angles and Contact Angle Hysteresis. *J. Colloid Interface Sci.* **1977**, *62*, 205–212.

(97)   Callaghan, P. T.; Godefroy, S.; Ryland, B. N. Use of the Second Dimension in PGSE NMR Studies of Porous Media. In *Magnetic Resonance Imaging*; Elsevier Inc., 2003; Vol. 21, pp

243–248.

(98)   Friebolin, H. *Basic One- and Two-Dimensional NMR Spectroscopy - Fifth, Completely Revised and Updated Edition*, 5th Editio.; Weinheim, Germany, 2011.

(99)   Claridge, T. D. W. *High-Resolution NMR Techniques in Organic Chemistry*; Elsevier, 2009.

(100)   Nagashima, K. A. Z.; Velan, S.; Kuchel, P. W.; Page, G.; Vijayaragavan, V.; Nagarajan, V.; Chuang, K. A. I. H. Stejskal – Tanner Equation Derived in Full. **2012**, No., 205–214.

(101)   Thommes, M.; Kaneko, K.; Neimark, A. V.; Olivier, J. P.; Rodriguez-Reinoso, F.; Rouquerol, J.; Sing, K. S. W. Physisorption of Gases, with Special Reference to the Evaluation of Surface Area and Pore Size Distribution (IUPAC Technical Report). *Pure Appl. Chem.* **2015**, *87*, 1051–1069.

(102)   Thommes, M.; Kaneko, K.; Neimark, A. V; Olivier, J. P.; Rodriguez-Reinoso, F.; Rouquerol, J.; Sing, K. S. W. IUPAC Technical Report Physisorption of Gases, with Special Reference to the Evaluation of Surface Area and Pore Size Distribution (IUPAC Technical Report). *Pure Appl. Chem* **2015**, No., aop.

(103)   Türkün, L. Ş.; Türkün, M. Effect of Bleaching and Repolishing Procedures on Coffee and Tea Stain Removal from Three Anterior Composite Veneering Materials. *J. Esthet. Restor. Dent.* **2004**, *16*, 290–301.

(104)   Rojvoranun, S.; Chavadej, S.; Scamehorn, J. F.; Sabatini, D. A. Mechanistic Studies of Particulate Soil Detergency: II: Hydrophilic Soil Removal. *J. Surfactants Deterg.* **2012**, *15*, 663–677.

(105)   Matusiak, M.; Walawska, A.; SybIlska, W. Comparison of Spectrophotometric and Digieye Colour Measurements of Woven Fabrics. *Tekst. ve Konfeksiyon* **2017**, *27*, 53–59.

(106)   Sharpe, L. T.; Stockman, A.; Jagla, W.; Jägle, H. A Luminous Efficiency Function, VD65* (λ), for Daylight Adaptation: A Correction. *Color Res. Appl.* **2011**, *36*, 42–46.

(107)   Rosell-Llompart, J.; Grifoll, J.; Loscertales, I. G. Electrosprays in the Cone-Jet Mode: From Taylor Cone Formation to Spray Development. *J. Aerosol Sci.* **2018**, *125*, 2–31.

(108)   Rayleigh F R S. On the Equilibrium of Liquid Conducting Masses Charged with Electricity. *J. Sci.* **1882**, *14*, 184–186.

(109)   Tang, K.; Smith, R. D. Theoretical Prediction of Charged Droplet Evaporation and Fission in Electrospray Ionization. *Int. J. Mass Spectrom.* **1999**, *185*, 97–105.

(110)   Mengual, O.; Meunier, G.; Cayre, I. Turbiscan Ma 2000: Multiple Light Scattering

Measurement for Concentrated Emulsion and Suspension Instability Analysis. *Talanta* **2000**, *50*, 445–456.

(111) Chanamai, R.; McClements, D. J. Dependence of Creaming and Rheology of Monodisperse Oil-in-Water Emulsions on Droplet Size and Concentration. *Colloids Surfaces A Physicochem. Eng. Asp.* **2000**, *172*, 79–86.

(112) Sips, R. On the Structure of a Catalyst Surface. *J. Chem. Phys.* **1948**, *16*, 490–495.

(113) Pakula, C.; Stamminger, R. Electricity and Water Consumption for Laundry Washing by Washing Machine Worldwide. *Energy Effic.* **2010**, *3*, 365–382.

(114) Stejskal, E. O.; Tanner, J. E. Spin Diffusion Measurements: Spin Echoes in the Presence of a Time-Dependent Field Gradient. *J. Chem. Phys.* **1965**, No.

(115) Rouquerol, Françoise Rouquerol, J.; Sing, K. S. .; Llewellyn, P.; Maurin, G. *Adsorption by Powders and Porous Solids: Principles, Methodology and Applications*, 2nd ed.; Academic Press, 2014.

(116) Brunauer, S.; Emmett, P. H.; Teller, E. Adsorption of Gases in Multimolecular Layers. *J. Am. Chem. Soc.* **1938**, *60*, 309–319.

(117) Barret, E. P.; Joyner, L. G.; Halenda, P. P. The Determination of Pore Volume and Area Distributions in Porous Substances. I. Computations from Nitrogen Isotherms. *J. Am. Chem. Soc.* **1951**, *73*, 373–380.

(118) Grancaric, A. M.; Tarbuk, A.; Pusic, T. Electrokinetic Properties of Textile Fabrics. *Color. Technol.* **2005**, *121*, 221–224.

(119) Zimmermann, R.; Freudenberg, U.; Schweiß, R.; Küttner, D.; Werner, C. Hydroxide and Hydronium Ion Adsorption — A Survey. *Curr. Opin. Colloid Interface Sci.* **2010**, *15*, 196–202.

(120) Ghosal, P. S.; Gupta, A. K. Development of a Generalized Adsorption Isotherm Model at Solid-Liquid Interface: A Novel Approach. *J. Mol. Liq.* **2017**, *240*, 21–24.

(121) Li, H.; Jiao, Y.; Xu, M.; Shi, Z.; He, B. Thermodynamics Aspect of Tannin Sorption on Polymeric Adsorbents. *Polymer (Guildf).* **2004**, *45*, 181–188.

(122) Jeppu, G. P.; Clement, T. P. A Modified Langmuir-Freundlich Isotherm Model for Simulating PH-Dependent Adsorption Effects. *J. Contam. Hydrol.* **2012**, *129–130*, 46–53.

(123) Ho, Y. S.; Chiu, W. T.; Wang, C. C. Regression Analysis for the Sorption Isotherms of Basic Dyes on Sugarcane Dust. *Bioresour. Technol.* **2005**, *96*, 1285–1291.

(124) Giles, C. H.; Smith, D.; Huitson, A. A General Treatment and Classification of the Solute Adsorption Isotherm. *J. Colloid Interface Sci.* **1974**, *47*, 755–765.

(125) Luxbacher, T. *The Zeta Guide – Principles of the Streaming Potential Technique*.

(126) Chang, Y. Bin; Tu, P. C.; Wu, M. W.; Hsueh, T. H.; Hsu, S. H. A Study on Chitosan Modification of Polyester Fabrics by Atmospheric Pressure Plasma and Its Antibacterial Effects. *Fibers Polym.* **2008**, *9*, 307–311.

(127) Volkov, V. I.; Korotchkova, S. A.; Nesterov, I. A.; Ohya, H.; Guo, Q.; Huang, J.; Chen, J. The Self-Diffusion of Water and Ethanol in Cellulose Derivative Membranes and Particles with the Pulsed Field Gradient NMR Data. *J. Memb. Sci.* **1996**, No.

(128) Holz, M.; Heila, S. R.; Saccob, A. Temperature-Dependent Self-Diffusion Coefficients of Water and Six Selected Molecular Liquids for Calibration in Accurate 1H NMR PFG Measurements. *Phys. Chem. Chem. Phys.* **2000**, *2*, 4740–4742.

(129) Callaghan, P. T. *Translational Dynamics and Magnetic Resonance : Principles of Pulsed Gradient Spin Echo NMR*.

(130) Wende, C.; Schonhoff, M. Dynamics of Water in Polyelectrolyte Multilayers: Restricted Diffusion and Cross-Relaxation. *Langmuir* **2010**, *26*, 8352–8357.

(131) Bellissent-Funel, M.-C. Status of Experiments Probing the Dynamics of Water in Confinement. *Eur. Phys. J. E* **2003**, *12*, 83–92.

(132) Monson, P. A. Understanding Adsorption/Desorption Hysteresis for Fluids in Mesoporous Materials Using Simple Molecular Models and Classical Density Functional Theory. *Microporous Mesoporous Mater.* **2012**, *160*, 47–66.

(133) Bardestani, R.; Patience, G. S.; Kaliaguine, S. Experimental Methods in Chemical Engineering: Specific Surface Area and Pore Size Distribution Measurements—BET, BJH, and DFT. *Can. J. Chem. Eng.* **2019**, *97*, 2781–2791.

(134) Grassert, I.; Schmidt, U.; Ziegler, S.; Fischer, C.; Oehme, G. Use of Rhodium Complexes with Amphiphilic and Nonamphiphilic Ligands for the Preparation of Chiral α-Aminophosphonic Acid Esters by Hydrogenation in Micellar Media. *Tetrahedron Asymmetry* **1998**, *9*, 4193–4202.

(135) Myers, D. *Surfactant Science and Technology*, 3rd editio.; Wiley-Interscience, Ed.; A John Wiley & Sons, Inc. Publication: New York, 2006.

(136) Yan, P.; Xiao, J. X. Polymer-Surfactant Interaction: Differences between Alkyl Sulfate and Alkyl Sulfonate. *Colloids Surfaces A Physicochem. Eng. Asp.* **2004**, *244*, 39–44.
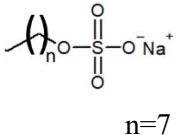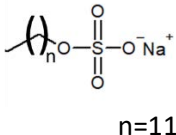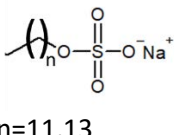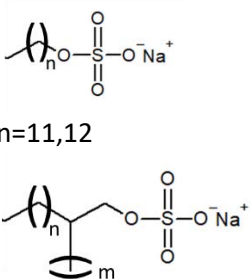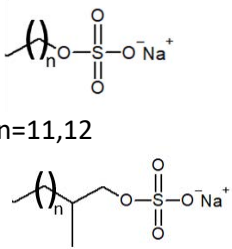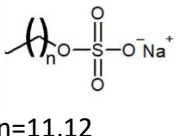
(137)   Jacobasch, H. J.; Bauböck, G.; Schurz, J. Problems and Results of Zeta-Potential Measurements on Fibers. *Colloid Polym. Sci.* **1985**, *263*, 3–24.

(138)   Collins, G. E.; Buckley, L. J. Conductive Polymer-Coated Fabrics for Chemical Sensing. *Synth. Met.* **1996**, *78*, 93–101.

(139)   Yang, Z.; Peng, H.; Wang, W.; Liu, T. Crystallization Behavior of Poly(ε-Caprolactone)/Layered Double Hydroxide Nanocomposites. *J. Appl. Polym. Sci.* **2010**, *116*, 2658–2667.

(140)   Kolhe, S. M.; Kumar, A. Radiation-Induced Grafting of Vinyl Benzyl Trimethyl Ammonium Chloride onto Nylon-6 Fabric. *Radiat. Phys. Chem.* **2007**, *76*, 901–906.

(141)   Saïhi, D.; El-Achari, A.; Vroman, I.; Cazé, C. Graft Copolymerization of Methacryloyloxyethyl Trimethyl Ammonium Chloride Monomer onto Polyamide 66 Fibres. *J. Text. Apparel, Technol. Manag.* **2004**, *4*, 1–8.

(142)   Azizinejad, F.; Talu, M.; Abdouss, M.; Shabani, M. An Investigation of the Grafting of Acrylic Acid/Methyl Methacrylate Mixture onto Poly(Ethylene Terephthalate) Fibres. *Iran. Polym. J.* **2005**, *14*, 33–38.

(143)   Birdi, K. S. *Handbook of Surface and Colloid Chemistry*; CRC Press, 2016.

(144)   Jadoon, Q.; Bibi, I.; Mehmood, K.; Sajjad, S.; Nawaz, M.; Ali, F.; Bibi, S.; Ur-Rehman, W.; Bano, S.; Usman, M. Interaction of Surfactants with Block-Copolymer Systems in the Presence of Hofmeister Anions. *Mater. Res. Express* **2017**, *4*, 1–10.

(145)   Gamboa, C.; Olea, A. F. Association of Cationic Surfactants to Humic Acid: Effect on the Surface Activity. *Colloids Surfaces A Physicochem. Eng. Asp.* **2006**, *278*, 241–245.

(146)   Wertz, P. W. Human Synthetic Sebum Formulation and Stability under Conditions of Use and Storage. *Int. J. Cosmet. Sci.* **2009**, *31*, 21–25.

(147)   Naquiah, N.; Nizar, A.; Mohamed, J.; Marikkar, N.; Hashim, D. M. Differentiation of Lard , Chicken Fat , Beef Fat and Mutton Fat by GCMS and EA-IRMS Techniques. *J. Oleo Sci.* **2013**, *62*, 459–464.

(148)   Bukackova, M.; Rusnok, P.; Marsalek, R. Mathematical Methods in the Calculation of the Zeta Potential of BSA. *J. Solution Chem.* **1234**, *47*, 1942–1952.

(149)   Shi, Q.; Zhou, Y.; Sun, Y. Influence of PH and Ionic Strength on the Steric Mass-Action Model Parameters around the Isoelectric Point of Protein. *Biotechnol. Prog.* **2008**, *21*, 516–523.
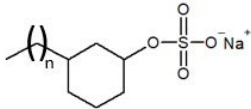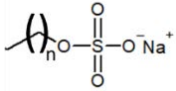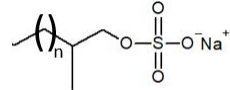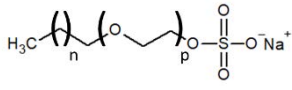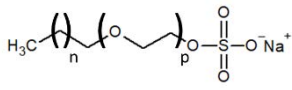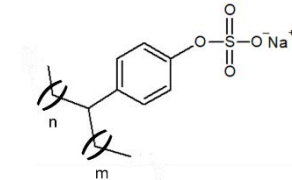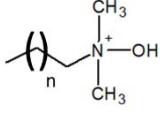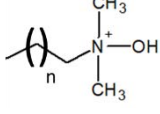
(150) Ang, W. S.; Elimelech, M. Protein (BSA) Fouling of Reverse Osmosis Membranes: Implications for Wastewater Reclamation. *J. Memb. Sci.* **2007**, *296*, 83–92.

(151) Hu, J.; Li, S.; Liu, B. Adsorption of BSA onto Sulfonated Microspheres. *Biochem. Eng. J.* **2005**, *23*, 259–263.

(152) Gao, Y.; Cranston, R. Recent Advances in Antimicrobial Treatments of Textiles. *Text. Res. J.* **2008**, *78*, 60–72.

(153) Lang, Frank-Peter; Laborda, Steve; Borchers, Georg; Morschhaeuser, R. Anionic Soil Release Polymers. US 0036641 A1, 2009.

(154) Dominic Wai-Kwing Yeung, Vance Bergeron, Jean-Francois Bodet, Mark Robert Sivik, Bernard William Kluesener, W. M. S. Block Polymers, Composition and Methods for Use for Foams, Laundry Detergents and Shower Rinses and Coagulants. US 9,044,413 B2, 2015.

(155) Mira, I. Interactions between Surfactants and Starch: From Starch Granules to Amylose Solutions - Doctoral Thesis, Royal Institute of Technology, Stockholm, Sweden, 2006.

(156) Tanford, C. Micelle Shape and Size. *J. Phys. Chem.* **1972**, *76*, 3020–3024.

(157) Chodankar, S.; Aswal, V. K.; Kohlbrecher, J.; Vavrin, R.; Wagh, A. G. Surfactant-Induced Protein Unfolding as Studied by Small-Angle Neutron Scattering and Dynamic Light Scattering. *J. Phys. Condens. Matter* **2007**, *19*, 1–12.

(158) Shweitzer, B.; Zanette, D.; Itri, R. Bovine Serum Albumin (BSA) Plays a Role in the Size of SDS Micelle-like Aggregates at the Saturation Binding : The Ionic Strength Effect. *J. Colloid Interface Sci.* **2004**, *277*, 285–291.

(159) Valstar, A. Protein-Surfactant Interactions - Doctoral Thesis, Acta Universitatis Upsaliensis, Uppsala,Sweden, 2000.

(160) Yang, C.; Rathman, J. F. Adsorption-Solution Structure Relationships of PET/POET Polymeric Surfactants in Aqueous Solutions. *Polymer (Guildf).* **1996**, *37*, 4621–4627.

(161) Valstar, A.; Almgren, M.; Brown, W. The Interaction of Bovine Serum Albumin with Surfactants Studied by Light Scattering. *Langmuir* **2000**, *16*, 922–927.
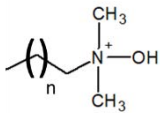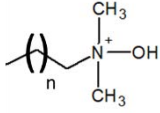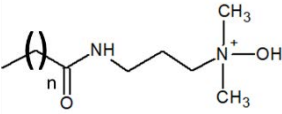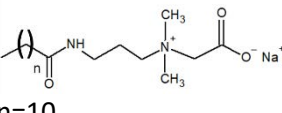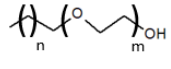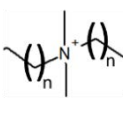
Appendix

Appendix I

List of surfactants used in this research classified by group head charge. All the structures and main structural features are proposed.

Surfactant charge	name	notation	Molecular structure	Structural feature	Supplier
anionic	Octyl alkyl sulfate	C8 AS	 n=7	linear	Sigma Aldrich
	Sodium dodecyl sulfate	SDS	 n=11	linear	Sigma Aldrich
	Sodium Lauryl sulfate	SLS	 n=11,13	linear	Sigma Aldrich
	Shell Alkyl sulfate	Shell AS	 n=11,12 n=1-4, m=8→5, 9→6	42% C12, 56% C13, 18% branched	Shell
	Lial Alkyl Sulfate	Lial AS	 n=11,12 n=8,9	43% C12, 57% C13, 55% branched	
	Safol Alkyl Sulfate	Safol AS	 n=11,12	48% C12, 47% C13, 50% branched	

			n=5,6		
	Isalchem Alkyl sulfate	Isalchem AS	n=11,12 n=8,9	43% C12, 57% C13, 95% branched	
	Alkyl mono-ethoxy-sulfate	AE_1S	n=11,13, p=0,1	C12-C14 AS C12-C14 AE_1S	
	Alkyl tri-ethoxy-sulfate	AE_3S	n=11,13, p=0,1,2,3	C12-C14 AS C12-C14 AE_1S C12-C14 AE_2S C12-C14 AE_3S	
	Lauryl Alkyl-benzen Sulfonate	LAS	n=7 →4 m=1→4 n=8 →5 m=1→4 n=10 →7 m=1→4	C11-C12-C14 LAS, 50% branched	
amphoteric	C10 Dimethyl Amine oxide	C10 AO	n=8	linear	
	C11 Dimethyl Amine oxide	C11 AO	n=9	linear	

	C9-C11 Dimethyl Amine oxide	C9-C11 AO	 n=7,9	linear	
	C12-C14 Dimethyl Amine oxide	C12-C14 AO	 n=10,12	linear	
	Cocoamido propyl amine oxide	CapAO	 n=10	Linear, big head	BASF
	Cocoamido propyl Betaine	CapBetaine	 n=10	Linear, big head	BASF
non-ionic	Decil-octaethoxy alchool	Marlipal	 n=8, m=8	linear	Sasol
cationic	Dodecyl dimethyl ammonium chloride	DDAC	 n=9	QUAT	Sasol

Appendix II

a) Differential scanning calorimetry plot of SRN240. A conventional DSC scan was run, using a heating rate of 10 °C.
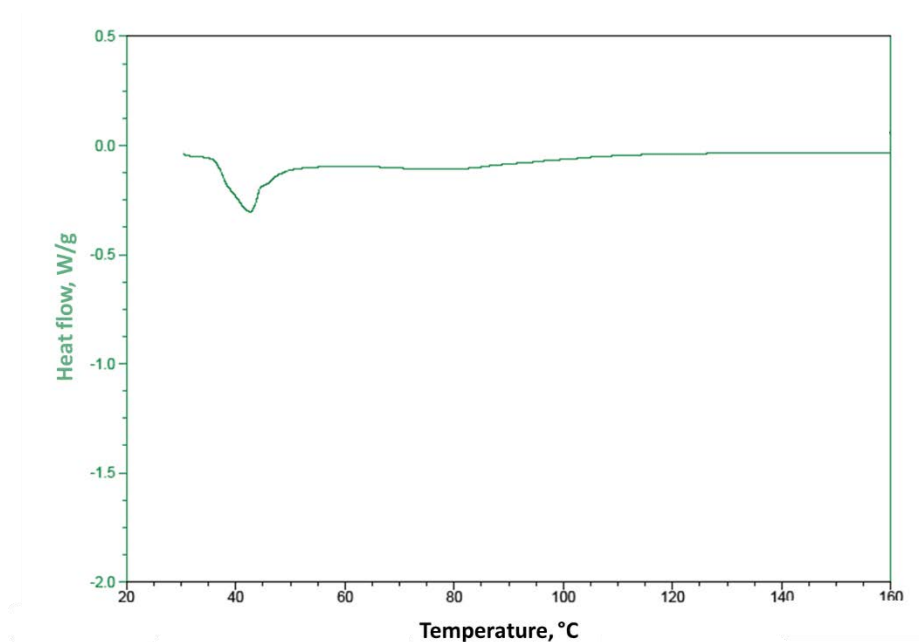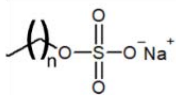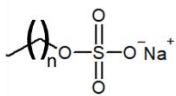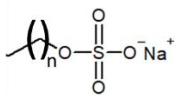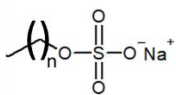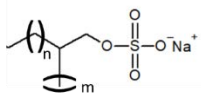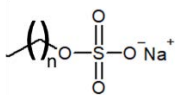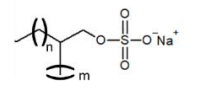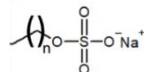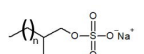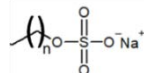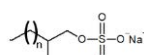

b) Differential scanning calorimetry plot of SRA300. A conventional DSC scan was run, using a heating rate of 10 °C.
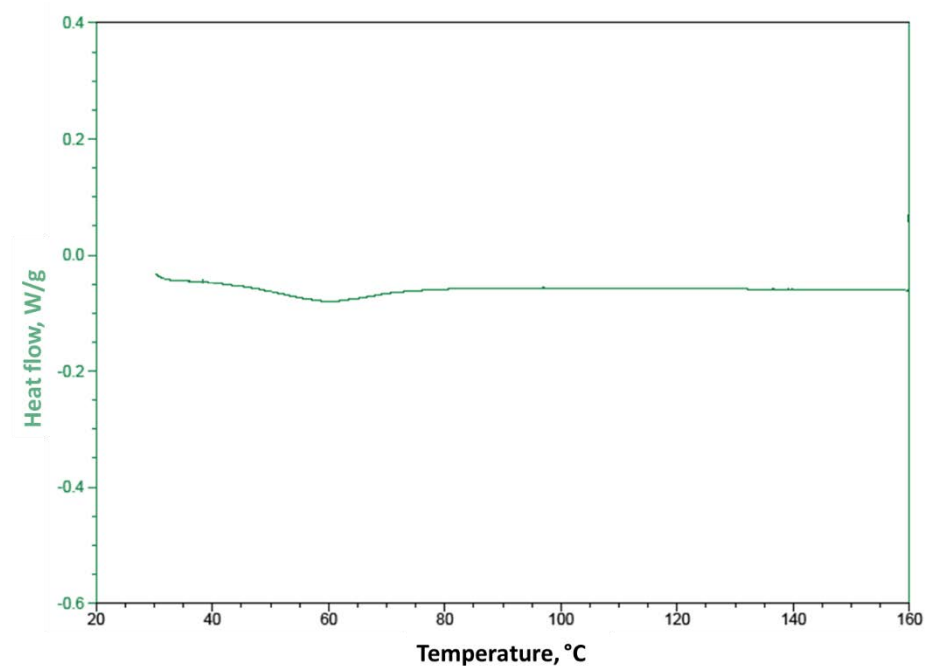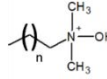
Appendix III

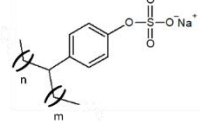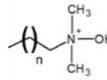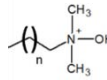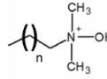List of m/z ratio present in each of the surfactants analysed in this thesis and that were used for surfactant quantification in presence and in absence of soil. For each m/z ratio, the chemical structure is presented, as well as the relative content of each m/z in each surfactant and the branching degree.
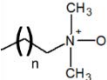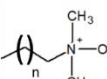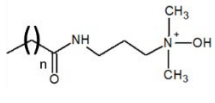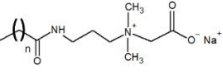
Surfactants	ESI mode	m/z	Isomer		Chemical structure	
Octyl sulphate	(-)-ESI	209.4	C8 AS	Linear		n=7
Sodium dodecyl sulphate	(-)-ESI	265.5	C12 AS	Linear		n=11
Sodium Lauryl sulphate	(-)-ESI	265.5	C12 AS	Linear		n=11
		293.4	C14 AS	Linear		n=13
Shell AS	(-)-ESI	265.5	C12 AS (42%)	18% branched		n=11
						n=1 → 4 m=8→5
		279.4	C13 AS (56%)			n=13
						n=1 → 4 m=9→6
Lial AS	(-)-ESI	265.5	C12 AS (43%)	55% branched	n=11 n=8	
		279.4	C13 AS (57%)		n=12 n=9	

Safol AS	(-)-ESI	265.5	C12 AS (48%)	50% branched		n=11		n=5
		279.4	C13 AS (47%)			n=12		n=6
Isalchem AS	(-)-ESI	265.5	C12 AS (43%)	95% branched		n=11		n=8
		279.5	C13 AS (57%)			n=12		n=9
Alkyl mono-ethoxy-sulphate (AE1S)	(-)-ESI	265.5	C12 AS	Linear		n=11		
		293.5	C14 AS			n=13		
		309.6	C12 AE1S			n=10 p=1		
		353.6	C14 AE1S			n=10 p=2		
Alkyl tri-ethoxy-sulphate (AE3S)	(-)-ESI	265.5	C12 AS	linear		n=11		
		293.6	C14 AS			n=13		
		309.6	C12 AE1S			n=10 p=1		
		337.6	C14 AE1S			n=14 p=1		
		353.6	C12 AE2S			n=10 p=2		
		381.6	C14 AE2S			n=14 p=2		
		397.6	C12 AE3S			n=10 p=3		
		425.7	C14 AE3S			n=14 p=3		
Linear Alkyl Benzen Sulphonate (LAS)	(-)-ESI	297.5	C11 LAS	50% branched		n=7 →4 m=1→4		
		311.5	C12 LAS			n=8 →5 m=1→4		

177

		325.5	C14 LAS			n=10 →7 m=1→4
C10 Dimethyl Amine oxide	(+)-ESI	202.5	C10 AO	linear		n=8
C11 Dimethyl Amine oxide	(+)-ESI	216.4	C11 AO	linear		n=9
C9-11 Dimethyl Amine oxide	(+)-ESI	202.5	C9 AO	linear		n=7
		216.5	C11 AO			n=9
C12-C14 Dimethyl Amine oxide	(+)-ESI	230.5	C12 AO	linear		n=10
		258.5	C14 AO			n=12
Cocoamido propyl amine oxide (CapAO)	(+)-ESI	301.5	C11 CapAO	linear		n=10
Cocoamido propyl Betaine	(+)-ESI	343.6	C11 CapBetaine	linear		n=10

List of publications

- Valentini, A.; Mateos, H.; Robles, E.; Brooker, A.; Cioffi, N.; Palazzo, G. Measurement of the Zeta-Potential of Solid Surfaces through Laser Doppler Electrophoresis of Colloid Tracer in a Dip-Cell: Survey of the Effect of Ionic Strength, pH, Tracer Chemical Nature and Size. *Colloids and Surfaces A*, **2019**, 576.

- Valentini, A.; Gkatzionis, K.; Palazzo, G.; Cioffi, N.; Franco, C. Di; Robles, E.; Brooker, A.; Britton, M. M. Combined Use of Streaming Potential and UV / Vis to Assess Surface Modification of Fabrics via Soil Release Polymers. *Ind. Eng. Chem. Res.* **2019**, 58.

- Mateos, H.; Valentini, A.; Colafemmina, G.; Murgia, S.; Robles, E.; Brooker, A.; Palazzo, G. Binding Isotherms of Surfactants Used in Detergent Formulations to Bovine Serum Albumin. Colloids Surfaces A **2020**, 598, 124801.

- Mateos, H.; Valentini, A.; Lopez, F. Surfactant Interactions with Protein-Coated Surfaces: Comparison between Colloidal and Macroscopically Flat Surfaces. Biomimetics 2020, 5, 31.